

1984

THE AUTOMATIC CONTROL OF LARGE SHIPS IN CONFINED WATERS

BURNS, ROLAND STEPHEN

<http://hdl.handle.net/10026.1/2689>

<http://dx.doi.org/10.24382/3427>

University of Plymouth

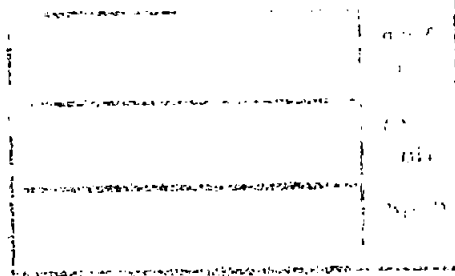
All content in PEARL is protected by copyright law. Author manuscripts are made available in accordance with publisher policies. Please cite only the published version using the details provided on the item record or document. In the absence of an open licence (e.g. Creative Commons), permissions for further reuse of content should be sought from the publisher or author.

THE AUTOMATIC CONTROL OF LARGE SHIPS
IN CONFINED WATERS

By

ROLAND STEPHEN BURNS

*This thesis is submitted to the Council for National Academic Awards
in partial fulfilment of the requirements for the degree of Doctor
of Philosophy.*



Sponsoring Establishment: Plymouth Polytechnic
Collaborating Establishment: University College, London.

September, 1984

PLYMOUTH POLYTECHNIC LIBRARY	
Accn. No.	5500163-8
Class. No.	T 623.88 BUR
Contl. No.	X 700496202

THE AUTOMATIC CONTROL OF LARGE SHIPS IN CONFINED WATERS

R. S. Burns

ABSTRACT

The design and evaluation of a control system, which can be utilised for the automatic guidance of large ships in confined or restricted waters, is investigated.

The vessel is assumed to be a multivariable system and it is demonstrated that a non-linear, time-varying mathematical model most accurately describes the motion of the hull, particularly in tight manoeuvres.

A discrete optimal controller has been designed to control simultaneously track, heading and forward velocity. The system is most effective whilst operating under a dual-mode policy. It is shown that feedback matrix adaption is necessary to deal with changes in forward velocity and a form of gain scheduling is proposed. Active disturbance control is employed to counteract effects of wind and tide.


An inertial navigation system, together with an optimal controller and filter, is installed on-board a car ferry model. Free-sailing tests show that the performance characteristics of the system are in accordance with theoretical predictions.

The feasibility of implementation on a full-size vessel is considered.

DECLARATION

I declare that:

1. While registered as a candidate for the Council's research degree,
I have not been a registered candidate or enrolled student for
another award of the CNAA or other academic or professional inst-
itution.
2. No material contained in this thesis has been used in any other
submission for an academic award.
3. The work undertaken in this thesis is concerned with the design and
evaluation of an optimal controller, which is part of a joint research
project into the study of automatic pilotage of large ships in
confined waters.
4. During the course of the investigation, the following advanced studies
have been undertaken in connection with the programme of research:-
 - (a) Advanced Reading Course - Modern Control Theory, Statistical
Techniques, Adaptive and Optimal Control, Multivariable Control.
 - (b) Short Course - Microprocessor Interface and Software Development.
City of Birmingham Polytechnic.
 - (c) Attendance at the following conferences/symposia:-
 - (i) First International Conference on Systems Engineering.
Coventry Lanchester Polytechnic, Sept. 1980.
 - (ii) Second International Conference on Systems Engineering.
Coventry Lanchester Polytechnic, Sept. 1982.
 - (iii) Symposium on Application of Multivariable Systems Theory.
Royal Naval Engineering College, Plymouth, Oct. 1982.
5. Appendix 7 contains a copy of the published paper "Automatic Pilotage
of Large Ships in Confined Waters" presented at symposium (iii) above.

Signature of Candidate 
(R. S. Burns)

Date ... 1/9/84 ...

CONDITIONS OF USAGE


To the Librarian of:- a) British Library
b) Plymouth Polytechnic

I give permission for my thesis entitled The Automatic Control of Large Ships in Confined Waters to be made available forthwith for consultation by readers in respective libraries or to be sent away on temporary loan if requested by other institutions. I also give my permission for the production of a microfilm of this thesis by the British Library, as required by the regulations of the Council of National Academic Awards (CNAA).

This thesis is made available on the understanding that the reader will not publish in any form either the whole or any part of it without written permission from both the holding library and the author. Where the regulations of the CNAA and of the holding library allow, I give permission for the thesis to be photocopied in whole or in part for the purpose of private study.

The copyright of this thesis belongs to the author.

Signature of Author:


..... (R.S. Burns)

Permanent Address:

16 Torridge Close,
Plympton,
Plymouth,
Devon.
PL7 3DH

Date:

1st September, 1984.

The Quiberon, Flag-Ship of Brittany Ferries,
Safely Berthed at Millbay Docks, Plymouth.



TABLE OF CONTENTS

	Page
Abstract	i
Declaration	ii
Conditions of Usage	iii
Acknowledgements	ix
List of Figures	x
List of Tables	xiv
 Chapter 1.	
Introduction and Review of Ship Autopilot Control Systems	
1.1 Introduction	1
1.2 PID Autopilots	2
1.3 Adaptive Autopilots	5
1.3.1 Model Reference Adaption	6
1.3.2 Self-Tuning Autopilots	8
1.3.3 Cost Functions for Adaptive Course-Keeping Autopilots	9
1.4 Path and Track-Keeping Autopilots	11
1.4.1 Dynamic Positioning	13
1.5 Commercial Autopilots on the Market	14
1.6 Integrated Navigational Systems	15
1.7 Present Study	16
 Chapter 2.	
Ship Mathematical Model	
2.1 Introduction	19
2.2 Co-ordinate Systems and Sign Conventions	19
2.3 Euler's Equations of Motion for a Rigid Body	20
2.4 Selection of System Variables	21
2.5 Linear Time-Invariant Model	24

		Page
2.5.1	Steering Gear and Main Engines	24
2.5.2	State-Space Formulation	25
2.5.3	Discrete Solution of the State Equation	26
2.5.4	Transfer Function Approach	26
2.5.5	Co-ordinate System Transformation	27
2.6	Quasi-Linear Time-Variant Model	28
2.6.1	Non-Dimensional Model	29
2.7	Non-Linear Time-Variant Model	30
2.7.1	Non-Linear Equations of Motion	30
2.7.2	Non-Linear Control Parameters	32
Chapter 3	Disturbance Modelling	
3.1	Introduction	35
3.2	Current	35
3.2.1	Hydrodynamic Coefficients	36
3.2.2	The Dynamics of Tidal Streams	37
3.2.3	Tidal Stream Direction	39
3.3	Wind	40
3.3.1	Aerodynamic Coefficients	41
3.3.2	Wind Dynamics	43
3.4	Disturbance Recursive Equation Set	46
3.4.1	Frequency Spectrum	46
Chapter 4.	Simulation of Ship Manoeuvres and Experimental Determination of Hydrodynamic Coefficients	
4.1	Introduction	49
4.2	Simulation Program	49
4.3	Manoeuvring Simulations	50
4.3.1	Turning Circle Manoeuvres	50
4.3.2	Dieudonne Spiral Manoeuvre	50
4.3.3	Kempf Zig-Zag Manoeuvre	52

		Page
4.3.4	Starting Trials	52
4.4	Analysis of Results	52
4.5	Important Non-Linear Coefficients	54
4.6	Experimental Determination of Hydrodynamic Coefficients for Car Ferry Hull 5502	55
4.7	Description of Tests	57
4.7.1	Hull Resistance	57
4.7.2	Bollard Pulls	57
4.7.3	Self Propulsion Experiments	57
4.7.4	Rudder Experiments	58
4.7.5	Drift Angle Experiments	58
4.7.6	Added Mass Coefficients	59
4.7.7	Free-Sailing Tests	59
Chapter 5	Controller Design	78
5.1	Introduction	78
5.2	The Ship Control Problem	79
5.3	Controllability and Observability	80
5.4	Multivariable System Control	83
5.4.1	Stochastic Optimal Control	83
5.4.2	Deterministic Optimal Control	84
5.5	Optimal Closed-Loop Pole Assignment	87
5.6	Disturbance Control	93
5.7	Adaptive Optimal Control	96
Chapter 6	Controller Performance	
6.1	Introduction	104
6.2	Desired State Trajectories	105
6.3	Ship Related State Variable Feedback	106
6.3.1	Reverse-Time Integration	108
6.3.2	Dual-Mode Control with Way-Point Anticipation	110

		Page
6.4	Ship and Earth Related State Variable Feedback	114
6.5	Selection of Control Policy	117
Chapter 7	System Implementation	
7.1	Introduction	140
7.2	Measurement System	140
7.2.1	Review of Measurement Techniques	140
7.2.2	Prototype Measurement System	142
7.2.3	Initial Tests	144
7.2.4	Measurement System Component Characteristics	145
7.3	The Measurement Package	148
7.4	Rudder and Engine Servo-Systems	148
7.4.1	Rudder Servos	148
7.4.2	Engine Speed Control	152
7.5	Microcomputer Hardware	154
7.5.1	General Features of the TMS 9900	154
7.5.2	System Configuration	155
7.5.3	A/D and D/A Conversion	156
7.6	Commissioning Trials	158
7.6.1	Commissioning Test 1. 19.7.83	158
7.6.2	Commissioning Test 2. 3.8.83	159
7.6.3	Commissioning Test 3. 12-20.9.83	161
Chapter 8	Free-Sailing Trials	
8.1	Introduction	163
8.2	Selection of State Variables for Model	164
8.2.1	Reduced State Equations	164
8.3	Controller Parameters	165
8.4	Real-Time Software Development	168
8.4.1	Program Structure	169
8.4.2	Computation of Mathematical Model	170

		Page
8.4.3	Bench Testing	171
8.5	Test Procedure	172
8.6	Test Results	174
8.7	Analysis of Results	176
Chapter 9	Conclusions	
9.1	Introduction	198
9.2	Modelling Techniques	198
9.3	Controller Design and Evaluation	200
9.4	Performance Characteristics	202
9.5	Implementation and Testing	205
9.6	Future Developments	206
	References	210
	Nomenclature	224
Appendix 1	Mathematical Model Parameters	A1.1
Appendix 2	Mariner Hull Hydrodynamic Coefficients	A2.1
Appendix 3	Towing Tank Results Car Ferry Hull 5502	A3.1
Appendix 4	Optimal Filter	A4.1
Appendix 5	Elements of A and B matrices	A5.1
Appendix 6	Computer Programs	A6.1
Appendix 7	Application of Multivariable Systems Theory, October, 1982. "Automatic Pilotage of Large Ships in Confined Waters - A Multivariable Approach"	

ACKNOWLEDGEMENTS

The candidate would like to express his sincere gratitude to his supervisors, Professor T.H. Lambert, Mr. T.H. Bouncer and Dr. D.R. Broome for their guidance, assistance and advice throughout the course of the work and in the preparation of this thesis.

I am grateful to Professor D.E. Fussey for making available the facilities of the Department of Mechanical Engineering and to all technician staff throughout the Polytechnic who have helped with this project. Particular thanks must go to Mr. M.J. Stringer for his aid in development of both hardware and software for the physical model. My thanks also to the staff of the Computer Centre.

I would also like to acknowledge the co-operation given by the following organisations, without whose approval the sailing trials could never have taken place:

1. Brittany Ferries
2. The National Trust
3. South West Water Authority
4. Plymouth Model Boat Club

Finally, I am indebted to my wife, Janet, for typing this thesis and to my whole family for their support and encouragement during the period in which the work was completed.

LIST OF FIGURES

<u>Figure Number</u>	<u>Title</u>	<u>Page</u>
1.1	Proposed Guidance System	16
2.1	Ship Co-ordinate System	20
2.2	Multivariable System	22
3.1	Relative Current	36
3.2	Turbulent Current Energy Spectrum	37
3.3	Relative Wind	40
3.4	Ship as a Lifting Surface	41
3.5	Horizontal Wind Energy Spectrum	43
3.6	Gust Co-ordinate System	44
3.7	Correlated Stochastic Components of Tidal Stream Velocity and Direction	47
3.9(a)	Smoothed Frequency Spectrum for Tide and Wind Velocity	47
3.8	Correlated Stochastic Components of Wind Velocity and Direction	48
3.9(b)	Smoothed Frequency Spectrum for Tide and Wind Direction	48
4.1	Flow-Chart for Manoeuvring Simulation	51
4.12	Photograph: Model Car Ferry Hull 5502	56
4.13	Photograph: Model Attached to Towing Gantry	56
4.2a,b,c,d	Turning Circle Simulation, Full-Size Mariner Hull, 7.717 m/s Approach, 20° Starboard Rudder	62/63
4.3	Advance	64
4.4	Transfer	65
4.5	Tactical Diameter	66
4.6	Final Diameter	67
4.7(a)	Final Forward and Lateral Velocities Approach Speed 7.717 m/s.	68
4.7(b)	Final Forward and Lateral Velocities Approach Speed 2.572 m/s.	69
4.8	Dieudonne Spiral	70

<u>Figure Number</u>	<u>Title</u>	<u>Page</u>
4.9	Kempf Zig-Zag Manoeuvre	71
4.10	Step Change in Demanded Engine Speed	71
4.11a,b,c,d	Turning Circle Simulation, Model Car Ferry Hull, 0.5 m/s Approach, 30° Starboard Rudder	72
5.1	Ship Automatic Pilotage Control System	79
5.2	Separation Principle	84
5.3	Optimal Controller For a Tracking System	86
5.4	Surge Optimal Closed-Loop Pole Trajectories	90
5.5	Effect of q_{55} on Sway and Yaw Optimal Closed-Loop Pole Trajectories	90
5.6	Effect of q_{77} on Sway and Yaw Optimal Closed-Loop Pole Trajectories	91
5.7	Complete Optimal Root Locus Diagram	92
5.8	Effect of Forward Velocity Reduction on Open-Loop Eigenvalues	96
5.9	Effect of 30 Degree Port Turn on Open-Loop Eigenvalues	97
5.10	Departure of Closed-Loop Eigenvalues from Optimal Positions During a Speed Reduction	97
5.11	Departure of Closed-Loop Eigenvalues from Optimal Positions During a 30 Degree Port Turn	98
5.12	Variation in Closed-Loop Poles During a Speed Reduction. Feedback Matrix Re-calculated with Constant Q and R .	99
5.13	Optimal Root Locus Diagrams for Forward Speeds of 5.145 and 2.572 m/s.	99/100
5.14	Feedback Matrix Adaption to Changes in Forward Speed	102
6.1	Desired Track Into Plymouth Sound	105
6.2	Co-ordinate Transformation	108
6.4	Optimal Control Without Command Equations	112
6.6	Way-Point Advance	113
6.9	Generalised Performance Indices	121
6.3a,b,c	Simulation Runs 1, 2 and 3	122-124
6.5a,b	Simulation Runs 4 and 5	125/126
6.7	Simulation Run 6	127

<u>Figure Number</u>	<u>Title</u>	<u>Page</u>
6.8a,b	Simulation Runs 7 and 8	128
6.10	Simulation Run 9	129
6.11a,b	Simulation Runs 10 and 11	130/131
6.12a,b	Simulation Runs 12 and 15	132/133
6.13a,b	Simulation Runs 13 and 16	134/135
6.14a,b	Simulation Runs 14 and 17	136/137
6.15a,b	Simulation Runs 18 and 19	138/139
7.1	Schematic Representation of Guidance System	140
7.2	Strap-Down Inertial Navigation System	143
7.3	800 ADA Servoed Linear Accelerometer	145
7.4	900 Series Servoed Rate Gyroscope	146
7.5	Heading Gyroscope Measurement Bridge	147
7.6	Photograph: Measurement Package	149
7.11	Photograph: Top View of TMS 9900 Computer, Power Supplies and Heading Gyroscope	149
7.7	Instrumentation Power Supplies	150
7.8(a)	Schematic Diagram of Rudder Servo-System	150
7.8(b)	Photograph: Rudder Servo-System	151
8.12	Photograph: Model in a Tight Turn on the Reservoir	151
7.9	Schematic Diagram of Engine Speed Control	153
7.10	TMS 9900 Memory-Map	157
7.12	Commissioning Test 1	160
7.13	Commissioning Test 3	160
8.1	90 Degree Track-Changing Simulation (Model), Dual-Mode Control	167
8.3	Bench-Test: TMS 9900 Microcomputer Interfaced to Instrumentation Package	167
8.2	Order of Operations in Real-Time Program	168
8.4	Plan of Crownhill Reservoir	172
8.11(a)	Photograph: Run 5: Track-Keeping	177
8.11(b)	Photograph: Run 10: Track-Changing	177

<u>Figure Number</u>	<u>Title</u>	<u>Page</u>
8.5a,b,c	Reservoir Run 3	180-182
8.6a,b,c	Reservoir Run 5	183-185
8.7a,b,c	Reservoir Run 9	186-188
8.8a,b,c	Reservoir Run 10	189-191
8.9a,b,c	Reservoir Run 12	192-194
8.10a,b,c	Reservoir Run 19	195-197
A3.1	Hull Resistance	A3.8
A3.5	Determination of \bar{X}_{vv}	A3.8
A3.2	Bollard Pulls	A3.9
A3.3	Non-Dimensional X-Direction Rudder Force	A3.10
A3.4	Non-Dimensional Y-Force and N-Moment Against Rudder Angle	A3.11
A3.6	Non-Dimensional Y-Force and N-Moment Against Lateral Velocity	A3.12
A4.1	Optimal Filter	A4.1

LIST OF TABLES

<u>Table Number</u>	<u>Title</u>	<u>Page</u>
4.1	Advance After 90 Degrees Change of Heading	74
4.2	Transfer After 90 Degrees Change of Heading	74
4.3	Tactical Diameter After 180 Degrees Heading Change	75
4.4	Steady-State Turn Diameter	75
4.5	Final Forward and Lateral Velocities	76
4.6	Dieudonne Spiral Manoeuvre	76
4.7	Important Hydrodynamic Coefficients	77
4.8	Hydrodynamic Coefficients for Car Ferry Hull 5502	77
6.1	Desired Headings and Way-Points	106
6.2	Desired State Vector	107
6.3	Controller Settings	109
6.4	Generalised Performance Indices	111
8.1	Details of Test Runs	175
8.2	Generalised Performance Indices for Mathematical and Physical Models	179
8.3	Mathematical Model Validity Indices	179
9.1	Closed-Loop Characteristics of Model	206
A2.1	Mariner Hull Hydrodynamic Coefficients	A2.2
A3.1	Hull Resistance	A3.1
A3.2(a)	Bollard Pulls - Both Propellers Ahead	A3.2
A3.2(b)	Port Screw Ahead and Astern	A3.3
A3.3	Self Propulsion Points - Both Screws Ahead	A3.3
A3.4	Non-Dimensional Rudder Forces and Moments on Hull	A3.4
A3.5	Drift Angle Experiments	A3.6

CHAPTER 1

INTRODUCTION AND REVIEW OF SHIP AUTOPILOT CONTROL SYSTEMS

1.1. Introduction

The history of the modern automatic pilot (autopilot) for ship steering has its origin near the beginning of this century, following the invention of the gyrocompass. Elmer Sperry discussed the problems of automatic steering in 1922 (1) in terms of an application of the gyrocompass and describes what was possibly the first installation aboard ship. In the same year Minorsky presented the basic theory for directional stability of automatically steered ships (2) and summarised various control equations that might be applied. Sperry's system, although completely mechanical, had all the elements that make up the control loop of an automatic course-keeping system, namely: rudder, steering gear, ship, gyrocompass and autopilot. By 1932, four hundred of Sperry's systems had been installed on merchant ships throughout the world.

The autopilot of this era was a very simple device in which the heading error produced a corrective signal for the steering gear (proportional control). The proportional gain, or so-called rudder adjustment could be varied to suit different loading conditions of the ship. In heavy seas however, a proportional autopilot produced excessive working of the steering gear and many manufacturers provided a "weather adjustment". In most cases this consisted of lost motion, or

backlash between the autopilot output and the control actuating device, so that when the ordered rudder angle changed direction the control system did not respond until a specified small angle had been exceeded, thus reducing rudder activity. Backlash, or alternatively, dead-band weather adjustment was employed in many autopilots and with some, an added feature was the application of "bias" by which an initial constant rudder angle or "kick" was applied as soon as the dead-band was exceeded.

Another scheme introduced in early autopilots was to include in the rudder adjustment a form of delayed feedback which insured that rudder motion, once started, would continue to some predetermined angle before stopping. It is claimed that this had the effect of checking the ship's initial swing off course and also meeting the return swing of the ship, thus tending to prevent overshoot. Nomoto (3) describes this approach as "negative backlash" and explains that its purpose is to compensate for the phase lag caused by "weather adjustment" backlash. He adds that it is set to overcompensate for idle movement in telemotor links so as to yield a "phase lead". He refers to it as "over-telemotor adjust" and comments that the mechanism is another kind of damping to raise the stability of autopilots.

1.2. PID Autopilots

Proportional autopilots of a mainly mechanical nature were used in ships up to about 1950. They were not entirely satisfactory as over-telemotor adjust did not always prevent transient oscillation. The introduction of control terms proportional to the first or higher derivatives of the heading error had the combined advantage of producing increased damping, improved stability and introducing an anticipatory effect that helped compensate for control and steering gear

lags. According to Luke and West (4) the first commercial autopilot with rate-of-turn control action was installed on the S.S. United States in 1951.

About this time also another addition to the control equation was a term proportional to the integral of heading error. This allowed the course to be maintained in the presence of a steady disturbance such as a cross wind. The control law for a proportional, integral and derivative (PID) controller can be written:

$$\delta_D = K_1 \psi_e + K_2 \dot{\psi}_e + K_3 \int \psi_e dt \quad (1.1)$$

Sometimes just the derivative of the actual heading $\dot{\psi}_A$, rather than $\dot{\psi}_e$ is employed in equation (1.1). This has the effect of producing a single closed-loop zero in the closed-loop transfer function, whereas equation (1.1) as it stands will yield a pair of real or complex conjugate closed-loop system zeros.

One disadvantage of derivative terms are that they lead to large, and ineffective, rudder movement at high frequencies of encounter (i.e. in bow seas). This high frequency rudder movement has little effect on the ship's heading due to the dynamics of the hull, but it does cause unnecessary wear on the steering gear and adds to the ship resistance.

The use of a low-pass filter for avoiding excessive steering in rough seas as an alternative to backlash or dead-band was first proposed by Motora (5). Rydill (6) observed that a simple first-order filter tended to reduce directional stability and suggests that a 'quadratic delay' or second-order filter gives a sharper reduction in rudder movement at high frequencies, with less detrimental effect on

stability.

When Laplace Transforms are taken of equation (1.1) and coupled with Rydill's filter the autopilot transfer function takes the form:

$$\frac{\delta_D}{\psi_e}(s) = \frac{K_2 s^2 + K_1 s + K_3}{s(K_4 s^2 + K_5 s + 1)} \quad (1.2)$$

By factorising the second order terms equation (1.2) may be expressed in the standard form of the PID ship control algorithm as described by Bech (7)

$$\frac{\delta_D}{\psi_e}(s) = \frac{K_R (1 + T_{PH} s) (1 + K_{CR} T_{CR} s)}{T_{PH} (1 + T_{CR} s) (1 + T_D s) s} \quad (1.3)$$

Bech suggests the following range of autopilot setting to be suitable for most ships:

K	(rudder gain)	0.5 - 3
R		
T	(automatic permanent helm)	120 - ∞ seconds
PH		
K	(counter rudder gain)	1 - 8
CR		
T	(counter rudder time constant)	3.5 - 28 seconds
CR		
T	(damping time constant)	0.1 - 3.75 seconds
D		

Along with changes in control laws came the required change to electronic hardware in order to implement more complex designs. The PID autopilots of the sixties were analogue in nature and employed operational amplifiers to perform addition, integration and differentiation. In discussing the "Sperry Gyropilot" Wesner (8) explains that a single operational amplifier with associated components is used to differentiate and filter the heading error. A further amplifier integrates the heading error to generate the "automatic weather helm" signal. Summing firstly the proportional and rate terms and then finally the integral signal produces the composite rudder output

signal. The "Sperry Gyropilot" was designed mainly with the large tanker in mind, but Brook, chief engineer for S.G. Brown, when describing an autopilot specifically for the needs of commercial shipping (9), chose a control algorithm similar to Wesner. These control equations differ from the standard form of Bech in that the first-order rate filter converts them into a classical lead-lag network with an added integral term as follows:

$$\frac{\delta_D}{\psi_e}(s) = \frac{K_R (1 + K_{CR} T_{CR} s)}{(1 + T_{CR} s)} + \frac{1}{T_{PH} s} \quad (1.4)$$

When the autopilot was tested on a range of vessels Brown found that the product $K_{CR} T_{CR}$ which he refers to as the lower break frequency time constant should have a value of 10 seconds for a ship of 1000 tonnes displacement and up to 22 seconds for super tankers that displace 252,000 tonnes at normal cruising speeds. He selected a decade between the break frequencies so that the upper break frequency time constant T_{CR} ranges between 1 and 2.2 seconds. The weather helm integrator time constant T_{PH} was set at 80 seconds.

1.3 Adaptive Autopilots

The disturbances acting upon a vessel may be classified according to their influence on the ship's behaviour and placed in the following categories:

1. Disturbances that cause deviations from the set course.
2. Disturbances which affect the steering characteristics of the ship.

Wind, waves and tide belong to the first group. Heading error

due to this class of disturbance can be mainly overcome by feedback, providing the autopilot is correctly set.

The second class of disturbances relate to ship handling qualities and include such factors as loading, depth of water under keel and forward velocity.

The dynamics of a super tanker for example, manoeuvring in coastal waters may be subject to large parameter variation that could lead to course instability. Manual autopilot adjustment under these conditions would demand a significant level of judgment by operating personnel.

1.3.1 Model Reference Adaption

This form of automatic adaption compares directly the responses of the actual ship with an ideal mathematical model when both are subjected to the same input. A criterion function is generated in terms of the difference between the responses. The autopilot is then so adjusted that the minimum (or maximum) of the criterion function is approached.

(a) Sensitivity Models

Much pioneer work was done at Delft University of Technology by Honderd and Winkelman (10) who in 1972 simulated a model reference adaptive control system, obtaining data regarding the ship's dynamics from measurements taken aboard the Dutch training ship "Prinses Margriet". The dynamics of the model in the adaptive system corresponded to the dynamics of the actual ship in deep water. Adaption took place by defining a quadratic criterion of the form:

$$J = \frac{1}{2} e^2 \quad (1.5)$$

with
$$e = \dot{\psi}_m - \dot{\psi}_A \quad (1.6)$$

The quantity e was multiplied by a sensitivity coefficient available from the sensitivity model and the result used to adjust a

parameter in the system. The sensitivity model has the same structure as the system, but with a different input and is arrived at by analysis of how the non-linear function $H(\dot{\psi})$, the steady-state relationship between δ_A and $\dot{\psi}_A$, is affected by loading and other category 2 disturbances.

The product of the sensitivity coefficient and error quantity adjusts the magnitude of the signal obtained from a rate gyroscope, so adaption takes place by varying the amount of rate feedback in the control loop.

(b) Liapunov Approach

This technique is based on the second method of Liapunov where the system and reference model are assumed to be of the same order. If there are differences between the state vectors of the model and system, the parameters of the system are adjusted in order to minimise the difference.

Following the Liapunov approach, Van Amerongen and Udink ten Cate (11), 1973, demonstrated that when a Liapunov function V of the system error is formed, its time derivative \dot{V} will be negative definite with respect to the error if certain adaptive laws are fulfilled. They go on to explain that such an adaptive system will be asymptotically stable and for ships with linear dynamics the Liapunov method is straightforward to apply. Difficulties were experienced however in forming a suitable Liapunov function for non-linear ship dynamics but by applying Ingwerson's method (12) a function was formed and following the techniques of Winsor and Roy (13) a rate feedback adaptive law was obtained. After simulation tests on both sensitivity model and Liapunov autopilots, Van Amerongen and Udink ten Cate concluded there was little difference between the two, although the latter

required a low-pass filter in the presence of measurement noise.

Udink ten Cate and Verstoep pursued Liapunov model reference adaptive control (MRAC) systems further (14) and in 1974 presented a method of improving performance by employing a new type of error noise rejection filter. The possibility of an alternative design method of Liapunov MRAC systems using a function of the parameter misalignment was investigated and it was demonstrated that this approach had better convergence properties and was less dependent on input signal frequencies compared with other design methods.

1.3.2 Self-Tuning Autopilots

As discovered by Honderd and Winkelman (10) one of the main problems of a model reference system is the selection of the reference model dynamic characteristics. In recent years aspects of system identification have been refined and a survey by Astrom and Eykhoff (15) in 1971 reports that many techniques such as linear least squares, generalised least squares, maximum likelihood and instrumental variable methods can all be used, the choice depending on available a priori knowledge.

Subsequently, in 1973 Astrom and Wittenmark discussed a "self-tuning regulator" (16) based on a least squares parameter estimator and a minimum variance control strategy. The analysis was restricted to a single-input, single-output system with constant, but unknown parameters. It was demonstrated that the control law was identical with that which would have been computed had the system parameters been known. The minimum variance cost function employed in the self-tuning regulator had two limitations in the fact that there was no set point specified and no penalty on control effort.

A more generalised "self-tuning controller" was first proposed by Clarke and Gawthrop (17) and recent work by Mort and Linkens (18)

and Hodder and Shields (19) on this algorithm indicates that the autopilot works satisfactorily under both constant and changing parameter conditions, although difficulties may possibly exist in applying the algorithm to ship manoeuvring control.

Following their work on maximum likelihood identification of ship steering dynamics, Astrom and Kallstrom (20) (21) returned to the problem of adaptive self-tuning autopilots, particularly for tankers (22). The dependence of the ship velocity was handled by gain scheduling and in the more complex alternative proposed, a Kalman filter was employed to obtain a reliable smooth estimate of the heading, sway velocity and yaw rate. It was concluded that the adaptive autopilot could reduce the drag by up to two percent compared with values obtained from well-tuned PID regulators.

1.3.3 Cost Functions for Adaptive Course-Keeping Autopilots

In confined waters and areas of high traffic density accurate steering is necessary and in general a PID autopilot will perform this function. During the seventies, when the cost of fuel oil increased dramatically, it was realised that on the ocean, good course-keeping qualities were not so important as energy saving strategies.

It was suggested as long ago as 1966 by Nomoto and Motoyama (23) that a ship left to yaw naturally in a seaway without the application of frequent corrective rudder movements will in fact suffer less propulsion loss than if helm is repeatedly being applied. During a 400 mile passage it is estimated that heading deviations of ± 2 degrees increase the distance no more than a quarter of a mile which means little in terms of fuel consumed. On the other hand, every departure of the rudder from the mid-position exercises an element of

drag and consequently a braking effect on the forward speed. Additional drag is created by the vast mass of water carried round by the ship during an induced turn.

Among the first to consider the use of a cost function were Koyama (24) in 1970 and Norrbín (25). They independently proposed a function of the type:

$$J = \frac{1}{t} \int_0^t (\psi_e^2 + \lambda \delta_A^2) dt \quad (1.7)$$

The choice of the weighting factor λ led to a great deal of conjecture. Koyama suggests values of between 8 to 10 whilst Norrbín indicates a much smaller value. Broome and Lambert (26) conducted experiments on a scale model of a fast container ship and demonstrated how the cost function could be minimised for a given value of derivative gain.

Continuing this work, Marshall and Broome (27) constructed a three dimensional surface whose topology described cost function variation against rudder proportional gain K and counter rudder time constant T . Employing a cost function of the form:

$$J = \frac{1}{t} \int_0^t \psi_e^2 dt + \frac{0.5}{t} \int_0^t \delta_A^2 dt \quad (1.8)$$

it was demonstrated that for certain classical ship models an optimum setting of the autopilot occurred for values of T of about 50 seconds and K of approximately 0.5.

Clarke (28) suggested a similar cost function of the form:

$$J = \frac{1}{t} \int_0^t (A\psi_e^2 + B\dot{\psi}_A^2 + C\delta_A^2) dt \quad (1.9)$$

A simulation exercise based on the results of an analytical solution for a 200,000 tonne tanker provided the following range of

constants:

A	0.5 to 1.5
B	1600 to 79000
C	0.9 to 4.7

The variation of values were as a result of assuming different engine conditions, i.e. constant revolutions, constant power, constant torque or constant thrust.

1.4 Path and Track-Keeping Autopilots

Ship autopilots can be designed to perform the following tasks:

1. Course-Keeping
2. Course-Changing
3. Track-Keeping
4. Track-Changing

In terms of classical control theory, 1 and 3 present the regulator problem whilst 2 and 4 the tracking, or servomechanism problem.

The first recorded track-keeping system was in 1892 when a British patent was granted for a leader-cable system. This type of system consists of an electric cable, carrying alternating current, that lies along the sea bed following the desired track. A pair of coils on-board the ship experience induced voltages, their difference indicating whether the cable lies to port or starboard of the vessel and the magnitudes representing the distance between the cable and ship. Though the idea of leader-cables has not been fully abandoned, as yet it has never found general application.

At the end of the second world war interest arose in track-keeping systems as a result of minesweeping operations, where areas of sea needed to be searched accurately. In 1966 Goclowski and Gelb (29)

suggested the use of radio beacons to obtain position fixes and designed a lead-lag autopilot based on perpendicular distance off track, heading and yaw-rate feedback. An automatic track guidance system for a minesweeper discussed by Horst (30) derived the perpendicular distance off track from the plotting table and employed a control algorithm:

$$\delta_A = a_0 \int y_t dt + a_1 y_t + a_2 \psi_e + a_3 \dot{\psi}_A \quad (1.10)$$

He explains that ψ_e and $\dot{\psi}_A$ were used since \dot{y}_t and \ddot{y}_t were not available.

Zuidweg (31) (32) was amongst the first to consider automatic guidance and track-keeping in the light of modern control theory. He demonstrated the feasibility of stochastic linear optimal control and estimation for a ship whose dynamics are constant and known. In 1973 Millers (33) applied modern control theory to the problem of manoeuvring a ship through a narrow passage and developed a recursive filtering and control strategy to cope with stochastic current and measurement errors. Also in the same year Canner (34) discussed the linking of a Decca Navigator to an autopilot through an Omnitrac computer and suggests a cheaper alternative would be to extract path error from an x, y, t plotter.

In a later paper (35) he explores the use of avionic radar responder position fixing devices. Yakushenkov (36) also at this time discusses the synthesis of a ship's control system based on the minimisation of the mean square estimate of the deviation from the desired track, employing filtered data from radio-navigational receiver, gyrocompass and log.

The problem of controlling surface ships along prescribed paths in a manoeuvring situation where an adaptive autopilot is required to adjust for changes in system parameters was investigated by Parsons

and Cuong (37) in 1980. Their approach was to design a control system with two loops - an inner or control loop comprising of both state estimator and optimal controller together with an outer, or gain update loop consisting of an on-line parameter estimator.

An adaptive autopilot for both track-keeping and track-changing was discussed by Van Amerongen and Land (38). A Kalman filter state estimation algorithm coupled with an optimal controller are employed in the track-keeping mode, but he suggests changing to a course-keeping mode at turning points to ensure smooth transition.

1.4.1 Dynamic Positioning

Dynamic Positioning (DP) may be considered as the special case of track-keeping where the desired track is some point on the ocean bed. Interest in DP has arisen due to the discovery in recent years of vast mineral deposits on and below the floors of the ocean and has resulted in a great increase in the number of offshore mining projects. This has led to the need for accurate positioning of surface ships, for example, drilling vessels.

Dynamic Positioning systems have been manufactured since the early sixties, the traditional approach to the control problem being the implementation of PID controllers (39). The positional accuracy of these systems depend upon the measurement techniques employed, some of the most common being:

1. Taut wire angle and length measurement.
2. Acoustic transponder and hydrophone array.
3. Shore based radio stations such as Decca Hi-Fix
when the vessel is positioned near land.

In 1975 A/S Kongsberg Vapenfabrikk of Norway initiated the development of a DP system based on the concept of Kalman filtering

and optimal control. The first installation was tested during 1977 on board the vessel M/V Seaway Eagle. Jenssen et. al (40) reported that the operational performance was in accordance with expectations, the vessel having a drift of less than 10 m over a five minute period.

1.5 Commercial Autopilots on the Market

A 1983 autopilot survey shows that there are about twelve major autopilot manufacturers in the world. Most produce a series of models each of which is designed for vessels within a defined tonnage range.

Autopilots, on the whole, are still of PID design but the adaptive autopilot is starting to make its mark on the commercial market. The Sperry approach to adaptivity is an add-on, microprocessor based, Adaptive Steering Module (ASM) that may be interfaced with their UGP Universal Gyropilot, a PID autopilot. Coleman and Wang (41) explain that the ASM can adjust the parameters of the Gyropilot for the following operating regimes:

1. Open sea course-keeping, optimised control for minimum fuel usage.
2. Course-changing manoeuvres, minimum overshoot and constant rate of turn.
3. Confined water course-keeping, minimum heading error.

In 1981 a new company was formed by Racal-Decca to launch what was asserted to be the most sophisticated adaptive autopilot on the market - the DP780, developed by a team directed by Bech. This model referenced autopilot costs about £13,500 and Racal-Decca claim that a 2 per cent fuel saving at present prices would pay for a DP780 in 114 days cargo ship steaming, or after only 33 days at sea for a super tanker.

Other major manufacturers include Plath who produce an adaptive

autopilot Navipilot AD, which has three control strategies, open-sea, confined waters and heavy weather conditions. Adaptive autopilot control by Kockumation is, like that of Sperry, achieved by means of an add-on module following broadly similar principles.

1.6 Integrated Navigational Systems

On ocean going ships, various kinds of navigational instruments are installed usually according to some safety rules and regulation requirements. On larger vessels these will include:

1. Gyrocompass.
2. Doppler sonar or electromagnetic logs.
3. Satellite navigator.
4. Loran-C, Omega and/or Decca receivers.

These instruments work independently, each with their own measurements errors, many of which may be considered of a random nature. The original work of Kalman and Bucy (42) demonstrated the existence of a method of estimation based on a statistical filter. Dove (43) points out that the so-called Kalman filter, first used in navigation of space vehicles and then in aircraft systems is now available as part of a maritime integrated navigational system.

Grimble (44) explains the discrete-time Kalman filter is a predictor-corrector mechanism. If the estimate of the states at time kT is known, and the system mathematical model is available, the predicted states at time $(k+1)T$ can be computed. When the difference between the measurements and the predicted states are weighted by the Kalman gain matrix, a corrected best estimate is arrived at by summing the predicted states with the weighted errors. The basic Kalman filter is designed for linear systems, but more recently it has been extended to cope with systems that have non-linear dynamics (45).

Hashiguchi (46) describes an integrated automatic navigational system manufactured by Hitachi Shipbuilding under the trade name "Transoline" that links together an autopilot with an integrated navigational system. Transoline is intended for open-sea operation and tests performed on the container ship S.S. Yashima-Maru indicate that the system works satisfactorily.

1.7 Present Study

The concept of automatic pilotage has been brought about by the increasing density of marine traffic in confined waters, particularly port approaches where the risk of collision is high. The practical realisation of such a system has been made possible by recent advances in navigational aids, particularly the Navstar Global Positioning System (GPS) which employs eighteen satellites, and is due to become operational around 1990. GPS has a three-dimensional positional accuracy of a few metres. When integrated with other navigational instruments and a suitable autopilot, it has the potential to bring a ship safely into port anywhere in the world.

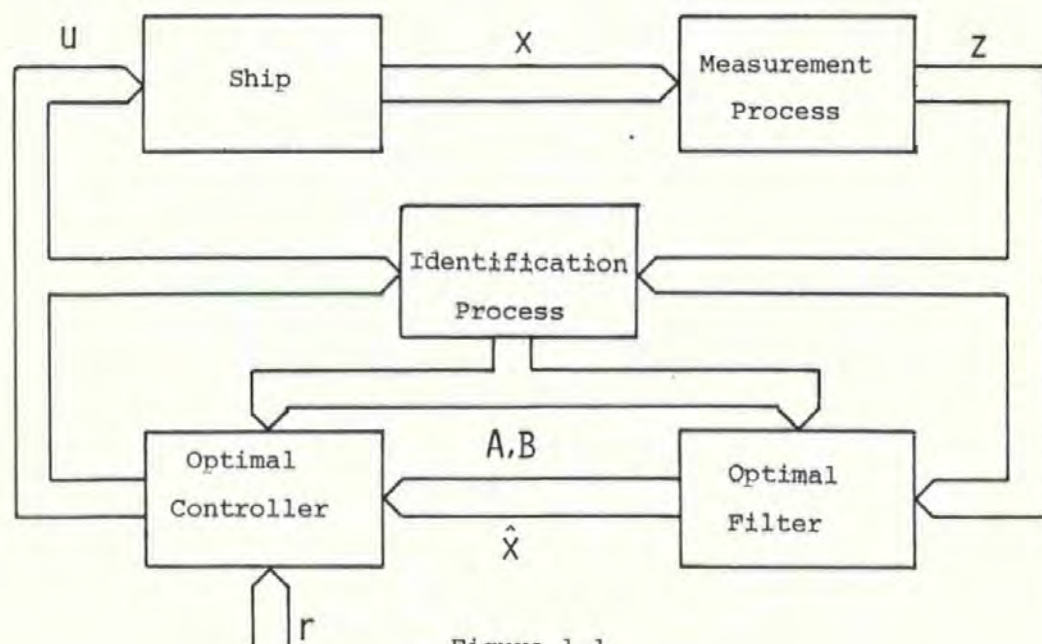


Figure 1.1

Proposed Guidance System

This present investigation concerns a feasibility study of a guidance system for automatically controlling a large vessel in the pilotage phase of its voyage. The proposed system is shown in Figure 1.1.

The project is part of an integrated scheme where members of a research team have concentrated separately on the following areas:

1. State Estimation and Digital Filtering.
2. Optimal and Sub-Optimal Controller Design.
3. Ship Modelling and Identification.

The aim of the investigation described in this thesis is the design of an optimal or sub-optimal controller for the automatic pilotage of large ships in confined waters. In the case of the optimal controller the problem is treated in a multivariable manner so that several parameters such as position, heading and forward speed can be controlled simultaneously. In simulation studies Burns, Bouncer and Dove have demonstrated such a technique to be very effective (47).

This is a new approach since the recent emphasis by other researchers (37) (38) involved in the study of control systems for manoeuvring in confined waters has been focused on the minimisation of scalar error quantities, for example heading or track error.

The programme of work has three distinct phases:

1. Ship Mathematical Models

Chapter 2 describes the choice of state variables and the development of linear time-invariant, quasi-linear time-variant and non-linear time-variant ship mathematical models.

Chapter 3 deals with disturbance modelling, derivation of aerodynamic derivatives and Gauss-Markov relationships for wind and tidal streams.

Chapter 4 is concerned with computer model verification employing (a) data for the Mariner hull obtained from the literature and (b) linear and non-linear hydrodynamic coefficients evaluated for a model car-ferry hull from towing-tank tests at N.M.I., and free-sailing tests on the river Plym.

2. Controller Design and Guidance System Simulation

Chapter 5 explains the criteria and strategies employed in the design of sub-optimal and optimal controllers, disturbance counteraction and adaption to cater for time-varying and non-linear ship dynamics.

Chapter 6 explores the effectiveness of different control policies in terms of (a) stability, (b) accuracy, (c) integrity when simulating the automatic guidance of a full-size vessel into Plymouth Sound.

3. Free-Sailing Model Performance

Chapter 7 describes the measurement system and on-board computing facility employed to implement the guidance system on the physical model. The results of the commissioning tests are given.

Chapter 8 looks at the modifications to the mathematical model and the software required to enable an optimal control policy to work in real-time, interfaced with the measurement system on-board the model car-ferry hull. A performance analysis is conducted on the results of the free-sailing tests.

Chapter 9 reviews the principal conclusions and observations based on the work and considers the possibility of future developments.

CHAPTER 2

SHIP MATHEMATICAL MODEL

2.1 Introduction

Mathematical models of ship dynamics are required for many different purposes, amongst which the most important include: prediction of ship manoeuvres, autopilot analysis, navigational filters and design for optimum ship performance. There are two different approaches to the problem, theoretical modelling, based upon physical laws and experimental modelling, derived from measured input-output relationships.

2.2. Co-ordinate Systems and Sign Conventions

A ship may be considered to be a rigid body with six degrees of freedom. It is convenient to describe its motion in terms of translation and rotation about a moving system of three mutually perpendicular axes x, y, z , referred to as the ship longitudinal axis, lateral axis and vertical axis respectively. These axes, shown in Figure 2.1, form a consistent right-hand co-ordinate system.

A second right-handed system of orthogonal axes x_o, y_o, z_o , referred to as the earth co-ordinate system, is fixed so that the x_o axis, to conform with standard navigational practice, is aligned with the direction of True North.

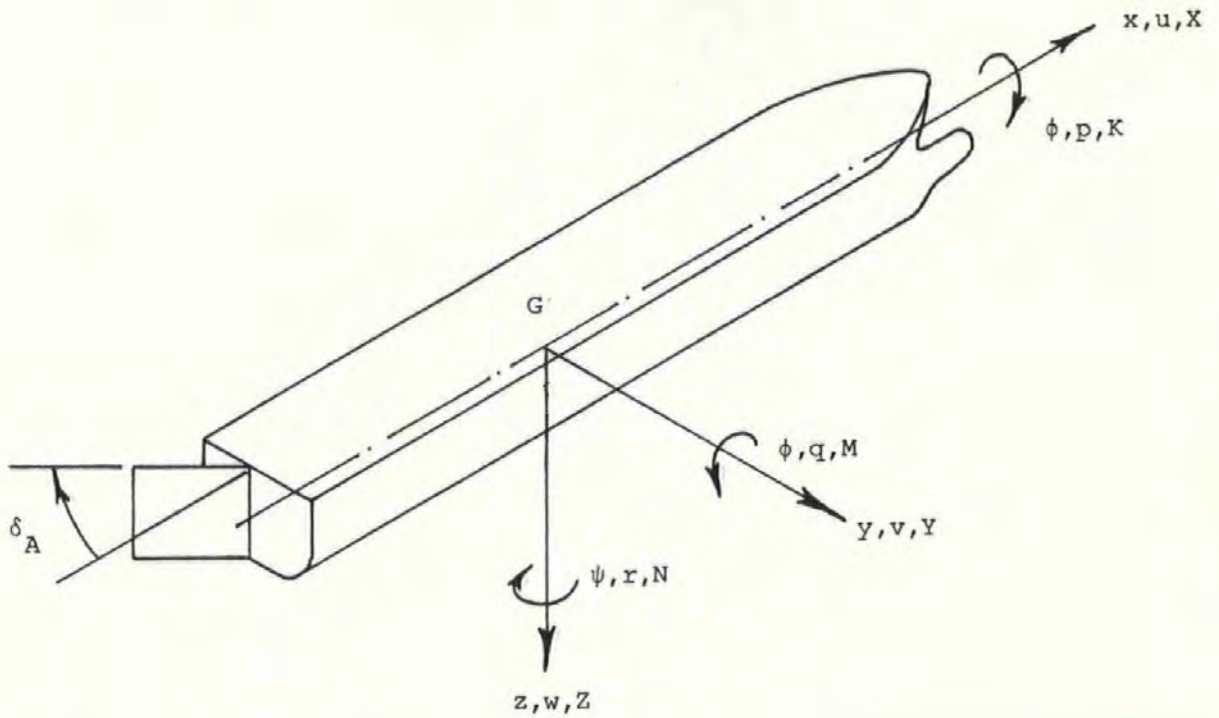


Figure 2.1

Ship Co-ordinate System

2.3 Euler's Equations of Motion for a Rigid Body

Employing equations for linear and angular momentum Abkowitz (48) demonstrated that the three force equations (surge, sway and heave) and the three moment equations (roll, pitch and yaw) may be written as a Eulerian set:

$$m\{\dot{u} + qw - rv - X_G(q^2 + r^2) + Y_G(pq - \dot{r}) + Z_G(pr + \dot{q})\} = X$$

$$m\{\dot{v} + ru - pw - Y_G(r^2 + p^2) + Z_G(qr - \dot{p}) + X_G(qp + \dot{r})\} = Y$$

$$m\{\dot{w} + pv - qu - Z_G(p^2 + q^2) + X_G(rp - \dot{q}) + Y_G(rq + \dot{p})\} = Z$$

$$I_x \dot{p} + (I_z - I_y)qr + m\{Y_G(\dot{w} + pv - qu) - Z_G(\dot{v} + ru - pw)\} = K$$

$$I_y \dot{q} + (I_x - I_z)rp + m\{Z_G(\dot{u} + qw - rv) - X_G(\dot{w} + pv - qu)\} = M$$

$$I_z \dot{r} + (I_y - I_x)pq + m\{X_G(\dot{v} + ru - pw) - Y_G(\dot{u} + qw - rv)\} = N$$

(2.1)

When manoeuvring in the approaches to a port, it will be assumed that ship motions in roll, pitch and heave are small enough to be neglected. Under these conditions equations (2.1) reduce to:

$$m(\dot{u} - rv - X_G r^2) = X$$

$$m(\dot{v} + ru + X_G \dot{r}) = Y$$

$$I_z \dot{r} + mX_G(\dot{v} + ru) = N$$

(2.2)

If the origin of the ship co-ordinate system is selected to coincide with the mass centre of the vessel, then equations (2.2) become:

$$m(\dot{u} - rv) = X$$

$$m(\dot{v} + ru) = Y$$

$$I_z \dot{r} = N$$

(2.3)

2.4 Selection of System Variables

In the formulation of the multivariable control problem it is necessary to view the ship as a dynamic system with multiple inputs and outputs as shown in Figure 2.2.

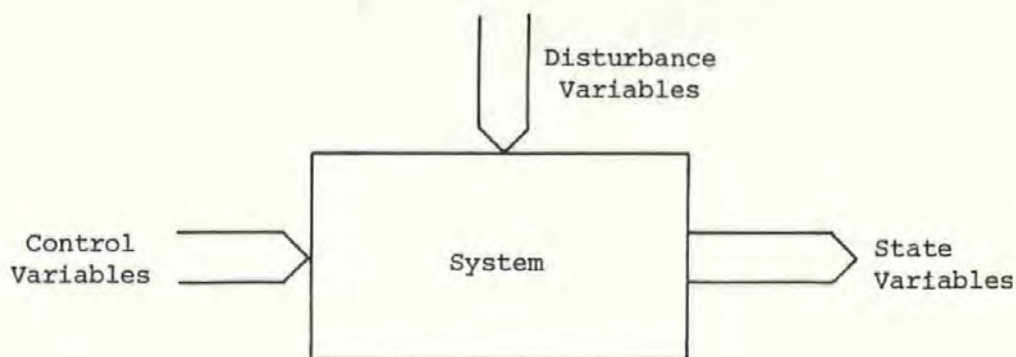


Figure 2.2
Multivariable System

If a true representation of the system behaviour is to be achieved, care must be taken over the selection of the system variables.

(a) State Variables

The choice of variables that make up the state vector has been made from consideration of those parameters which are felt important when defining the "state" of a vessel in a manoeuvring situation. The state vector which most fully describes this condition is :

$$X^T = (\delta_A \ n_A \ x \ u \ y \ v \ \psi_A \ r) \quad (2.4)$$

All of these state variables relate to the ship co-ordinate system. The first two states δ_A and n_A become necessary if the dynamics of rudder and main engines are to be taken into account. The remaining six states constitute position and its derivative in the surge, sway and yaw directions.

A further set of earth-related states may be defined:

$$y^T = (x_o \ u_o \ y_o \ v_o) \quad (2.5)$$

The transformation from ship to earth co-ordinate system, which takes place after the state computations, is given by:

$$y = T(t)x \quad (2.6)$$

where $T(t)$ is a time-varying transformation matrix.

(b) Control and Disturbance Variables

When choosing the control vector it is assumed that the ship has a single screw and rudder but no bow thruster, so that:

$$U_c^T = (\delta_D \ n_D) \quad (2.7)$$

Equation (2.7) will equally apply to vessels with twin screws and rudders, provided the latter are linked and both engines maintain the same revolutions.

When considering the two categories of disturbances mentioned in Chapter 1, wind and tidal stream have been selected as being the most important parameters that will deflect the ship from some desired track. With regard to the ship handling class of disturbance, the most important variable in a manoeuvring condition is forward velocity. Other effects such as shallow water and loading are not included at this stage.

The vector of disturbances, expressed with respect to the ship co-ordinate system, is:

$$W^T = (u_c \ v_c \ u_a \ v_a) \quad (2.8)$$

It is sometimes convenient to combine the control and disturbance vectors into an augmented forcing vector of the form:

$$U^T = (\delta_D \ n_D \ u_c \ v_c \ u_a \ v_a) \quad (2.9)$$

2.5. Linear Time-Invariant Model

The forces and moments acting on a ship's hull are as a result of hydrodynamic, aerodynamic and control surface effects. In general, they are highly non-linear, but if the vessel is travelling at constant forward velocity with only small variations in heading, the expressions may be linearised using a first order Taylor expansion about the given equilibrium condition of motion (49). Hence, the sway and yaw components of equations (2.3) may be written in dimensionalised form as:

$$\begin{aligned} m\dot{v} + mru &= Y_{\dot{v}}\dot{v} + Y_v(v + v_c) + Y_{\dot{r}}\dot{r} + Y_r r + Y_{\delta} \delta_A + Y_n n_A + Y_a v_a \\ I_z \dot{r} &= N_{\dot{v}}\dot{v} + N_v(v + v_c) + N_{\dot{r}}\dot{r} + N_r r + N_{\delta} \delta_A + N_n n_A + N_a v_a \end{aligned} \quad (2.10)$$

Rearranging equation (2.10) gives,

$$\begin{aligned} \dot{v} &= \left(\frac{Y_{\delta}}{m - Y_{\dot{v}}} \right) \delta_A + \left(\frac{Y_n}{m - Y_{\dot{v}}} \right) n_A + \left(\frac{Y_v}{m - Y_{\dot{v}}} \right) v + \left(\frac{Y_r - mu}{m - Y_{\dot{v}}} \right) r \\ &+ \left(\frac{Y_{\dot{r}}}{m - Y_{\dot{v}}} \right) \dot{r} + \left(\frac{Y_v}{m - Y_{\dot{v}}} \right) v_c + \left(\frac{Y_a}{m - Y_{\dot{v}}} \right) v_a \end{aligned}$$

and,

$$\begin{aligned} \dot{r} &= \left(\frac{N_{\delta}}{I_z - N_{\dot{r}}} \right) \delta_A + \left(\frac{N_n}{I_z - N_{\dot{r}}} \right) n_A + \left(\frac{N_v}{I_z - N_{\dot{r}}} \right) v + \left(\frac{N_{\dot{v}}}{I_z - N_{\dot{r}}} \right) \dot{v} \\ &+ \left(\frac{N_r}{I_z - N_{\dot{r}}} \right) r + \left(\frac{N_v}{I_z - N_{\dot{r}}} \right) v_c + \left(\frac{N_a}{I_z - N_{\dot{r}}} \right) v_a \end{aligned} \quad (2.11)$$

2.5.1. Steering Gear and Main Engines

The steering gear and main engines are both modelled by first

order linear differential equations:-

$$\begin{aligned}\delta_A + T_R \dot{\delta}_A &= \delta_D \\ n_A + T_N \dot{n}_A &= n_D\end{aligned}\quad (2.12)$$

2.5.2. State-Space Formulation

After suitable re-arrangement and combination of equations (2.11) and (2.12), the system equation set may be written,

$$\begin{aligned}\dot{\delta}_A &= f_{11} \delta_A + g_{11} \delta_D \\ \dot{n}_A &= f_{22} n_A + g_{22} n_D \\ \dot{x} &= u \\ \dot{u} &= 0 \\ \dot{y} &= v \\ \dot{v} &= f_{61} \delta_A + f_{62} n_A + f_{66} v + f_{68} r + g_{64} v_c + g_{66} v_a \\ \dot{\psi} &= r \\ \dot{r} &= f_{81} \delta_A + f_{82} n_A + f_{86} v + f_{88} r + g_{84} v_c + g_{86} v_a\end{aligned}\quad (2.13)$$

Equation set (2.13) can be expressed as a vector matrix differential equation as shown in (2.14), which is the general form of the state variable equation for a linear time-invariant system.

$$\begin{bmatrix} \dot{\delta}_A \\ \dot{n}_A \\ \dot{x} \\ \dot{u} \\ \dot{y} \\ \dot{v} \\ \dot{\psi} \\ \dot{r} \end{bmatrix} = \begin{bmatrix} f_{11} & 0 & 0 & 0 & 0 & 0 & 0 & 0 \\ 0 & f_{22} & 0 & 0 & 0 & 0 & 0 & 0 \\ 0 & 0 & 0 & 1 & 0 & 0 & 0 & 0 \\ 0 & 0 & 0 & 0 & 0 & 0 & 0 & 0 \\ 0 & 0 & 0 & 0 & 0 & 1 & 0 & 0 \\ f_{61} & f_{62} & 0 & 0 & 0 & f_{66} & 0 & f_{68} \\ 0 & 0 & 0 & 0 & 0 & 0 & 0 & 1 \\ f_{81} & f_{82} & 0 & 0 & 0 & f_{86} & 0 & f_{88} \end{bmatrix} \begin{bmatrix} \delta_A \\ n_A \\ x \\ u \\ y \\ v \\ \psi \\ r \end{bmatrix} + \begin{bmatrix} g_{11} & 0 & 0 & 0 & 0 & 0 & 0 & 0 \\ 0 & g_{22} & 0 & 0 & 0 & 0 & 0 & 0 \\ 0 & 0 & 0 & 0 & 0 & 0 & 0 & 0 \\ 0 & 0 & 0 & 0 & 0 & 0 & 0 & 0 \\ 0 & 0 & 0 & 0 & 0 & 0 & 0 & 0 \\ 0 & 0 & 0 & g_{64} & 0 & g_{66} & 0 & 0 \\ 0 & 0 & 0 & 0 & 0 & 0 & 0 & 0 \\ 0 & 0 & 0 & g_{84} & 0 & g_{86} & 0 & 0 \end{bmatrix} \begin{bmatrix} \delta_D \\ n_D \\ u_c \\ v_c \\ u_a \\ v_a \\ \psi \\ r \end{bmatrix} \quad (2.14)$$

or,

$$\dot{X}(t) = F X(t) + G U(t) \quad (2.15)$$

The elements of the F and G matrices are constant and a complete list is given in Appendix A1.1.

2.5.3. Discrete Solution of the State Equation

Equation (2.15) may be solved in discrete-time and proof of the reverse exponential matrix method for computation of state, control and disturbance transition matrices as employed by Cadzow (50) and Bouncer (51) is given in Appendix A1.5.

The discrete solution of the state equation is:

$$X((k+1)T) = A(T) X(kT) + B(T) U(kT) \quad (2.16)$$

When the control and disturbance variables are separated, equation (2.16) takes the form:

$$X((k+1)T) = A(T) X(kT) + B(T) U_c(kT) + C(T) W(kT) \quad (2.17)$$

2.5.4. Transfer Function Approach

Eliminating v and \dot{v} from equations (2.11) gives the classical

linear differential equation governing yaw response to rudder motion, first used by Nomoto (52) in 1966:

$$T_1 T_2 \ddot{\psi}_A + (T_1 + T_2) \dot{\psi}_A + \psi_A = K_n (\delta_A + T_3 \ddot{\delta}_A) \quad (2.18)$$

Appendix A1.4 lists the relationships between T_1, T_2, T_3 and K_n with the ship's mass, moment of inertia and dimensionalised hydrodynamic coefficients.

From equation (2.18) the transfer function becomes:

$$\frac{\psi_A}{\delta_A}(s) = \frac{K_n (1+T_3 s)}{s(1+T_1 s)(1+T_2 s)} \quad (2.19)$$

2.5.5. Co-ordinate System Transformation

To convert from ship to earth co-ordinates we may use:

$$\begin{aligned} u_o &= u \cos \psi_A - v \sin \psi_A \\ v_o &= u \sin \psi_A + v \cos \psi_A \\ x_o &= \int u_o dt \\ y_o &= \int v_o dt \end{aligned} \quad (2.20)$$

or, in terms of transformation matrix $T(t)$,

$$\begin{pmatrix} u_o \\ v_o \end{pmatrix} = \begin{pmatrix} 0 & 0 & 0 & \cos \psi_A & 0 & -\sin \psi_A & 0 & 0 \\ 0 & 0 & 0 & \sin \psi_A & 0 & \cos \psi_A & 0 & 0 \end{pmatrix} \begin{pmatrix} X \end{pmatrix} \quad (2.21)$$

The discrete transformation takes place by assuming that during the k th sampling period the ship's co-ordinate system has a fixed angle $\psi_A(kT)$ with respect to earth axes, so that:

$$\begin{aligned} x_o((k+1)T) &= x_o(kT) + (x((k+1)T) - x(kT)) \cos(\psi_A(kT)) \\ &\quad - (y((k+1)T) - y(kT)) \sin(\psi_A(kT)) \end{aligned}$$

$$\begin{aligned}
y_o((k+1)T) &= y_o(kT) + (y((k+1)T) - y(kT))\cos(\psi_A(kT)) \\
&\quad + (x((k+1)T) - x(kT))\sin(\psi_A(kT)) \\
u_o((k+1)T) &= u((k+1)T)\cos(\psi_A(kT)) - v((k+1)T)\sin(\psi_A(kT)) \\
v_o((k+1)T) &= v((k+1)T)\cos(\psi_A(kT)) + u((k+1)T)\sin(\psi_A(kT))
\end{aligned} \tag{2.22}$$

2.6. Quasi-Linear Time-Variant Model

If, whilst in the approach to the final berthing position say, a ship undergoes large changes in forward velocity then equations (2.16) and (2.17) are not valid since matrices $A(T)$, $B(T)$ and $C(T)$ are now time-varying. The problem can be overcome with a discrete model by assuming that the values remain constant during the sample period and then re-computed at each sample instant.

Together with the sway and yaw equations (2.10) it now becomes necessary to include the surge expression from equation (2.3):

$$m\dot{u} - mrv = X_u \dot{u} + X_u(u + u_c) + X_n n_A + X_a u_a \tag{2.23}$$

which may be written:

$$\begin{aligned}
\dot{u} &= \left(\frac{X_n}{m - X_u} \right) n_A + \left(\frac{X_u}{m - X_u} \right) u + \left(\frac{mr}{m - X_u} \right) v \\
&+ \left(\frac{X_u}{m - X_u} \right) u_c + \left(\frac{X_a}{m - X_u} \right) u_a
\end{aligned} \tag{2.24}$$

Combining equation (2.24) with (2.11) yields the equation set (2.13) with the modification:

$$\dot{u} = f_{42} n_A + f_{44} u + f_{46} v + g_{43} u_c + g_{45} u_a \tag{2.25}$$

The matrix equation for the quasi-linear model is similar to (2.14) except there will be entries f_{42} , f_{44} and f_{46} in the F matrix

plus g_{43} and g_{45} in the G matrix. The values of the additional parameters are given in Appendix A1.2.

To use the quasi-linear state equations the hydrodynamic coefficients have to be re-dimensionalised at each sampling instant according to the new total velocity:

$$U((k+1)T) = \{u((k+1)T)^2 + v((k+1)T)^2\}^{1/2} \quad (2.26)$$

As a result, every element in both the F and G matrices will change so that the state, control and disturbance transition matrices also need to be calculated.

The state equation for the quasi-linear time-variant system is:

$$\dot{X}(t) = F(t) X(t) + G(t) U(t) \quad (2.27)$$

and the corresponding discrete solution,

$$X((k+1)T) = A(T, kT) X(kT) + B(T, kT) U_c(kT) + C(T, kT) W(kT) \quad (2.28)$$

2.6.1 Non-Dimensional Model

A method employed by some researchers (53) to avoid re-calculation of the system matrices is to use a non-dimensional mathematical model that does not require scaling as a function of forward velocity. The system that finds most common usage is the prime system, based on the ship length L and total velocity U . The fundamental non-dimensional quantities are:

<u>length</u>	$x' = \frac{x}{L}$	
<u>time</u>	$t' = \left(\frac{U}{L}\right) t$	
<u>mass</u>	$m' = \frac{m}{\rho / 2 L^3}$	(2.29)

Formulation of the state equations is a similar process to that described in 2.6 except that the F and G matrices are calculated once only, using non-dimensional hydrodynamic coefficients. The non-dimensional state variables become:

$$X'(t') = \left(1 \frac{L}{U} \frac{1}{L} \frac{1}{U} \frac{1}{L} \frac{1}{U} 1 \frac{L}{U} \right) X(t) \quad (2.30)$$

This technique was tested, computing a set of non-dimensional state variables during a turning manoeuvre. Their values, upon re-dimensionalising, were the same as those obtained using the standard quasi-linear model.

2.7. Non-Linear Time-Variant Model

It is well known that in a manoeuvring situation where a vessel is executing tight turns, the linear equations of motion become inaccurate when attempting to predict the ship's movements. In 1969 Bech (54) observed that the Nomoto equation (2.18) was only valid for a small range of $\dot{\psi}_A$ and δ_A and suggested the equation be re-written:

$$\ddot{\psi}_A + \left(\frac{1}{T_1} + \frac{1}{T_2} \right) \dot{\psi}_A + \frac{K}{T_1 T_2} H(\dot{\psi}_A) = \frac{K_n}{T_1 T_2} (\delta_A + T_3 \dot{\delta}_A) \quad (2.31)$$

Here the main non-linearities have been lumped in the steering characteristics $H(\dot{\psi}_A)$ which describes $\dot{\psi}_A$ as a function of δ_A in the steady-state and is written as a polynomial expression:

$$H(\dot{\psi}_A) = c_0 + c_1 \dot{\psi}_A + c_2 \dot{\psi}_A^2 + c_3 \dot{\psi}_A^3 \quad (2.32)$$

$H(\dot{\psi}_A)$ can be determined, in general, by the reversed spiral test, or in the case of dynamic stability by the Dieudonne spiral test.

2.7.1 Non-Linear Equations of Motion

The surge equation (2.23) when expressed in terms of a Taylor

expansion up to third order becomes:

$$\begin{aligned}
 \dot{m}\dot{u} - mrv = & \{X_{\dot{u}}\dot{u} + X_u(u+u_c) + X_{\delta}\delta_A + X_n n_A + X_a u_a\} \\
 & + \frac{1}{2}! \{X_{\dot{u}\dot{u}}\dot{u}^2 + X_{uu}(u+u_c)^2 + X_{\delta\delta}\delta_A^2 + X_{nn}n_A^2 \\
 & + X_{aa}u_a^2 + 2X_{u\dot{u}}\dot{u}(u+u_c) \\
 & + 2X_{u\delta}\dot{u}\delta_A + \dots + 2X_{na}n_A u_a\} \\
 & + \frac{1}{3!} \{X_{\dot{u}\dot{u}\dot{u}}\dot{u}^3 + X_{uuu}(u+u_c)^3 + \dots + X_{aaa}u_a^3 \\
 & + 3X_{\dot{u}\dot{u}\dot{u}}\dot{u}^2(u+u_c) + 3X_{\dot{u}\dot{u}\delta}\dot{u}^2\delta_A + \dots + 3X_{nna}n_A^2 u_a\}
 \end{aligned} \tag{2.33}$$

where,

$$X_{\dot{u}} = \frac{\partial X}{\partial \dot{u}} ; \quad X_{\dot{u}\dot{u}} = \frac{\partial^2 X}{\partial \dot{u}^2}$$

$$X_{\dot{u}\delta} = \frac{\partial^2 X}{\partial \dot{u} \partial \delta} ; \quad X_{\dot{u}\dot{u}\dot{u}} = \frac{\partial^3 X}{\partial \dot{u}^3 \partial u} \quad \text{etc.}$$

Similar expressions exist for the sway and yaw equations.

Abkowitz (48) shows that terms above third order are unimportant. He also demonstrates that as a consequence of symmetry in the X-direction, functions with even powers (e.g. δ_A^2) will be predominant. In contrast, expressions for Y and N will contain mainly terms with odd powers (e.g. δ_A , δ_A^3).

The selection of important non-linear coefficients has been made by reviewing the work of Strom-Tejsen (55), Lewison (56), Gill (57) and Eda and Crane (58).

These are:

Surge Equation, terms in: u^2 , u^3 , v^2 , r^2 , δ_A^2 , $u n_A$ and n_A^2 .

Sway Equation, terms in: n_A^2 , v^3 , rv^2 , δ_A^3 and $\delta_A v^2$.

Yaw Equation, terms in: n_A^2 , v^3 , rv^2 , δ_A^3 , $\delta_A v^2$ and $u_a v_a$.

2.7.2. Non-Linear Control Parameters

In addition to hull coefficients, the control parameters themselves (rudder and propeller) are non-linear functions.

Propeller Characteristics

O'Brien (59) shows that the thrust exerted by a propeller is:

$$T_p = \rho n_A^2 d^4 K_t \quad (2.34)$$

Gill (57) assumes that $\frac{\partial K_t}{\partial J_a}$ can be approximated to the straight-line relationship:

$$K_t = p_1 J_a + p_2 \quad (2.35)$$

where J_a , the screw advance coefficient is expressed by:

$$J_a = \frac{(1-w_T)u}{n_A d} \quad (2.36)$$

From equations (2.34), (2.35) and (2.36):

$$T_p = \rho d^4 \left\{ p_1 \frac{(1-w_T)}{d} u n_A + p_2 n_A^2 \right\} \quad (2.37)$$

But the actual thrust is,

$$T_a = (1-t_d) T_p \quad (2.38)$$

so that:

$$T_a = \rho d^3 (1-t_d) \{ p_1 (1-w_T) u n_A + p_2 d n_A^2 \} \quad (2.39)$$

or:

$$T_a = X_{un} u n_A + \bar{X}_{nn} n_A^2 \quad (2.40)$$

Rudder Characteristics

Let the speed of advance of a propeller and rudder be u_{av} , and

assume the rudder sits in the propeller race which has velocity u_r . It may be shown that the rate of change of axial momentum across the propeller is:

$$\frac{dM}{dt} = \frac{\rho}{2} A_p (u_r^2 - u_{av}^2) \quad (2.41)$$

where:

$$u_{av} = u(1-w_T) \quad (2.42)$$

From Newton's second law, equating (2.37) and (2.41) gives:

$$u_r^2 = (1-w_T)u^2 + \frac{2d^3}{Ap} \left\{ p_1 \frac{(1-w_T)}{d} u n_A + p_2 n_A^2 \right\} \quad (2.43)$$

The lateral force on a ship's hull due to rudder action is therefore:

$$Y_r = \frac{1}{2} \rho L^2 u_r^2 (Y_{\delta \delta A}' + \bar{Y}_{\delta \delta \delta A} \delta_A^3) \quad (2.44)$$

When dimensionalising the rudder terms it is important to use u_r in equation (2.44) and not u , so that the effect of the propeller race on the rudder is taken into account when manoeuvring at low forward speeds.

The complete set of non-linear equations of motion now become:

$$\begin{aligned} m\dot{u} - mr\dot{v} &= X_u \dot{u} + X_u (u + u_c) + \bar{X}_{uu} (u^2 + u_c^2) + \bar{X}_{uuu} (u^3 + u_c^3) \\ &\quad + \bar{X}_{vv} v^2 + \bar{X}_{rr} r^2 + \bar{X}_{\delta \delta} \delta_A^2 + X_{un} u n_A + \bar{X}_{nn} n_A^2 + X_{a a} u_a \\ m\dot{v} + mru &= Y_v \dot{v} + Y_v (v + v_c) + Y_r r + Y_r \dot{r} + Y_{\delta \delta} \delta_A + \bar{Y}_{nn} n_A^2 \\ &\quad + \bar{Y}_{vvv} (v^3 + v_c^3) + \bar{Y}_{rvv} r (v^2 + v_c^2) + \bar{Y}_{\delta \delta \delta} \delta_A^3 + \bar{Y}_{\delta vv} \delta_A (v^2 + v_c^2) \\ &\quad + Y_{a a} v_a \\ I_z \dot{r} &= N_v \dot{v} + N_v (v + v_c) + N_r r + N_r \dot{r} + N_{\delta \delta} \delta_A + \bar{N}_{\delta vv} \delta_A (v^2 + v_c^2) \\ &\quad + N_{a a} v_a + N_{uva} u v_a + \bar{N}_{nn} n_A^2 + \bar{N}_{vvv} (v^3 + v_c^3) + \bar{N}_{rvv} r (v^2 + v_c^2) + \bar{N}_{\delta \delta \delta} \delta_A^3 \end{aligned} \quad (2.45)$$

In the above equations Clarke's bar notation (60) has been adopted, i.e.:

$$\bar{X}_{uu} = \frac{1}{2}X_{uu} ; \bar{X}_{uuu} = \frac{1}{6}X_{uuu} \quad \text{etc.}$$

Equations (2.45) may now be arranged in a set of the form (2.13) but with entries in the fourth equation that will correspond to those in (2.25).

Since there are many cross-coupled terms, some state variables appear in the F and G matrices themselves. For example, with the term mr_v , v is considered the state variable and the product mr inserted in the F matrix using the current value $r(kT)$.

A list of the non-linear state equation parameters is given in Appendix A1.3. As with the quasi-linear model, they are re-calculated at each sampling instant.

CHAPTER 3

DISTURBANCE MODELLING

3.1. Introduction

The principal factors causing disturbing forces and moments on a ship in the pilotage phase of its voyage are wind and current. When attempting to model their effect on a hull the computational algorithm requires the following information:

- (a) Components of wind and current velocities in x and y directions.
- (b) The hydrodynamic and aerodynamic coefficients of the vessel concerned.
- (c) The stochastic nature of the disturbances themselves.

3.2 Current

From equations (2.45) it is seen that the total velocity of the hull relative to the water is $(u + u_c)$ in the x-direction and $(v + v_c)$ in the y-direction. The positive sign in these terms requires that an anti-phase convention be adopted when describing values of current on the earth and ship co-ordinate systems.

The relative motion vector diagram is shown in Figure 3.1. The components of OU_c in the x and y directions are:

$$\begin{aligned}u_c &= U_c \cos(\alpha_c - \psi_A) \\v_c &= U_c \sin(\alpha_c - \psi_A)\end{aligned}\tag{3.1}$$

Velocity vectors OU and OU_c act through the centre of pressure P_c and vector $U_c U$ is the total velocity of the hull relative to the water.

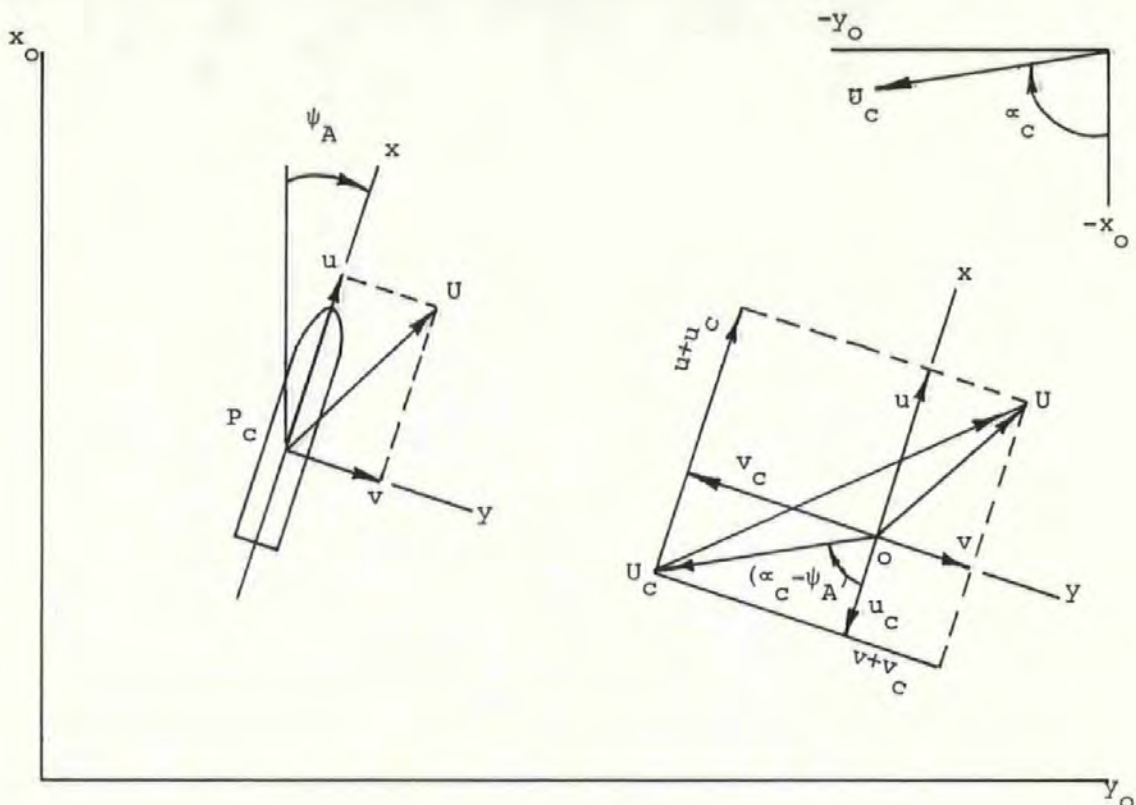


Figure 3.1

Relative Current

3.2.1. Hydrodynamic Coefficients

Initial experiments using a first-order Taylor expansion gave rise to larger than expected errors in force and moment calculations and, since the information was available, all non-linear terms were eventually employed.

The forces and moments exerted on the hull due to current are:

$$\begin{aligned}
 X_c &= X_{u_c} + \bar{X}_{uu_c} u_c^2 + \bar{X}_{uuu_c} u_c^3 \\
 Y_c &= Y_{v_c} + \bar{Y}_{vv_c} v_c^3 + \bar{Y}_{rvv_c} r v_c^2 + \bar{Y}_{\delta vv_c} \delta_A v_c^2 \\
 N_c &= N_{v_c} + \bar{N}_{vv_c} v_c^3 + \bar{N}_{rvv_c} r v_c^2 + \bar{N}_{\delta vv_c} \delta_A v_c^2
 \end{aligned} \tag{3.2}$$

These terms are included in the complete non-linear system equations (2.45).

3.2.2. The Dynamics of Tidal Streams

Bowden and Proudman (61) have examined the longitudinal component of turbulence in the Mersey Narrows using a Doodson current meter, both on the sea bed and near the surface. They found that turbulent energy input had a bandwidth of about 1 cycle per minute up to 1 Hertz as shown in Figure 3.2.

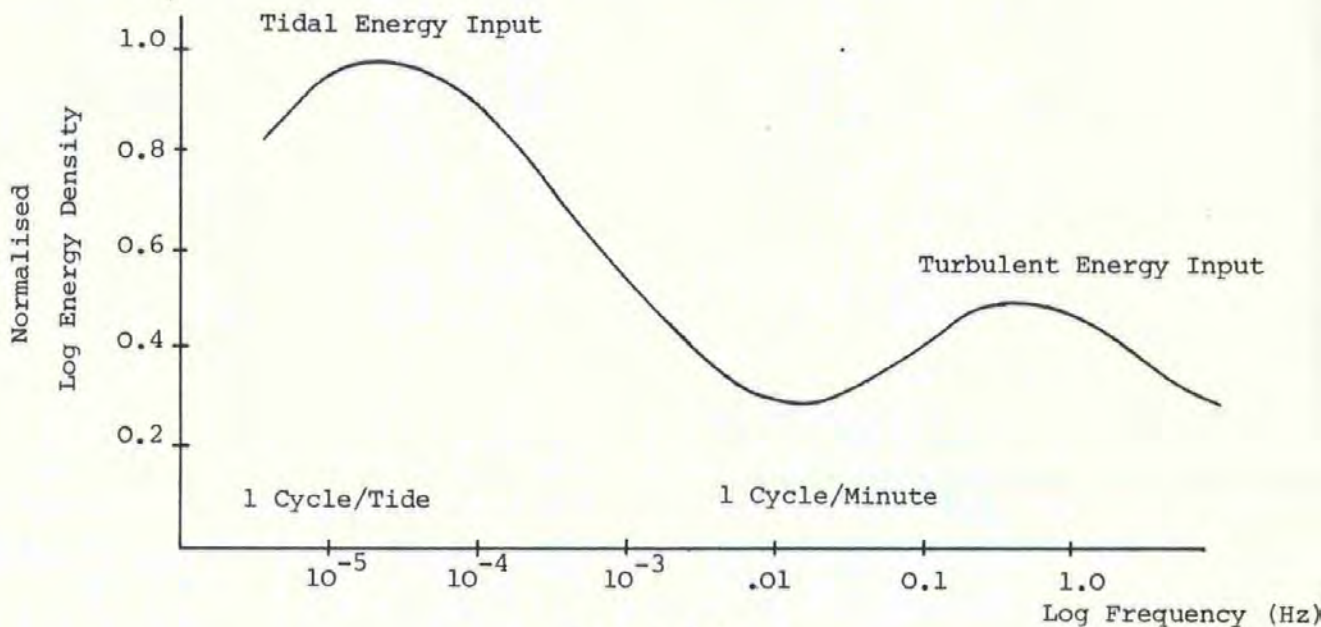


Figure 3.2

Turbulent Current Energy Spectrum

The amplitude of horizontal turbulent fluctuation of the current was observed to be a linear function of the mean value, in the order of 10%.

Discrete Stochastic Process

One method of describing the random nature of the turbulence is to assume a first order Gauss-Markov function:

$$U_c(k+1) = a_c U_c(k) + w_c(k) \quad (3.3)$$

where a_c is a non-negative constant smaller than unity and $w_c(k)$ is a gaussian random process for which:

$$E\{w_c(k)\} = (1-a_c)u_{cm}$$

$$\text{cov}\{w_c(k_1), w_c(k_2)\} = \begin{cases} q_c & \text{if } k_1 = k_2 \\ 0 & \text{if } k_1 \neq k_2 \end{cases} \quad (3.4)$$

From the characterisation of $U_c(k)$ it follows that:

$$E\{U_c(k)^2\} = \frac{q_c}{1-a_c^2} = \sigma_c^2 \quad (3.5)$$

Coefficient a_c may be obtained from the exponential term:

$$a_c = e^{-\frac{T}{T_c}} \quad (3.6)$$

If the current is assumed to have a constant mean value u_{cm} while the ship is entering port, the deterministic and stochastic components may be separated:

$$U_c(k+1) = C_{dl}\{u_{cm} + a_c U_c(k) + b_c w_c(k)\} \quad (3.7)$$

The coefficient b_c is given by

$$b_c = 1 - e^{-\frac{T}{T_c}} = 1 - a_c \quad (3.8)$$

and the overall scaling factor C_{dl} allows different conditions of current whilst maintaining a constant ratio between mean and stochastic elements.

In choosing the parameters for equations (3.7) and (3.8), T was selected to be the same as the sampling time for the main ship model, 5 seconds, and T_c was set at 10 seconds which corresponds to a turbulent energy break frequency of 0.0159 Hz.

Standard Weather Conditions

A set of standard weather conditions were employed in most simulation tests. These conditions existed in Plymouth Sound on 26th October 1982 between 10.30 and 11.00 a.m.

Values for the tidal stream mean and standard deviation during this period were:

$$\begin{aligned} u_{cm} &= 0.669 \text{ m/s} & \sigma_c &= 0.2 \text{ m/s} \\ \sigma \{w_c(k)\} &= 0.378 \text{ m/s} & E\{w_c(k)\} &= 0 \end{aligned} \quad (3.9)$$

The stochastic component of the current for this parameter set is shown in Figure 3.7(a).

3.2.3. Tidal Stream Direction

The direction of the current during the considered period is taken to comprise of a constant mean value together with a stochastic component. The process may be described by:

$$\begin{aligned} \alpha_c(k+1) &= \alpha_{cm} + C_{d2} \{a_{cd} \alpha_c(k) + b_{cd} w_{cd}(k)\} \\ E\{w_{cd}(k)\} &= 0 \\ \text{cov}\{w_{cd}(k_1), w_{cd}(k_2)\} &= \begin{cases} q_{cd} & \text{if } k_1 = k_2 \\ 0 & \text{if } k_1 \neq k_2 \end{cases} \end{aligned} \quad (3.10)$$

The scaling constant C_{d2} only affects the stochastic component and the gaussian random process $w_{cd}(k)$ must have high correlation with $w_c(k)$ as explained in 3.3.2. This is achieved by setting:

$$w_{cd}(k) = \frac{\sigma\{w_{cd}(k)\}}{\sigma\{w_c(k)\}} w_c(k) \quad (3.11)$$

Parameters a_{cd} and b_{cd} are computed according to equations (3.6) and (3.8) where T_c has a value of 5 seconds. The mean direction has been taken as a south-westerly incoming tide with a standard deviation

of 20 degrees, so that:

$$\alpha_{cm} = 3.665 \text{ rad.} \quad \sigma_{cd} = 0.35 \text{ rad.}$$

$$\sigma\{w_{cd}(k)\} = 0.492 \text{ rad.} \quad (3.12)$$

The stochastic component of tidal stream direction is shown in Figure 3.7(b) and the correlation with Figure 3.7(a) can be seen.

3.3 Wind

The aerodynamic forces and moments acting on a ship may be treated in a similar manner to the hydrodynamic effects of current. Again an anti-phase sign convention is used and the relative wind vector diagram is shown in Figure 3.3.

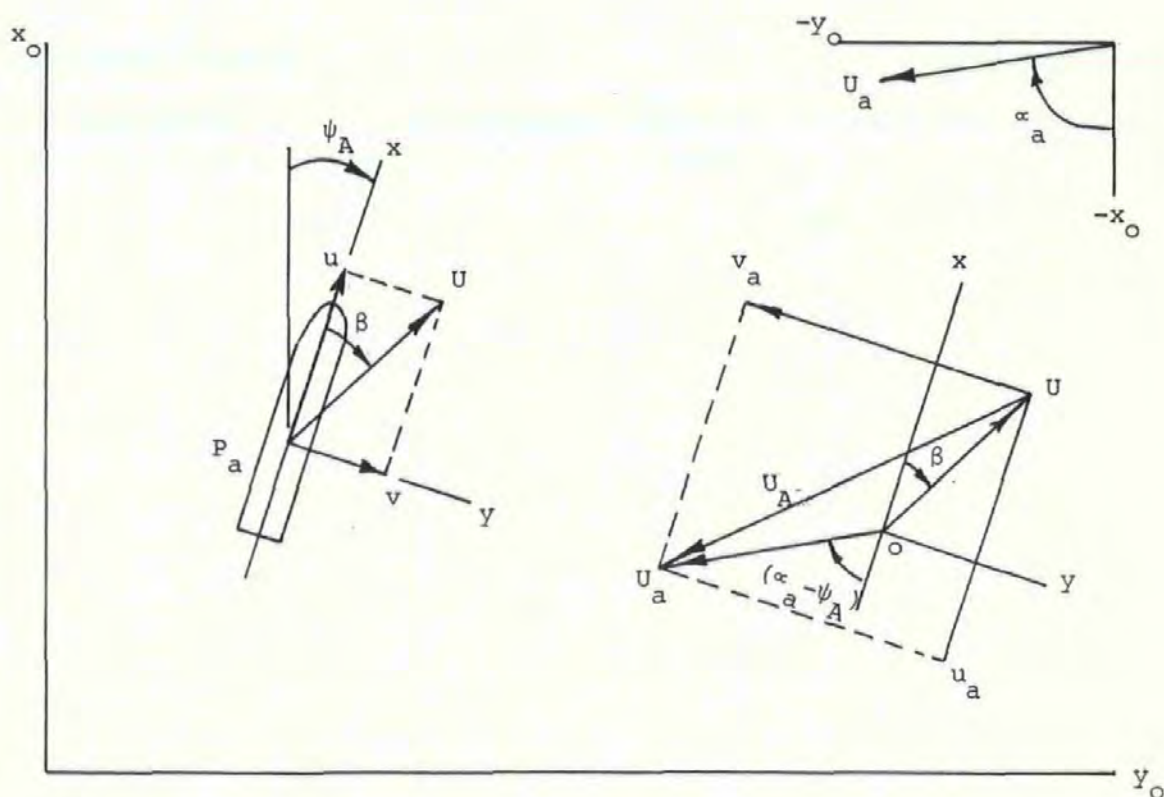


Figure 3.3

Relative Wind

Vectors OU and OU_a pass through the centre of pressure P_a ($P_a \neq P_c$) and vector UU_a , or U_A is the total wind velocity relative to the ship, its components in the x and y directions being:

$$u_a = U_a \cos(\alpha_a - \psi_A) + U \cos \beta$$

or,

$$u_a = U_a (\cos \alpha_a \cos \psi_A + \sin \alpha_a \sin \psi_A) + u \quad (3.13)$$

and,

$$v_a = U_a \sin(\alpha_a - \psi_A) + U \sin \beta$$

which may be rewritten:

$$v_a = U_a (\sin \alpha_a \cos \psi_A - \cos \alpha_a \sin \psi_A) + v \quad (3.14)$$

3.3.1 Aerodynamic Coefficients

A ship may be considered to be a lifting surface as shown in Figure 3.4.

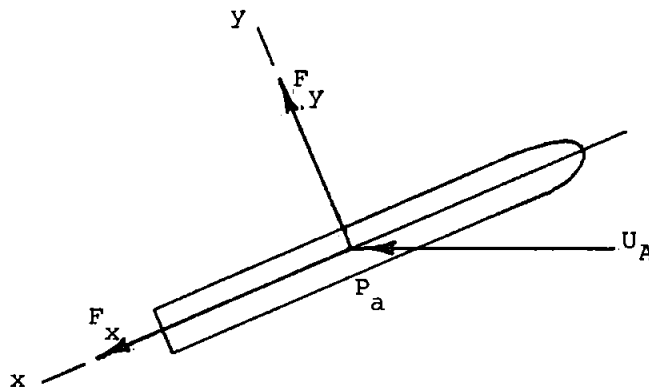


Figure 3.4

Ship as a Lifting Surface

The components of force in the x and y directions (drag and lift) may be written:

$$\begin{aligned} F_x &= \frac{1}{2} \rho C_{a x} \Lambda_A u_a^2 \\ F_y &= \frac{1}{2} \rho C_{a y} \Lambda_A v_a^2 \end{aligned} \quad (3.15)$$

The correction factor Λ depends upon the aspect ratio, which,

for a body sitting on a flat surface is:

$$\lambda_a = \frac{2L}{D} \quad (3.16)$$

In terms of non-dimensional aerodynamic coefficients X'_a and Y'_a equations (3.15) may be expressed:

$$\begin{aligned} F_x &= \{(\rho_a L_a^2 u_a) X'_a\} u_a \\ F_y &= \{(\rho_a L_a^2 v_a) Y'_a\} v_a \end{aligned} \quad (3.17)$$

Comparing equations (3.15) and (3.17) we get:

$$X'_a = \frac{C_x \Lambda L_b D}{L^2} \quad ; \quad Y'_a = \frac{C_y \Lambda D}{L} = \frac{2C_y \Lambda}{\lambda_{ay}} \quad (3.18)$$

Zuidweg (31) suggests that for a ship the product $C_y \Lambda$ is usually in the order of -0.9. For a y-direction aspect ratio λ_{ay} of 20, this gives:

$$Y'_a = -0.09 \quad (3.19)$$

A close approximation to $C_x \Lambda$ is also about -0.9, and, if it is assumed for a typical ship that,

$$\frac{L_b}{L} = 0.16$$

$$\frac{D}{L} = 0.1$$

then,

$$X'_a = -0.0144 \quad (3.20)$$

Eda (62) shows that wind-tunnel tests on a model of a Mariner-class vessel mounted on a ground board produced the following non-dimensional aerodynamic coefficients:

$$Y'_a = -0.056$$

$$X'_a = -0.015 \quad (3.21)$$

He also demonstrates that the total non-dimensional moment acting on the vessel is given by the relationship:

$$N'_w = N'_a v'_a + N'_{uva} u'_a v'_a$$

where,

$$N'_a = -0.0017$$

$$N'_{uva} = -0.0046 \quad (3.22)$$

3.3.2 Wind Dynamics

Measurements made by Van Der Hoven (63) at Brookhaven, New York, of the horizontal wind energy spectrum at a height of 10 metres is shown in Figure 3.5.

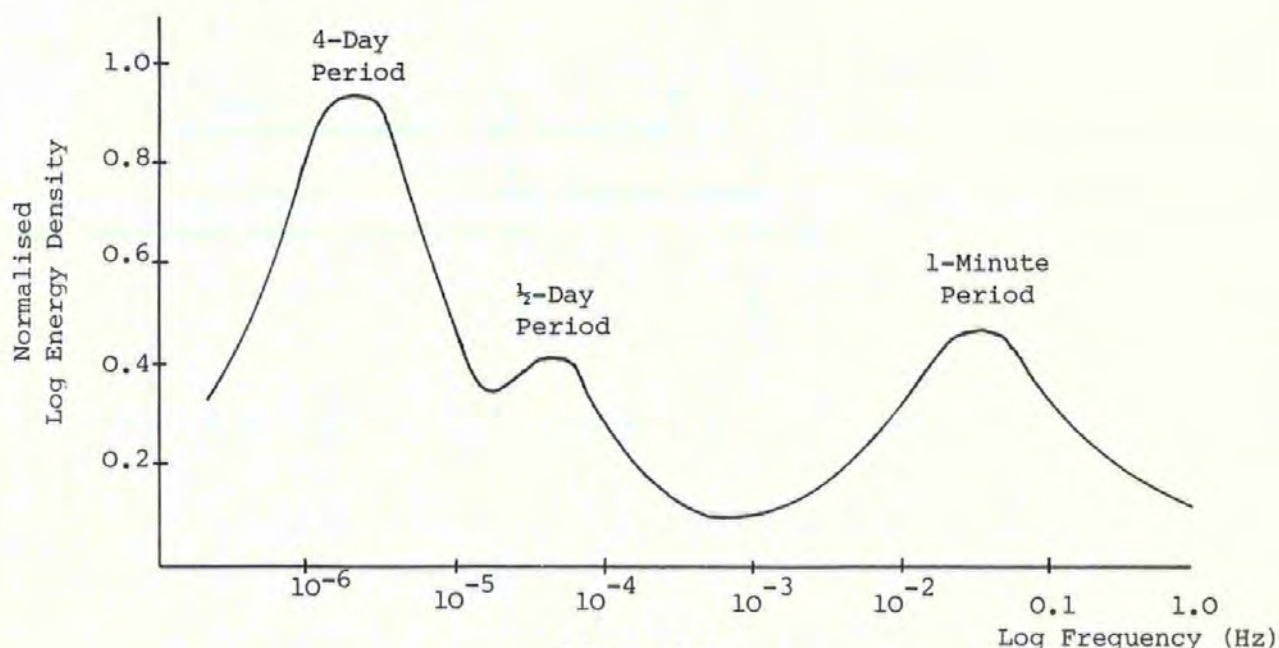


Figure 3.5

Horizontal Wind Energy Spectrum

The curve has several points of interest. First, the four-day cycle represents the frequency of anti-cyclones in the Westerly zones. Second, the half-day period indicates the effect of daily temperature variation and third, the one minute period which is the cyclic repetition of gusts.

Correlation between Gust Magnitude and Direction

Consider a 3-dimensional gust to have rectangular co-ordinates x_w, y_w, z_w that are aligned with the mean speed direction as shown in Figure 3.6.

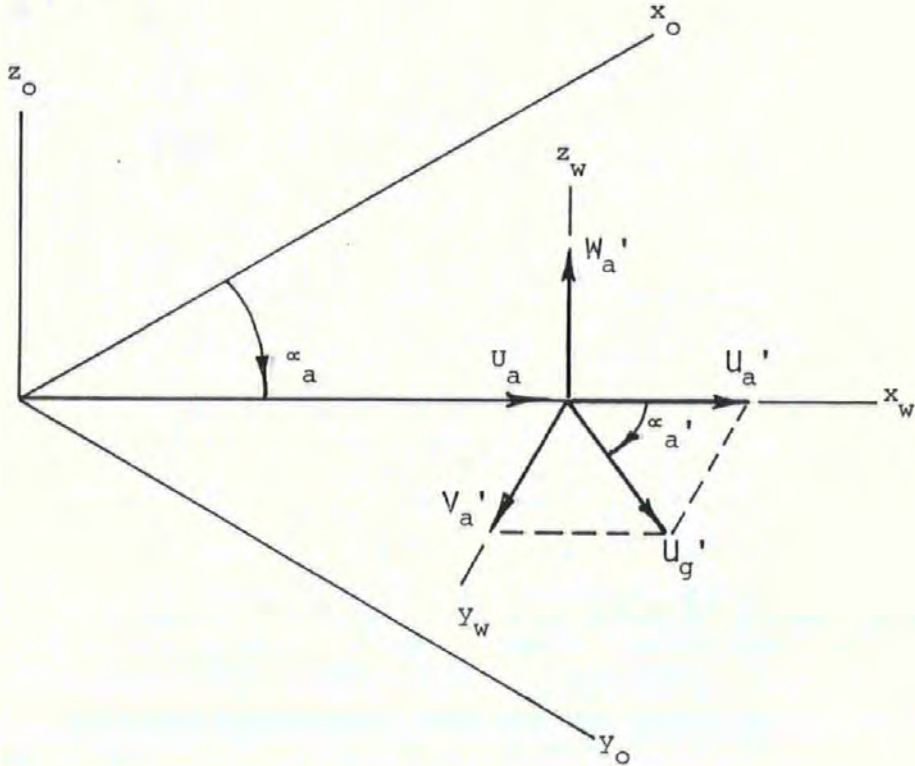


Figure 3.6

Gust Co-ordinate System

The gust magnitude and direction is given by:

$$U_g' = U_a' + V_a' + W_a'$$

If the W_a' component is ignored,

$$U_g' = U_a' + V_a' \quad (3.23)$$

From equation (3.23) it is seen that a gust increase $\Delta U_g'$ will affect its components $\Delta U_a'$ and $\Delta V_a'$, causing the gust direction to veer. For this to occur, there must be correlation between the statistical properties of U_a' and V_a' .

Correlated Discrete Stochastic Processes

The wind magnitude and direction may be described by correlated Gauss-Markov functions with separate deterministic and stochastic components:

$$U_a(k+1) = C_{d3} \{ u_{am} + a_a U_a(k) + b_a w_a(k) \}$$

$$E\{w_a(k)\} = 0$$

$$\text{cov}\{w_a(k_1), w_a(k_2)\} = \begin{cases} q_a & \text{if } k_1 = k_2 \\ 0 & \text{if } k_1 \neq k_2 \end{cases} \quad (3.24)$$

$$\alpha_a(k+1) = \alpha_{am} + C_{d4} \{ a_{ad} \alpha_a(k) + b_{ad} w_{ad}(k) \}$$

$$E\{w_{ad}(k)\} = 0$$

$$\text{cov}\{w_{ad}(k_1), w_{ad}(k_2)\} = \begin{cases} q_{ad} & \text{if } k_1 = k_2 \\ 0 & \text{if } k_1 \neq k_2 \end{cases}$$

$$w_{ad}(k) = \frac{\sigma\{w_{ad}(k)\}}{\sigma\{w_a(k)\}} w_a(k) \quad (3.25)$$

Parameters a_a and b_a are found from equations (3.6) and (3.8) with T and T_c set to 5 seconds and 10 seconds respectively, giving a wind energy break frequency equal to that of the tidal stream, 0.0159 Hz.

Close inspection of anemogram records presented by Watts (64), shows on all traces the wind direction to contain higher frequency components than the wind velocity. No explanation is given for this phenomenon, but to include its effect in both the wind and tidal-stream models, parameters a_{ad} , b_{ad} , a_{cd} and b_{cd} are calculated from equations (3.6) and (3.8) with $T_c = T = 5$ seconds, giving a break frequency of 0.0318 Hz.

The standard weather conditions prevailing in Plymouth Sound on

26th October, 1982 produces the following wind data:

$$\begin{aligned} u_{am} &= 10.29 \text{ m/s} & \sigma_a &= 3 \text{ m/s} \\ \sigma\{w_a(k)\} &= 5.674 \text{ m/s} \\ \alpha_{am} &= 3.927 \text{ rad.} & \sigma_{ad} &= 0.35 \text{ rad.} \end{aligned}$$

$$\sigma\{w_{ad}(k)\} = 0.492 \text{ rad.} \quad (3.26)$$

Correlated stochastic components of wind velocity and direction for these values are shown in Figures 3.8(a) and 3.8(b).

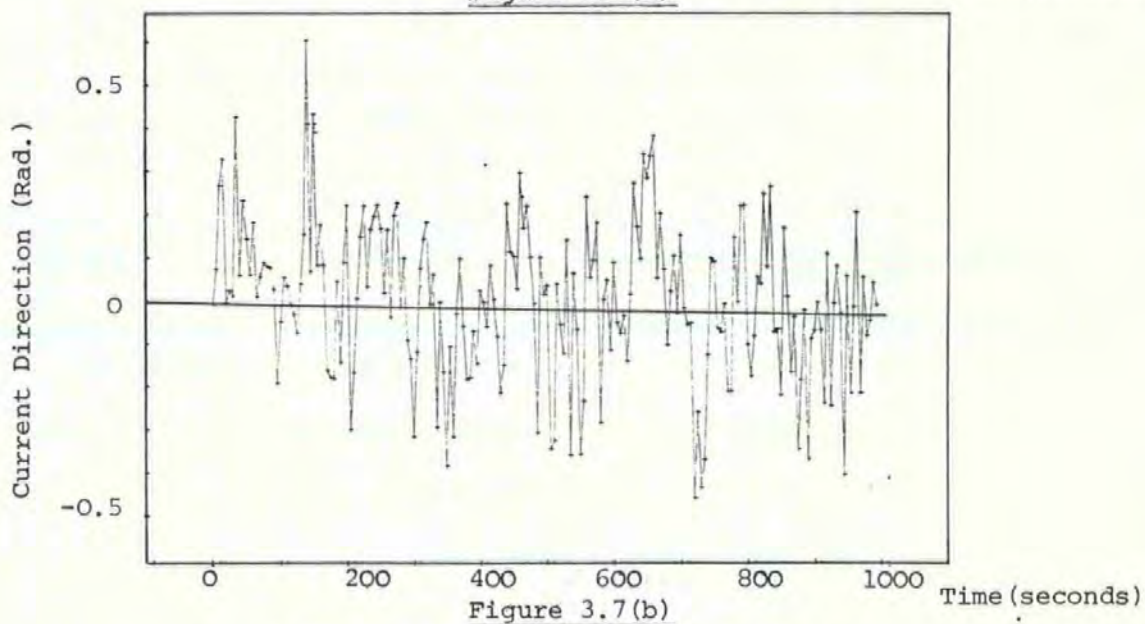
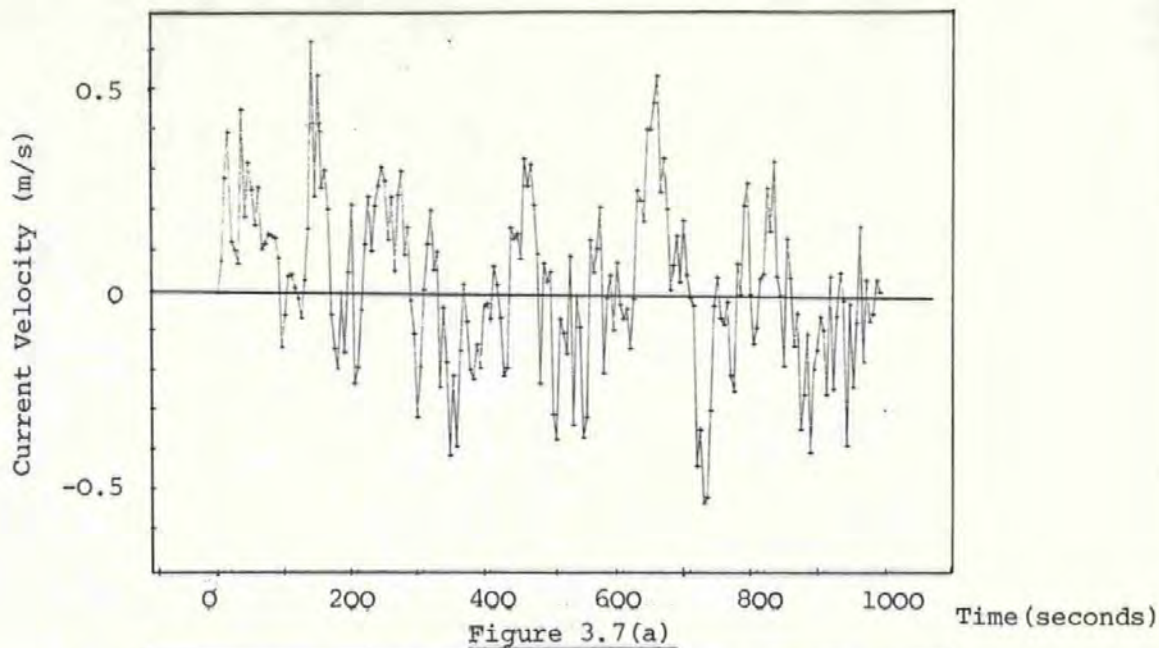
3.4. Disturbance Recursive Equation Set

Using the values given in sections 3.2 and 3.3 the disturbance recursive equation set for the standard weather conditions ($C_{d1} = C_{d2} = C_{d3} = C_{d4} = 1$) become:

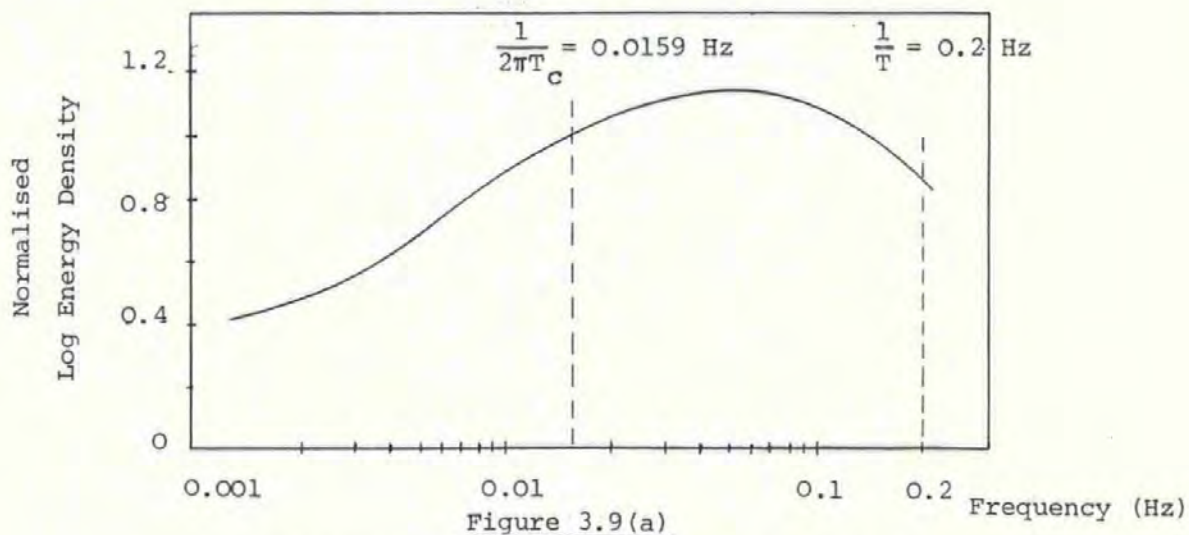
$$\begin{aligned} U_c(k+1) &= 0.669 + 0.606U_c(k) + 0.394w_c(k) \\ \alpha_c(k+1) &= 3.665 + 0.368\alpha_c(k) + 0.632w_{cd}(k) \\ U_a(k+1) &= 10.29 + 0.606U_a(k) + 0.394w_a(k) \\ \alpha_a(k+1) &= 3.927 + 0.368\alpha_a(k) + 0.632w_{ad}(k) \end{aligned} \quad (3.27)$$

3.4.1 Frequency Spectrum

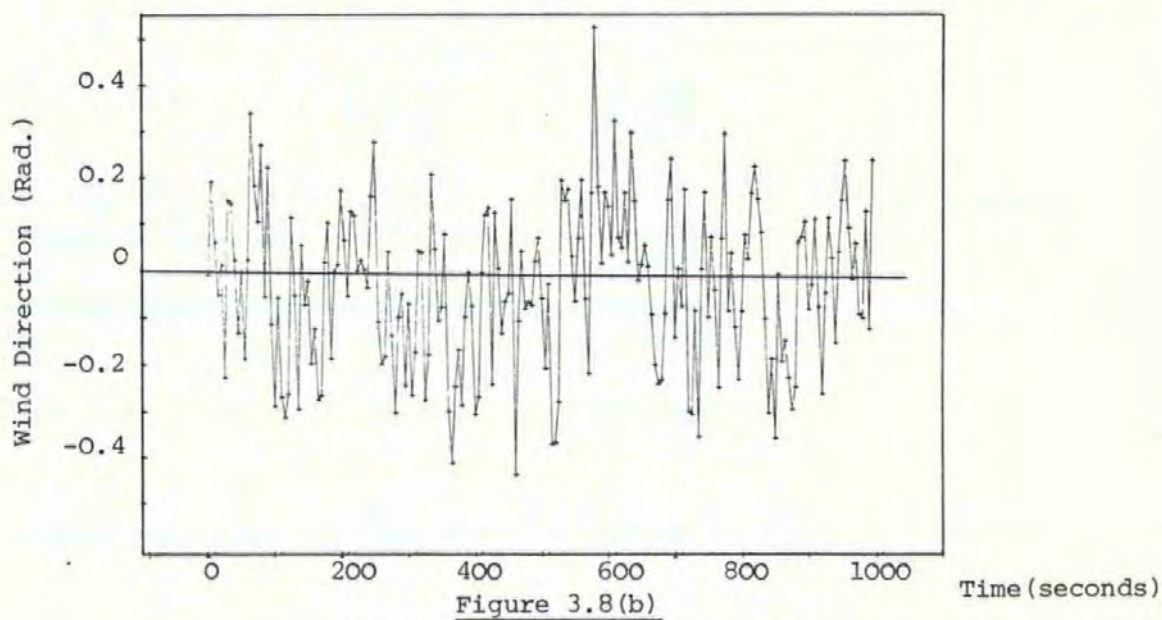
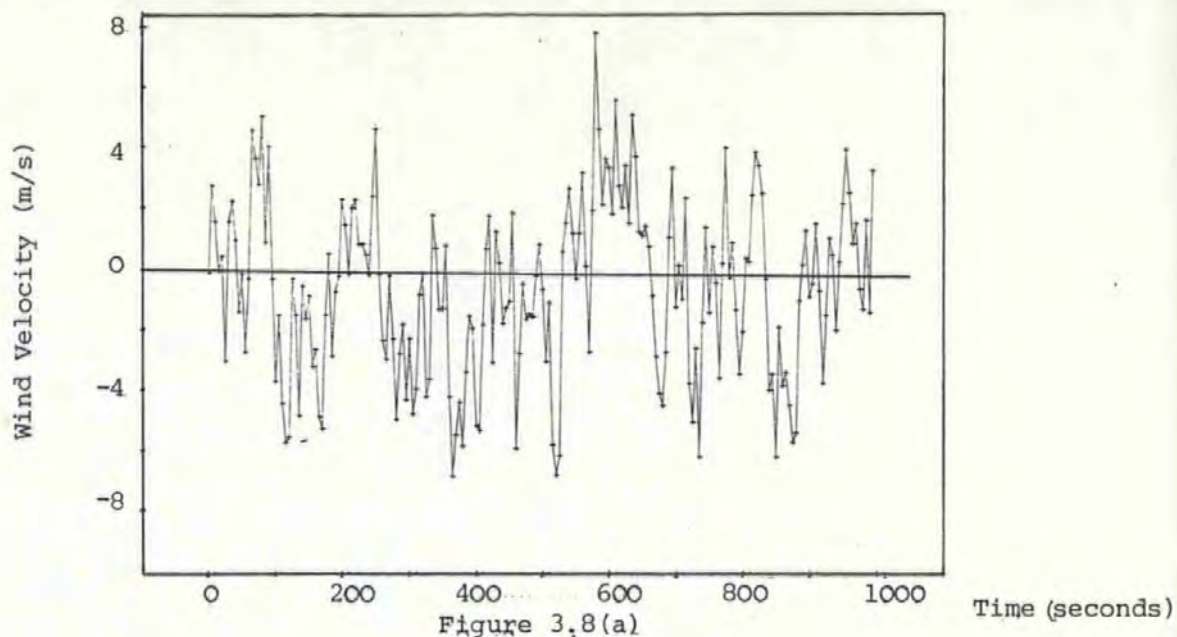
The smoothed frequency spectrum of the discrete time series generated by equations (3.27) may be evaluated using a Fast Fourier Transform (FFT) algorithm together with either a Bartlett, Turkey or Parzan smoothing window. Figure 3.9(a) illustrates the nature of the smoothed spectrum for tide and wind velocity over the bandwidth 0.001 to 0.2 Hz and Figure 3.9(b) indicates the slightly higher spectrum for tide and wind direction.



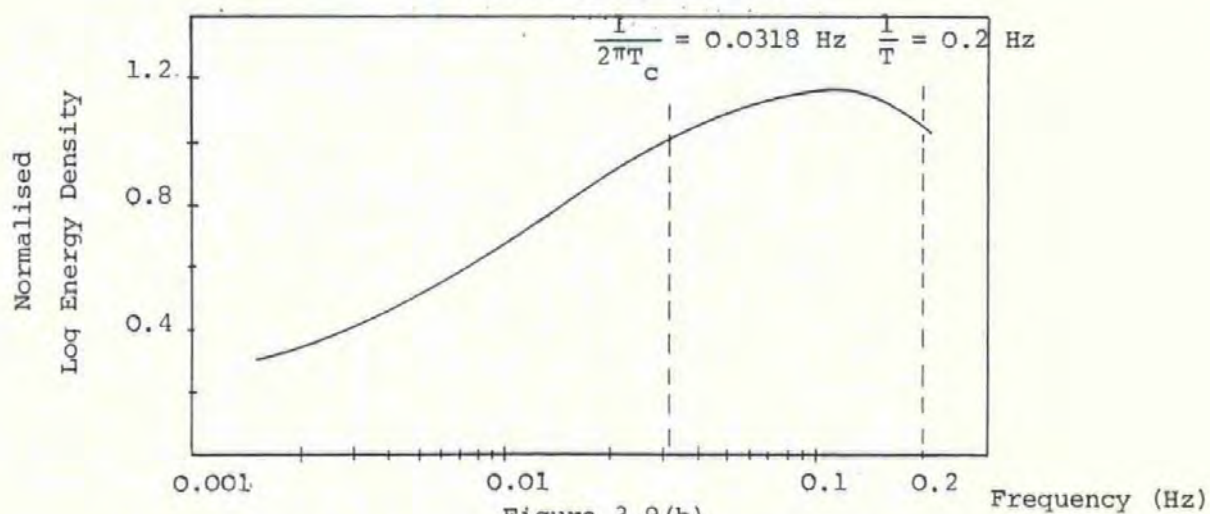
Correlated Stochastic Components of
Tidal Stream Velocity and Direction



Smoothed Frequency Spectrum for Tide and Wind Velocity



Correlated Stochastic Components of
Wind Velocity and Direction



Smoothed Frequency Spectrum for Tide and Wind Direction

CHAPTER 4

SIMULATION OF SHIP MANOEUVRES AND EXPERIMENTAL DETERMINATION OF HYDRODYNAMIC COEFFICIENTS

4.1 Introduction

In order to assess the accuracy of the three mathematical models proposed in Chapter 2 to describe the motion of a vessel during tight manoeuvres, a comprehensive computer simulation study was conducted. This consisted of subjecting each of the models to a set of standard steering tests as laid down by the B.S.R.A. (65).

A comparative evaluation with full-scale measurements taken by Morse and Price for the USS Compass Island (66) was then undertaken and the best mathematical model selected.

The USS Compass Island was constructed with a Mariner hull form, and a complete set of hydrodynamic coefficients for this class of vessel have been measured by Chislett and Strom-Tejsen (67) using a planar-motion mechanism. These, together with the particulars of the full-size vessel, are given in Appendix 2.

4.2 Simulation Program

The computer program for simulating ship manoeuvres is written in FORTRAN, all major calculations being carried out in either subroutine LAB (Linear A and B) for the linear/quasi-linear models and NAB (Non-linear A and B) for the non-linear model. Both routines

are similar and a listing for the latter is given in Appendix A6.1

A flow-chart for the order of operations during a simulation run is shown in Figure 4.1.

4.3 Manoeuvring Simulations

4.3.1 Turning Circle Manoeuvres

Turning circles are used to determine the effectiveness of the rudder to produce steady-state turning characteristics. Simulation runs using approach speeds of 7.717 m/s (15 knots) for all three mathematical models and 2.572 m/s (5 knots) for the quasi-linear and non-linear models only, were performed for rudder angles of ± 5 , 10, 15, 20, 25 and 30 degrees.

A total of 60 simulation runs were carried out and a typical set of results are given in Figure 4.2. Tables 4.1 to 4.4 summarise the results in terms of advance, transfer, tactical diameter and final diameter as defined in Figure 4.2(a) and the data is plotted in Figures 4.3 to 4.6 for the two approach speeds. The results for steady-state loss in forward speed and increase in lateral velocity due to a turning manoeuvre are listed in Table 4.5 and shown in Figure 4.7(a) and 4.7(b).

4.3.2 Dieudonne Spiral Manoeuvre

The Dieudonne spiral manoeuvre is used to provide a qualitative measure of course stability for surface ships. Steady-state yaw-rate is plotted as a function of rudder angle in a gradually increasing, and then decreasing spiral manoeuvre. Results are given in Table 4.6 and Figure 4.8 along with the Morse-Price data.

The simulation was performed at approach speeds of 7.717 m/s and 2.572 m/s. In each case the rudder was set to +25 degrees and then decremented in steps of -5 degrees to -25 degrees (finer steps being

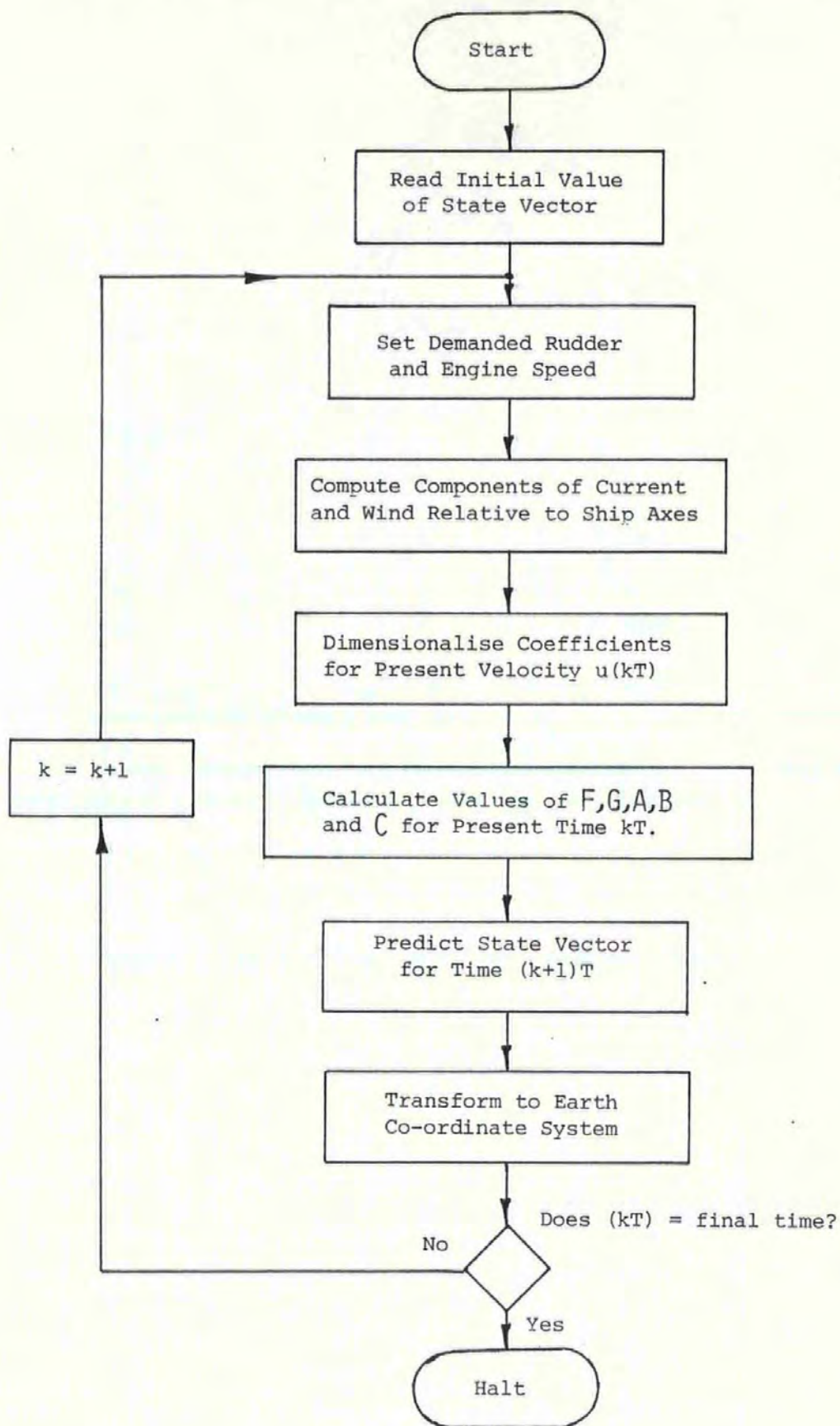


Figure 4.1

Flow-Chart for Manoeuvring Simulation

used around the origin) and incremented back again to +25 degrees in steps of +5 degrees. At each increment the ship was allowed to settle into a steady turn and the corresponding yaw-rate noted.

4.3.3 Kempf Zig-Zag Manoeuvre

This manoeuvre gives an indication of the effectiveness of the rudder to initiate and check changes of heading. Results are shown in Figure 4.9.

The simulation was conducted at a single approach speed of 7.717 m/s as no data for the real ship was available at the slower speed. Initially the demanded rudder was set to +20 degrees then, as the simulation continued, a check was made on the heading, and when it lay within a tolerance band of 18-22 degrees, the demanded rudder was switched to -20 degrees. The process was repeated for several changes in demanded rudder.

4.3.4 Starting Trials

These were performed to compare the dynamics of the vessel in the x-direction with data extracted from the Morse-Price trials. With the propeller moment and side-thrust terms removed (so that the ship would travel in a straight line) and the vessel stationary with rudder amidships, a step change in demanded engine speed was ordered. The resulting responses are shown in Figure 4.10.

The final steady-state relationship between forward speed and engine revolutions obtained from these trials were used as initial conditions for the turning circle, Dieudonne and Kempf manoeuvres.

4.4 Analysis of Results

The three phases of the turning circle manoeuvre, advance and transfer, tactical diameter and final diameter provide a measure of the accuracy of the mathematical models in terms of (a) initial transient, (b) final transient, (c) steady-state performance.

Figures 4.3 and 4.4 show that all the mathematical models are reasonably accurate in the initial transient, but Figure 4.5 and 4.6 reveal that towards the end of the transient and into the steady-state, only the non-linear model retains its accuracy. For example, with 20 degrees of starboard rudder, the final diameter of the real ship and the non-linear model is about 1000 m, compared with about 500 m for the linear and quasi-linear models. This tightness of turn in the latter case explains the excessive speed loss and lateral velocity experienced by the quasi-linear model shown in Figure 4.7.

The Dieudonne spiral results of Figure 4.8 again emphasise that only the non-linear model provides an accurate rudder to yaw-rate relationship over the rudder angle range ± 25 degrees. Note, however, that over the range ± 5 degrees, the slope (which is the gain constant K_n in the Nomoto model) is correct for all three mathematical models. A further by-product of this test is the conclusion that the vessel has controls-fixed stability, although a close inspection of the Morse-Price data around the origin for the USS Compass Island shows a slight tendency towards instability.

Results for the Kempf manoeuvre given in Figure 4.9 illustrate that, as with the turning circle, all three mathematical models produce fairly accurate results in a manoeuvre which is primarily an initial transient test.

Figure 4.10 indicates that both non-linear and quasi-linear models very closely represent the x-direction dynamics of the vessel.

Conclusions

The conclusions that must be drawn from this set of tests is that the non-linear model is the only mathematical model to accurately represent the three degrees of freedom ship motion in all manoeuvring regimes, particularly tight manoeuvres.

4.5 Important Non-Linear Coefficients

Since the next stage of work involved measurement of hydrodynamic coefficients for a car ferry hull, an analytical survey of the important coefficients on the Mariner hull was conducted so as not to waste time measuring coefficients that have no significant effect on the hull's performance.

To assess the relative importance of each coefficient, the vessel, under simulation, was steered into a tight turn and allowed to settle to its steady-state turning circle. Using the dimensionalised coefficients the equations of static equilibrium were employed to compute the forces and moments acting on the hull arising from each term. These were then expressed in percentage form.

Using an approach speed of 7.717 m/s and a demanded rudder of -20 degrees, the steady turning circle contained the following state variables:

$$\begin{aligned}\delta_A &= -0.349066 \text{ rad} \\ n_A &= 7.15509 \text{ rad/s} \\ u &= 5.8033 \text{ m/s} \\ v &= -0.897414 \text{ m/s} \\ r &= 0.012489 \text{ rad/s}\end{aligned}$$

The steady-state forces and moments acting on the hull as a result of these state variables are given as a percentage in Table 4.7. The terms deemed as "negligible" were not measured for the car-ferry hull, unless they were available from polynomial curve fitting expressions.

The turning circle simulation was again repeated for a demanded rudder of -20 degrees with the "negligible" terms omitted and the recorded state variables remained unaltered to within three significant figures.

4.6 Experimental Determination of Hydrodynamic Coefficients for Car Ferry Hull 5502

The Department of Mechanical Engineering at Plymouth Polytechnic has on loan from the National Maritime Institute (NMI) the scale model of a twin screw car ferry hull shown in Figure 4.12, NMI designation 5502. The particulars of the model and full-size vessel are:

	<u>Model 5502A</u>	<u>Full-Size Ship 5502B</u>
Lpp	3.419 m	150 m
Beam	0.565 m	24.8 m
Draught	0.134 m	5.9 m
Displacement	166.4 kg	14.4x10 ⁶ kg
Block Coefficient	0.64	0.64
I_z about mass centre	149.8937 kg m ²	24.364x10 ⁹ kg m ²
Propellers	3-bladed, inward turning.	-

The majority of the coefficients were determined from experiments conducted on the Number Two Towing Tank at the National Physical Laboratories, Teddington, during October 1981. The remainder of the coefficients were obtained from tests on the river Plym during the late summer of 1982.

The NPL experiments required a three-axis dynamometer (surge, sway and yaw) to be inserted in the model to measure the hydrodynamic forces and moments on the hull. This was attached via a trailing link to the towing gantry as shown in Figure 4.13.

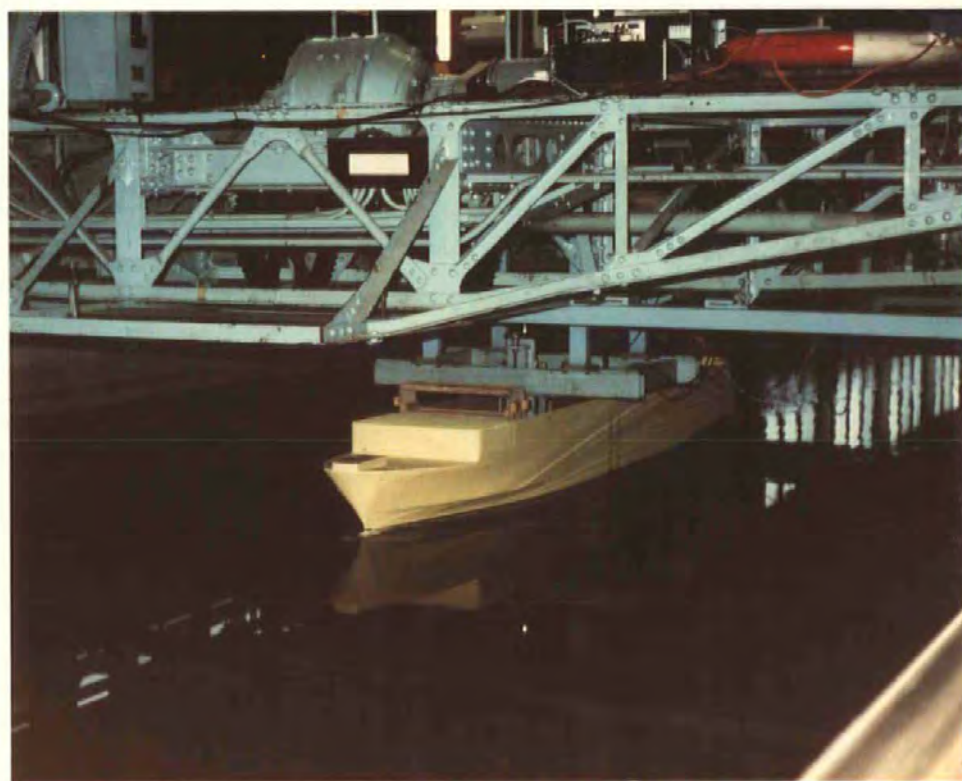
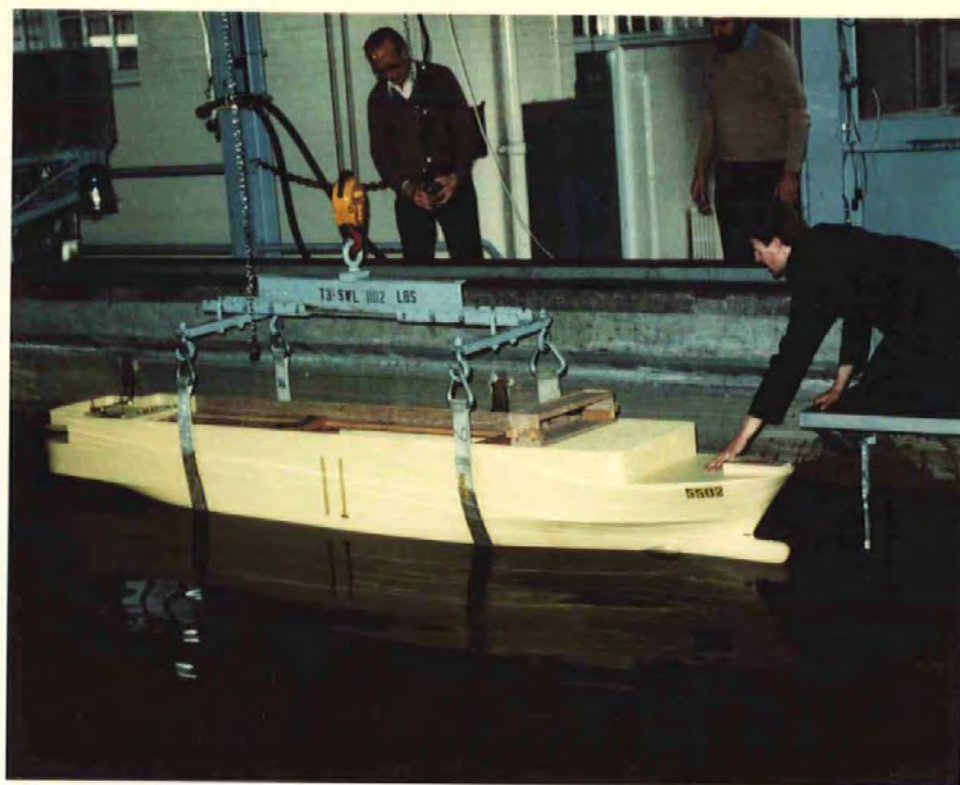
A total of 64 runs were made in the towing tank. The tests are described in 4.7 and the results summarised in Appendix 3.

Figure 4.12

Model Car Ferry Hull 5502

Figure 4.13

Model Attached to Towing Gantry



4.7 Description of Tests

4.7.1 Hull Resistance

The hull was towed at six different speeds with none-rotating propellers and zero angle of drift, measurements being taken of drag force and forward velocity. A least-squares fit of a third-order polynomial through the results shown in Table A.3.1. produced the curve in Figure A.3.1 and hence the coefficients X_u , \bar{X}_{uu} and \bar{X}_{uuu} .

4.7.2 Bollard Pulls

These were performed with the hull stationary, measurements being taken of thrust against propeller speed for (a) both propellers ahead, (b) single propeller ahead and astern as shown in Tables A.3.2(a) and (b).

The coefficient \bar{X}_{nn} was obtained from the slope of a least-squares straight-line fit of thrust against the square of propeller speed, given in Figure A.3.2(a) for case (a) above.

The single propeller results were fitted to a third-order polynomial as illustrated in Figure A.3.2(b) thus overcoming the negative thrust problem (a square-law relationship still provides positive thrust when the propeller is driven in reverse).

4.7.3. Self Propulsion Experiments

The self propulsion point was obtained for the three different forward speeds given in Table A.3.3 by adjusting the angular velocity of the propellers to give zero dynamometer reading in the x-direction for each case. This corresponds to the condition under which the model is not being towed, but is self propelled.

The difference between the bollard pull thrust at this engine speed and the hull resistance at the self propulsion point enables the coefficient X_{un} to be calculated.

The model towing speed was selected to be 0.75 m/s for most of

the remaining tests. This corresponds to a Froude number of 0.13 and represents a forward velocity of 5 m/s for the full-size ship.

4.7.4 Rudder Experiments

The rudder experiments were conducted with both rudders linked together, the hull travelling at a forward speed of 0.75 m/s with zero drift angle and the engines running at the self propulsion velocity. Table A.3.4 lists the non-dimensional surge and sway forces and yaw moments in rudder angle increments of 5 degrees over the range ± 30 degrees.

Figure A.3.3(a) shows the X-force/rudder angle relationship which is clearly a square law. The straight-line fit of X' against δ_A^2 in Figure A.3.3(b) has a slope whose value is $\bar{X}_{\delta\delta}'$.

A cubic polynomial least-squares fit of the non-dimensional sway force Y' against rudder angle, shown in Figure A.3.4(a) produces the Y_{δ}' and $\bar{Y}_{\delta\delta\delta}'$ coefficients. Similarly, fitting a cubic polynomial to the non-dimensional yaw moment N' and rudder angle data as seen in Figure A.3.4(b) provides N_{δ}' and $\bar{N}_{\delta\delta\delta}'$.

4.7.5 Drift Angle Experiments

These were again conducted with rudders linked and a hull speed of 0.75 m/s, propellers at self-propulsion velocity. The drift angle was adjusted in 2 degree increments over a range of ± 10 degrees. For each value of drift angle the rudders were rotated through ± 30 degrees at 10 degree increments. At each rudder position, measurements of surge and sway forces and yaw moment were taken.

This involved only 30 runs because fortunately the tank was long enough to allow 2 different rudder settings to be made per run. Table A.3.5 gives the non-dimensional forces and moments for the positive and negative drift angles.

Figure A3.5 shows the non-dimensional X-force plotted against v^2 . It will be seen that the results are scattered and the Mariner hull data is included for reference. A least-squares straight line fit produces the \bar{X}_{vv} coefficient, obtained from the slope of the line.

A cubic polynomial fit to the non-dimensional Y'-force/sway velocity data as shown in Figure A.3.6(a) yields the Y_v' and \bar{Y}_{vvv}' coefficients. A similar fit to the non-dimensional N' moments/sway velocity information provides N_v' and \bar{N}_{vvv}' as shown in Figure A.3.6(b).

4.7.6 Added Mass Coefficients

No acceleration measurements were taken in the towing tank as the gantry control mechanism was only designed for constant speed operation. In the absence of measurements, it was considered reasonable to assume the ratio of non-dimensional added mass to non-dimensional ship mass to be the same for both the Mariner and car ferry hulls, since both have similar block coefficients.

Mariner Hull

$$\begin{aligned}
 \frac{X_u'}{m'} &= -0.05263 \\
 \frac{Y_v'}{m'} &= -0.93734 \\
 \frac{N_v'}{m'} &= -0.34213 \\
 \frac{Y_r'}{I_z'} &= -0.21939 \\
 \frac{N_r'}{I_z'} &= -1.1148
 \end{aligned} \tag{4.1}$$

4.7.7 Free-Sailing Tests

The yaw-rate dependant coefficients Y_r' , N_r' , \bar{Y}_{rvv}' and \bar{N}_{rvv}' were

obtained from steady-state turning circle trials on the river Plym. A calm day was selected and the tests performed during the turn of the tide.

The vessel was put in a tight turn with +30 degrees of rudder. When steady conditions were arrived at, the diameter of the circle was measured and the time for one revolution noted. To take into account slight differences in the speed of the port and starboard screws, the tests were repeated with -30 degrees of rudder and the mean values which are listed below, were then computed.

$$\delta_A = \pm 30 \text{ degrees.}$$

$$\text{Mean Circle Diameter} = 14.75 \text{ m}$$

$$\text{Mean Time for One Revolution} = 150 \text{ seconds}$$

$$\text{Track Velocity } U = 0.3089 \text{ m/s}$$

$$\text{Forward Velocity } u = 0.3034 \text{ m/s}$$

$$\text{Lateral Velocity } v = 0.0578 \text{ m/s}$$

$$\text{Yaw Rate } r = \pm 0.0419 \text{ rad/s}$$

$$\text{Approach Speed} = 0.5 \text{ m/s}$$

$$\text{Mean Propeller Speed} = 480 \text{ rev/min}$$

Under steady turning conditions the dimensionalised non-linear sway and yaw equations of motion (2.45) become:

$$\begin{aligned} mru &= Y_v v + Y_r r + Y_{\delta} \delta_A + \bar{Y}_{vvv} v^3 + \bar{Y}_{rvv} rv^2 + \bar{Y}_{\delta\delta\delta} \delta_A^3 \\ 0 &= N_v v + N_r r + N_{\delta} \delta_A + \bar{N}_{vvv} v^3 + \bar{N}_{rvv} rv^2 + \bar{N}_{\delta\delta\delta} \delta_A^3 \end{aligned} \quad (4.2)$$

It will be noted that there are 2 equations and 4 unknowns. In the absence of further information, the principle of hull similarity was again employed using the following force and moments ratios obtained for the Mariner hull under a 30 degree rudder turn:

$$\frac{\bar{Y}_{rvv}rv^2}{Y_r} = 1.630$$

$$\frac{\bar{N}_{rvv}rv^2}{N_r} = 0.771 \quad (4.3)$$

These relationships can be substituted into equations (4.2) and a force and moment balance obtained.

Table 4.8 lists the set of hydrodynamic coefficients and dimensionalising factors for car ferry hulls 5502A (model) and 5502B (full-size). Figures 4.11(a) to 4.11(d) show a set of simulation results for the model when 30 degrees of starboard rudder is applied. It will be noted that they correspond very closely to the free-sailing results measured on the river Plym.

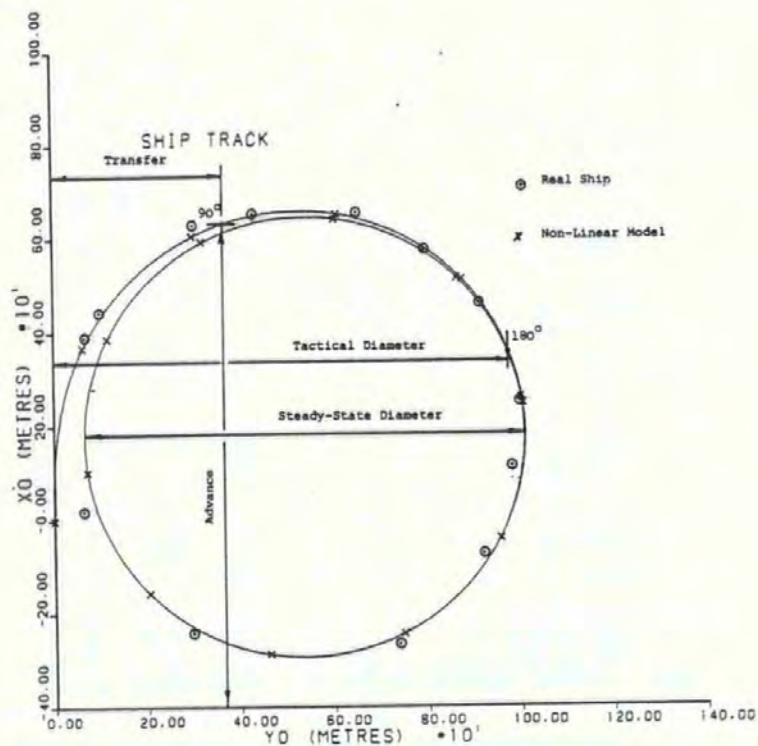


Figure 4.2(a)

Ship Track

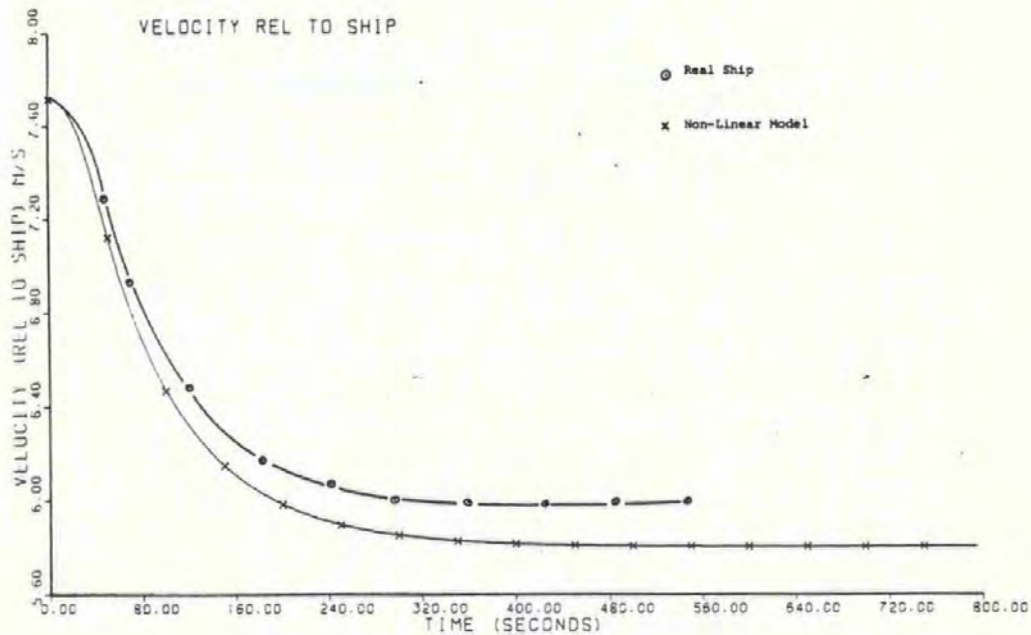


Figure 4.2(b)

Forward Velocity Transient

Turning Circle Simulation, Full-Size Mariner Hull,
7.717 m/s Approach, 20° Starboard Rudder

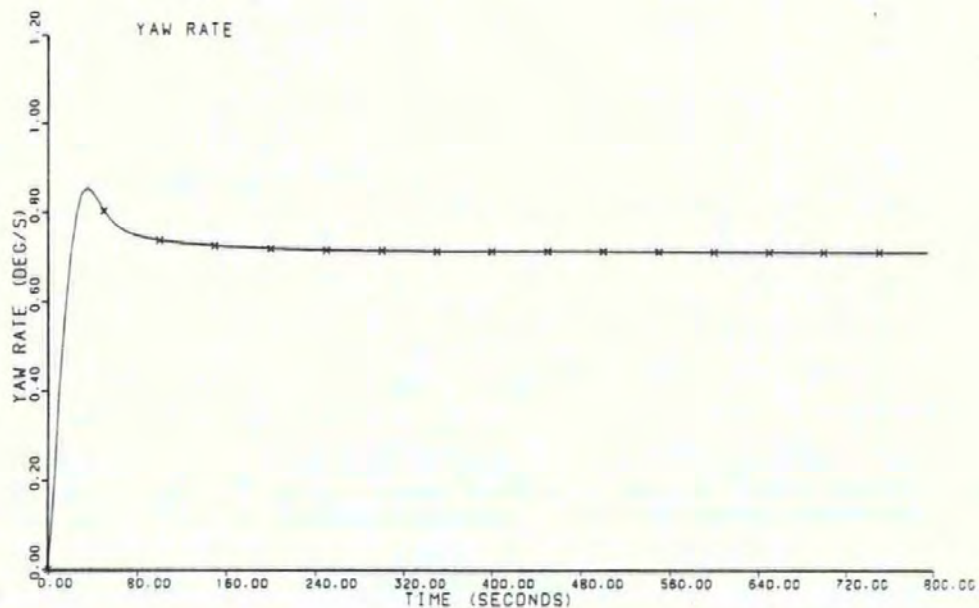


Figure 4.2(c)
Yaw-Rate Transient

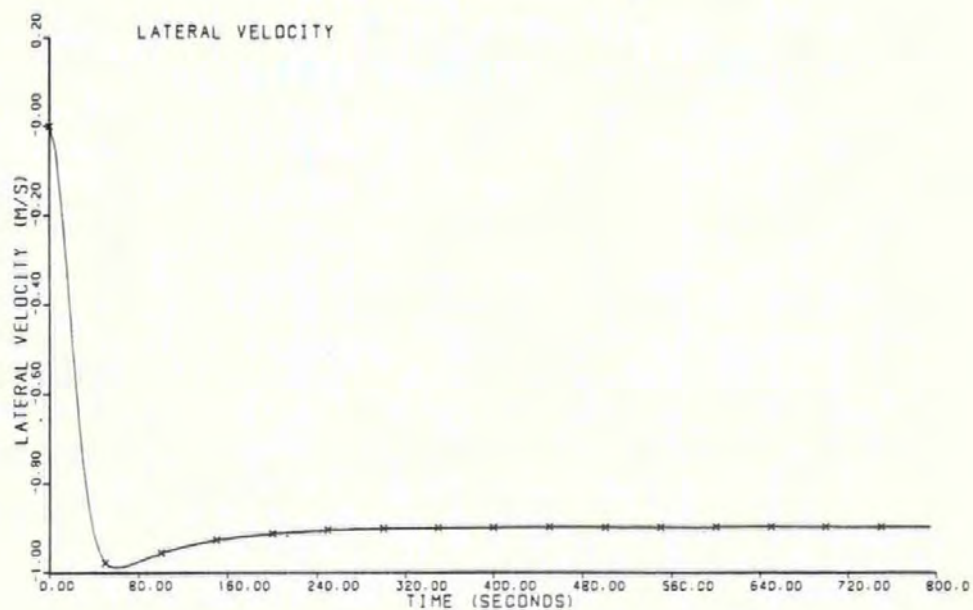
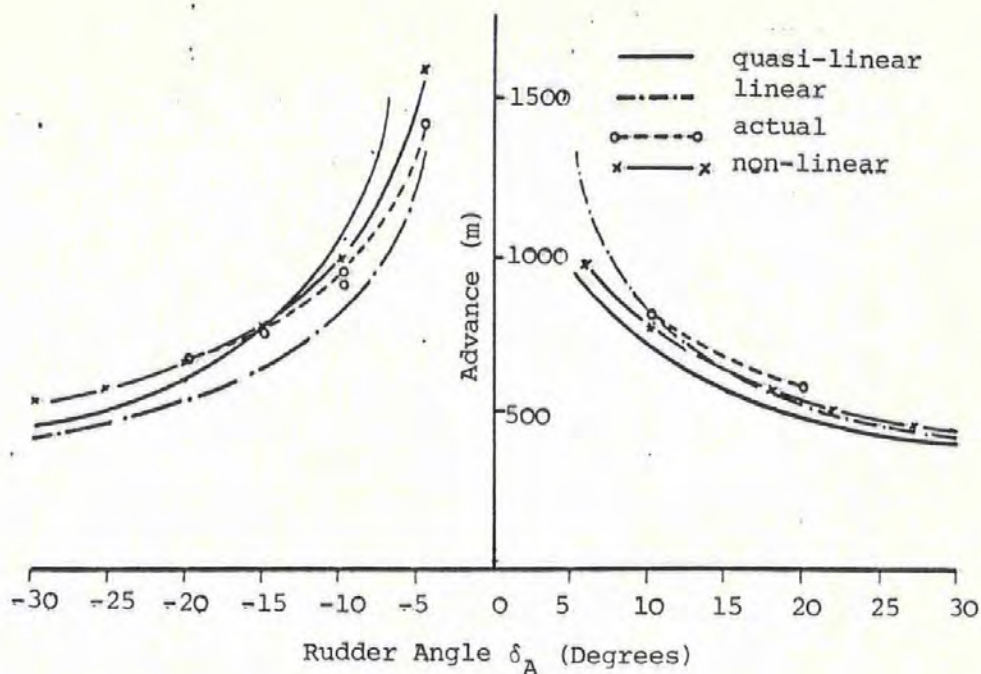
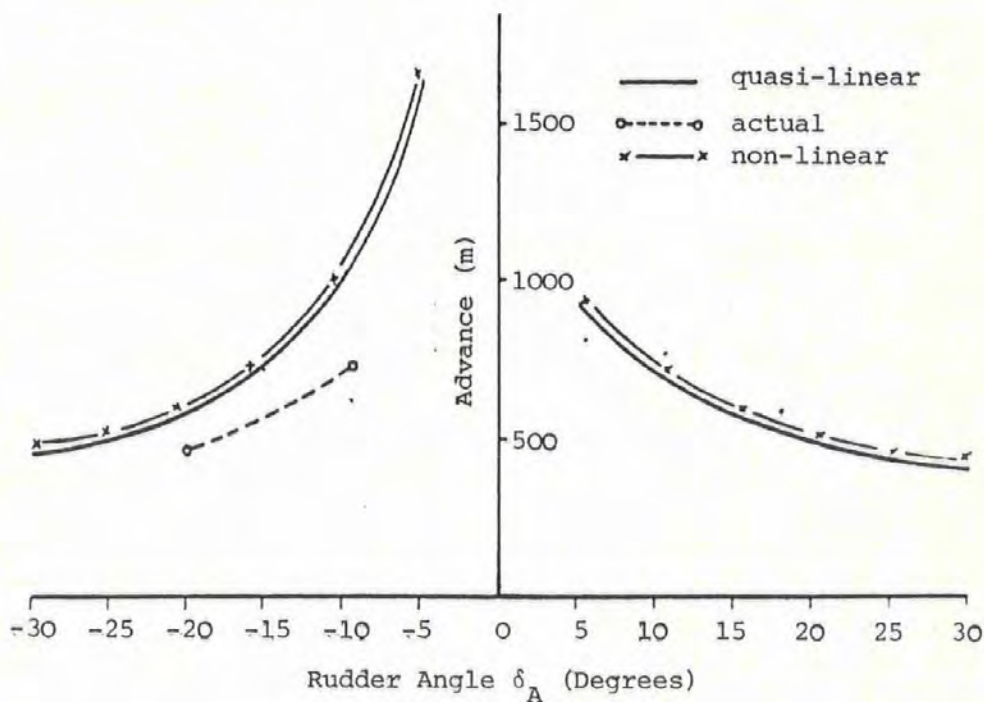


Figure 4.2(d)
Lateral Velocity Transient



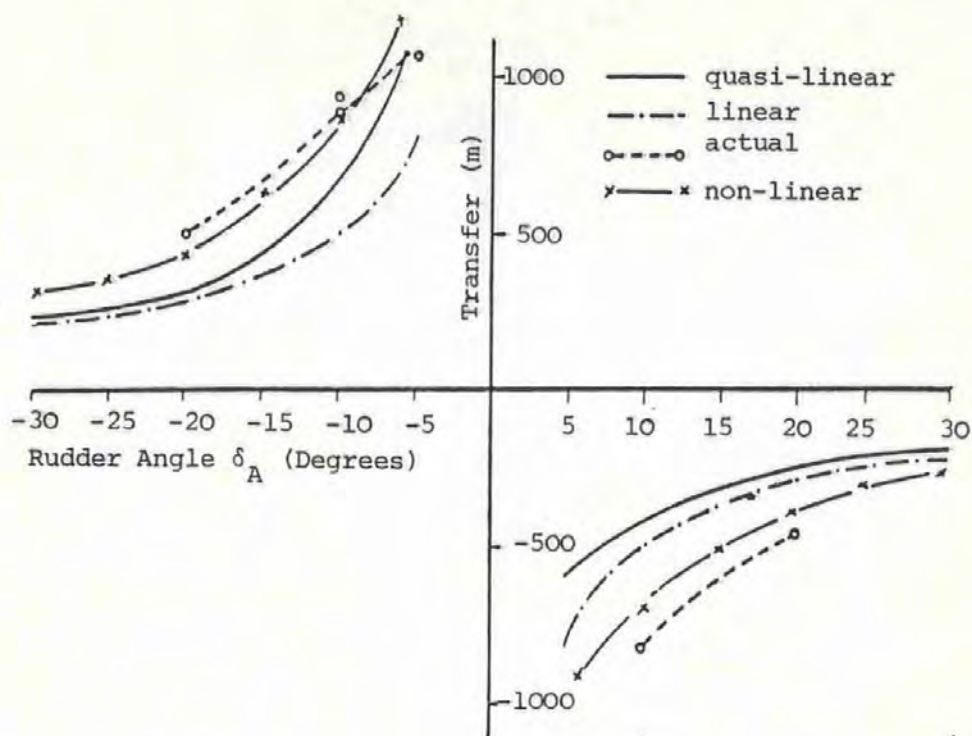
(a) 7.717 m/s Approach



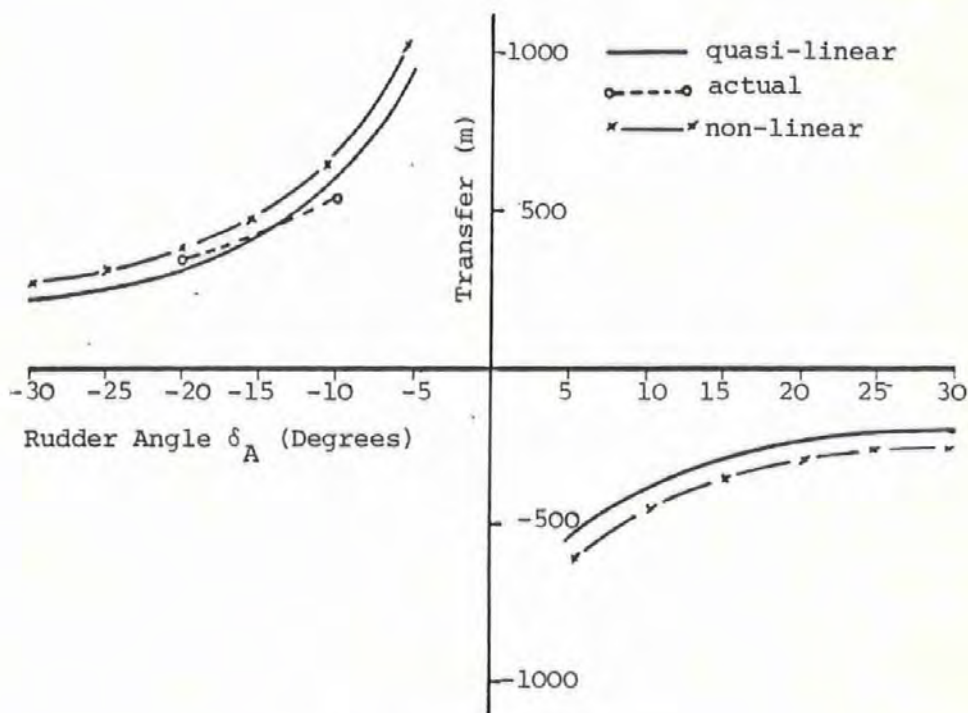
(b) 2.572 m/s Approach

Figure 4.3

Advance



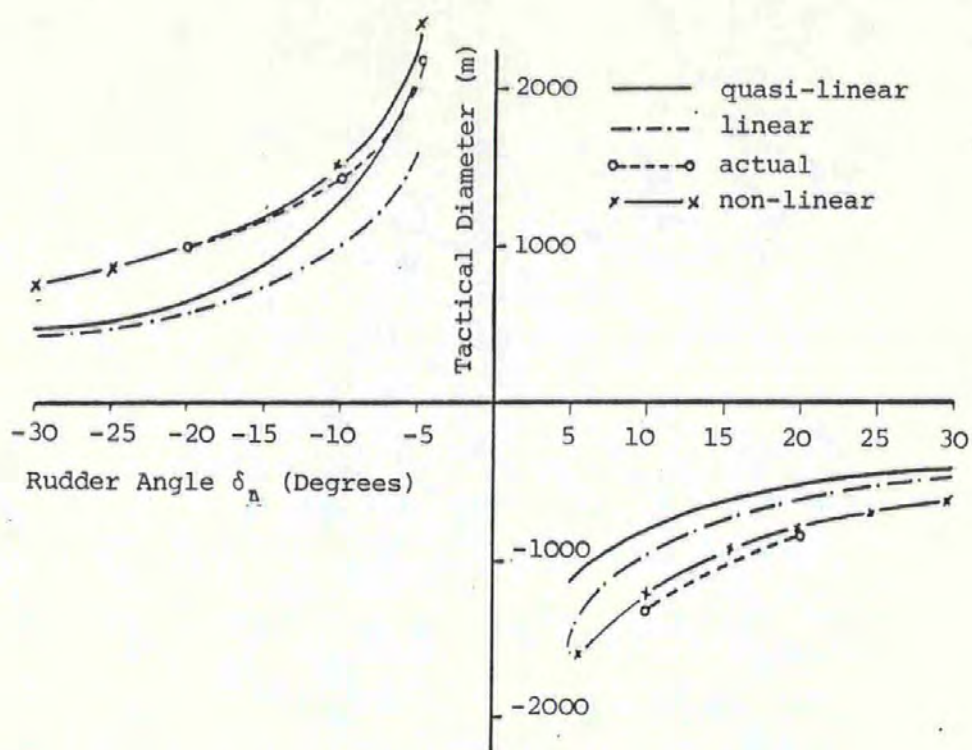
(a) 7.717 m/s Approach



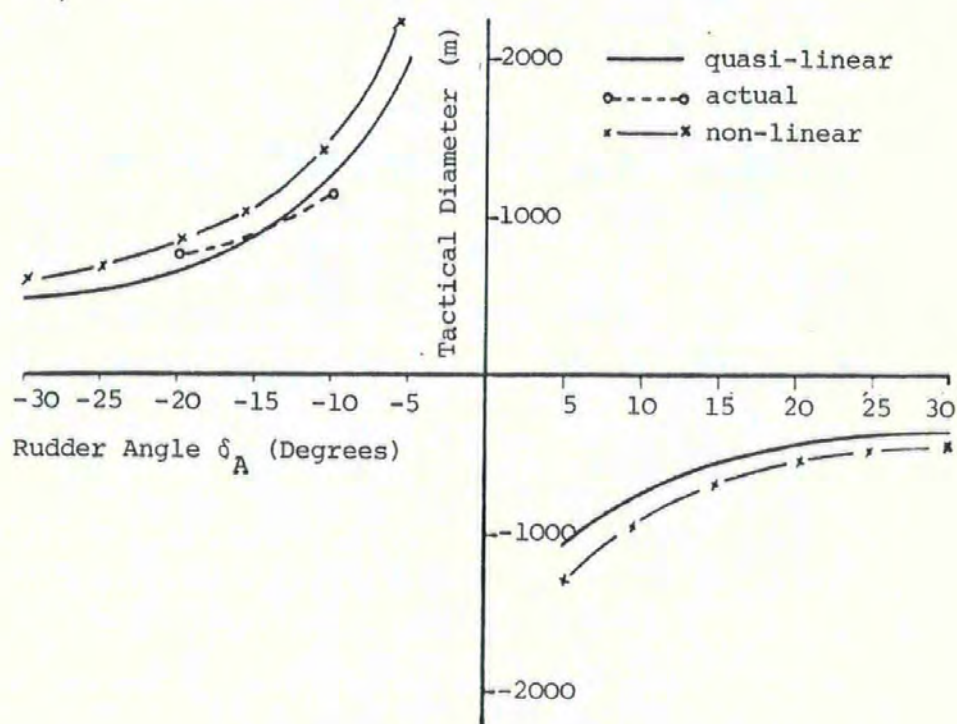
(b) 2.572 m/s Approach

Figure 4.4

Transfer



(a) 7.717 m/s Approach



(b) 2.572 m/s Approach

Figure 4.5

Tactical Diameter

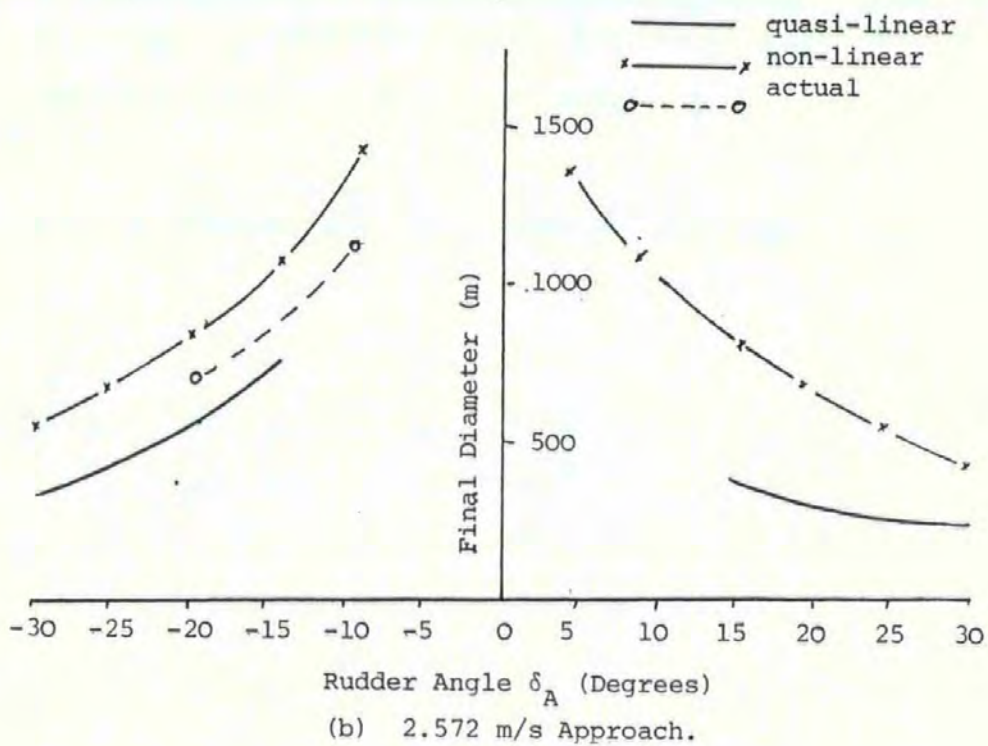
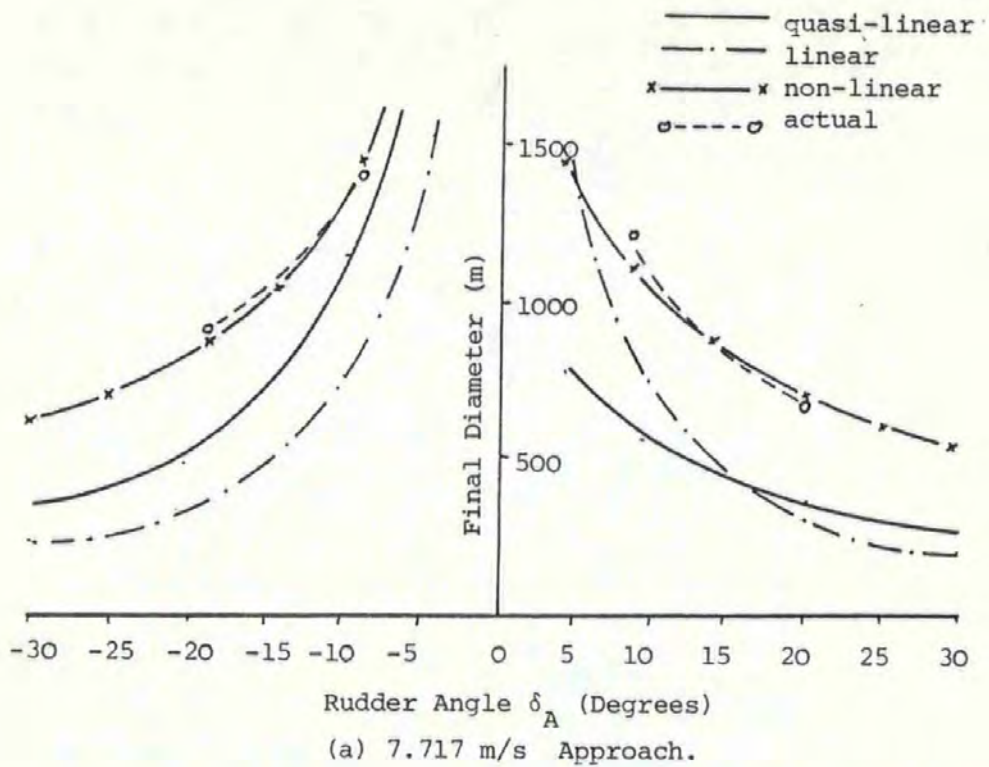


Figure 4.6

Final Diameter

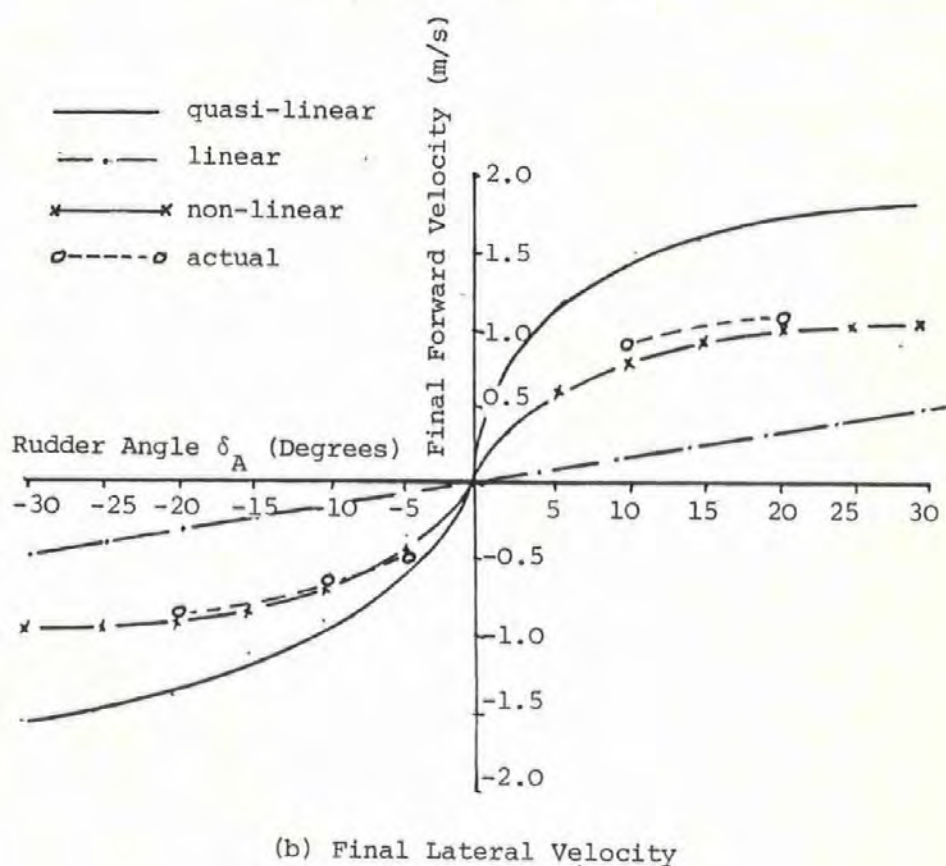
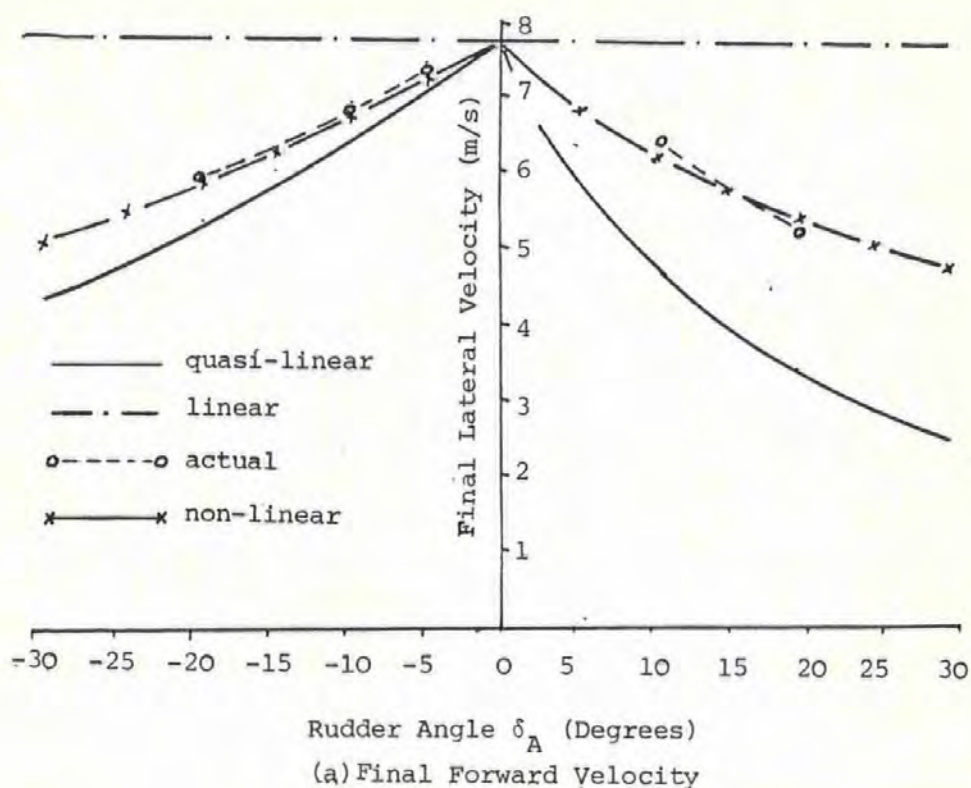
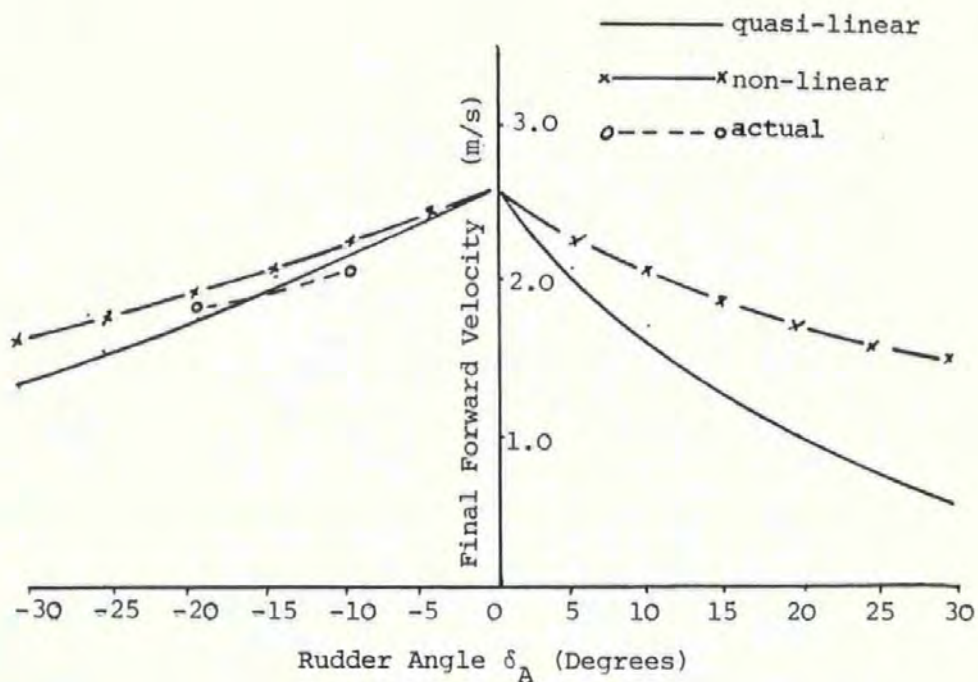
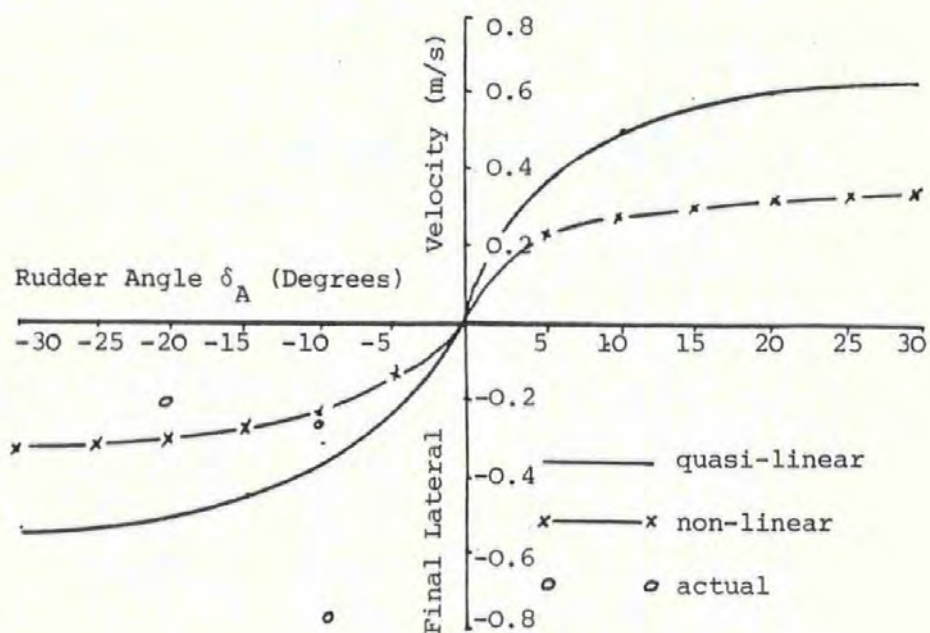


Figure 4.7(a)

Final Forward and Lateral Velocities Approach Speed 7.717 m/s.



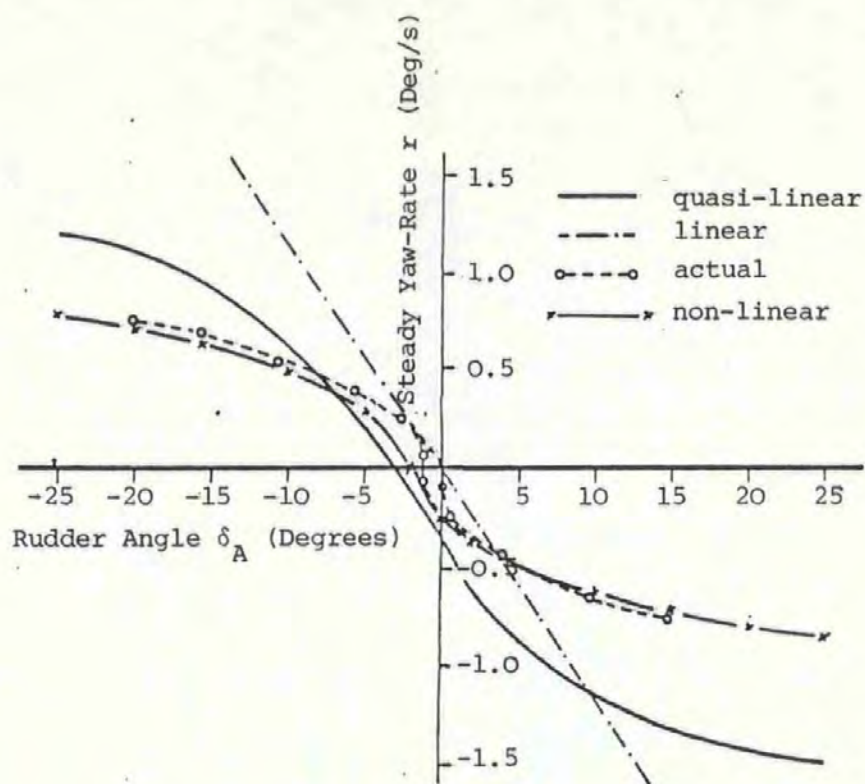
(a) Final Forward Velocity



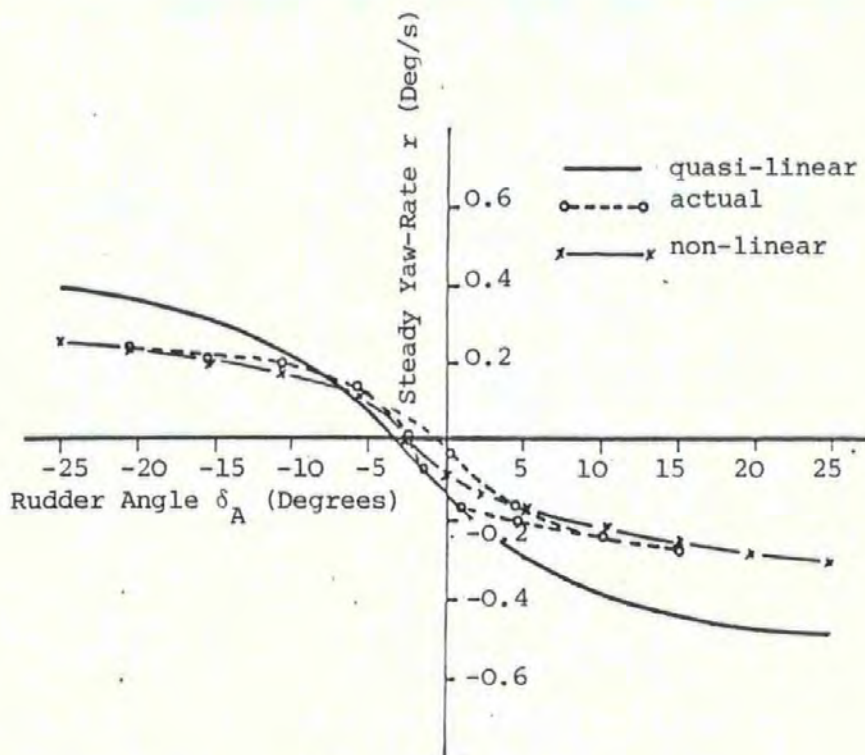
(b) Final Lateral Velocity

Figure 4.7(b)

Final Forward and Lateral Velocities Approach Speed 2.572 m/s.



(a) 7.717 m/s Approach



(b) 2.572 m/s Approach

Figure 4.8

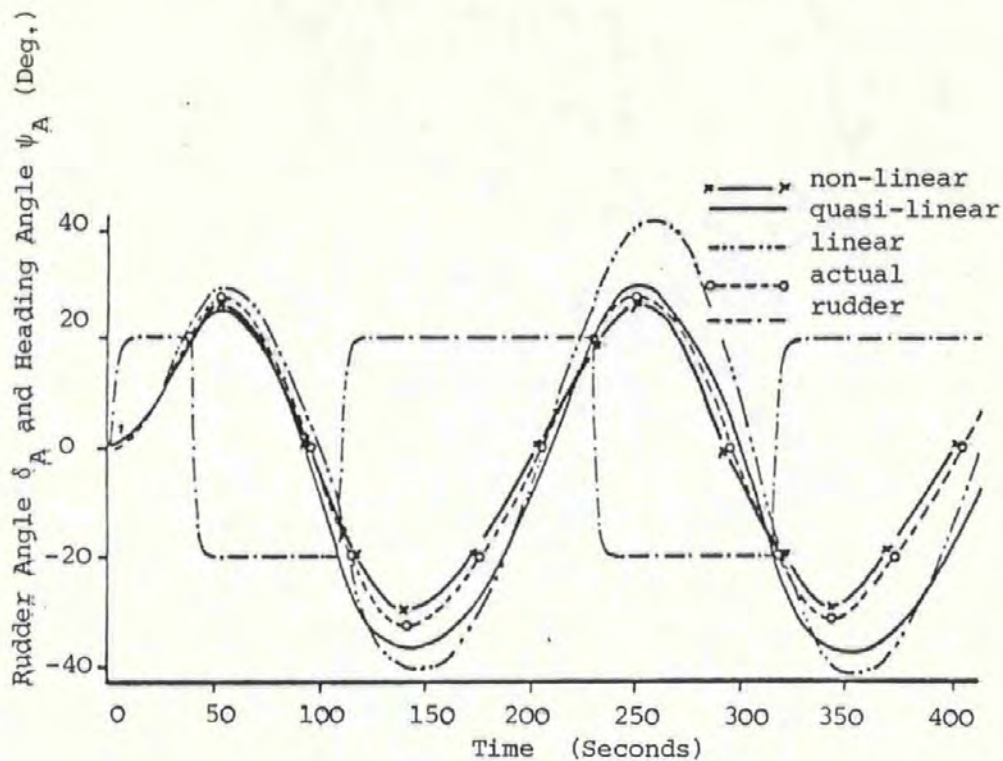


Figure 4.9

Kempf Zig-Zag Manoeuvre.

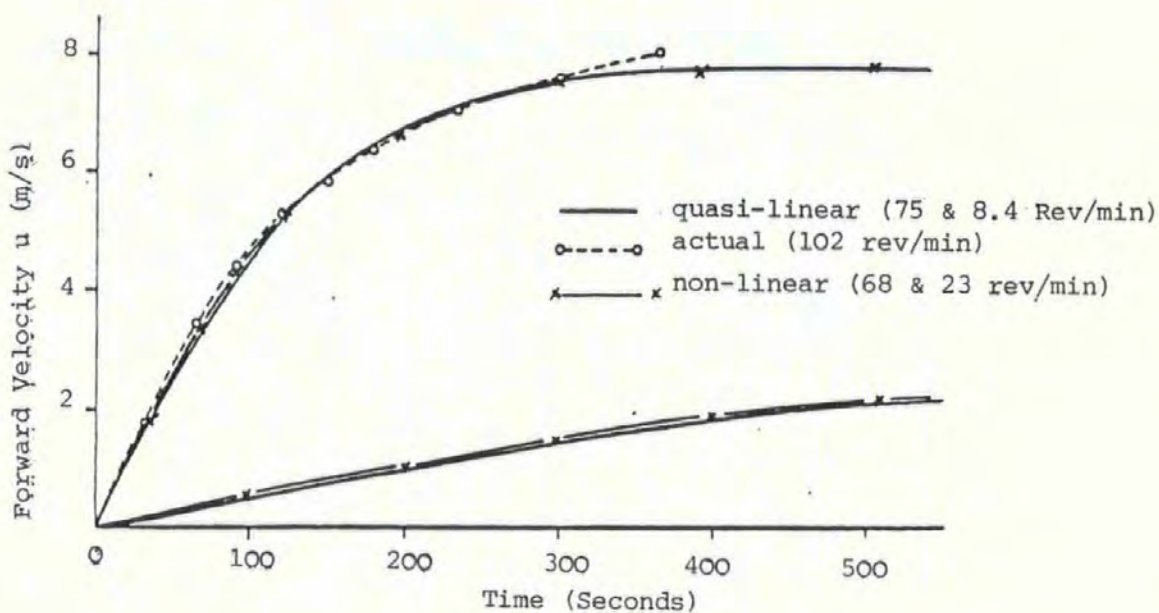


Figure 4.10

Step Change in Demanded Engine Speed

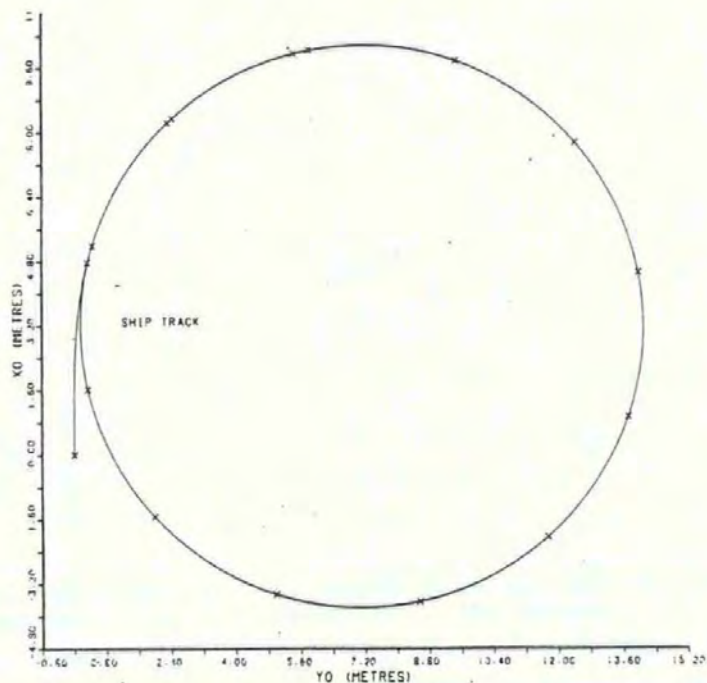


Figure 4.11(a)

Ship Track

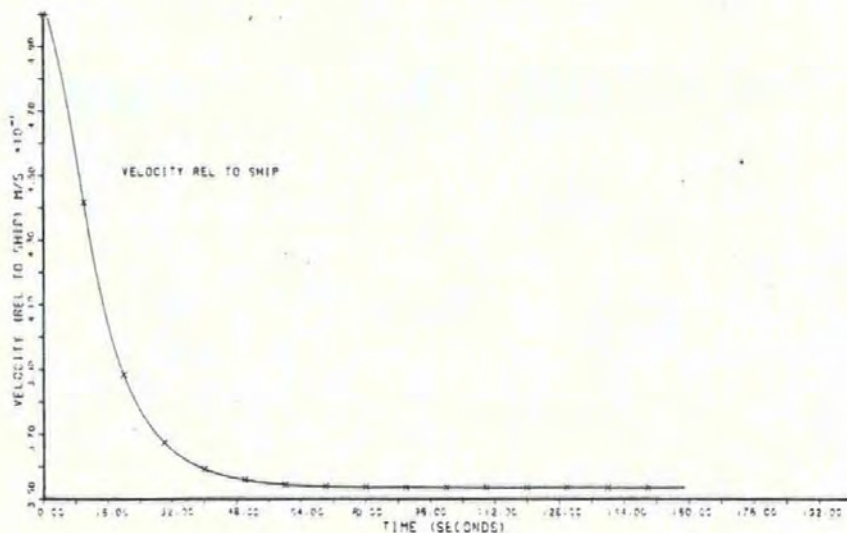


Figure 4.11(b)

Forward Velocity Transient

Turning Circle Simulation, Model Car Ferry Hull,
0.5 m/s Approach, 30° Starboard Rudder

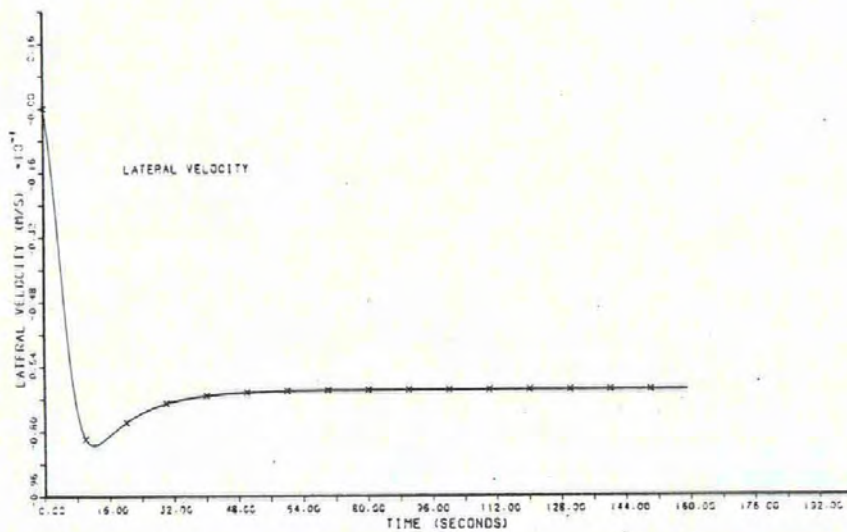


Figure 4.11(c)
Lateral Velocity Transient

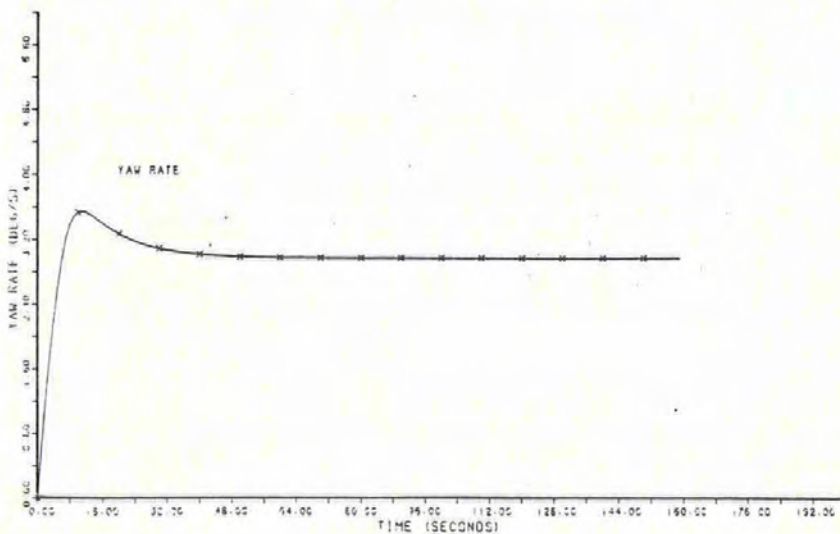


Figure 4.11(d)
Yaw-Rate Transient

Rudder Angle (degrees)	Advance after 90 degrees Change of Heading (m)							Approach Speed (m/s)
	Real	Linear	Error	Quasi- Linear	Error	Non- Linear	Error	
	Ship	Model	%	Model	%	Model	%	
30	-	427.17	-	403.24	-	474.69	-	7.717
25	-	477.91	-	448.74	-	512.57	-	7.717
20	589.8	540.62	8.34	503.39	14.65	565.87	4.06	7.717
15	-	669.65	-	576.20	-	641.40	-	7.717
10	832.1	818.31	1.66	704.11	15.38	756.09	9.13	7.717
5	-	1011.35	-	949.62	-	971.21	-	7.717
-5	1417.3	1011.35	28.64	2565.37	81.00	1829.88	29.11	7.717
-10	955.5	818.31	14.36	1059.61	10.86	1006.18	5.30	7.717
-15	-	669.65	-	749.42	-	776.73	-	7.717
-20	667.5	540.62	19.01	605.76	9.25	655.17	1.85	7.717
-25	-	477.91	-	518.97	-	580.53	-	7.717
-30	-	427.17	-	459.99	-	526.74	-	7.717
30	-	-	-	397.99	-	462.18	-	2.572
25	-	-	-	437.47	-	502.23	-	2.572
20	-	-	-	492.39	-	555.29	-	2.572
15	-	-	-	568.88	-	627.05	-	2.572
10	-	-	-	691.56	-	743.66	-	2.572
5	-	-	-	934.04	-	957.29	-	2.572
-5	-	-	-	-	-	1803.54	-	2.572
-10	704.0	-	-	1037.31	47.35	988.05	40.35	2.572
-15	-	-	-	736.69	-	759.05	-	2.572
-20	457.2	-	-	595.83	30.32	641.01	40.20	2.572
-25	-	-	-	510.69	-	566.02	-	2.572
-30	-	-	-	452.85	-	512.30	-	2.572

Table 4.1
Advance After 90 Degrees Change of Heading

Rudder Angle (degrees)	Transfer after 90 degrees Change of Heading (m)							Approach Speed (m/s)
	Real	Linear	Error	Quasi- Linear	Error	Non- Linear	Error	
	Ship	Model	%	Model	%	Model	%	
30	-	-210.69	-	-189.96	-	-335.09	-	7.717
25	-	-252.07	-	-233.40	-	-355.98	-	7.717
20	-457.2	-288.40	36.92	-272.02	40.50	-401.85	12.11	7.717
15	-	-341.04	-	-300.38	-	-470.94	-	7.717
10	-658.4	-489.04	25.72	-406.36	38.28	-555.38	15.65	7.717
5	-	-713.92	-	-593.22	-	-727.50	-	7.717
-5	1078.9	713.92	33.83	1954.90	81.19	1355.52	25.64	7.717
-10	731.5	-489.04	33.15	674.26	7.83	731.43	0.00	7.717
-15	-	-341.04	-	413.37	-	567.40	-	7.717
-20	512.1	-288.40	41.68	317.18	38.06	468.20	8.57	7.717
-25	-	-252.07	-	261.23	-	415.96	-	7.717
-30	-	-210.69	-	225.43	-	369.78	-	7.717
30	-	-	-	-169.52	-	-327.66	-	2.572
25	-	-	-	-193.46	-	-362.20	-	2.572
20	-	-	-	-232.58	-	-408.04	-	2.572
15	-	-	-	-283.61	-	-445.34	-	2.572
10	-	-	-	-369.17	-	-543.45	-	2.572
5	-	-	-	-546.40	-	-698.58	-	2.572
-5	-	-	-	-	-	1337.47	-	2.572
-10	548.6	-	-	635.16	15.78	725.17	32.19	2.572
-15	-	-	-	403.53	-	543.97	-	2.572
-20	347.5	-	-	303.69	12.61	461.70	32.86	2.572
-25	-	-	-	245.38	-	423.80	-	2.572
-30	-	-	-	207.84	-	358.42	-	2.572

Table 4.2
Transfer After 90 Degrees Change of Heading

Rudder Angle (degrees)	Tactical Diameter after 180 degrees Heading Change (m)							Approach Speed (m/s)
	Real Ship	Linear Model	Error %	Quasi- Linear Model	Error %	Non- Linear Model	Error %	
30	-	-472.14	-	-397.89	-	-709.11	-	7.717
25	-	-525.36	-	-443.34	-	-776.96	-	7.717
20	-850.4	-603.59	29.02	-509.03	40.14	-866.81	1.93	7.717
15	-	-733.76	-	-611.47	-	-989.70	-	7.717
10	-1325.9	-975.50	26.43	-772.61	41.73	-1171.93	11.61	7.717
5	-	1413.09	-	-1119.19	-	-1503.51	-	7.717
-5	2176.3	1413.09	35.07	-	-	2769.67	27.27	7.717
-10	1458.5	975.50	33.12	1326.42	9.06	1551.99	6.41	7.717
-15	-	733.76	-	864.57	-	1197.99	-	7.717
-20	1001.3	603.59	39.72	669.80	33.11	1009.16	0.78	7.717
-25	-	525.36	-	549.08	-	881.77	-	7.717
-30	-	472.14	-	477.47	-	791.86	-	7.717
30	-	-	-	-371.39	-	-699.87	-	2.572
25	-	-	-	-421.55	-	-767.84	-	2.572
20	-	-	-	-488.12	-	-858.31	-	2.572
15	-	-	-	-585.84	-	-976.92	-	2.572
10	-	-	-	-750.54	-	-1161.15	-	2.572
5	-	-	-	-	-	-1490.50	-	2.572
-5	-	-	-	-	-	2759.61	-	2.572
-10	1124.7	-	-	-	-	1541.78	37.08	2.572
-15	-	-	-	848.63	-	1188.72	-	2.572
-20	745.2	-	-	648.33	12.99	997.46	33.85	2.572
-25	-	-	-	530.79	-	872.47	-	2.572
-30	-	-	-	455.02	-	782.34	-	2.572

Table 4.3
Tactical Diameter After 180 Degrees Heading Change

Rudder Angle (degrees)	Steady-State Turn Diameter (m)							Approach Speed (m/s)
	Real Ship	Linear Model	Error %	Quasi- Linear Model	Error %	Non- Linear Model	Error %	
30	-	251	-	295	-	607	-	7.717
25	-	301	-	328	-	608	-	7.717
20	731.5	376	48.59	390	46.68	782	6.90	7.717
15	-	502	-	370	-	915	-	7.717
10	1202.4	752	37.46	510	57.58	1108	7.85	7.717
5	-	1505	-	843	-	1440	-	7.717
-5	2148.8	1505	29.96	-	-	2730	27.04	7.717
-10	1417.3	752	46.94	1210	14.63	1520	7.25	7.717
-15	-	502	-	770	-	1143	-	7.717
-20	964.7	376	61.02	586	39.26	940	2.56	7.717
-25	-	301	-	480	-	803	-	7.717
-30	-	251	-	423	-	702	-	7.717
30	-	-	-	222	-	588	-	2.572
25	-	-	-	272	-	661	-	2.572
20	-	-	-	355	-	759	-	2.572
15	-	-	-	392	-	896	-	2.572
10	-	-	-	-	-	1090	-	2.572
5	-	-	-	-	-	1425	-	2.572
-5	-	-	-	-	-	2710	-	2.572
-10	1133.9	-	-	-	-	1495	31.84	2.572
-15	-	-	-	764	-	1125	-	2.572
-20	722.4	-	-	547	24.28	922	27.63	2.572
-25	-	-	-	525	-	782	-	2.572
-30	-	-	-	434	-	681	-	2.572

Table 4.4
Steady-State Turn Diameter

Rudder Angle (degrees)	Final Forward Velocity (m/s)				Final Lateral Velocity (m/s)				Approach Speed (m/s)
	Real	Linear	Quasi- Linear	Non- Linear	Real	Linear	Quasi- Linear	Non- Linear	
	Ship	Model	Model	Model	Ship	Model	Model	Model	
30	-	7.717	2.571	4.868	-	0.494	1.821	1.011	7.717
25	-	7.717	2.901	5.156	-	0.412	1.816	0.994	7.717
20	5.196	7.717	3.356	5.478	1.137	0.329	1.793	0.966	7.717
15	-	7.717	4.010	5.839	-	0.247	1.728	0.921	7.717
10	6.585	7.717	4.977	6.245	0.921	0.165	1.569	0.851	7.717
5	-	7.717	6.323	6.711	-	0.083	1.198	0.734	7.717
-5	7.563	7.717	7.662	7.336	-0.468	-0.083	-0.319	-0.455	7.717
-10	6.894	7.717	6.954	6.708	-0.695	-0.165	-0.921	-0.709	7.717
-15	-	7.717	6.099	6.219	-	-0.247	-1.281	-0.827	7.717
-20	5.916	7.717	5.364	5.803	-0.818	-0.329	-1.489	-0.897	7.717
-25	-	7.717	4.776	5.439	-	-0.412	-1.614	-0.941	7.717
-30	-	7.717	4.307	5.119	-	-0.494	-1.694	-0.969	7.717
30	-	-	0.598	1.581	-	-	0.624	0.334	2.572
25	-	-	0.812	1.676	-	-	0.619	0.328	2.572
20	-	-	1.008	1.782	-	-	0.611	0.319	2.572
15	-	-	1.321	1.904	-	-	0.604	0.305	2.572
10	-	-	1.747	2.043	-	-	0.541	0.282	2.572
5	-	-	2.206	2.205	-	-	0.392	0.244	2.572
-5	-	-	2.559	2.432	-	-	-0.104	-0.151	2.572
-10	2.058	-	2.335	2.207	-0.746	-	-0.315	-0.236	2.572
-15	-	-	2.015	2.036	-	-	-0.443	-0.274	2.572
-20	1.749	-	1.727	1.894	-0.159	-	-0.505	-0.297	2.572
-25	-	-	1.512	1.772	-	-	-0.528	-0.311	2.572
-30	-	-	1.368	1.665	-	-	-0.534	-0.320	2.572

Table 4.5
Final Forward and Lateral Velocities

Rudder Angle (degrees)	Steady-State Yaw-Rate (Deg./s.)							
	Approach Speed 7.717 m/s.				Approach Speed 2.572 m/s.			
	Real Ship	Linear Model	Quasi- Linear Model	Non- Linear Model	Real Ship	Linear Model	Quasi- Linear Model	Non- Linear Model
25	-	-2.939	-1.481	-0.883	-	-	-0.489	-0.295
20	-	-2.351	-1.417	-0.817	-	-	-0.471	-0.273
15	-0.77	-1.763	-1.323	-0.714	-0.27	-	-0.438	-0.247
10	-0.68	-1.175	-1.166	-0.651	-0.24	-	-0.385	-0.217
5	-0.51	-0.588	-0.869	-0.534	-0.20	-	-0.292	-0.178
2.5	-0.39	-0.294	-0.639	-0.454	-0.17	-	-0.217	-0.152
0	-0.23	0	-0.359	-0.339	-0.125	-	-0.126	-0.114
-2.0	-0.1/0.19	-	-	-	-	-	-	-
-2.5	0.26	0.294	-0.058	-0.052	-0.01	-	-0.025	-0.019
-5	0.38	0.588	0.225	0.309	0.13	-	0.073	0.103
-10	0.54	1.175	0.659	0.512	0.19	-	0.224	0.170
-15	0.67	1.763	0.925	0.628	0.22	-	0.311	0.209
-20	0.74	2.351	1.089	0.716	0.235	-	0.363	0.238
-25	-	2.939	1.197	0.787	-	-	0.397	0.263
-20	0.74	2.351	1.090	0.716	0.235	-	0.364	0.238
-15	0.67	1.763	0.927	0.628	0.22	-	0.306	0.209
-10	0.54	1.175	0.659	0.512	0.17	-	0.215	0.170
-5	0.38	0.588	0.219	0.309	0.12	-	0.075	0.103
-2.5	0.26	0.294	-0.057	-0.052	0.09	-	-0.017	-0.017
0	0.18/-0.2	0	-0.357	-0.339	-0.05	-	-0.115	-0.114
2.5	-0.39	-0.294	-0.638	-0.454	-0.12	-	-0.209	-0.152
5	-0.51	-0.588	-0.869	-0.534	-0.16	-	-0.292	-0.178
10	-0.68	-1.175	-1.166	-0.651	-0.23	-	-0.385	-0.217
15	-0.77	-1.763	-1.323	-0.714	-0.27	-	-0.438	-0.247
20	-	-2.351	-1.417	-0.817	-	-	-0.471	-0.273
25	-	-2.939	-1.481	-0.883	-	-	-0.489	-0.295

Table 4.6
Dieudonne Spiral Manoeuvre

Force Terms in Steady-State Surge Equation				Force Terms in Steady-State Sway Equation			Moment Terms in Steady-State Yaw Equation		
Term	Force		Relative Importance	Term	Force %	Relative Importance	Term	Moment %	Relative Importance
	%	% Net Thrust							
$\bar{X}_{nn} n_A^2$	99.14	100	Major	mru	-62.2	Major	$N_{\delta} \delta_A$	63.5	Major
$X_{un} u_A$	-55.76		Major	Y_v	40.9	Major	$N_r r$	-46.9	Major
mrv	-16.98		Major	$Y_{\delta} \delta_A$	-35.5	Major	$N_{vv} v$	33.2	Major
$\bar{X}_{vv} v^2$	-8.54	-19.7	Major	$\bar{Y}_{rvv} rv^2$	28.3	Major	$\bar{N}_{rvv} rv^2$	-36.3	Major
$\bar{X}_{uuu} u^3$	-4.71	-10.86	Major	$Y_r r$	17.4	Major	$\bar{N}_{nn} n_A^2$	-9.7	Minor
$\bar{X}_{\delta\delta} \delta_A^2$	-4.70	-10.84	Major	$\bar{Y}_{nn} n_A^2$	5.4	Minor	$\bar{N}_{vvv} v^3$	-4.8	Negligible
$\bar{X}_{uu} u^2$	-5.56	-12.8	Major	$\bar{Y}_{vvv} v^3$	6.7	Minor	$\bar{N}_{\delta vv} \delta_A v^2$	3.3	Negligible
X_{uu}	-3.09	-7.1	Minor	$\bar{Y}_{\delta vv} \delta_A v^2$	-2.3	Negligible	$\bar{N}_{\delta\delta\delta} \delta_A^3$	-3.3	Negligible
$\bar{X}_{rr} r^2$	0.86	1.98	Negligible	$\bar{Y}_{\delta\delta\delta} \delta_A^3$	1.4	Negligible			

Major Importance 10-100%; Minor Importance 5-10%; Negligible Importance below 5%

Table 4.7
Important Hydrodynamic Coefficients

Surge Hydrodynamic Coefficients					Sway Hydrodynamic Coefficients			Yaw Hydrodynamic Coefficients		
Coefficient	Value			Dimensionalising Factor	Coefficient	Non-Dimensional Value	Dimensionalising Factor	Coefficient	Non-Dimensional Value	Dimensionalising Factor
	Non-Dimensional	Dimensional Model	Dimensional Full-Size Ship							
X_u	-	0.038462	76.1783	-	Y_{δ}'	0.0034178	$40L^2 u_r$	N_{δ}'	-0.0016011	$40L^3 u_r$
X_u'	-0.000426	-	-	$40L^3$	Y_v'	-0.0098675	$40L^2 u$	N_v'	+0.0043535	$40L^3 u$
\bar{X}_{uu}	-	-7.293782	-14446.16	-	Y_v'	-0.007583	$40L^3$	N_v'	-0.000230	$40L^4$
\bar{X}_{uuu}	-	-0.227298	-450.1888	-	Y_r'	0.0004926	$40L^3 u$	N_r'	-0.002143	$40L^4 u$
X_{un}	-	-0.040637	-39468.78	-	Y_r'	-0.0001368	$40L^4$	N_r'	-0.0006952	$40L^5$
X_a'	-0.015	-	-	$40L^2 u_A$	Y_a'	-0.087	$40L^2 u_A$	N_a'	-0.0026	$40L^3 u_A$
\bar{X}_{vv}'	-0.00617	-	-	$40L^2$	\bar{Y}_{vvv}'	-0.441178	$(40L^2)/U$	N_{uva}'	-0.00072	$40L^3$
$\bar{X}_{\delta\delta}'$	-0.00221	-	-	$40L^2 u^2$	\bar{Y}_{rvv}'	0.022934	$(40L^3)/U$	\bar{N}_{vvv}'	-0.0326335	$(40L^3)/U$
\bar{X}_{nn}	-	0.0011563	73339.8	-	$\bar{Y}_{\delta\delta\delta}'$	-0.0009569	$40L^2 u_r$	\bar{N}_{rvv}'	-0.047235	$(40L^4)/U$
								$\bar{N}_{\delta\delta\delta}'$	0.0007421	$40L^3 u_r$

Table 4.8
Hydrodynamic Coefficients for Car Ferry Hull 5502

CHAPTER 5

CONTROLLER DESIGN

5.1 Introduction

Control theory is a branch of applied mathematics devoted to the analysis and design of control systems. With the advent of the second world war, control engineering became a discipline in its own right due to the development of military systems designed on feedback control principles.

Classical control theory, based on the transfer function approach, owes much to the work of Nyquist (68) and Bode (69) in the frequency domain and Evans (70) in the s -plane. Such techniques have been in use since the late 1940's and early 1950's and are still employed in the design of many single input, single output systems. These methods were later extended to embrace non-linear systems via the describing function in the frequency domain and the phase-plane technique in the time domain. A further extension from continuous to discrete systems was effected with the development of z -transform operational methods. These latter techniques, together with matrix algebra, form the interface between classical and modern control theory.

The 1960's heralded the "state-space revolution" in control theory and provided the vehicle by which many advanced concepts could be investigated. Kalman (71) laid down the foundations of deterministic optimal control together with the maximum principle of

Pontryagin (72) and the dynamic programming method of Bellman (73). Towards the end of the decade the theory was expanded by Astrom (74) and others to include the effect of random disturbances and measurement errors, in the form of stochastic processes. About this time also there was a revived interest in frequency domain analysis as applied to multivariable systems, most notable being the Inverse Nyquist Array design method of Rosenbrock (75) based upon the concept of diagonal dominance.

During the 1970's there were further developments in frequency-response techniques, such as the sequential return difference method of Mayne (76). More recently work by MacFarlane and Postlethwaite (77) has extended the characteristics loci technique into a more generalised form by the use of Riemann surfaces to cover multivariable systems.

5.2. The Ship Control Problem

The essential features of a ship automatic pilotage control system are shown in Figure 5.1.

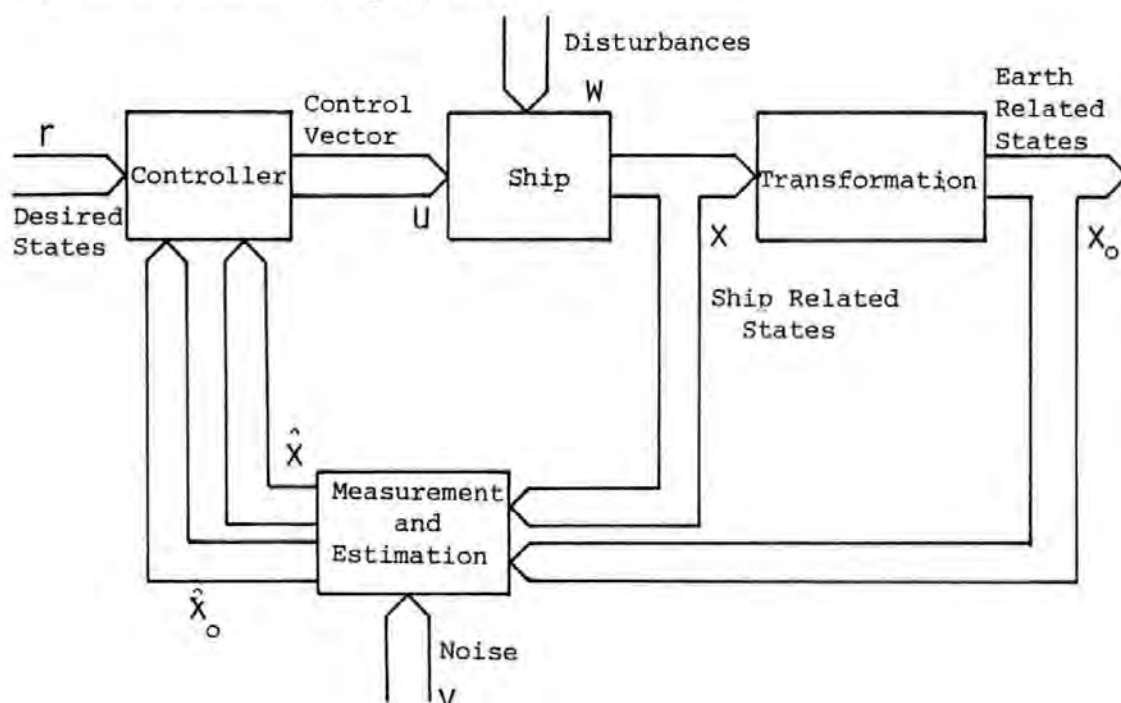


Figure 5.1

Ship Automatic Pilotage Control System

Single Input, Single Output Control

Minimises the error in a single variable such as heading or distance off track that has occurred due to changes in desired value or disturbance effects. The control action is taken without regard to its effect on any of the other system variables. Most existing commercial ship autopilots fall under this category.

Multivariable Control

Views the system in total and attempts to formulate a control policy that minimises the errors in all the state variables according to some predefined order of priority. Further, an optimal controller will seek to maximise the return from the system for a minimum cost.

In this chapter the design of a multivariable optimal controller is undertaken. An optimal control strategy is initially constructed under the assumption that the ship dynamics are linear and time-invariant. The effects of wind and current disturbances are then considered and finally the need for controller adaption, to accommodate the non-linear and time-variant characteristics of the real ship, is investigated.

5.3. Controllability and Observability

The concepts of controllability and observability were introduced by Kalman and play an important role in the control of multivariable systems. A system is controllable if a control vector $U(t)$ exists that will transfer the system from any initial state $X(t_0)$ to some desired state $X(t)$ in a finite time interval. If the state of the system can be determined by observation of the output over a finite time interval, the system is said to be observable. Work done by Dove (78) has demonstrated that in the context of this project all the states are observable. As a consequence, it can be

assumed that the controller will always receive a best estimate of the system states \hat{X} which, for initial design considerations, can be taken to be the values of the states themselves.

If a system is described by

$$\dot{X} = F X + G U \quad (5.1)$$

then a sufficient condition for complete state controllability is that the matrix

$$Q_c = \left[G \mid F G \mid \cdots \mid F^{n-1} G \right] \quad (5.2)$$

contains n linearly independent column vectors, i.e. is of rank n . A similar controllability matrix can be written in terms of the discrete state transition matrix A and control transition matrix B .

The F and G matrices for the full-size car ferry hull, moving in a straight line at a forward speed of 7.717 m/s are:

$$F = \begin{bmatrix} -0.5 & 0 & 0 & 0 & 0 & 0 & 0 & 0 \\ 0 & -0.5 & 0 & 0 & 0 & 0 & 0 & 0 \\ 0 & 0 & 0 & 1 & 0 & 0 & 0 & 0 \\ 0 & 0.0111 & 0 & -0.0091 & 0 & 0 & 0 & 0 \\ 0 & 0 & 0 & 0 & 0 & 1 & 0 & 0 \\ 0.1272 & 0 & 0 & 0 & 0 & -0.0306 & 0 & 0.3480 \\ 0 & 0 & 0 & 0 & 0 & 0 & 0 & 1 \\ -0.0047 & 0 & 0 & 0 & 0 & -0.0011 & 0 & -0.0840 \end{bmatrix} \quad (5.3)$$

From equation (5.2) the transpose of the controllability matrix may be constructed using equations (5.3) and (5.4).

$$G = \begin{bmatrix} 0.5 & 0 \\ 0 & 0.5 \\ 0 & 0 \\ 0 & 0 \\ 0 & 0 \\ 0 & 0 \\ 0 & 0 \\ 0 & 0 \end{bmatrix} \quad (5.4)$$

$$Q_c^T = \begin{bmatrix} 0.5 & 0 & 0 & 0 & 0 & 0 & 0 & 0 \\ 0 & 0.5 & 0 & 0 & 0 & 0 & 0 & 0 \\ -0.25 & 0 & 0 & 0 & 0 & 0.0636 & 0 & -0.00235 \\ 0 & -0.25 & 0 & 0.00554 & 0 & 0 & 0 & 0 \\ 0.125 & 0 & 0 & 0 & 0.0636 & -0.0346 & -0.00235 & 0.00130 \\ 0 & 0.125 & 0.0055 & -0.00282 & 0 & 0 & 0 & 0 \\ -0.0625 & 0 & 0 & 0 & -0.0346 & 0.0174 & 0.00130 & -0.00066 \\ 0 & -0.0625 & -0.00282 & 0.00141 & 0 & 0 & 0 & 0 \\ 0.03125 & 0 & 0 & 0 & 0.0174 & -0.0087 & -0.00066 & 0.00033 \\ 0 & 0.03125 & 0.0014 & -0.00071 & 0 & 0 & 0 & 0 \\ -0.0156 & 0 & 0 & 0 & -0.00871 & 0.00436 & 0.00033 & -0.00017 \\ 0 & -0.0156 & -0.00071 & 0.00035 & 0 & 0 & 0 & 0 \\ 0.00781 & 0 & 0 & 0 & 0.0044 & -0.0022 & -0.00017 & 0.00008 \\ 0 & 0.00781 & 0.0004 & -0.00018 & 0 & 0 & 0 & 0 \\ -0.00391 & 0 & 0 & 0 & -0.00218 & 0.00109 & 0.00008 & -0.00004 \\ 0 & -0.0039 & -0.00018 & 0.00009 & 0 & 0 & 0 & 0 \end{bmatrix} \quad (5.5)$$

The rank of the controllability matrix was determined using NAG routine F01BLF. This routine requires that for an $m \times n$ real matrix,

$m \geq n$, so the input to the routine was Q_c^T , which has the same rank as Q_c . Upon exit, the rank was computed as eight, i.e. equation (5.5) is non-singular and the system described by equation (5.1) with matrices (5.3) and (5.4) is fully state controllable.

5.4. Multivariable System Control

5.4.1. Stochastic Optimal Control

The problem of controlling a system with many inputs and outputs, which is subject to disturbances and measurement errors, such that the system's behaviour is optimised is referred to as stochastic optimal control.

The stochastic optimal control problem is to find a control U which causes the system

$$\dot{X} = g(X(t), U(t), W(t), t) \quad (5.6)$$

to follow an optimal trajectory $X(t)$ that minimises a performance criterion

$$J = \int_{t_0}^{t_1} h(X(t), U(t), t) dt \quad (5.7)$$

whilst being subjected to a measurement process

$$Z = f(X(t), V(t), t) \quad (5.8)$$

Separation Principle

This important feature of stochastic optimal control theory is illustrated in Figure 5.2. The separation principle allows a given optimisation problem to be reduced into two problems whose solutions are known, namely an optimal filter in cascade with a deterministic optimal controller. The filter design has been undertaken by Dove (78) and forms no part of the work described here.

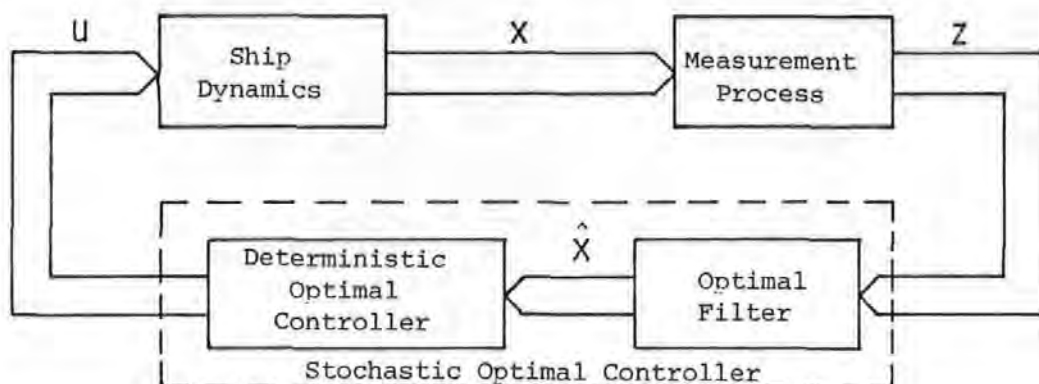


Figure 5.2

Separation Principle

5.4.2. Deterministic Optimal Control

Tracking Problem with Quadratic Performance Criterion

The tracking or servomechanism problem is one of applying a control U to drive a ship so that its states follow a desired trajectory in some optimal sense. The regulator problem is a special case of the tracking problem, the desired trajectory being a zero state.

Continuous Form

The quadratic criterion to be minimised is

$$J = \int_{t_0}^{t_1} \{ (X-r)^T Q (X-r) + U^T R U \} dt \quad (5.9)$$

where r is the desired value of the state vector. It can be shown (79) that constrained functional minimisation yields the matrix Riccati equations

$$\dot{W} = -W F - F^T W - Q + W G R^{-1} G^T W \quad (5.10)$$

The coefficients $W(t)$ are found by integration in reverse-time starting with the boundary condition:

$$W(t_1) = 0 \quad (5.11)$$

Should t_1 be infinite, or far removed from t_0 , the solutions of

$W(t)$ converge to constant values and the matrix Riccati equations may be written:

$$W F + F^T W + Q - W G R^{-1} G^T W = 0 \quad (5.12)$$

If the desired state vector r is known in advance, tracking errors may be reduced by allowing the system to follow a command vector m . This vector is obtained from the reverse-time differential equation set.

$$\dot{m} = (F - G R^{-1} G^T W)^T m - Q r \quad (5.13)$$

The boundary condition is:

$$m(t_1) = 0 \quad (5.14)$$

Inbuilt into vector m are all the system transient and steady-state errors for the desired state trajectory. This gives the optimal control law:

$$u_{opt} = -R^{-1} G^T (W X + m) \quad (5.15)$$

or,

$$u_{opt} = -(S X + R^{-1} G^T m) \quad (5.16)$$

where S is the optimal feedback gain matrix. An optimal controller for a tracking system is shown in Figure 5.3.

Discrete Form

The discrete quadratic performance criterion is:

$$J = \sum_{k=0}^{N-1} \{ (X(kT) - r(kT))^T Q (X(kT) - r(kT)) + U^T(kT) R U(kT) \} \quad (5.17)$$

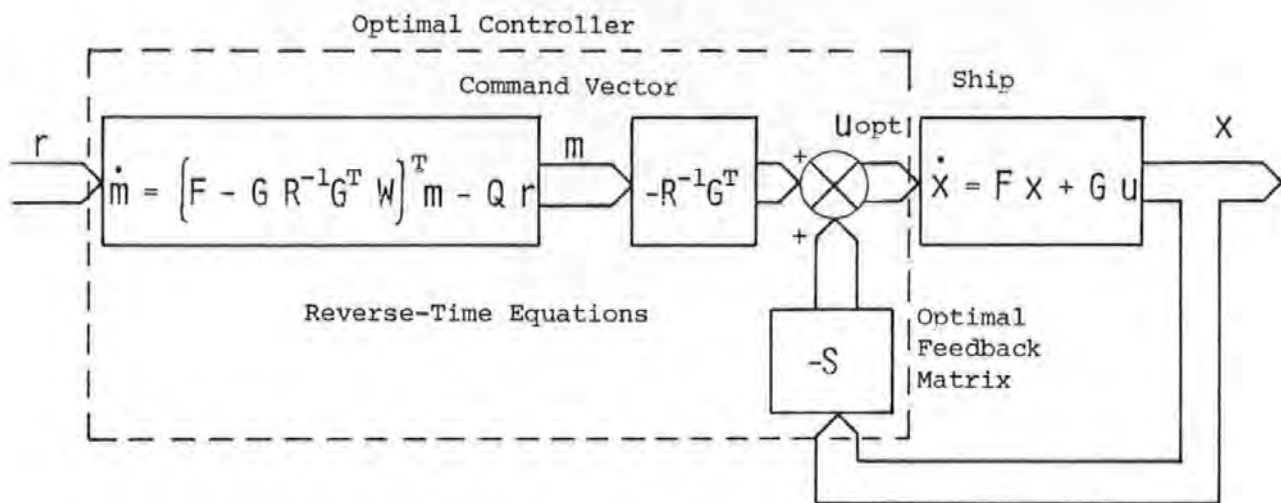


Figure 5.3

Optimal Controller For a Tracking System

Starting at the terminal boundary condition:

$$X^T(N-1)T W_0 X(N-1)T = 0 \quad (5.18)$$

the Riccati matrix W and the optimal feedback matrix S may be obtained from the set of recursive equations:

$$W(N-k)T = \{T Q + S^T(N-(k+1))T \cdot T R S(N-(k+1))T\} + \\ \{A - B S(N-(k+1))T\}^T W(N-(k+1))T \{A - B S(N-(k+1))T\} \quad (5.19)$$

where,

$$S(N-(k+1))T = \{T R + B^T W(N-(k+1))T B\}^{-1} B^T W(N-(k+1))T A \quad (5.20)$$

The command vector m is obtained from the difference equation:

$$m(N-k)T = D(T, kT) m(N-(k+1))T + E(T, kT) r(N-(k+1))T \quad (5.21)$$

having the boundary condition

$$m(N-1)T = 0 \quad (5.22)$$

producing the optimal control at time kT

$$U(kT)_{\text{opt}} = - S(N-(k+1))^T X(kT) - R^{-1} G^T m(N-(k+1))^T \quad (5.23)$$

or, if time kT is far removed from the terminal time $(N-1)T$

$$U(kT)_{\text{opt}} = S X(kT) - R^{-1} G^T m(N-(k+1))^T \quad (5.24)$$

5.5. Optimal Closed-Loop Pole Assignment

Consider the time-invariant continuous system described by the state equations

$$\dot{X} = F X + G U \quad (5.25)$$

together with an optimal control law:

$$U_{\text{opt}} = -R^{-1} G^T W X - R^{-1} G^T m \quad (5.26)$$

upon substitution of (5.26) into (5.25)

$$\dot{X} = (F - G R^{-1} G^T W) X - R^{-1} G^T m \quad (5.27)$$

or,

$$\dot{X} = (F - G S) X - R^{-1} G^T m \quad (5.28)$$

where the term $(F - GS)$ may be identified as the closed-loop state matrix of the optimal system. The optimal closed-loop eigenvalues (poles) are then given by:

$$| s I - (F - G S) | = 0 \quad (5.29)$$

It is apparent that when F and G are time-invariant the location of the optimal closed-loop poles depend upon the value of the feedback matrix S , which in turn is dependent upon weighting matrices Q and R . There exists then, an infinite number of closed-loop

poles, each being a measure of the optimality of the system as defined by relative weightings of Q and R .

Work has been undertaken by Kouvaritakis (80) and others in location of optimal closed-loop poles, particularly for the special condition:

$$Q = q_1 I$$

$$R = r_1 I \quad (5.30)$$

where I is the identity matrix and q_1 and r_1 two positive constants.

The weighting matrices Q and R are diagonal and of the form:

$$Q = \text{diag.}\{q_{11} \ q_{22} \ q_{33} \ q_{44} \ q_{55} \ q_{66} \ q_{77} \ q_{88}\}$$

$$R = \text{diag.}\{r_{11} \ r_{22}\} \quad (5.31)$$

Elements q_{11} and q_{22} are the rudder and main engines weightings and may be set at zero since the purpose of the control system is to employ the rudder and engines as control inputs, not as controlled variables. Surge dynamics are affected by variations in q_{33} and q_{44} together with r_{22} . The sway and yaw weightings are q_{55} , q_{66} and q_{77} , q_{88} respectively. Due to the coupling of sway and yaw, these elements, together with r_{11} closely interact, and changing any one value will affect all sway and yaw terms in the feedback matrix.

The Riccati matrix W and optimal feedback matrix S are calculated in reverse-time starting at the terminal boundary condition

as defined by equation (5.18). The recursive equations (5.19) and (5.20) are then employed to compute W and S , sufficient recursions being performed to allow steady-state convergence. These calculations take place in FORTRAN subroutine RICAL, a listing of which is given in Appendix A6.1.

When the optimal feedback matrix is known, the optimal closed-loop eigenvalues are given by equation (5.29). Variations in Q and R then will result in optimal trajectories being traced in the s -plane. These optimal root loci will always be stable, if a stable solution exists. The equations (5.30) cannot be used directly for the system under consideration since there are large differences of relative magnitude in individual elements. The alternative design procedure is to vary surge, sway and yaw weighting coefficients in turn, observing the effects on the optimal loci. Once relative weightings are established, overall scaling can then be used to position the final value of the optimal closed-loop poles.

If S is a null matrix then equation (5.29) provides the system open-loop poles, i.e. the eigenvalues of the F matrix defined in equation (5.3). When $u = 7.717$ m/s these are:

$$s = -0.5, -0.039, -0.0755, 0, 0, -0.5, 0, -0.00913 \quad (5.32)$$

Surge Weighting

Consider weighting matrices of the form:

$$\begin{aligned} Q &= \text{diag. } \{0 \quad 0 \quad q_{33} \quad 0 \quad 0 \quad 0 \quad 0 \quad 0\} \\ R &= \text{diag. } \{1 \quad 1\} \end{aligned} \quad (5.33)$$

Figure 5.4 shows the optimal trajectory as q_{33} is increased.

It is evident from Figure 5.4 that the surge open-loop eigenvalues are:

$$s = 0, -0.00913, -0.5$$

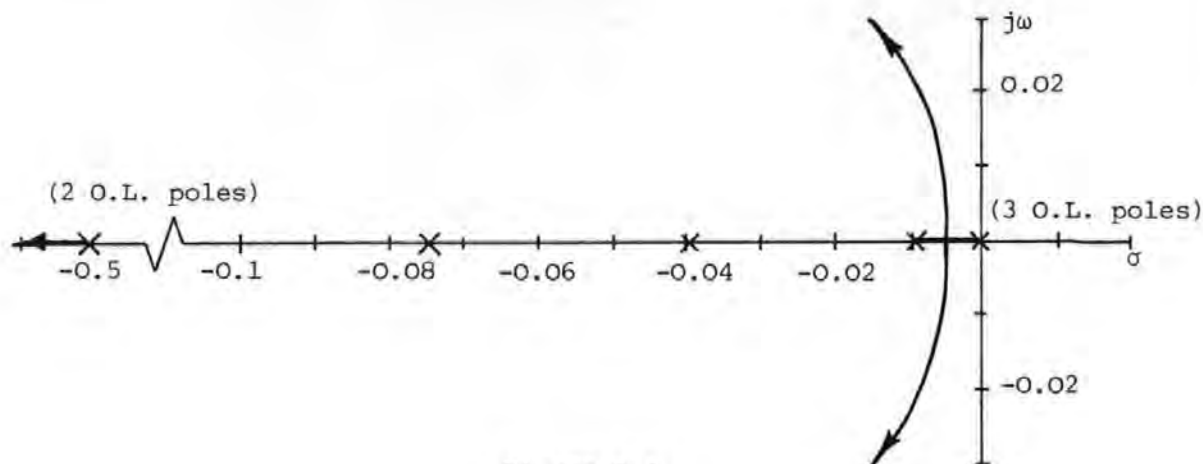


Figure 5.4

Surge Optimal Closed-Loop Pole Trajectories

The breakaway point occurs when q_{33} has a value of 0.000015 and values above 0.00005 produce excessive transient oscillation. This can be reduced by introducing the velocity term q_{44}

Sway Weighting

Here the weighting matrices become:

$$Q = \text{diag. } \{0 \quad 0 \quad 0 \quad 0 \quad q_{55} \quad 0 \quad q_{77} \quad 0 \quad 0\}$$

$$R = \text{diag. } \{1 \quad 1\}$$

(5.34)

With q_{77} maintained at a constant value of 0.1, Figure 5.5 illustrates the effect of increasing q_{55} .

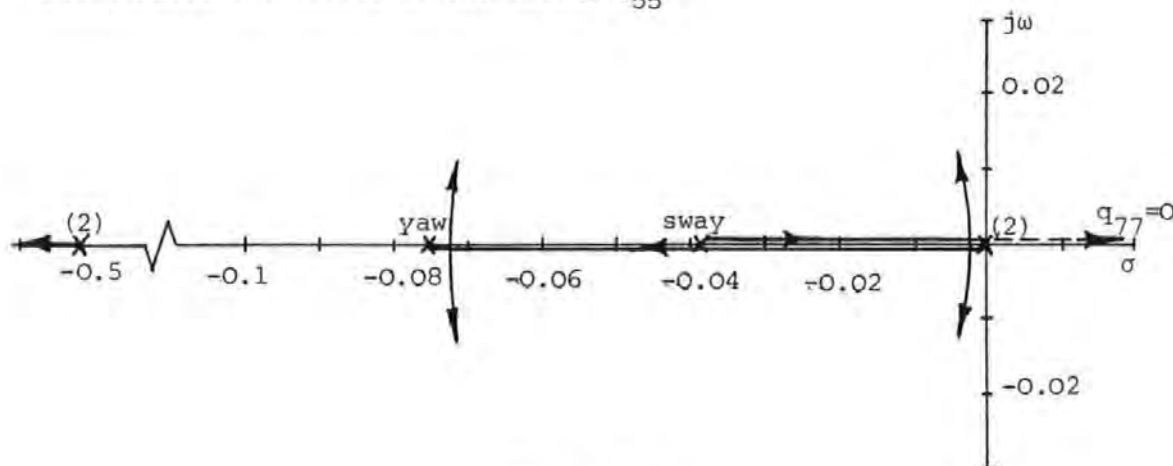


Figure 5.5

Effect of q_{55} on Sway and Yaw Optimal

Closed-Loop Pole Trajectories

It will be seen that the yaw loci breakaway is very close to the yaw open-loop pole and the sway breakaway point is almost at the origin. As an indication of the rate of travel along the real axis, when q_{55} is varied by a factor of 50 from 0.000001 to 0.00005 the sway locus moves from the open-loop pole of -0.039 to -0.0073. At the same time, the yaw locus, commencing at the origin, reaches a value of -0.059.

When q_{77} is set to zero the sway eigenvalue that approaches the origin is transferred to the right-hand side of the imaginary axis, producing a single unstable root. The consequence is that if the heading term s_{17} (that appears in the feedback matrix as a result of q_{77}) is zero, then no stable solution exists for the system as defined by the present set of state variables.

Yaw Weighting

The weighting matrices are:

$$\begin{aligned} Q &= \text{diag.} \{0 \quad 0 \quad 0 \quad 0 \quad 0 \quad 0 \quad q_{77} \quad 0\} \\ R &= \text{diag.} \{1 \quad 1\} \end{aligned} \quad (5.35)$$

The optimal trajectories are given in Figure 5.6.

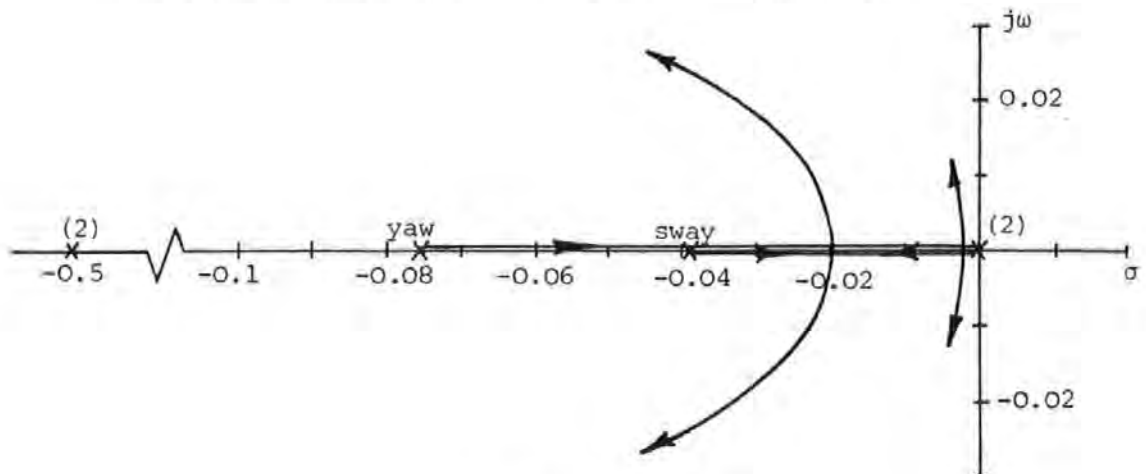


Figure 5.6

Effect of q_{77} on Sway and Yaw

Optimal Closed-Loop Pole Trajectories

The sway loci move quickly from their open-loop poles to breakaway at $q_{77} = 0.04$. Values of q_{77} above 0.5 produce undesirable transient oscillation. In contrast, the yaw loci move slowly from the open-loop pole positions, and, for example, at $q_{77} = 0.5$ the values are -0.0710 and 0.0 . This suggests the possibility of an open-loop zero in the vicinity of -0.07 .

Complete Optimal Root Locus Diagram

Having considered the effects of varying the individual elements of the Q matrix in order to obtain relative magnitudes, an overall scaling is now possible. Let Q and R be defined by:

$$\begin{aligned} Q &= q_1 \text{ diag.} \{0 \quad 0 \quad 0.00001 \quad 0.1 \quad 0.00001 \quad 0 \quad 0.2 \quad 0\} \\ R &= r_1 \text{ diag.} \{1 \quad 1\} \end{aligned} \quad (5.36)$$

Figure 5.7 shows the complete optimal root locus diagram as the ratio of q_1 to r_1 is increased.

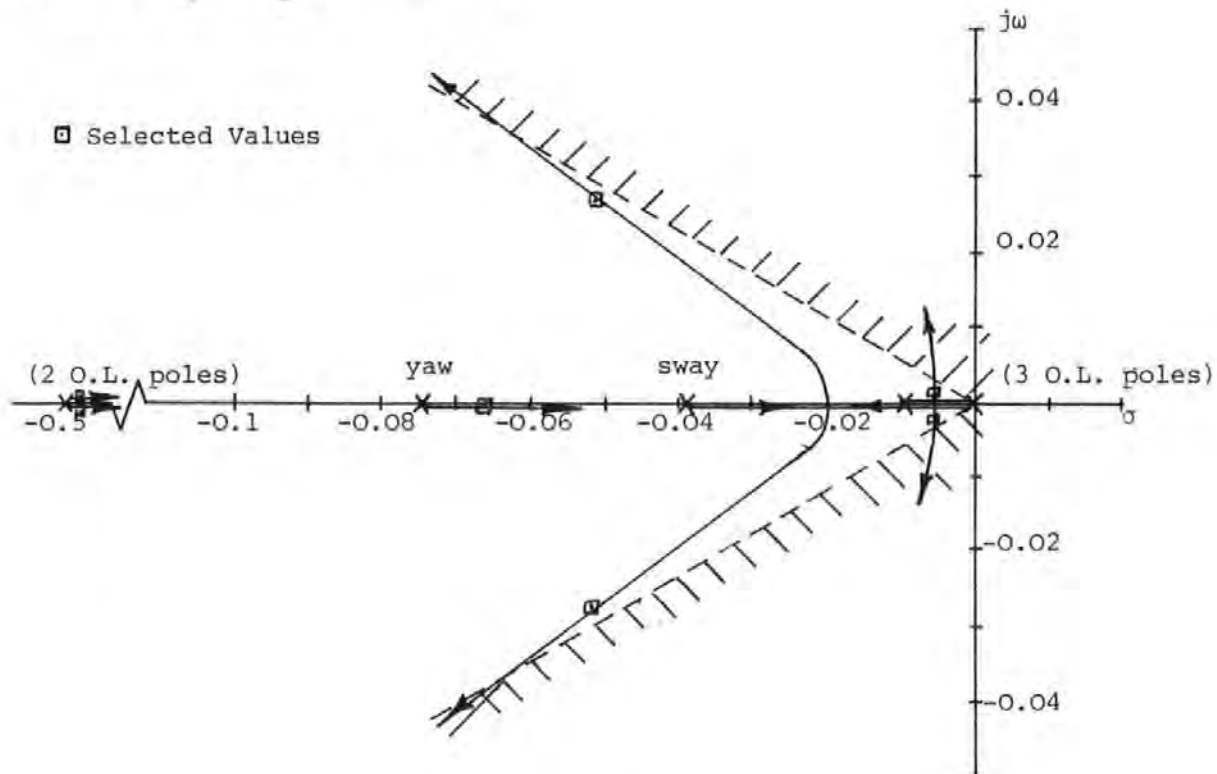


Figure 5.7

Complete Optimal Root Locus Diagram

The shaded area indicates the region of excessive transient oscillation and the ideal optimal closed-loop eigenvalues should lie outside this area and also as far to the left of the imaginary axis as possible. A set of eigenvalues that fulfill this requirement are:

$$s = -0.4990; -0.0516 \pm j0.0270; -0.0667; \\ -0.4999; -0.0086 \pm j0.0017; 0.0. \quad (5.37)$$

The associated weighting matrices are given in equations (5.36) where q_1 and r_1 are 5.0 and 1.0 respectively. When subroutine RICAL is used to compute S and W , their values become:

Optimal Feedback Matrix

$$S = \begin{bmatrix} 0.109 & 0 & 0 & 0 & -0.0013 & 0.1532 & -0.8419 & -8.047 \\ 0 & 0.0161 & 0.0069 & 0.729 & 0 & 0 & 0 & 0 \end{bmatrix} \quad (5.38)$$

Riccati Matrix

$$W = \begin{bmatrix} 0.237 & 0 & 0 & 0 & 0.0031 & 0.322 & -1.956 & -17.98 \\ 0 & 0.0326 & 0.0141 & 1.477 & 0 & 0 & 0 & 0 \\ 0 & 0.0141 & 0.0113 & 0.649 & 0 & 0 & 0 & 0 \\ 0 & 1.477 & 0.649 & 69.47 & 0 & 0 & 0 & 0 \\ 0.0031 & 0 & 0 & 0 & 0.095 & 1.57 & 2.99 & 42.05 \\ 0.322 & 0 & 0 & 0 & 1.57 & 26.36 & 47.67 & 677.5 \\ -1.956 & 0 & 0 & 0 & 2.99 & 47.67 & 123.2 & 1520.3 \\ -17.98 & 0 & 0 & 0 & 42.05 & 677.5 & 1520.3 & 20393.3 \end{bmatrix} \quad (5.39)$$

5.6 Disturbance Control

Conventional controllers employ integral control action to reduce steady-state disturbance errors. This is not possible under an optimal policy without affecting the closed-loop poles and an alternative method is active disturbance control. This technique,

used in dynamic positioning, relies upon knowledge of the disturbance model for the system in question. In the case of a ship it is the relationship between the instantaneous forces and moments acting upon the hull, and the disturbance variables. The existence of such a model allows prediction of hull forces and moments from measurement of disturbance variables (wind and current) and so makes possible the initiation of counteractive control action. Complete instantaneous force and moment cancellation can never be fully achieved due to the dynamics of the controls themselves. In addition, the control action available may not have sufficient flexibility to nullify the effect of all disturbances. For example, the deflection of a ship's rudder to balance the sway disturbance forces will not simultaneously balance yaw disturbance moments and so some form of compromise must be sought.

Equation (2.8) defines the disturbance vector W employed in the mathematical model. The disturbance elements of the augmented G matrix of equation (2.14) may be separated from the control elements and equation (2.15) may be written:

$$\dot{X}(t) = F X(t) + G U_{opt}(t) + G_d W(t) \quad (5.40)$$

When the disturbance control matrix G_c is included, the state equations become:

$$\dot{X}(t) = F X(t) + G U_{opt}(t) + G_d W(t) + G_c U_{dc}(t) \quad (5.41)$$

so that the complete control vector is now:

$$U(t) = U_{opt}(t) + U_{dc}(t) \quad (5.42)$$

Surge Disturbances

The surge forces due to current and wind may be extracted from equation (2.45).

$$X_c = -(X_u + \bar{X}_{uu} w(1) + \bar{X}_{uuu} w(1)^2) w(1) \quad (5.43)$$

$$X_w = -X_a w(3) \quad (5.44)$$

and the counteracting propeller thrust:

$$\begin{aligned} X_p &= \{X_{un} \sqrt{u^2 + v^2} + (\bar{X}_{nn} n_A^2)\} u_{dc}(2) \\ &= X_{pr} u_{dc}(2) \end{aligned} \quad (5.45)$$

so that,

$$u_{dc}(2) = \frac{X_c + X_w}{X_{pr}} \quad (5.46)$$

Yaw Disturbances

Again, from equation (2.45),

$$N_c = -\{N_v + \bar{N}_{rvv} r w(2) + \bar{N}_{vvv} w(2)^2 + \bar{N}_{\delta vv} A w(2)\} w(2) \quad (5.47)$$

$$N_w = -\{N_a + N_{uva} w(3)\} w(4) \quad (5.48)$$

and the rudder moment

$$N_r = - (N + \bar{N}_{\delta\delta\delta} \delta_A^2) u_{dc}(1)$$

$$N_{rd} = N_{rudd} u_{dc}(1) \quad (5.49)$$

giving,

$$u_{dc}(1) = \frac{N_c + N_w}{N_{rudd}} \quad (5.50)$$

Similar expressions exist for the sway equations but these were not employed since for good track-keeping performance, a moment balance is of prime importance if the vessel is not to wander from a desired track due to excessive yawing.

5.7 Adaptive Optimal Control

The optimal feedback matrix S described by equation (5.38) has been computed assuming the ship has linear time-invariant dynamics. In fact, reducing forward velocity has the effect of radically changing the system open-loop poles as shown in Figure 5.8.

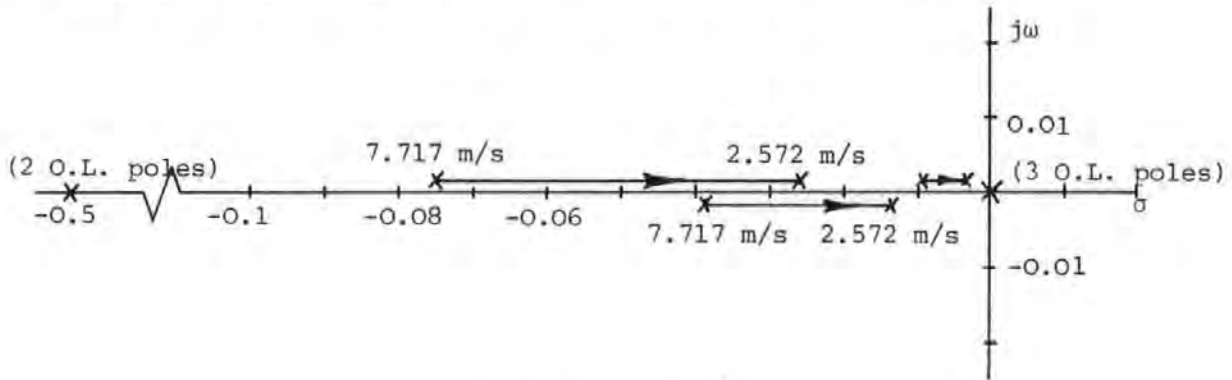


Figure 5.8

Effect of Forward Velocity

Reduction on Open-Loop Eigenvalues

The open-loop eigenvalues for $u = 2.572$ m/s are:

$$s = -0.5, -0.013, -0.0252, 0, 0, -0.5, 0, -0.00265 \quad (5.51)$$

These may be compared with those given in equation (5.32), which are for $u = 7.717$ m/s.

The system nonlinearities are most predominant when the vessel is executing a tight turn. Figure 5.9 indicates the open-loop eigenvalue variation during a 30 degree port turn, at an approach speed of 7.717 m/s.

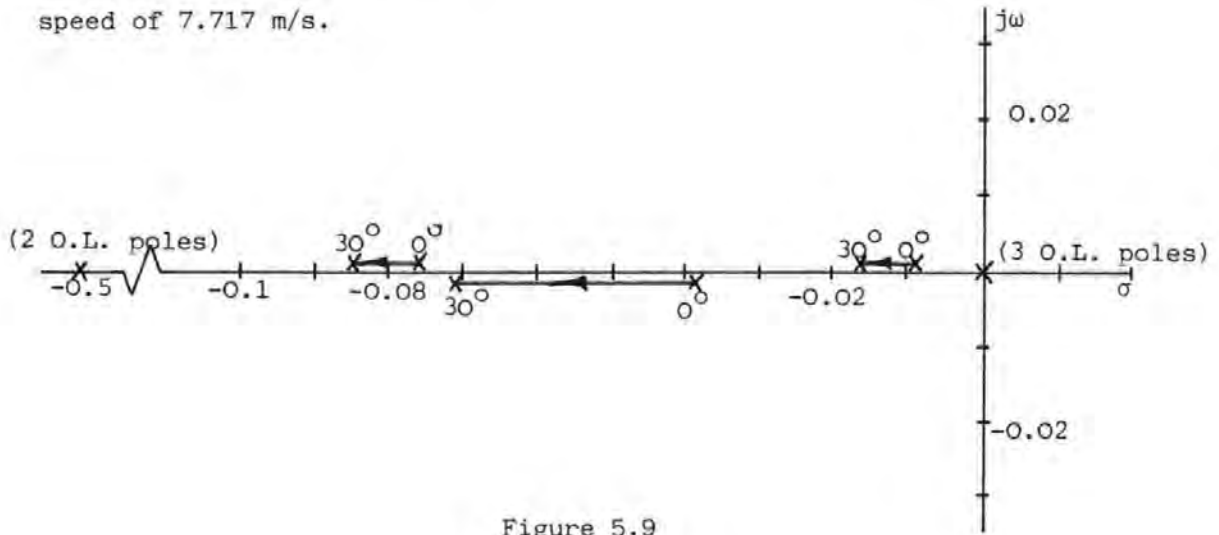


Figure 5.9
Effect of 30 Degree Port Turn
on Open-Loop Eigenvalues

When the feedback matrix S given in equation (5.38) is time-invariant during a forward speed reduction from 7.717 to 2.572 m/s, the closed-loop eigenvalues depart from their optimal positions in the manner shown in Figure 5.10.

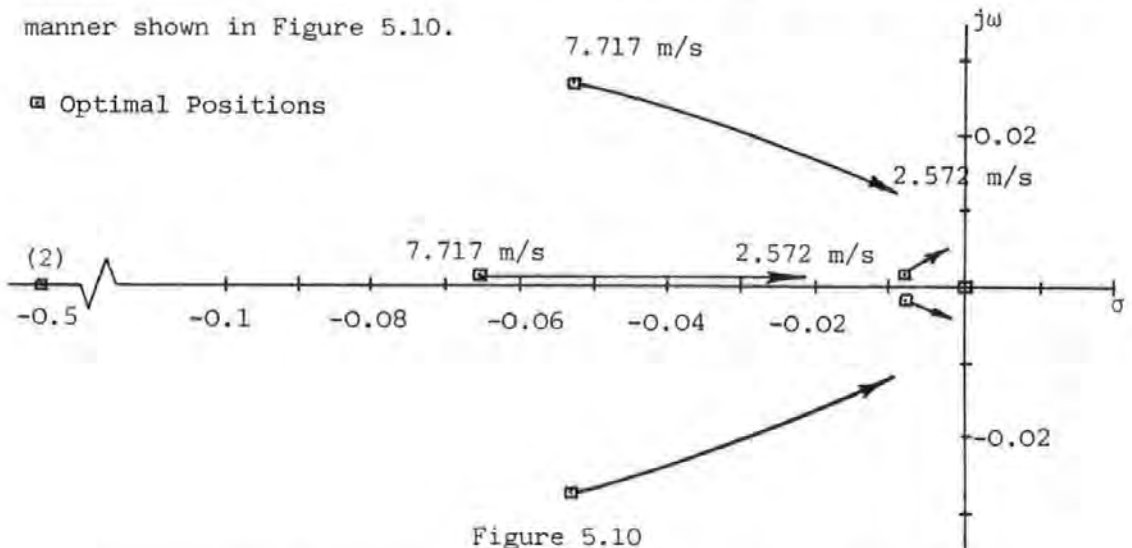


Figure 5.10
Departure of Closed-Loop Eigenvalues from Optimal Positions
During a Speed Reduction

In contrast, the variation in closed-loop eigenvalues during a tight turn is relatively small as can be seen in Figure 5.11 which shows the eigenvalue change during a 30 degree port turn with an approach speed of 7.717 m/s.

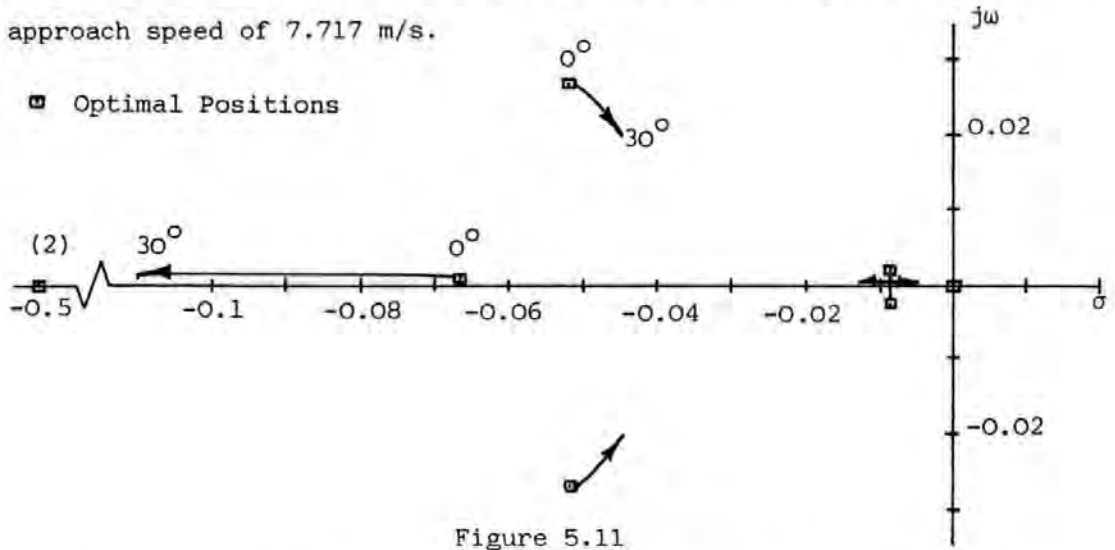


Figure 5.11

Departure of Closed-Loop Eigenvalues from Optimal Positions
During a 30 Degree Port Turn.

It is evident from Figure 5.11 that for turning manoeuvres, controller adaption is unnecessary. Forward speed variations, however, produce large changes in closed-loop eigenvalues as seen in Figure 5.10, such that at speeds below 2.5 m/s, the system is tending towards instability. Under these conditions an adaptive control strategy becomes very necessary to restore the closed-loop poles to their originally assigned optimal positions.

Let the closed-loop system matrix be defined by:

$$F_c = \left(F - G S \right) \quad (5.52)$$

If F_c has a constant known value when F is varying with time, the adaptive feedback matrix is:

$$S(t) = G^{-1} \left(F(t) - F_c \right) \quad (5.53)$$

Equation (5.53) only has a solution when G^{-1} exists which requires that G be a square matrix.

An alternative approach is to re-calculate the feedback matrix at different forward speeds with Q and R held at the values given in equation (5.36), q_1 and r_1 being 5.0 and 1.0 respectively. This technique does not maintain a fixed closed-loop pole array, and Figure 5.12 indicates the extent of variation as the forward speed is reduced from 7.717 to 2.572 m/s.

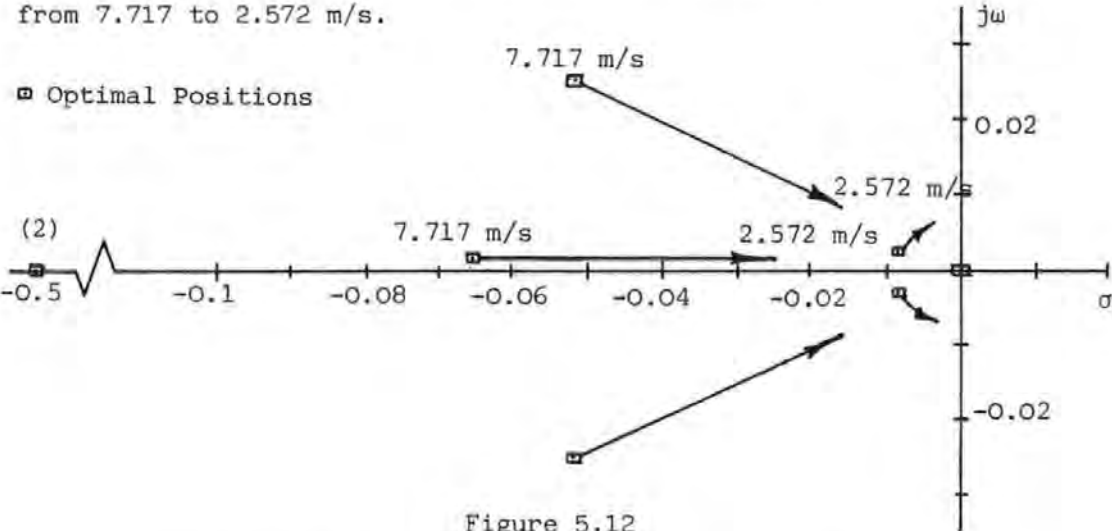
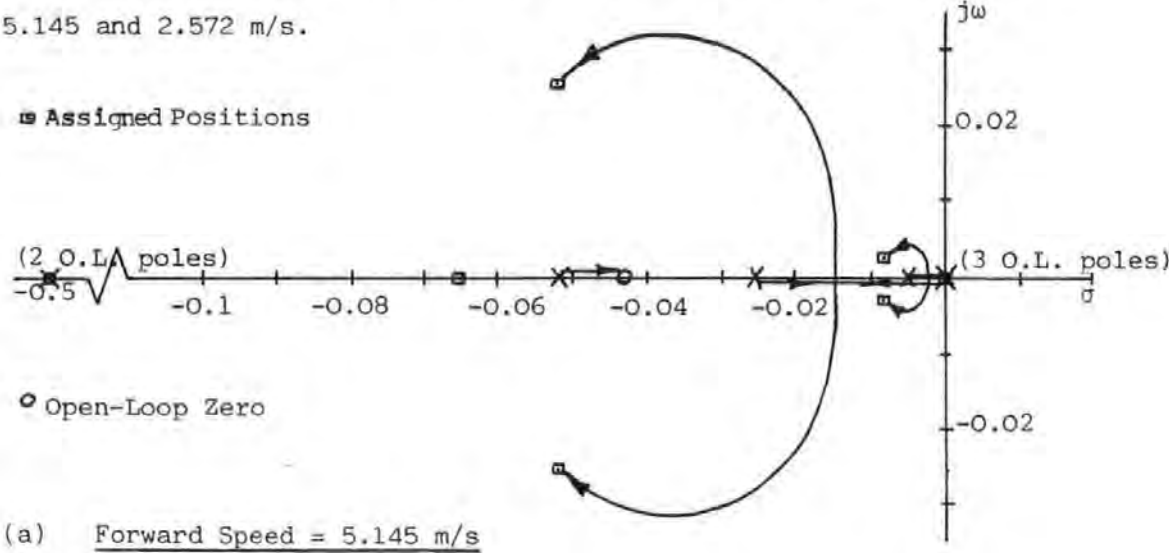


Figure 5.12
Variation in Closed-Loop Poles During a Speed Reduction
Feedback Matrix Re-calculated with Constant Q and R .

Figure 5.13(a) and (b) show the optimal root loci for speeds of 5.145 and 2.572 m/s.



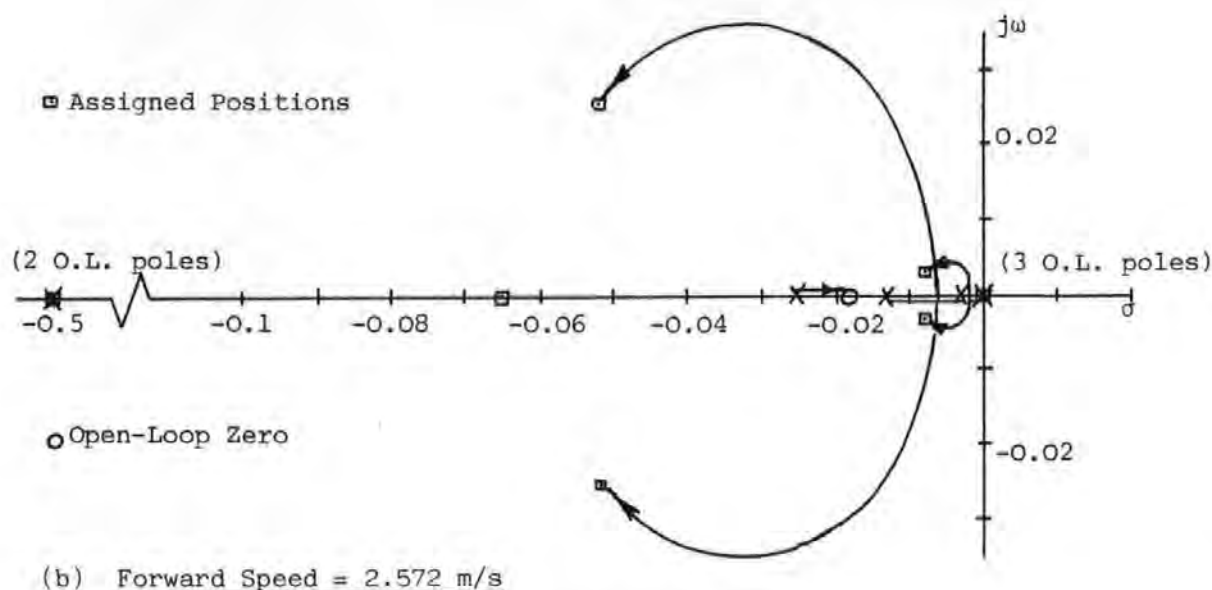


Figure 5.13

Optimal Root Locus Diagrams for Forward Speeds
of 5.145 and 2.572 m/s

The complex loci can be re-positioned to their original optimal values by increasing the $q_1 - r_1$ ratio together with q_{88} . Notice that in both cases the real axis locus does not depart far from the sway open-loop pole. This is also evident in Figure 5.7 and is indicative of the presence of an open-loop zero, as first suspected during the variation of individual matrix elements. The validity of this statement is supported by the Nomoto equation (2.19) which identifies the existence of an open-loop zero $\frac{1}{T_3}$. For the 5502 hull travelling at 7.717 m/s, $\frac{1}{T_3}$ has a value of -0.0611 and, as it lies just to the left of the open-loop sway pole in Figure 5.7, is the reason for the short real axis locus. The open-loop poles and zeros retain their relative positions on the real axis as the forward speed is varied. At low speeds then, adaptive control action will return the complex loci to their original optimality, but the real axis locus will be attracted to the system open-loop zero. Other finite but unknown real

open-loop zeros may be introduced by increasing the rate coefficients q_{44} , q_{66} and q_{88} in the Q matrix.

Adaptive Matrices, $u = 5.145$ m/s

The Q , R and S matrices to return the complex loci to their original ($u = 7.717$ m/s) positions are:

$$\begin{aligned} Q &= \text{diag.} \{0 \ 0 \ 0.00005 \ 0.5 \ 0.00005 \ 0.1 \ 100\} \\ R &= \text{diag.} \{0.2 \ 0.2\} \\ S &= \begin{pmatrix} 0.135 & 0 & 0 & 0 & -0.0029 & 0.3292 & -1.810 & -25.963 \\ 0 & 0.0267 & 0.0153 & 1.912 & 0 & 0 & 0 & 0 \end{pmatrix} \end{aligned} \quad (5.54)$$

which produce the closed-loop eigenvalue set:

$$\begin{aligned} s &= -0.4988; -0.0527 \pm j \ 0.0276; -0.0397; \\ &-0.4999; -0.0095 \pm j \ 0.0041; \ 0.0 \end{aligned} \quad (5.55)$$

Adaptive Matrices, $u = 2.572$ m/s

$$\begin{aligned} Q &= \text{diag.} \{0 \ 0 \ 0.00005 \ 0.5 \ 0.00005 \ 0 \ 1 \ 200\} \\ R &= \text{diag.} \{0.01 \ 0.01\} \\ S &= \begin{pmatrix} 0.175 & 0 & 0 & 0 & -0.0121 & 1.035 & -7.596 & -160.26 \\ 0 & 0.0553 & 0.0658 & 8.437 & 0 & 0 & 0 & 0 \end{pmatrix} \end{aligned} \quad (5.56)$$

with the closed-loop eigenvalues:

$$\begin{aligned} s &= -0.4982; -0.0539 \pm j \ 0.0273; -0.0196 \\ &-0.4998; -0.01876 \pm j \ 0.01167; \ 0.0 \end{aligned} \quad (5.57)$$

Figures 5.14(a) and (b) show to what extent the elements of the feedback matrix adapt to changes in forward speed. It can be seen that in general, the adaption is inversely proportional to the square

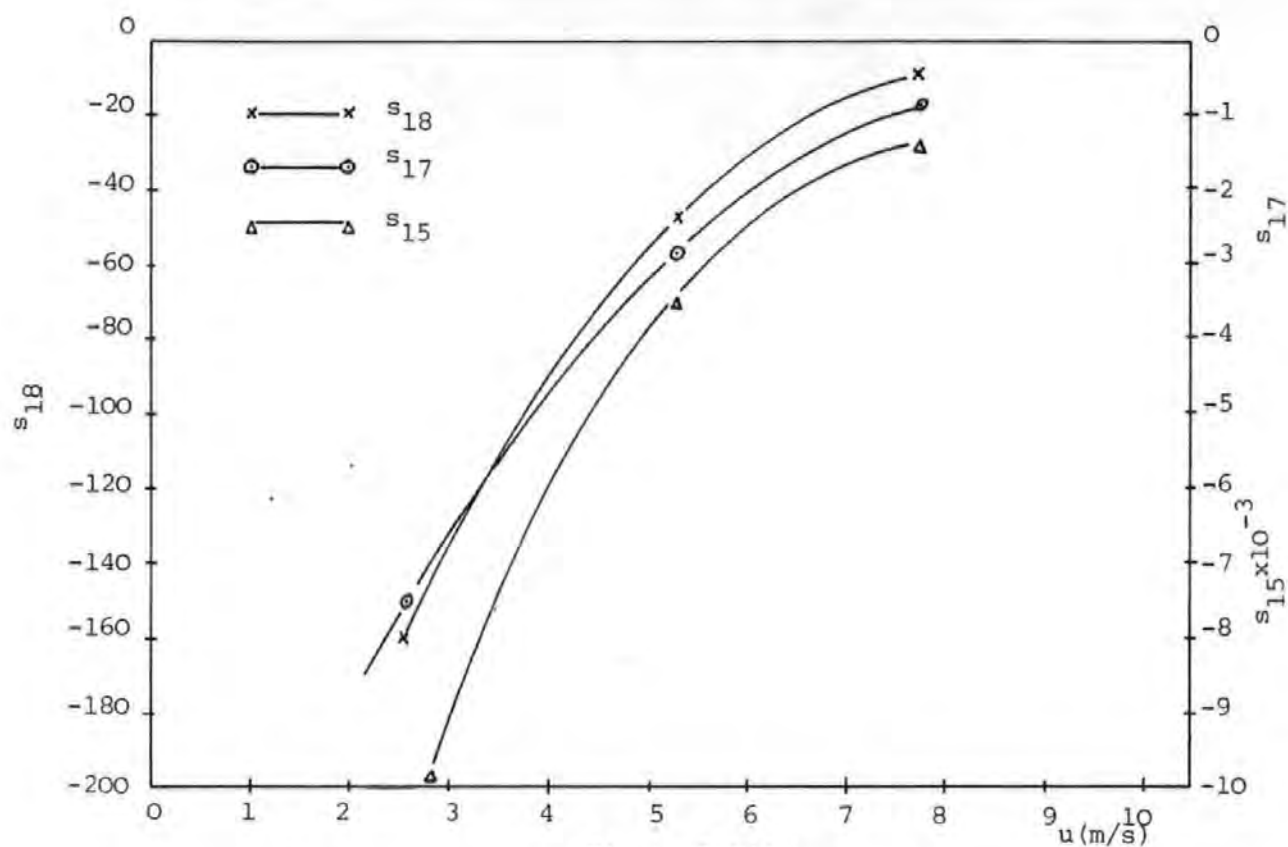


Figure 5.14(a)

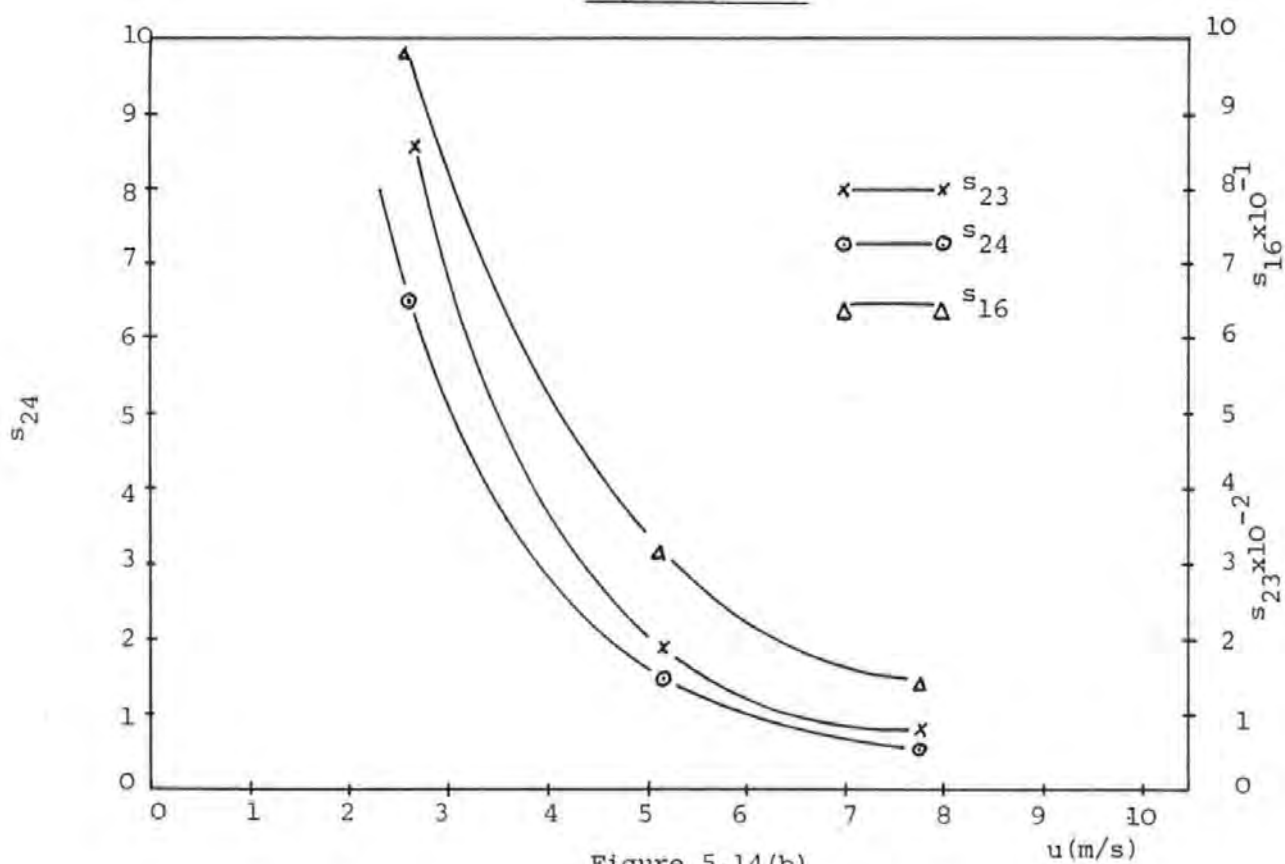


Figure 5.14(b)

Feedback Matrix Adaption to Changes in Forward Speed

of forward velocity. The adaptive equation set are:

$$\begin{aligned}s_{15} &= -0.08 u^{-2.0} \\s_{16} &= 6.0 u^{-1.8} \\s_{17} &= -50.0 u^{-2.0} \\s_{18} &= -2090.0 u^{-2.72} \\s_{23} &= 0.418 u^{-2.0} \\s_{24} &= 67.65 u^{-2.2}\end{aligned}\tag{5.58}$$

When expressed in this manner, the control algorithm is in the form of a "gain scheduling controller".

CHAPTER 6

CONTROLLER PERFORMANCE

6.1 Introduction

Having established a range of optimal controller feedback parameters, it becomes necessary to assess the effectiveness of the system under operational conditions in terms of (a) stability, (b) accuracy and (c) integrity. This chapter presents a computer simulation study of the automatic guidance of the full-size 5502 car ferry into Plymouth Sound whilst under an optimal control policy.

The control strategies considered are:

- (a) Ship related state variable feedback with reverse-time integration.
- (b) Ship related state variable feedback with dual-mode control and way-point anticipation.
- (c) Ship and earth related state variable feedback for dynamic position-keeping.

Generalised performance indices are employed to select the best policy and also to measure the degradation of system performance under:

- (i) adverse wind and tide conditions,
- (ii) variable forward speed adaption.

6.2. Desired State Trajectories

The recommended track for deep draught vessels into Plymouth Sound has been used as a basis for computing the desired value of the state variables. The track commences at a point 2,500 m south, 1000 m west of the breakwater lighthouse and, for the purpose of simulation, is assumed to consist of four straight-line elements as illustrated in Figure 6.1.

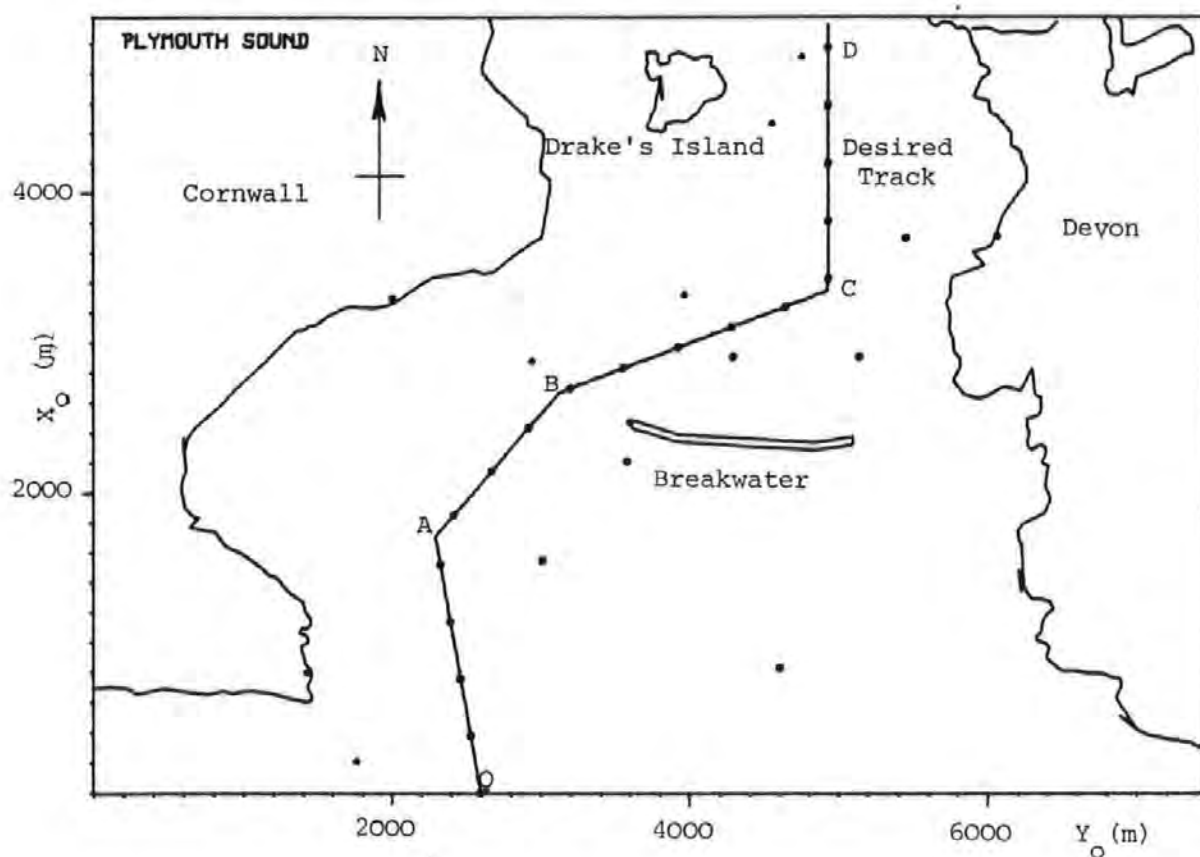


Figure 6.1

Desired Track Into Plymouth Sound

The desired headings and element intersections (way-points) are given in Table 6.1.

Element	Desired Heading (radians)	Way-Point	Co-ordinates Y _o , X _o (metres)
OA	-0.173076	O	2590.0, 0.0
AB	0.7135	A	2291.0, 1710.4
BC	1.209397	B	3124.3, 2673.1
CD	0.0	C	4928.9, 3355.2

Table 6.1

Desired Headings and Way-Points

6.3. Ship Related State Variable Feedback

The desired state vector relates to the ship co-ordinate system:

$$\mathbf{r}^T = (\delta_D, n_D, x_D, u_D, y_D, v_D, \psi_D, r_D) \quad (6.1)$$

Once the earth related state vector \mathbf{r}_o has been defined at $t = 0$, the remaining computations are performed with respect to the ship axes, as shown in Table 6.2.

$t = 0$

$$\mathbf{r}_o = \begin{pmatrix} x_{oD} \\ u_{oD} \\ y_{oD} \\ v_{oD} \end{pmatrix} = \begin{pmatrix} 0.0 \\ 7.602 \\ 2590.0 \\ -1.329 \end{pmatrix}$$

Tsamp = 5 seconds

kT (seconds)	x_D (metres)	u_D (m/s)	y_D (metres)	v_D (m/s)	ψ_D (radians)	r_D (rad/s)
0	0	7.717	0	0	-0.173076	0
5	38.585	7.717	0	0	-0.173076	0
10	77.17	7.717	0	0	-0.173076	0
15	115.755	7.717	0	0	-0.173076	0
20	154.34	7.717	0	0	-0.173076	0
etc.						

Table 6.2

Desired State Vector

Determination of Track Error

The lateral motion state variable y is not a measure of the track error, which may be obtained using the co-ordinate transformation shown in Figure 6.2.

Let the desired track at the i^{th} way-point be inclined at the desired heading angle $\psi_D(i)$ and assume that the vessel's position y_o , x_o on the earth's co-ordinate system is known. The position of the ship relative to co-ordinate system y_t, x_t , with origin at way-point $y(i)$, $x(i)$ is given by:

$$y_t = (y_o - y(i)) \cos \psi_D(i) - (x_o - x(i)) \sin \psi_D(i)$$

$$x_t = (x_o - x(i)) \cos \psi_D(i) + (y_o - y(i)) \sin \psi_D(i) \quad (6.2)$$

where y_t is the perpendicular distance off track and x_t the parallel distance travelled by the ship from the way-point.

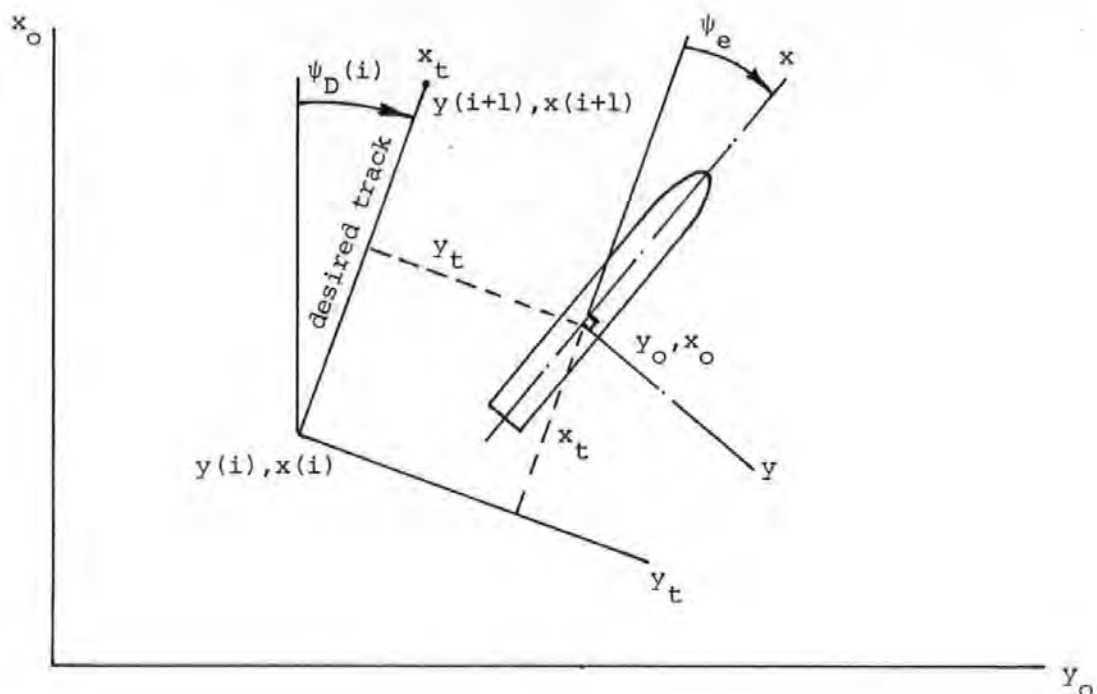


Figure 6.2

Co-ordinate Transformation

6.3.1. Reverse-Time Integration

This technique requires the generation of a reverse-time command vector \mathbb{M} using the difference equation (5.21) prior to the commencement of the simulation run. The controller details (weighting matrices) for each simulation are given in Table 6.3.

So that an overall comparison can be made, a set of generalised performance indices may be defined:

$$J_x = \int_{t_0}^{t_1} (x_D - x)^2 dt$$

$$J_u = \int_{t_0}^{t_1} (u_D - u)^2 dt$$

$$J_y = \int_{t_0}^{t_1} (y_D - y_t)^2 dt$$

$$J_\psi = \int_{t_0}^{t_1} (\psi_D - \psi_A)^2 dt$$

Run	Q MATRIX								R MATRIX	
No.	q ₁₁	q ₂₂	q ₃₃	q ₄₄	q ₅₅	q ₆₆	q ₇₇	q ₈₈	r ₁₁	r ₂₂
u = 7.717 m/s. Without Disturbances.										
1	0	0	0.5E-4	0	0	0	0.1	0	1	1
2	0	0	0.8E-4	0	0	0	0.5	0	0.1	1
3	0	0	0.8E-4	0	0	0	0.5	0	0.1	1
4	0	0	0.8E-4	0	0	0	0.5	0	0.1	1
5	0	0	0.5E-4	0.5	0.5E-4	0	1	0	1	1
6	0	0	0.5E-4	0.5	0.5E-4	0	1	0	1	1
7	0	0	0.5E-4	0.5	0.5E-4	0	1	0	1	1
8	0	0	0.5E-4	0.5	0.5E-4	0	1	0	1	1
u = 7.717 m/s. Including Disturbances.										
9	0	0	0.5E-4	0.5	0.5E-4	0	1	0	1	1
10	0	0	0.5E-4	0.5	0.5E-4	0	1	0	1	1
11	0	0	0.5E-4	0.5	0.5E-4	0	1	0	1	1
u = 5.145 m/s.										
12	0	0	0.5E-4	0.5	0.5E-4	0	1	0	1	1
13	0	0	0.5E-4	0.5	0.5E-4	0	1	0	1	1
14	0	0	0.5E-4	0.5	0.5E-4	0	1	100	0.2	0.2
u = 2.572 m/s.										
15	0	0	0.5E-4	0.5	0.5E-4	0	1	0	1	1
16	0	0	0.5E-4	0.5	0.5E-4	0	1	0	1	1
17	0	0	0.5E-4	0.5	0.5E-4	0	1	200	0.01	0.01
18	0	0	0.5E-4	0.5	0.5E-4	0	1	0	1	1
19	0	0	0.5E-4	0.5	0.5E-4	0	1	0	1	1

Table 6.3

Controller Settings

$$J_{\delta} = \int_{t_0}^{t_1} \delta_A^2 dt$$

$$J_n = \int_{t_0}^{t_1} n_A^2 dt \quad (6.3)$$

Table 6.4 lists the values of the performance indices for each simulation run, these being a representative selection of the many runs performed at the controller selection stage.

Figure 6.3(a), (b) and (c) shows simulations 1, 2 and 3 and illustrates the effect of increasing the heading weighting. It can be seen from Figure 6.3(b) that raising the weighting level increases the steady-state heading error. This error arises from the steady-state solution of equation (5.13):

$$\{(F - GS)^T\}^{-1} Q r = W x \quad (6.4)$$

when $x = r$,

$$\{(F - GS)^T\}^{-1} Q = W \quad (6.5)$$

These errors will be avoided if the command vector is adjusted according to equation (6.4). Simulation 3 shown in Figure 6.3(c) is a re-run of simulation 2 with the necessary corrections made.

6.3.2. Dual-Mode Control with Way-Point Anticipation

Way-point anticipation is a simple concept that allows the command equations (5.13) to be removed, thus reducing the optimal controller given in Figure 5.3 to the form shown in Figure 6.4.

Run	PERFORMANCE INDICES					
No.	J_x	J_u	J_y	J_ψ	J_δ	J_n
	u = 7.717 m/s. Without Disturbances.					
1	7.19E6	207.36	64.94E6	38.61	1.157	39.19E3
2	8.85E6	213.48	348.86E6	205.18	33.03	41.08E3
3	11.43E6	229.61	14.64E6	10.62	11.56	40.23E3
4	0.27E6	181.61	29.78E6	67.72	21.20	37.72E3
5	0.437E6	170.91	8.72E6	85.45	16.59	37.85E3
6	0.224E6	157.42	0.797E6	74.09	12.28	37.33E3
7	4.63E6	174.68	10.34E6	87.32	17.64	37.96E3
8	1.416E6	163.51	0.81E6	74.83	12.46	37.67E3
	u = 7.717 m/s. Including Disturbances.					
9	0.574E6	166.32	6.00E6	87.56	35.23	38.23E3
10	0.529E6	161.42	0.959E6	72.68	35.27	38.00E3
11	0.604E6	165.54	1.17E6	75.44	33.56	38.05E3
	u = 5.145 m/s.					
12	0.266E6	19.67	1.61E6	107.88	24.36	24.27E3
13	0.167E6	12.70	1.35E6	103.77	20.51	24.10E3
14	0.063E6	10.97	1.51E6	99.18	32.12	24.28E3
	u = 2.572 m/s.					
15	0.479E6	10.77	2.65E6	306.5	72.13	12.06E3
16	0.129E6	4.475	1.15E6	189.33	45.48	11.67E3
17	0.024E6	37.00	1.43E6	160.15	129.80	12.30E3
18	3.82E6	54.31	113.13E6	413.87	434.06	14.17E3
19	18.41E6	182.02	20.21E6	323.81	543.85	14.51E3

Table 6.4

Generalised Performance Indices

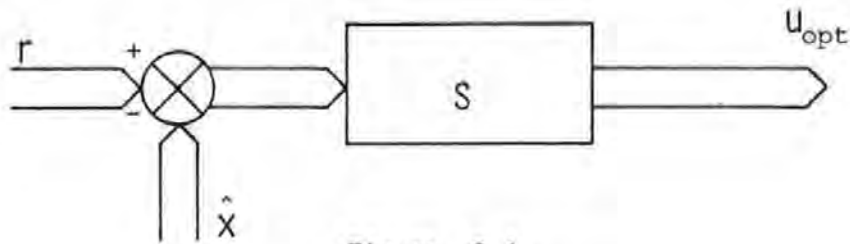


Figure 6.4

Optimal Control Without Command Equations

Here, the control equation (5.16) is now replaced by:

$$u_{opt} = S (r - \hat{x}) \quad (6.6)$$

It will be appreciated that equation (6.6) contains no anticipatory terms and simulations 4 and 5, shown in Figure 6.5(a) and (b) illustrate the transient overshoot effect on (i) heading weighting (ii) track-keeping weighting.

The turning circle manoeuvres described in Chapter 4 indicate the amount of advance 'A' that can be expected during a 90 degree turn for given rudder angles and approach speeds. Figure 4.3 shows that for large rudder angles the advance is reasonably independent of approach speed. This suggests that if a vessel is changing from track angle ψ_{DA} to ψ_{DB} , and the motion is assumed to form an arc of a circle of radius A_v , the way-point advance (the distance from the way-point that the rudder order has to be executed) to avoid overshoot is given by:

$$A_{wp} = A_v \sin (\psi_{DB} - \psi_{DA}) \quad (6.7)$$

Figure 6.6 shows a vessel initially on track and course that has reached an advanced way-point.

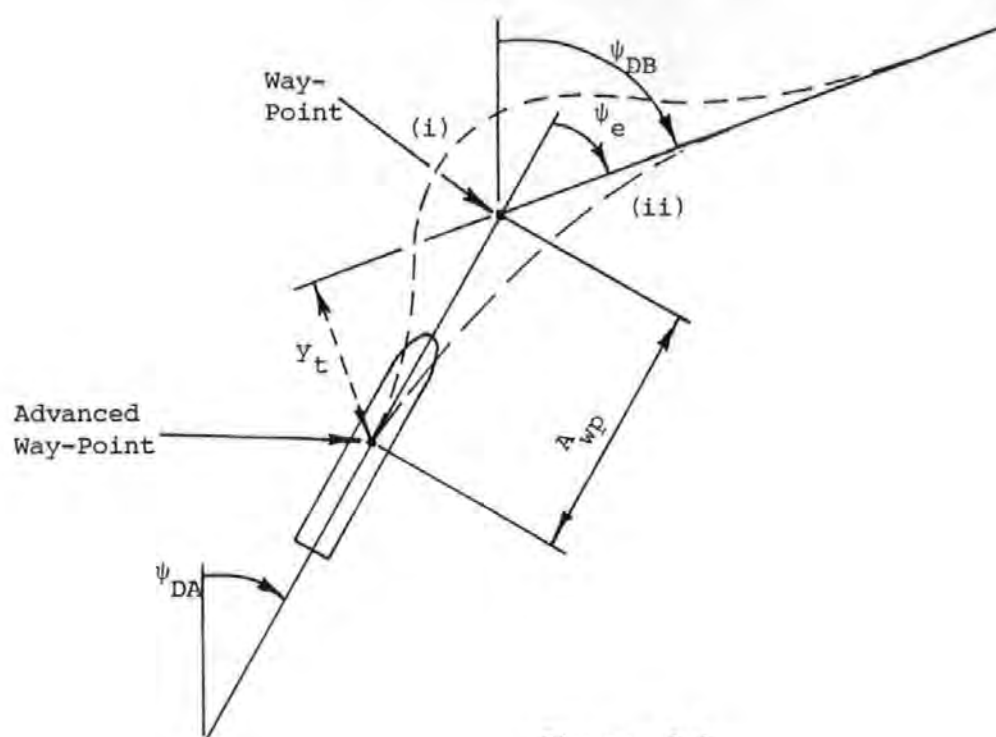


Figure 6.6

Way-Point Advance

If the instruction is now given to track the new segment, the controller accepts the track error y_t and course error ψ_e . When the control policy is weighted for track-keeping, terms in y_t will predominate, causing the ship to turn to port and follow trajectory (i). The problem may be overcome by employing a dual-mode controller that weights course-keeping terms if ψ_e exceeds some given angle (20/30 degrees was found to be suitable). Under a dual-mode policy, when the advanced way-point is reached, the controller switches from track to course weighting, thus suppressing terms in y_t and emphasising terms in ψ_e . The vessel now follows trajectory (ii) and reverts to track-keeping mode when ψ_e falls below 20 degrees.

Simulation run 6, shown in Figure 6.7 illustrates the hull response under dual-mode control. The normal operating controller mode has the track-keeping characteristics of simulation run 5, changing to the course-keeping setting of run 4 during turns.

The way-point advances are:

Point A, $A_{wp} = 309$ m

Point B, $A_{wp} = 347$ m

Point C, $A_{wp} = 502$ m

6.4. Ship and Earth Related State Variable Feedback

Marine position-fixing navigational equipment will always locate the position of a vessel relative to the earth co-ordinate system. With ship related state variable control, all positional information must be transformed to the ship axis system. The positional measurements may be used directly, however, if the state vector is re-defined as:

$$X^T = (\delta_A \ n_A \ x_O \ u \ y_O \ v \ \psi_A \ r) \quad (6.8)$$

This requires that the system matrix F be combined with the transformation matrix T to produce the system equation set:

$$\dot{\delta}_A = f_{11} \delta_A + g_{11} \delta_D$$

$$\dot{n}_A = f_{22} n_A + g_{22} n_D$$

$$x_O = u \cos \psi_A - v \sin \psi_A$$

$$\begin{aligned} \dot{u} = & f_{41} \delta_A + f_{42} n_A + f_{44} u + f_{46} v + \\ & f_{48} r + g_{43} u_c + g_{45} u_a \end{aligned}$$

$$y_O = u \sin \psi_A + v \cos \psi_A$$

$$\begin{aligned} \dot{v} = & f_{61} \delta_A + f_{62} n_A + f_{64} u + f_{66} v + \\ & f_{68} r + g_{64} v_c + g_{66} v_a \end{aligned}$$

$$\dot{\psi}_A = r$$

$$\begin{aligned} \dot{r} = & f_{81} \delta_A + f_{82} n_A + f_{84} u + f_{86} v + \\ & g_{84} v_c + g_{86} v_a \end{aligned} \quad (6.9)$$

which may be expressed as:

$$\dot{X}(t) = F_0(t, \psi_A) + G(t) U(t) \quad (6.10)$$

This combination of ship and earth related states allows a multivariable control strategy, referred to as dynamic position-keeping, to be used to control the vessel's heading and forward speed, together with its position on the earth's surface.

It will be seen from equation (6.10) that F_0 is a function of ψ_A which implies that the feedback matrix S becomes a function of ψ_D . This must be true for if a vessel is steaming north, errors in y_0 actuate the rudder whilst errors in x_0 operate the engines, whereas when it travels due east, y_0 errors operate the engines and x_0 errors actuate the rudder. The reversability of control action requires that x_0 and y_0 terms in the Q matrix (q_{33} and q_{55}) be identical. However, since the dynamics of the system have not been changed, the relative weightings in the Q and R matrices may remain unaltered.

The desired state vector r given in Table 6.2 will now have entries in x_{OD} , y_{OD} , the required earth related positional co-ordinates. If the reverse-time generated command vector M is not used, the dual-mode control action described in 6.3.2 may be employed.

Let the weighting matrices be defined by:

$$\begin{aligned} Q &= \text{diag. } \{0 \ 0 \ 0.00005 \ 0.5 \ 0.00005 \ 0 \ 1 \ 0\} \\ R &= \text{diag. } \{1 \ 1\} \end{aligned} \quad (6.11)$$

When the forward speed is 7.717 m/s, the feedback matrices for

each section of the desired track are:

$$S_{DA} = \begin{pmatrix} 0.109 & 0.92E-8 & -0.00023 & 0.48E-6 & -0.0013 & 0.1532 & -0.8419 & -8.047 \\ -0.18E-8 & 0.0161 & 0.0068 & 0.729 & -0.0012 & -0.51E-6 & -0.99E-6 & -0.13E-4 \end{pmatrix} \quad (6.12)$$

$$S_{AB} = \begin{pmatrix} 0.109 & 0.19E-6 & 0.00088 & 0.89E-5 & -0.00102 & 0.1532 & -0.8419 & -8.047 \\ 0.18E-6 & 0.0161 & 0.0052 & 0.729 & 0.0045 & -0.45E-6 & -0.22E-5 & -0.33E-4 \end{pmatrix} \quad (6.13)$$

$$S_{BC} = \begin{pmatrix} 0.109 & 0.24E-6 & 0.00126 & 0.12E-4 & -0.00048 & 0.1532 & -0.8419 & -8.047 \\ 0.24E-6 & 0.0161 & 0.00245 & 0.729 & 0.0065 & 0.16E-4 & 0.29E-4 & 0.00041 \end{pmatrix} \quad (6.14)$$

$$S_{CD} = \begin{pmatrix} 0.109 & 0 & 0 & 0 & -0.0013 & 0.1532 & -0.8419 & -8.047 \\ 0 & 0.0161 & 0.0069 & 0.729 & 0 & 0 & 0 & 0 \end{pmatrix} \quad (6.15)$$

It will be seen that the final section matrix S_{CD} in equation (6.15) is identical to the ship related feedback matrix given by equation (5.38) since at zero heading, F and F_0 are equivalent.

In equations (6.12), (6.13) and (6.14), entries s_{12} , s_{13} and s_{14} contribute to demanded rudder angle and entries s_{21} , s_{25} , s_{26} , s_{27} and s_{28} to demanded engine speed when the vessel is travelling in a direction other than north.

Simulation runs 7 and 8 shown in Figure 6.8(a) and (b) demonstrate the dynamic properties of ship and earth related feedback control under:

- (a) position-keeping mode,
- (b) dual-mode control.

The performance indices given in Table 6.4 for runs 7 and 8 are as specified in equation (6.3) with the exception that:

$$J_x = \int_{t_0}^{t_1} (x_{OD} - x_O)^2 dt$$

$$J_y = \int_{t_0}^{t_1} (y_{OD} - y_O)^2 dt$$

(6.16)

6.5. Selection of Control Policy

In choosing the best control policy, account must be taken not only of the values of performance indices, but also of the relative merits and disadvantages of each method.

Reverse-Time Integration

This technique provides the only true way of anticipating desired state trajectories. The settings in run 3 indicate a strategy that has reasonable track-keeping, excellent course-keeping and moderate forward speed control capability. The process of calculating a reverse-time command vector before entering a port, however, is time consuming and requires considerable computing power. Further, checks need to be made on the command vector to eliminate the possibility of steady-state errors accruing.

Dual-Mode Control

A practical and easily implemented solution to the problem of anticipating way-points. The main disadvantage of dual-mode control is that earth-related measurements must be transformed to ship axes prior to control action taking place. Figure 6.9 illustrates that for run 6, J_y has a global minimum, so that under dual-mode, the

controller provides very good track-keeping together with reasonable course-keeping and forward-speed performance.

Dynamic Position-Keeping

It will be observed that the performance indices for position-keeping runs 7 and 8 correspond to those for the dual-mode simulations 5 and 6, i.e. the net outcome of both strategies is the same, the difference lying in the manner in which the problem has been tackled. The use of a combination of ship and earth related state variables eases the measurement problem but with the incurred penalty of feedback matrix dependence upon desired heading.

In summary, reverse-time integration is a sophisticated solution but with practical difficulties, whilst dual-mode control and dynamic position keeping ultimately perform the same function, the former being more straight-forward to use. Hence a dual-mode policy, with way-point anticipation as displayed in run 6 was selected as the best control strategy in terms of;

- (a) overall performance,
- (b) ease of physical implementation.

Disturbance Control Performance

The standard weather conditions for all disturbance simulations are generated using the recursive equation set (3.27). These provide a mean current of 0.669 m/s and a mean wind speed of 10.29 m/s, both in a south-westerly direction. The stochastic components remain the same for each run thus enabling comparisons of control strategies to be made.

Simulation 9 shown in Figure 6.10 indicates the effectiveness of a dual-mode policy under the combined action of wind and current. It can be seen from the performance indices that although there is a marked increase in rudder activity, a significant deterioration in

overall performance, particularly in respect to track-keeping arises.

When the disturbance control terms of equation (5.42) are incorporated, the system performance is greatly enhanced. In simulation 10, shown in Figure 6.11(a), it is assumed that instantaneous measurements of wind and current are available for use by the controller. Under these conditions, there is little difference between the disturbed and non-disturbed response.

Run 11, shown in Figure 6.11(b), represents the simulated condition whereby no measured data is available and the controller operates with mean values of wind and current, obtained from local weather forecasts and chart tidal data. Admittedly, such information will be approximate, but any a priori knowledge on the nature of the disturbance vector will improve the quality of control, as can be seen when comparison is made between Figures 6.10 and 6.11(b), together with their respective performance indices.

Adaptive Control Performance

As the forward speed of the vessel reduces, the open-loop eigenvalues follow the real-axis trajectories shown in Figure 5.8 and Figure 5.10 traces the closed-loop loci for a fixed value feedback matrix. Dual-mode simulations 12 and 15, shown in Figure 6.12(a) and (b) are for forward speeds of 5.145 and 2.572 m/s respectively with constant feedback matrix settings using the 7.717 m/s values of equation (5.38). Clearly, the oscillatory track-keeping performance of run 15 is unsatisfactory, and some form of controller adaption is required.

Simulations 13 and 16, given in Figure 6.13(a) and (b) are again for speeds of 5.145 and 2.572 m/s, the feedback matrix S being recalculated, with constant Q and R at each forward speed. This

method of adaption, when observed in the s-plane (Figure 5.12) appears to produce significant deterioration in time-domain performance. Comparison of Figures 6.7, 6.13(a) and 6.13(b) however, show that at each forward speed, the vessel moves along an identical track, the adaptive controller time-scaling the closed-loop dynamics accordingly. This surprising and unexpected result, is in many ways more desirable than the control strategy employed in simulations 14 and 17, shown in Figure 6.14(a) and (b). Here, the complex closed-loop eigenvalues are returned to their original optimal positions by the use of adaptive equation set (5.58).

In a constant Q and R policy, the complete re-calculation of S via the Riccati matrix is unnecessary since the positional terms s_{15} , s_{17} and s_{23} remain unchanged and the velocity terms s_{16} , s_{18} and s_{24} are governed by the relationships:

$$\begin{aligned} s_{16} &= 1.172 u^{-1.0} \\ s_{18} &= -61.88 u^{-1.0} \\ s_{24} &= 2.76 u^{-0.65} \end{aligned} \quad (6.17)$$

Simulations 18 and 19, shown in Figure 6.15(a) and (b) illustrate the effect of wind and tidal stream on a vessel approaching Plymouth at a speed of 2.572 m/s under a constant Q and R policy. Run 18 is without disturbance correction and run 19 includes the correction algorithm. It appears from Figure 6.15(b) that at the beginning, and towards the end of the run, the corrective measures are not adequate to cope with disturbance surges.

When a vessel moves at low forward velocity, there is a corresponding reduction in rudder control forces and moments. The disturbance forces on the hull, however, do not reduce and so

eventually a saturation point occurs when the maximum control effort available is insufficient to match the disturbance effects. This condition is reached in run 19 and it can be seen in Figure 6.15(b) that for the first 8 minutes, and also after 30 minutes, the rudder is hard over to port. It is during these periods that the disturbances attain their peak values since both wind and tidal stream are almost perpendicular to the ship's track.

It is evident then that there comes a point of reduced forward velocity where the control system, although able to guide the vessel along its desired track, is unable to cope with disturbances of large magnitude. This condition of control saturation must be seen as a limitation of the system presented here. Should it be envisaged that significant low speed manoeuvring is to be performed by the ferry, then additional control effort (for example, bow thrusters) must be considered.

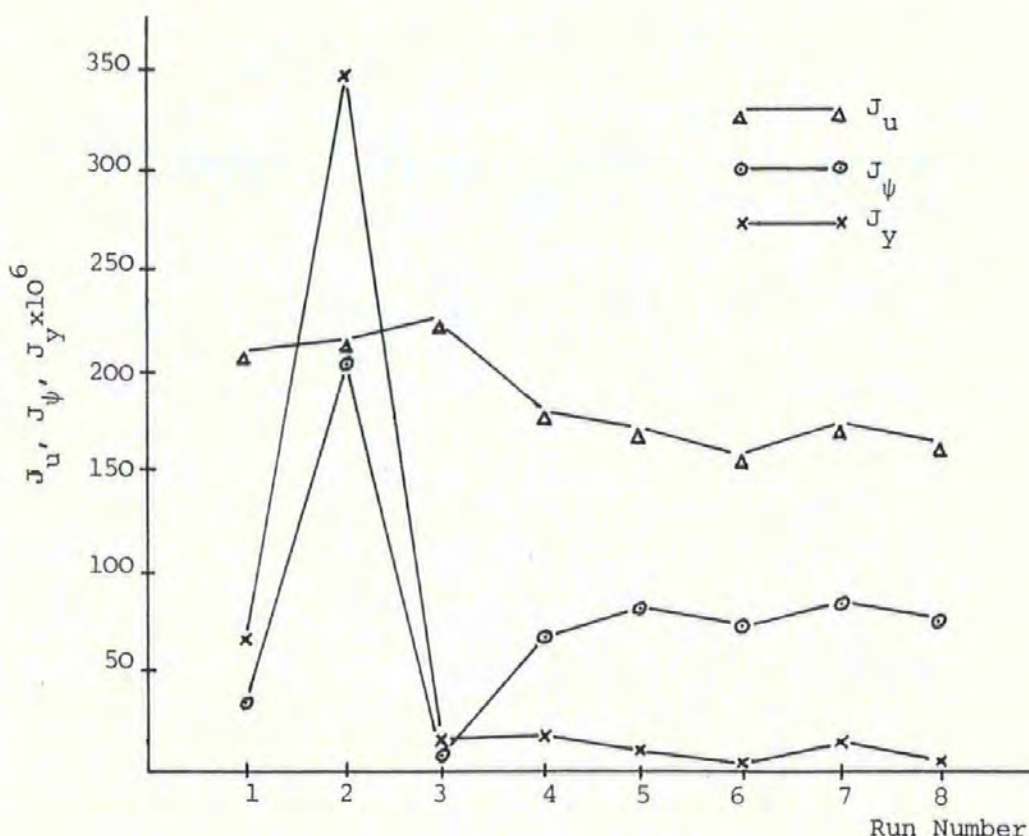


Figure 6.9

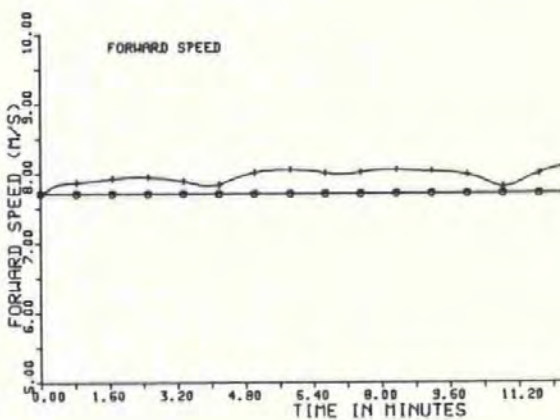
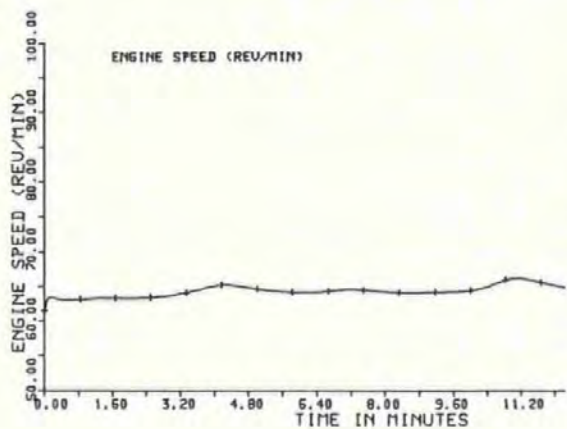
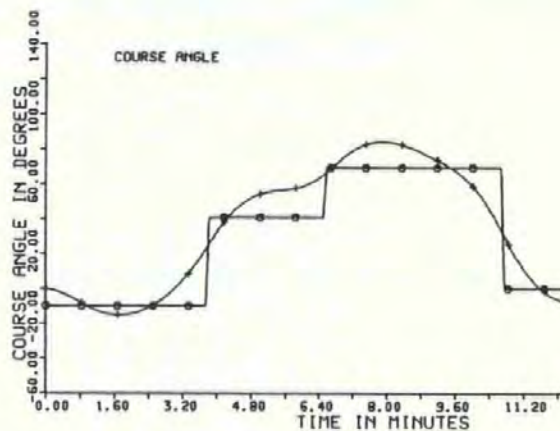
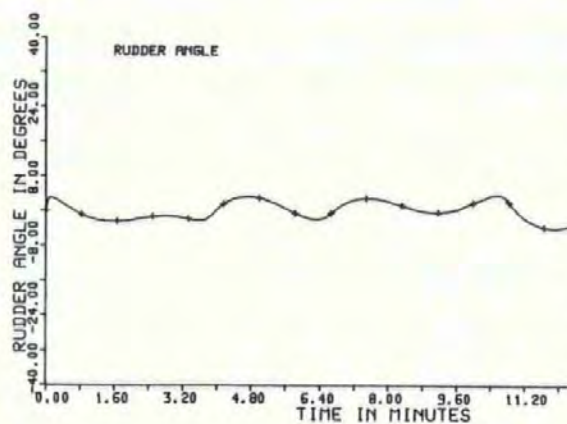
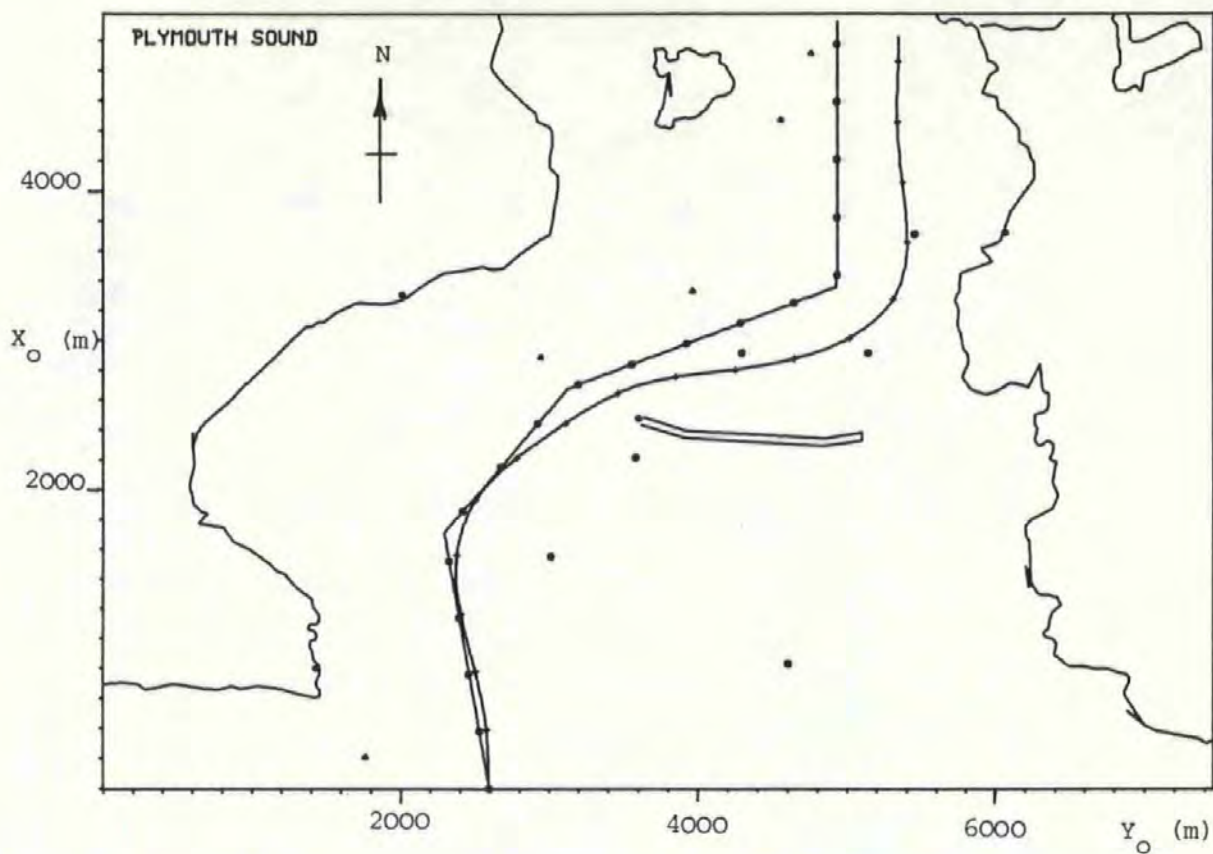


Figure 6.3(a)

Simulation 1

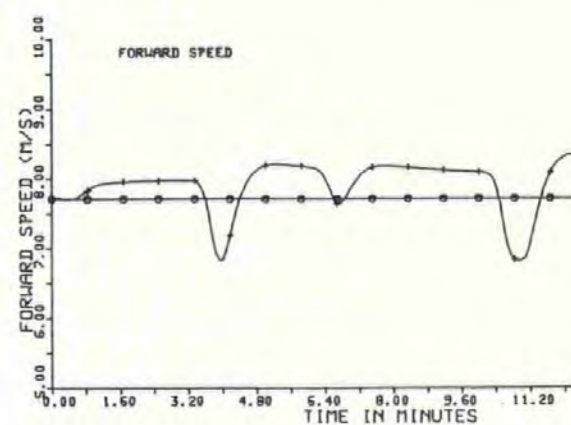
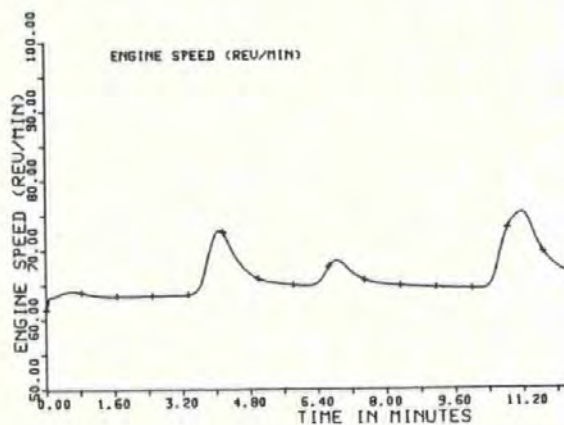
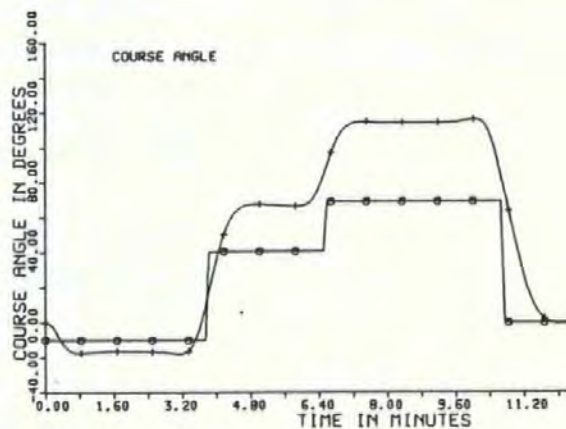
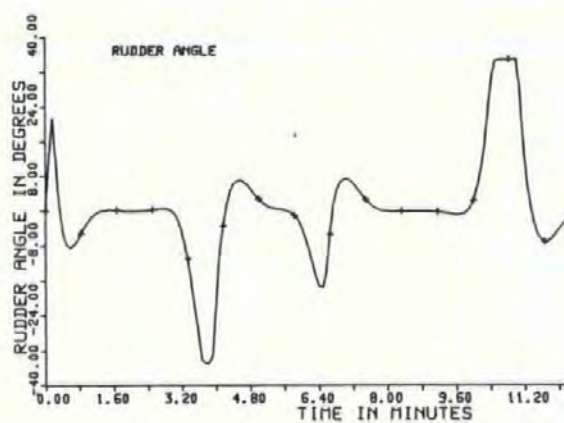
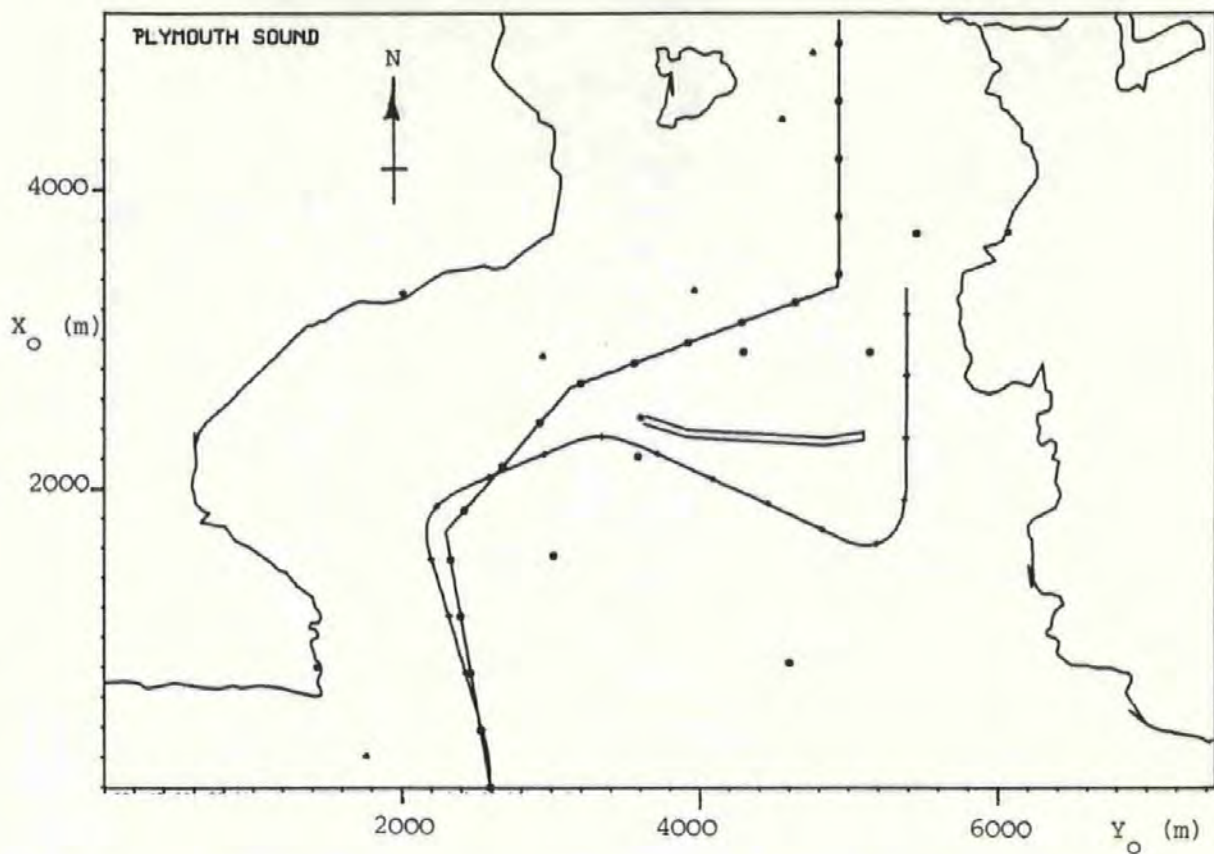


Figure 6.3(b)

Simulation 2

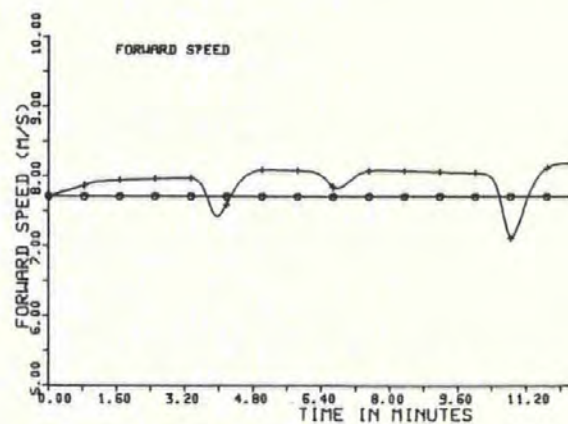
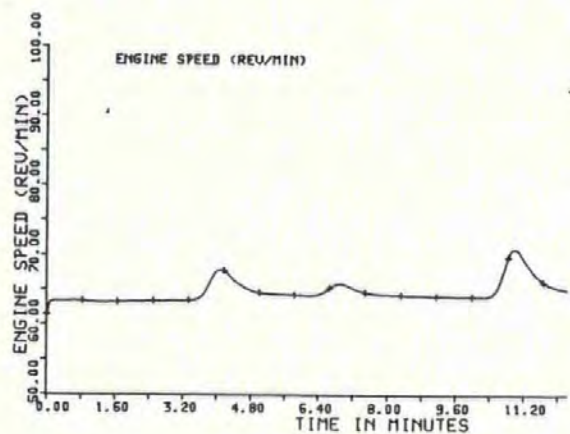
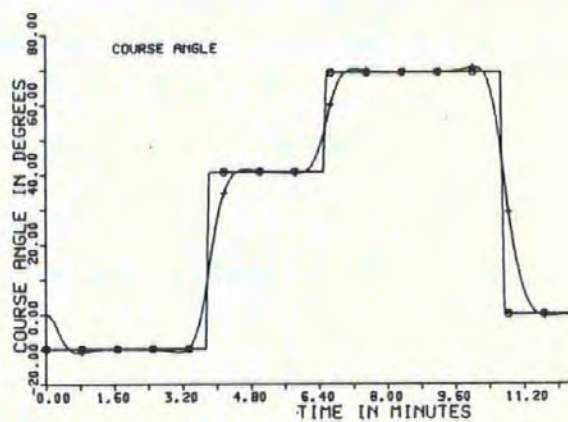
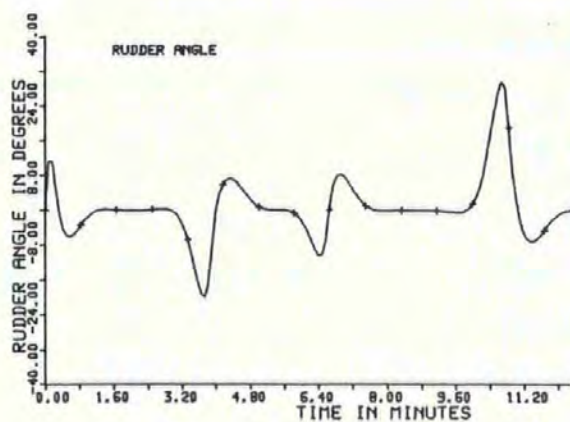
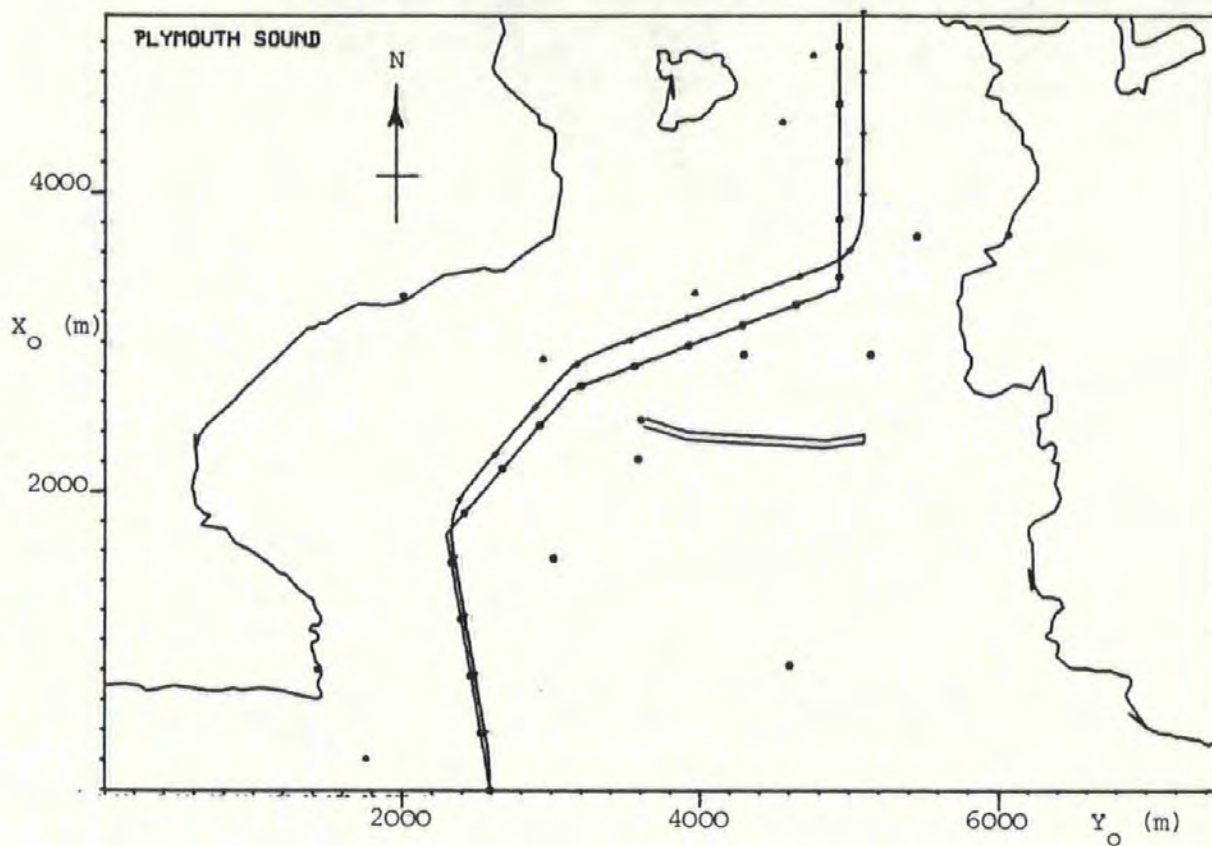


Figure 6.3(c)

Simulation 3

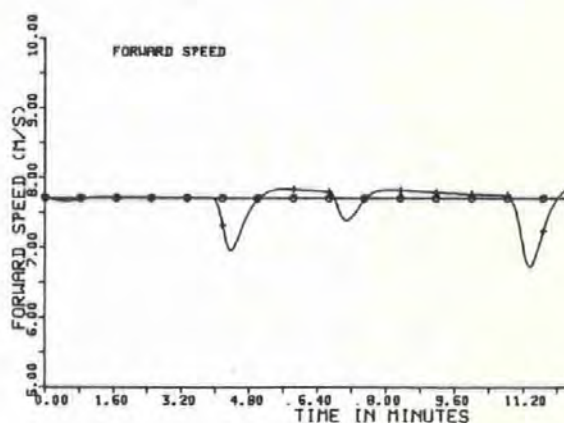
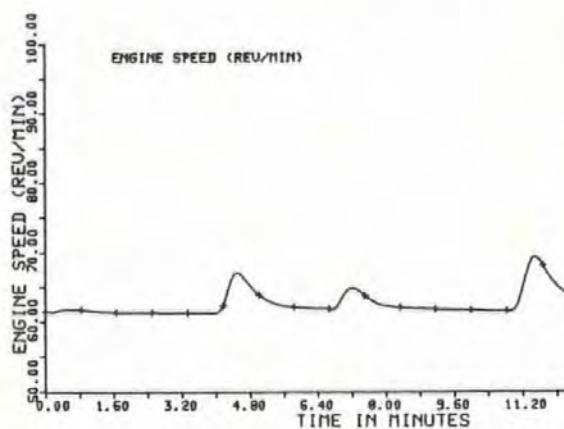
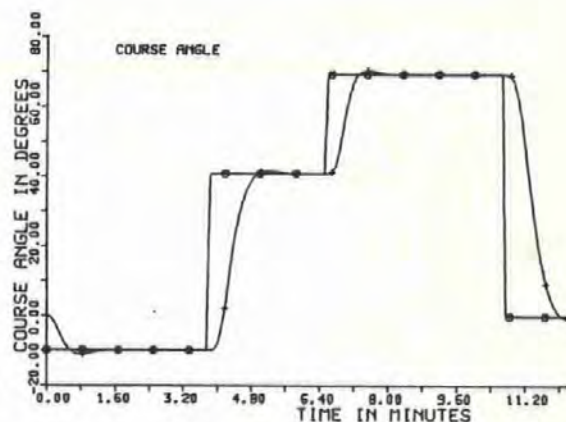
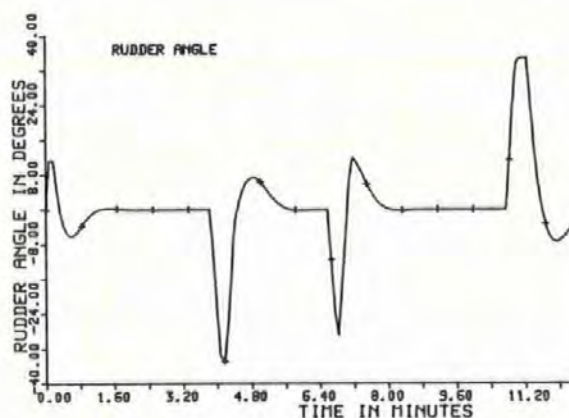
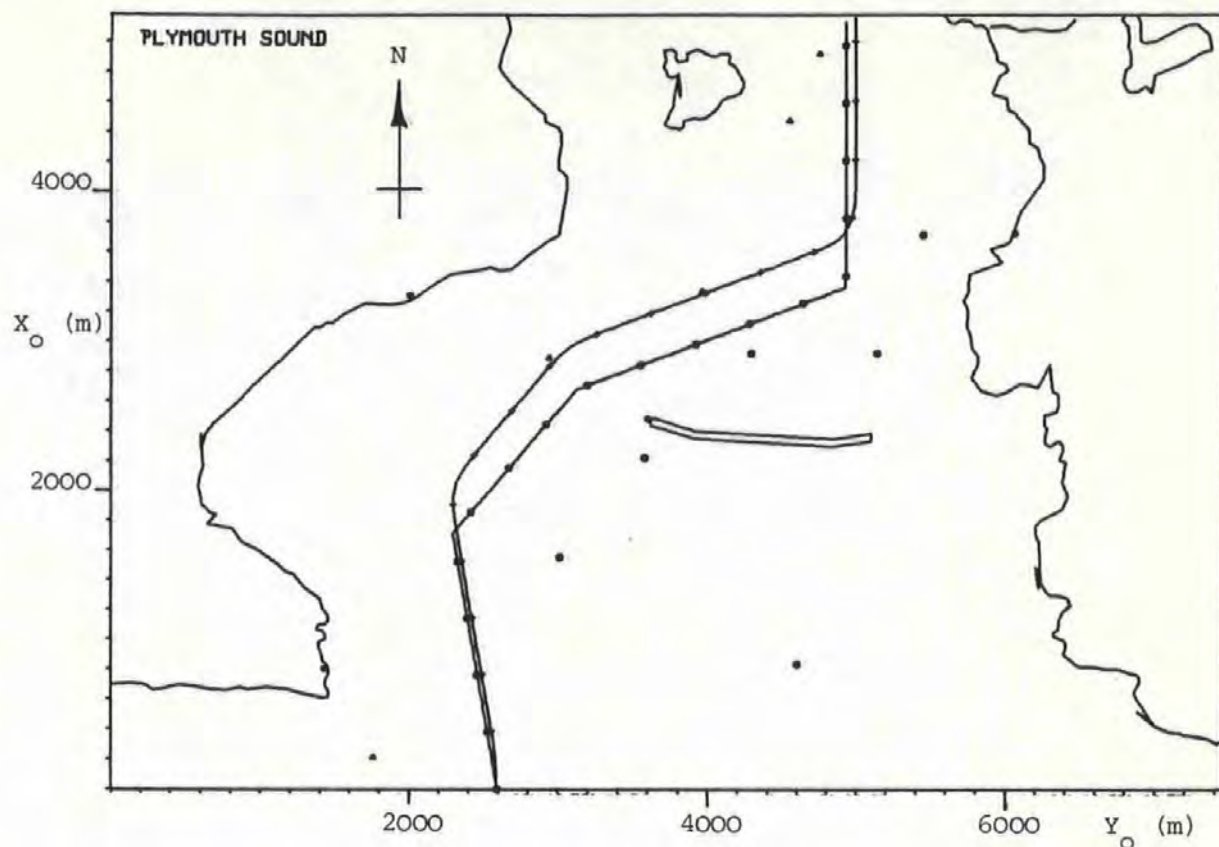


Figure 6.5(a)

Simulation 4

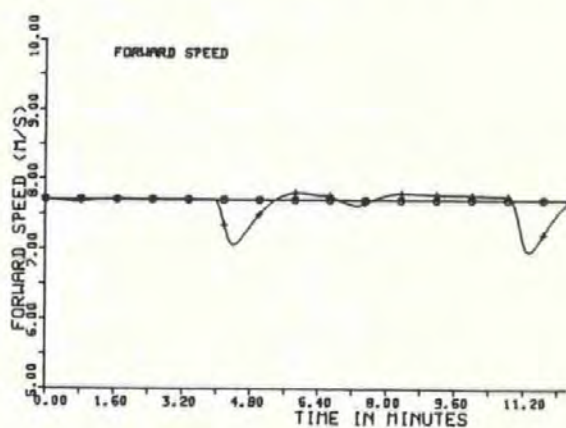
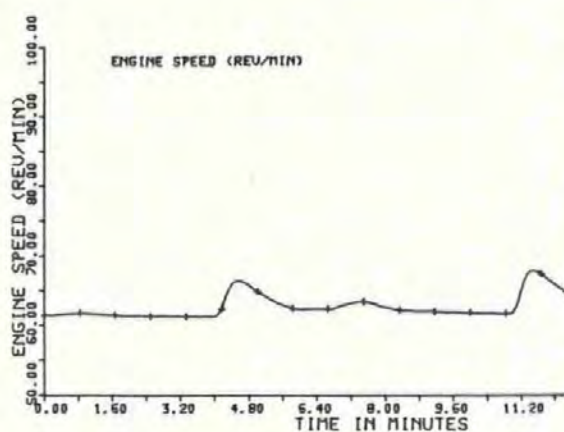
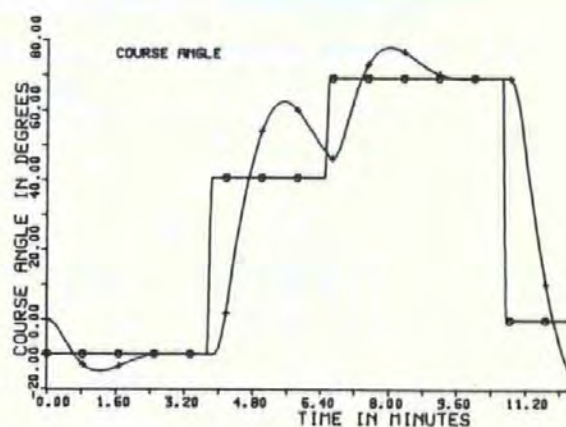
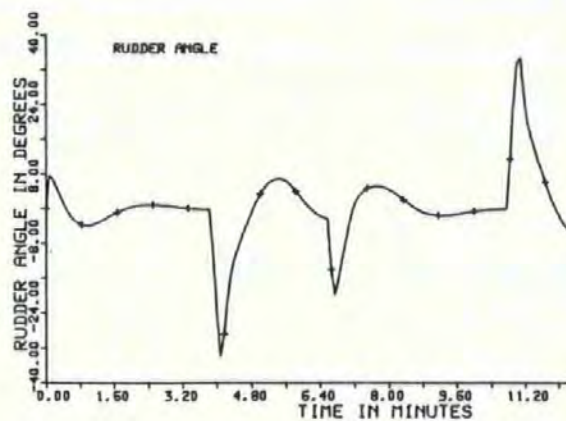
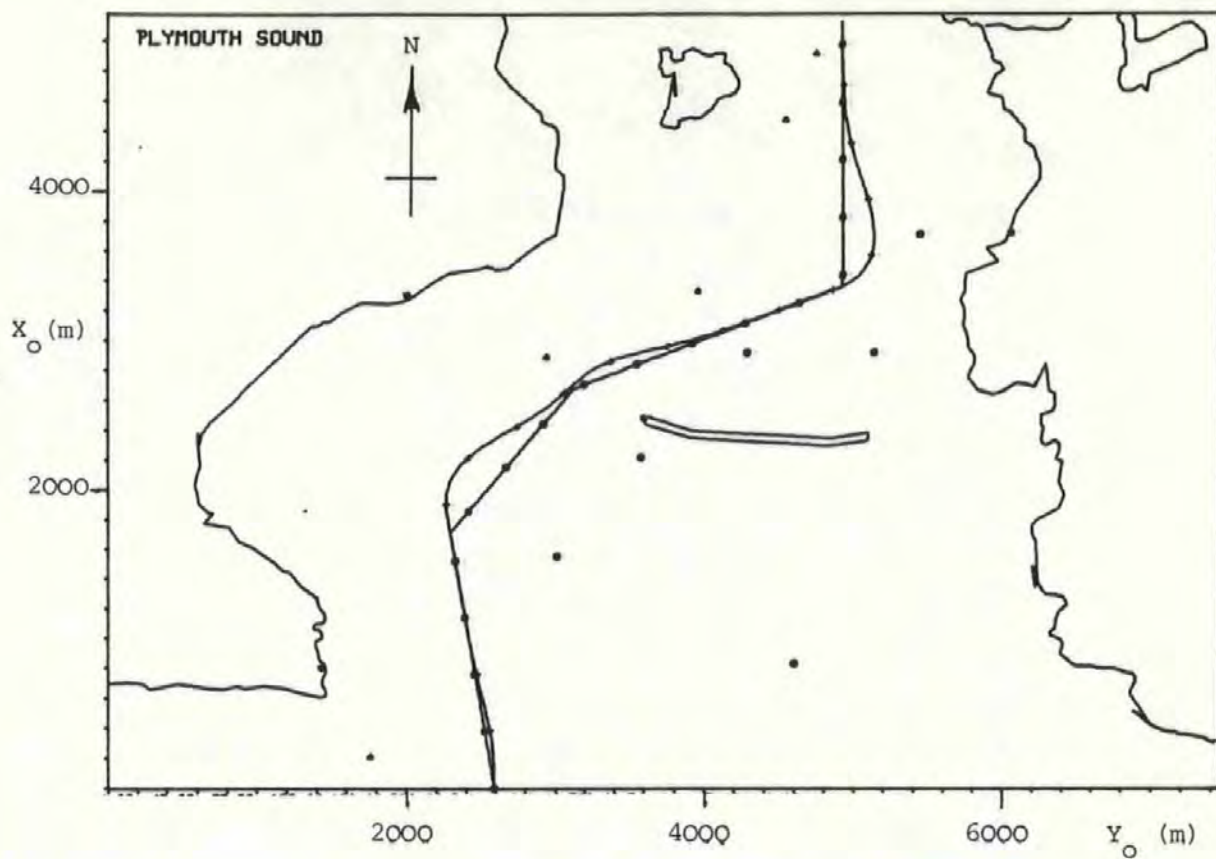


Figure 6.5(b)

Simulation 5

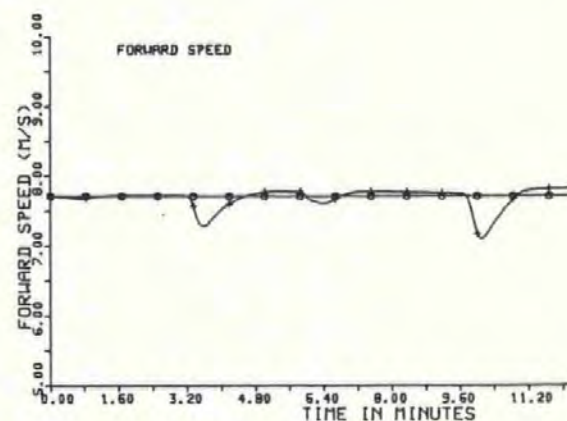
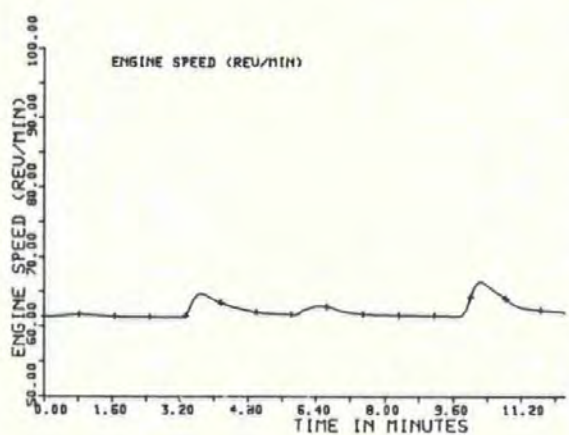
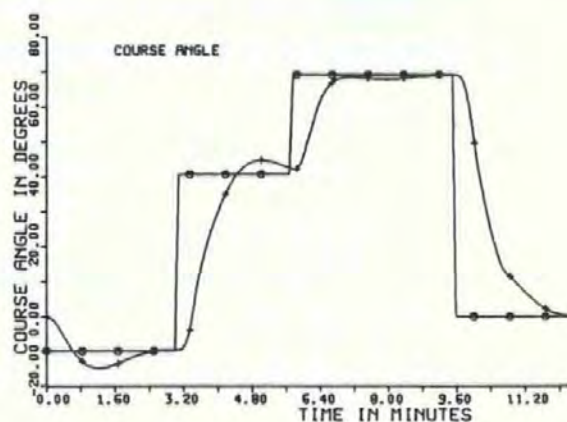
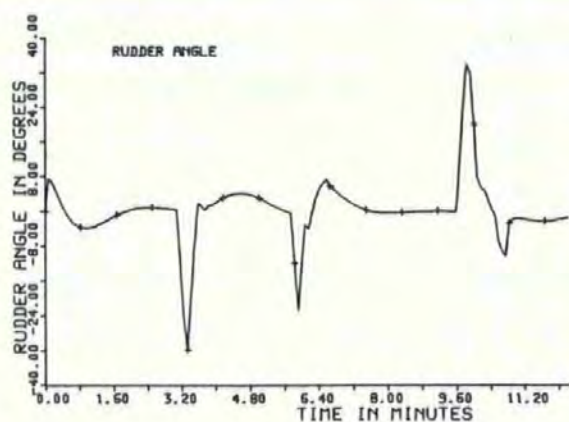
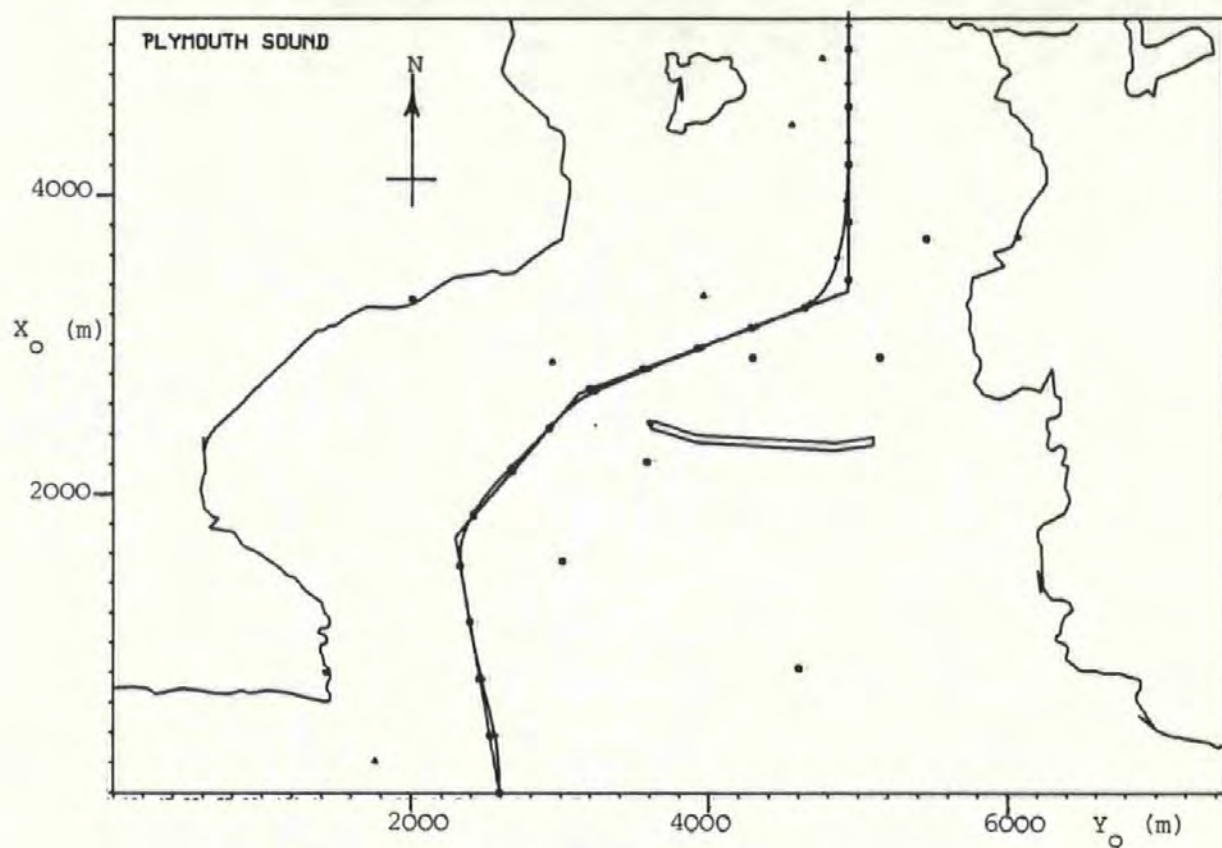


Figure 6.7

Simulation 6

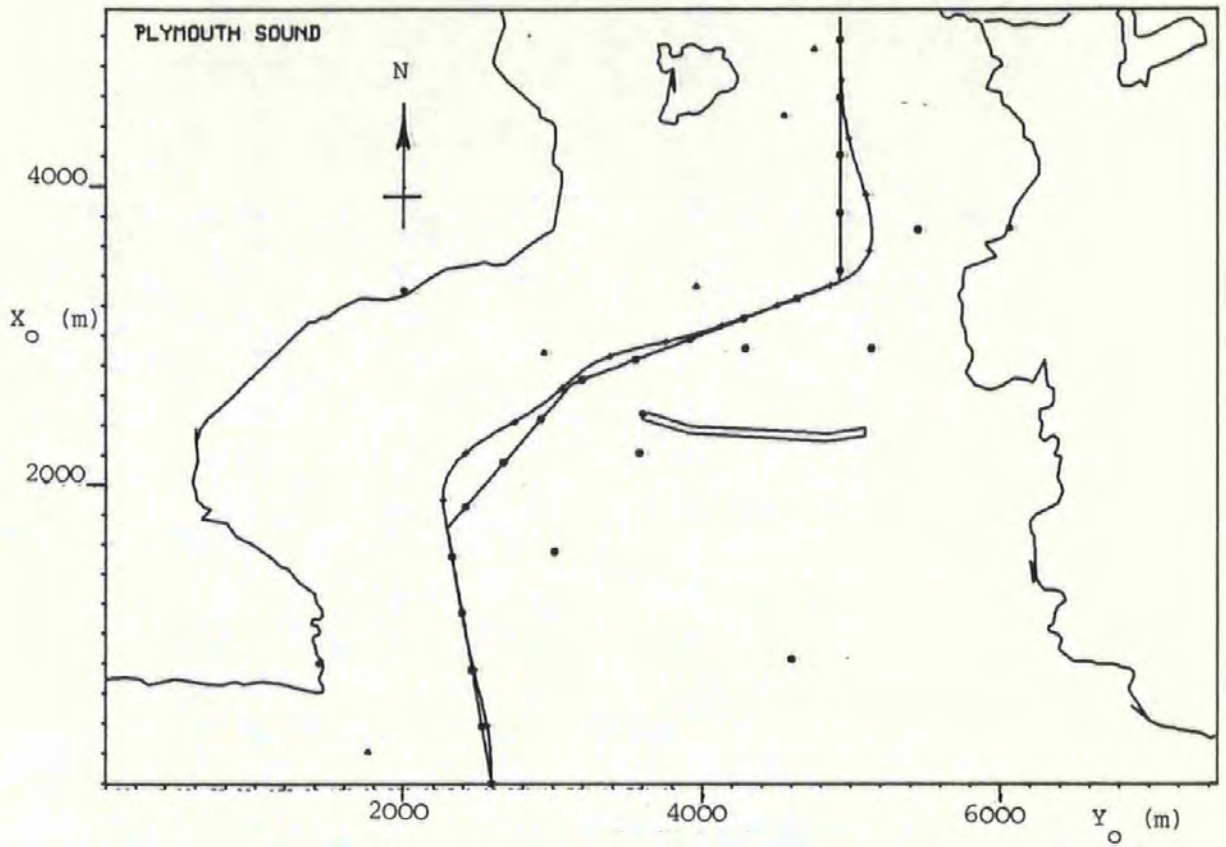


Figure 6.8(a)

Simulation 7

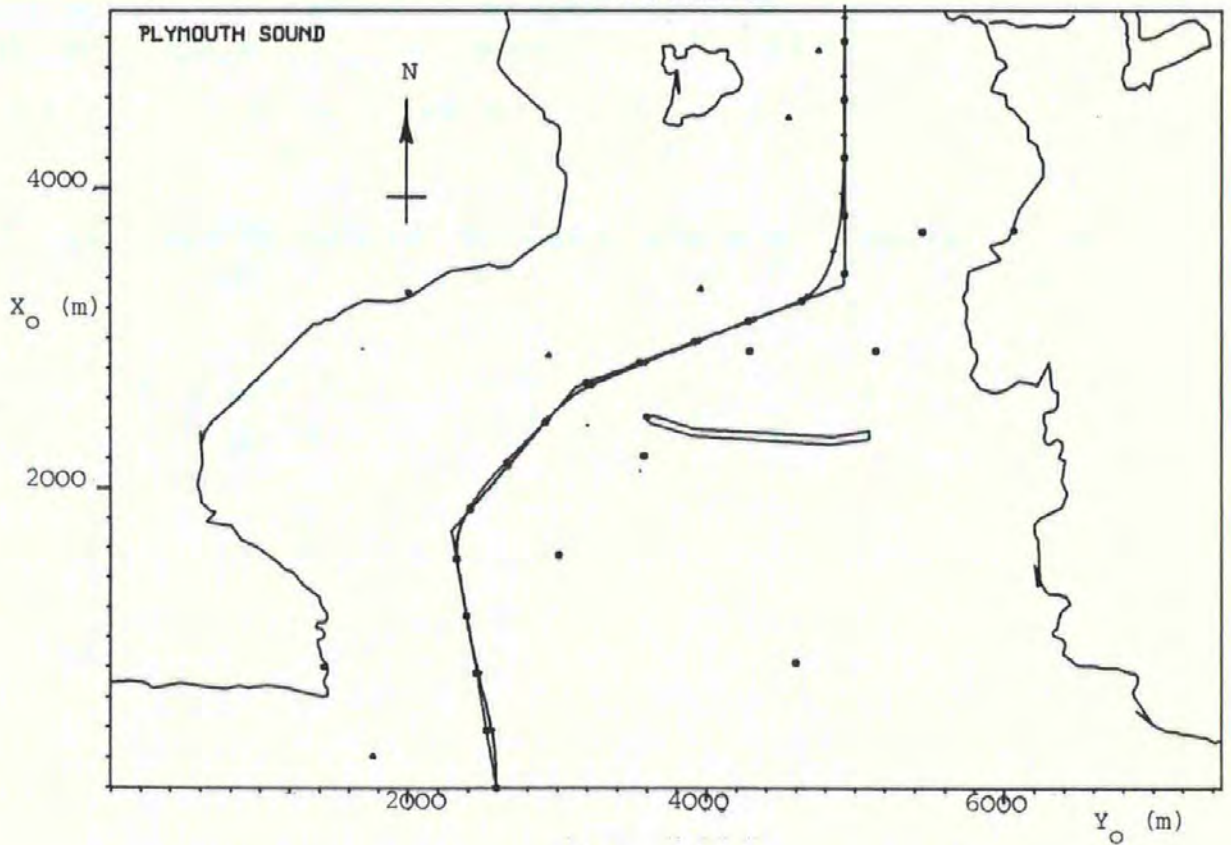


Figure 6.8(b)

Simulation 8

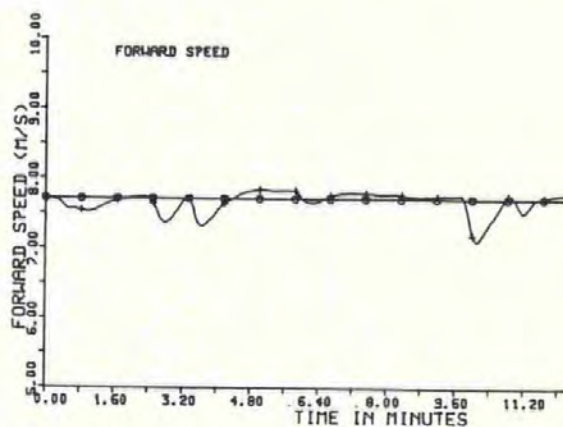
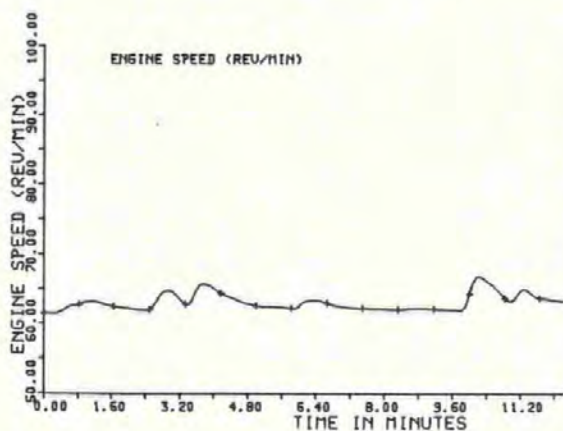
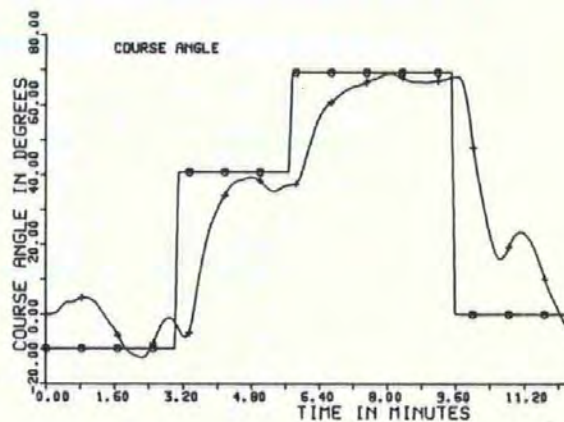
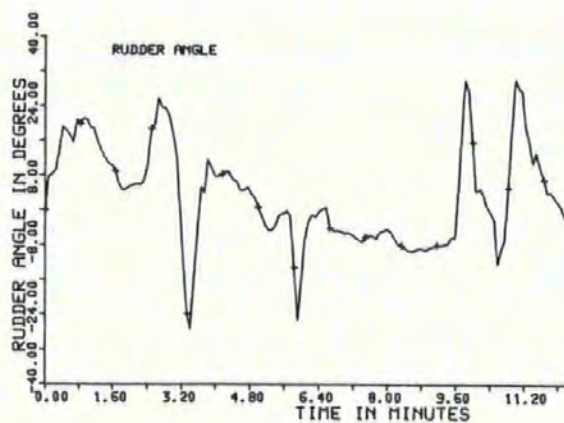
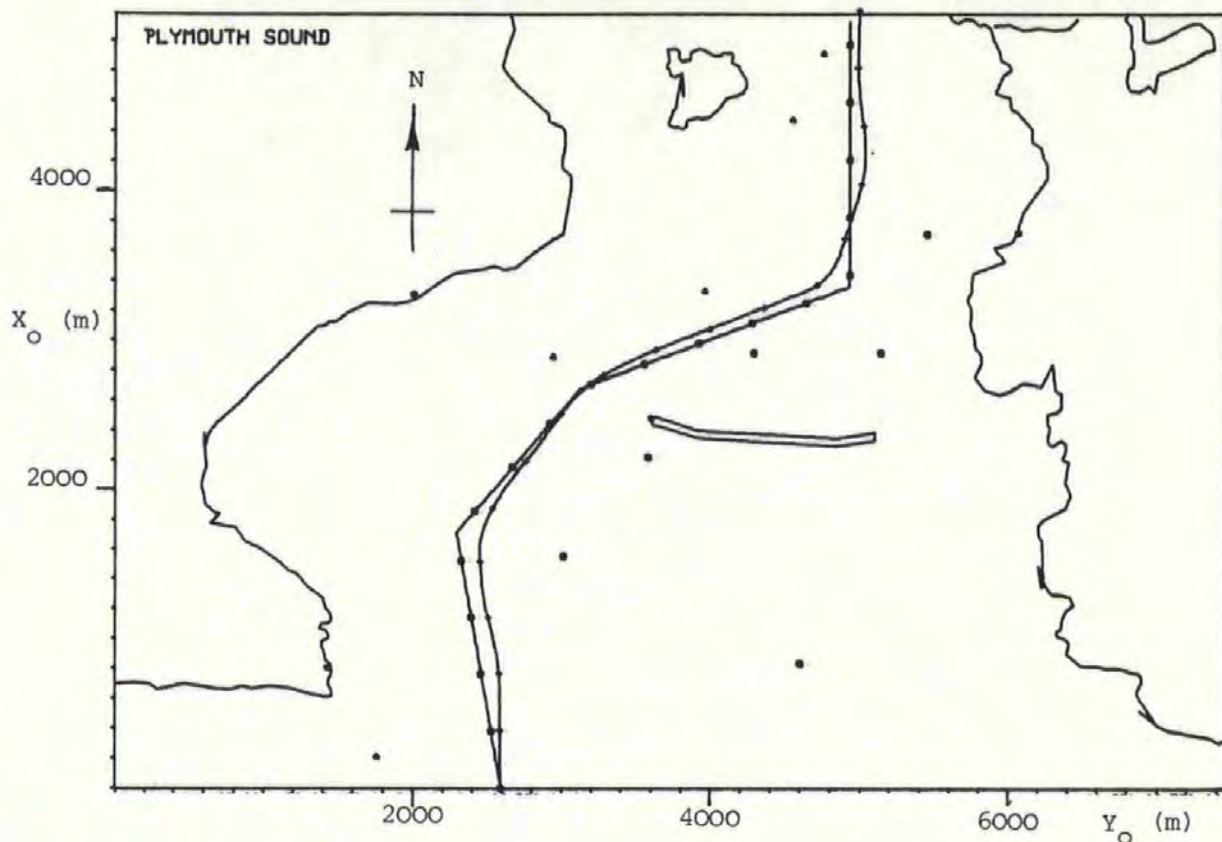


Figure 6.10

Simulation 9

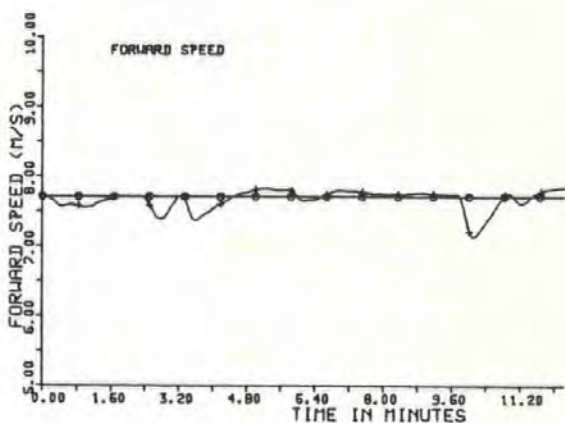
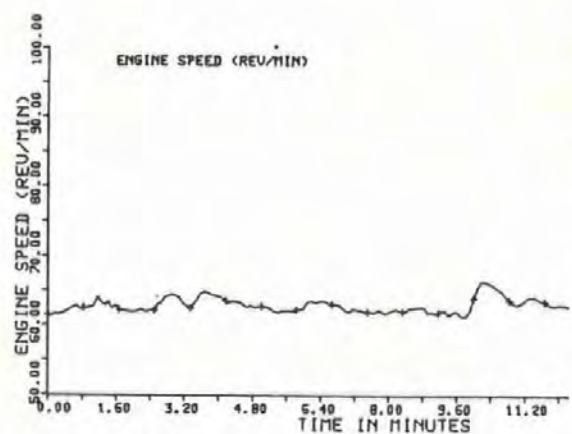
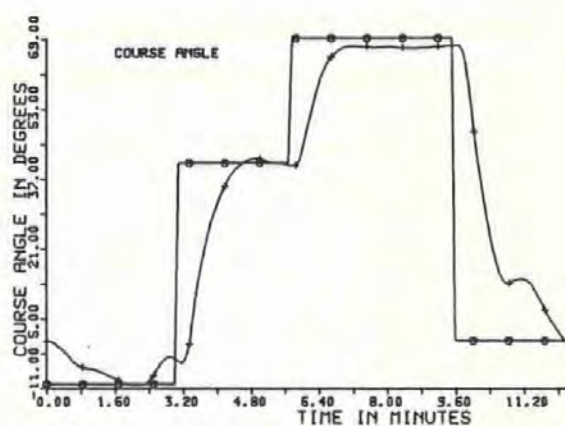
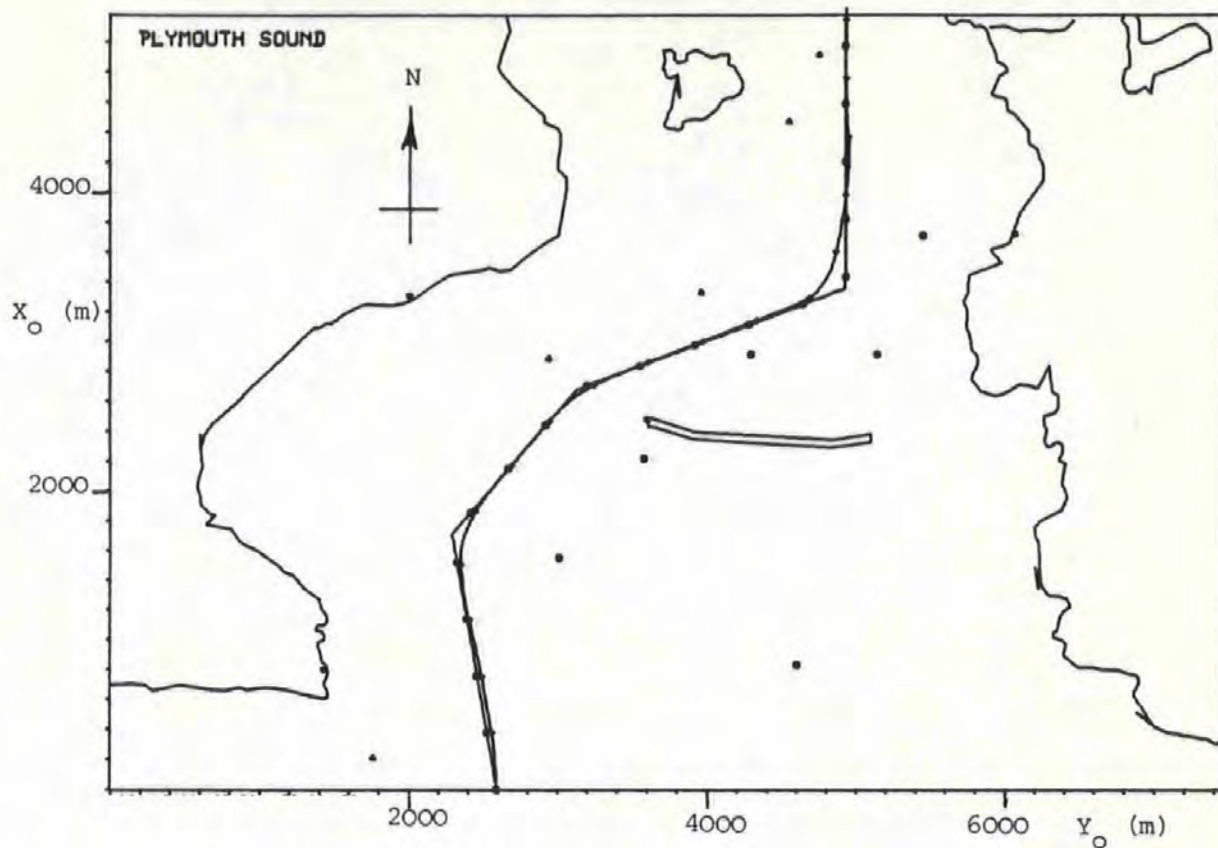


Figure 6.11(a)

Simulation 10

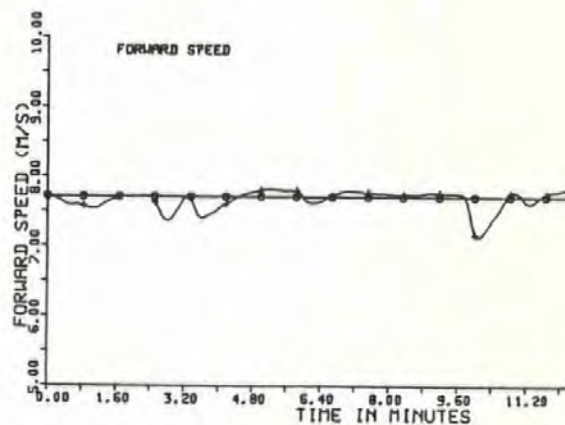
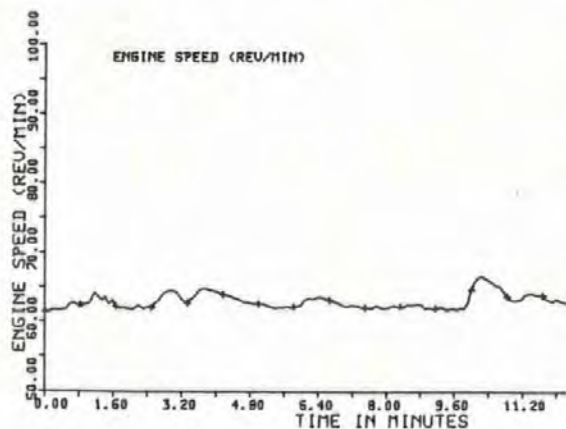
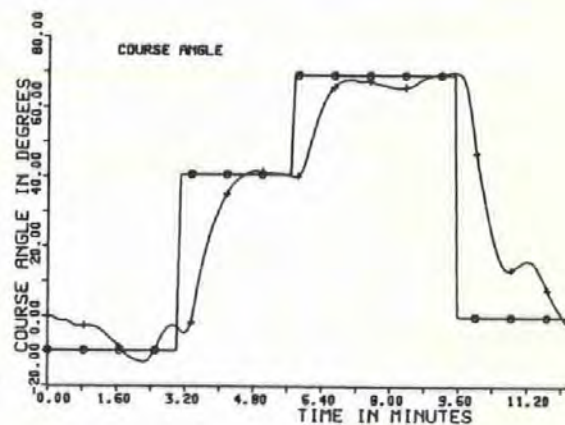
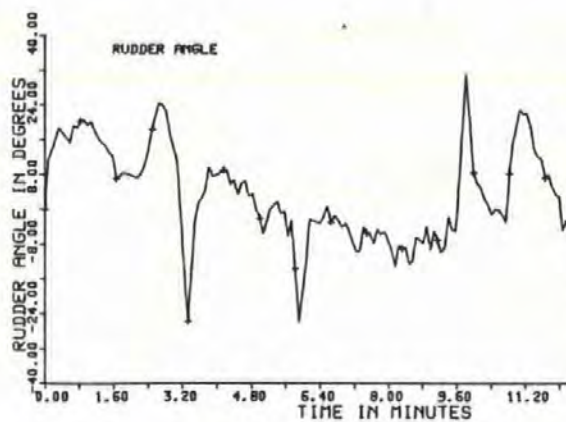
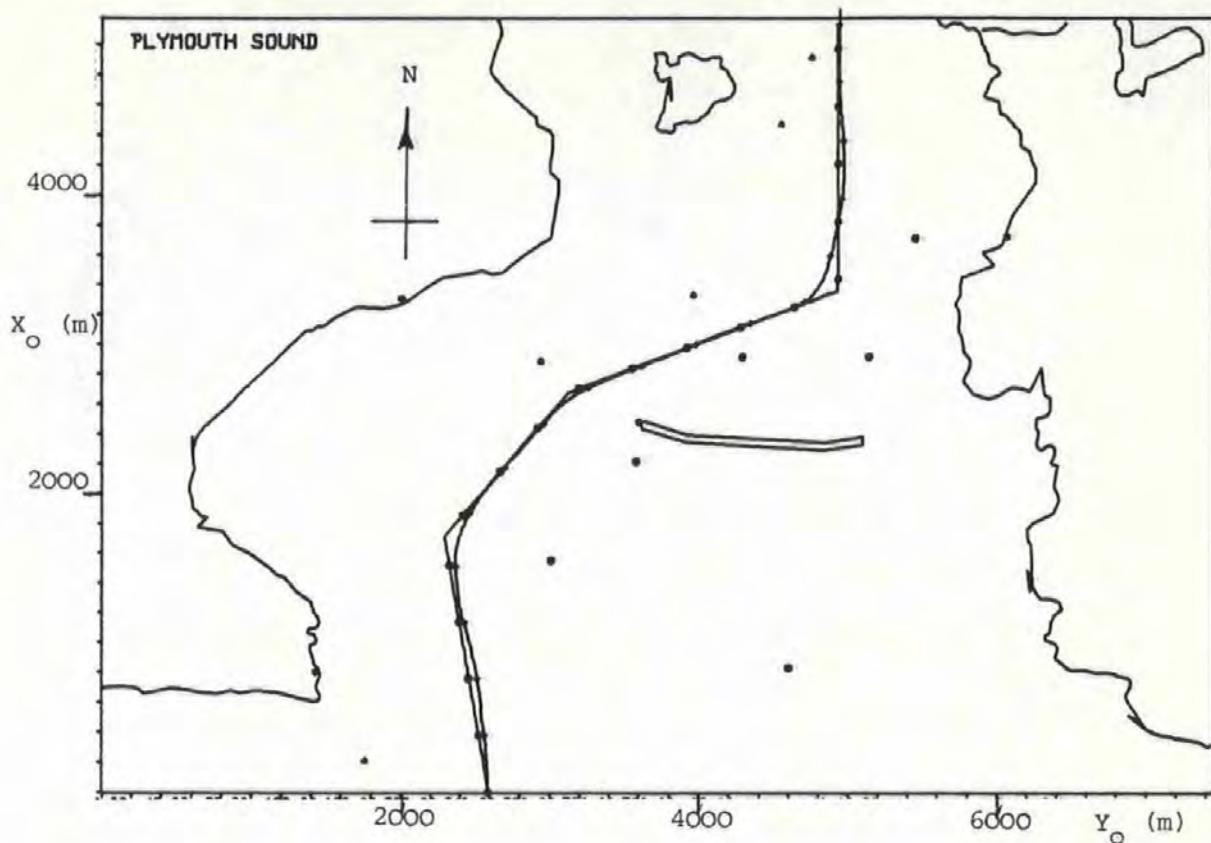


Figure 6.11(b)

Simulation 11

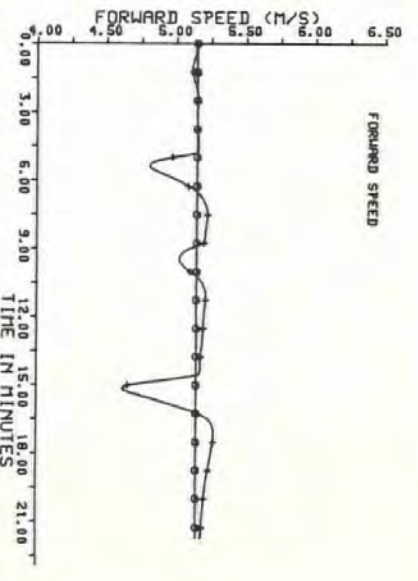
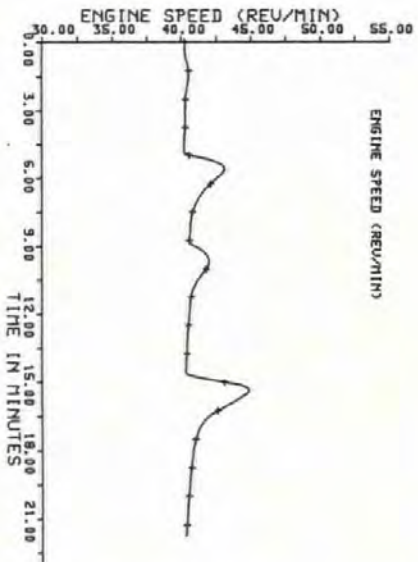
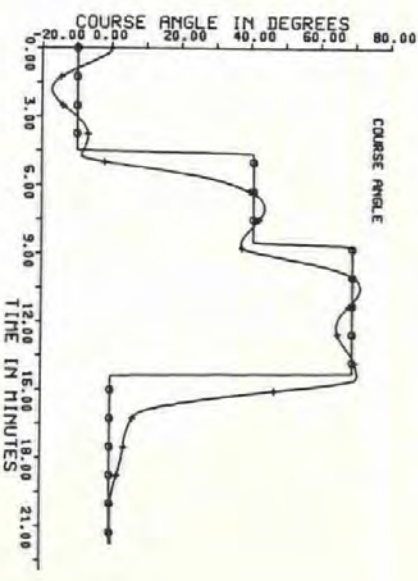
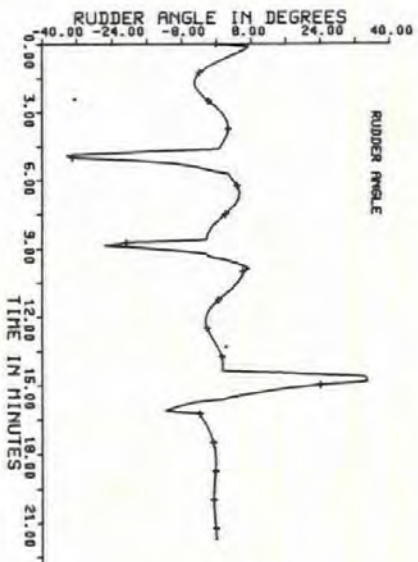
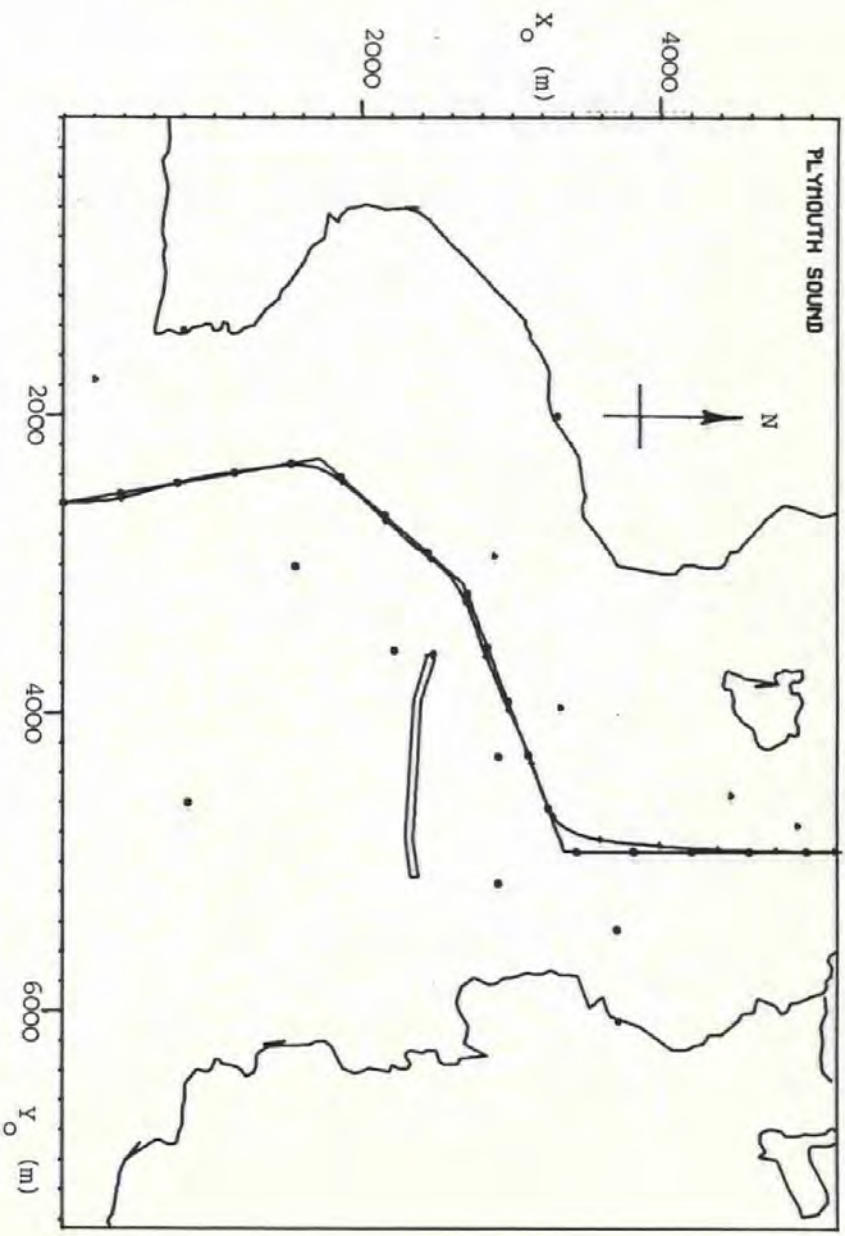


Figure 6.12(a)

Simulation 12

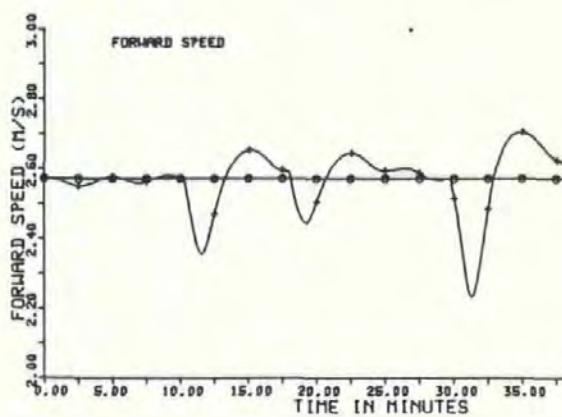
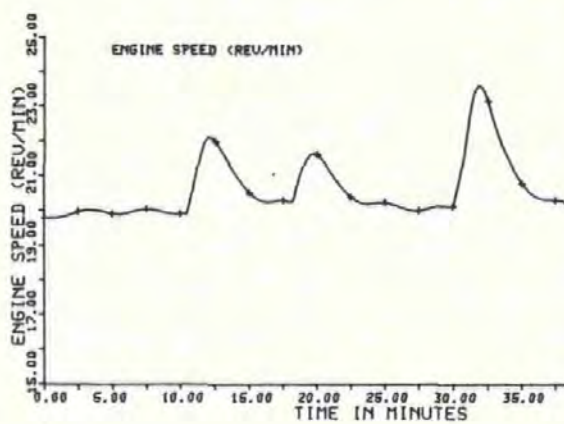
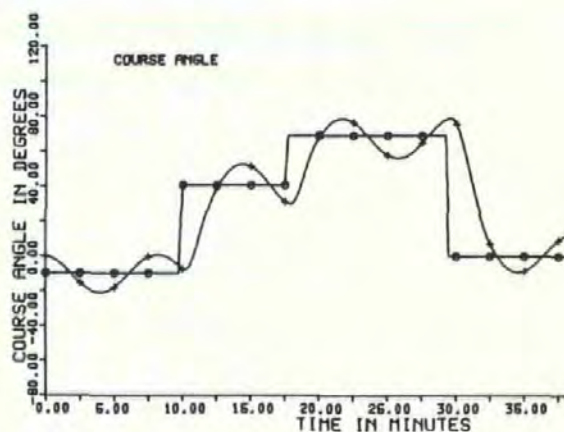
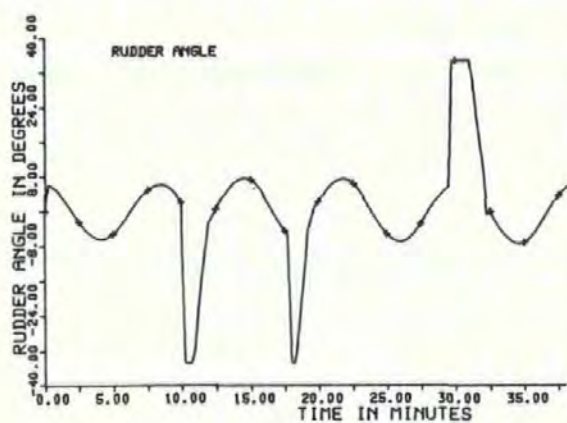
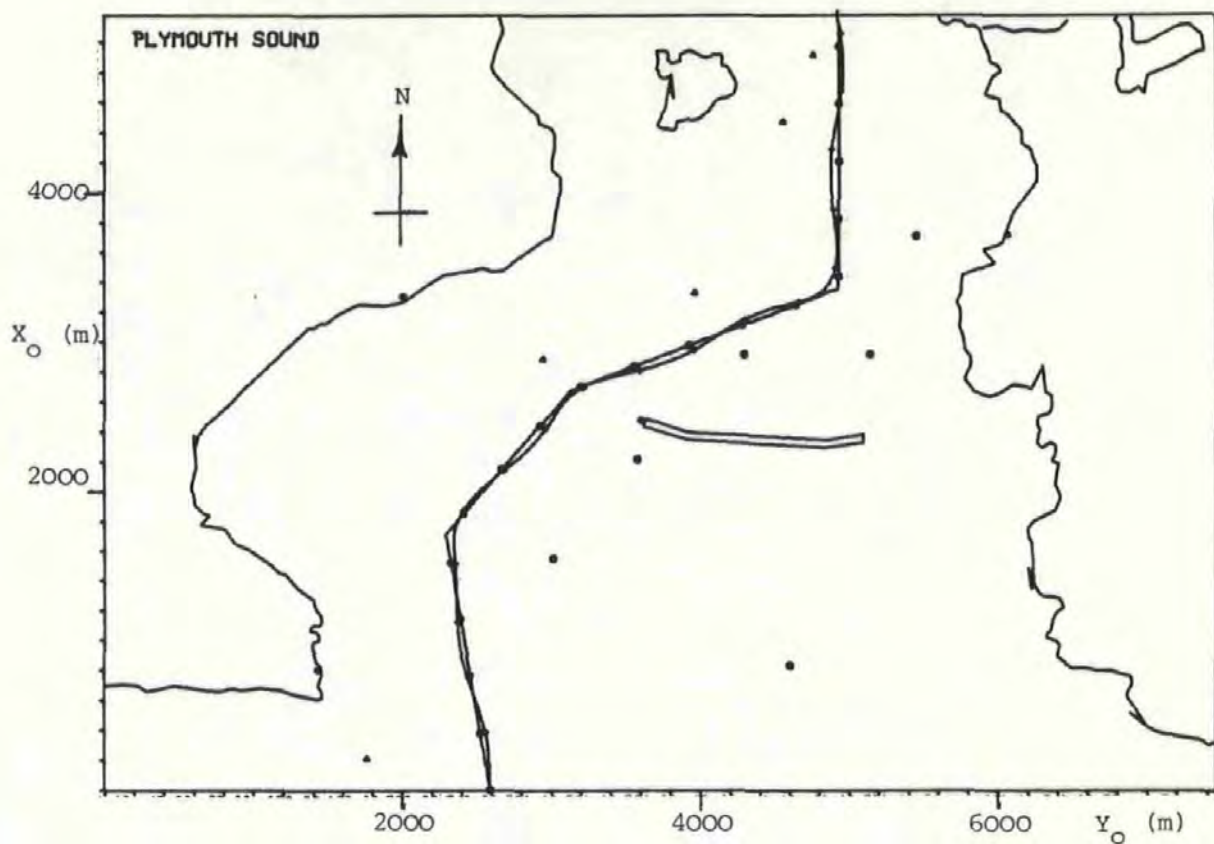


Figure 6.12(b)

Simulation 15

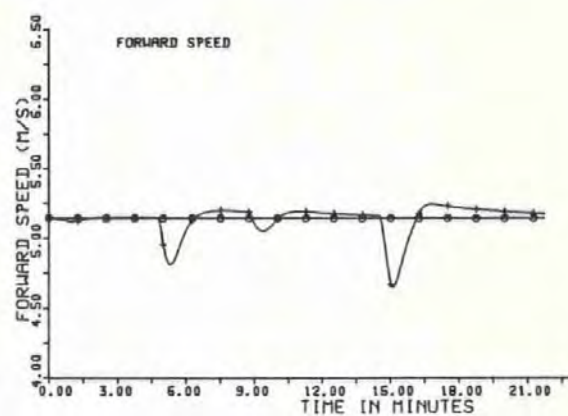
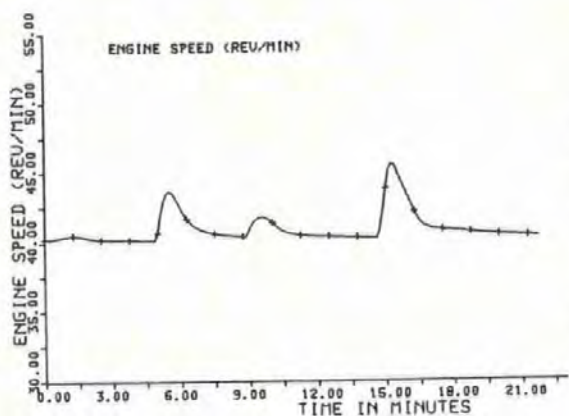
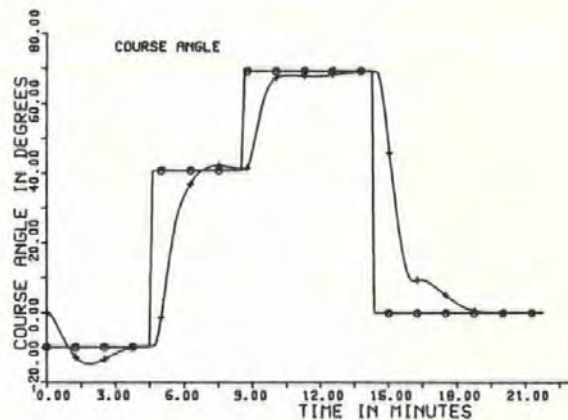
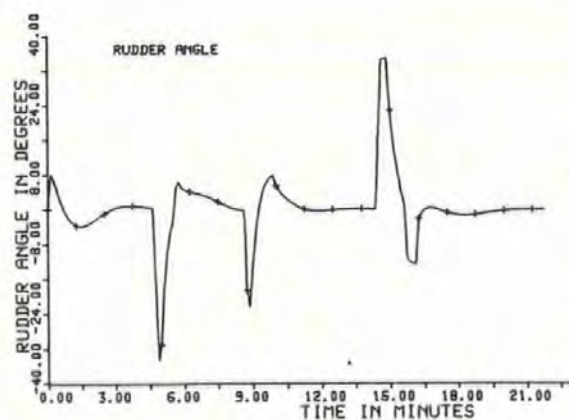
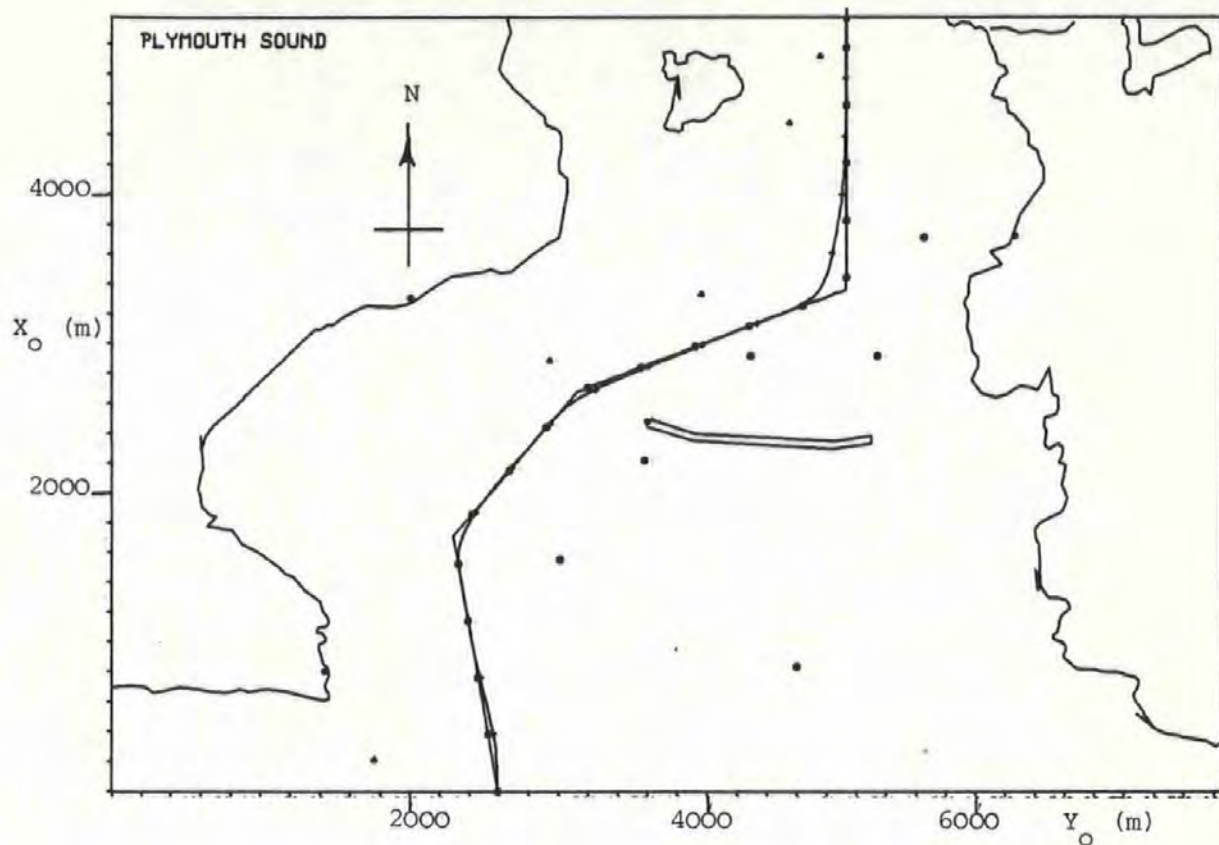


Figure 6.13(a)

Simulation 13

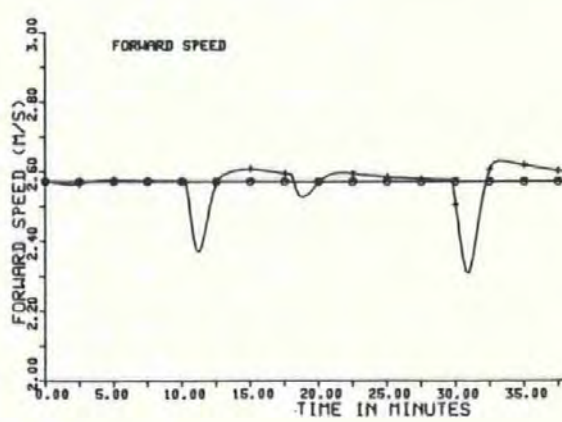
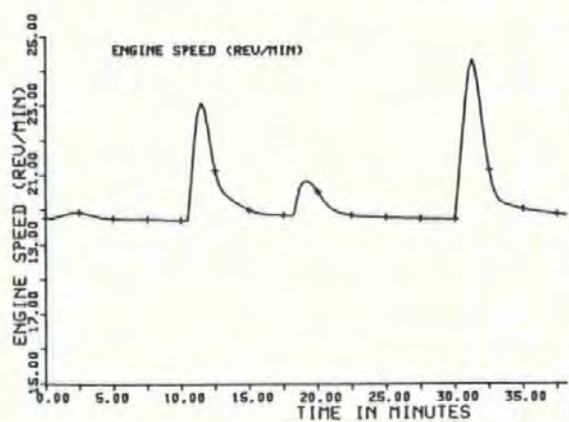
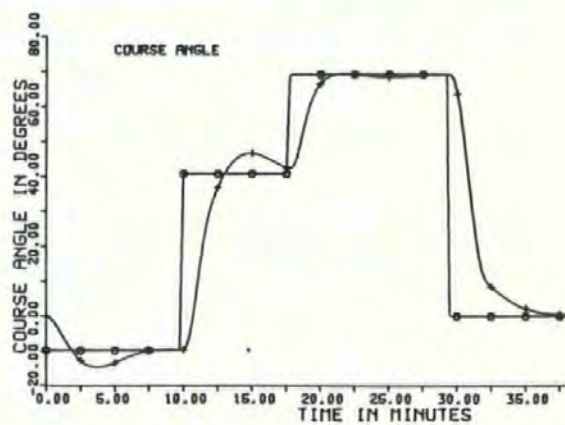
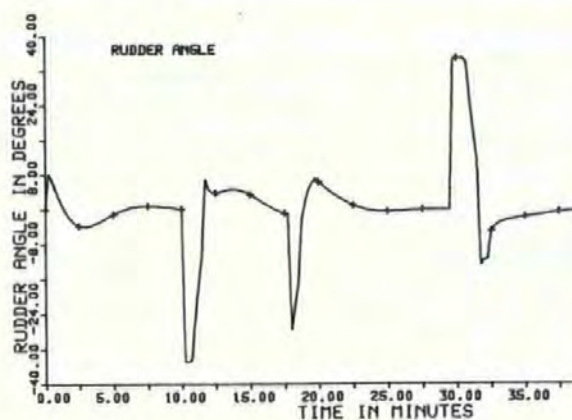
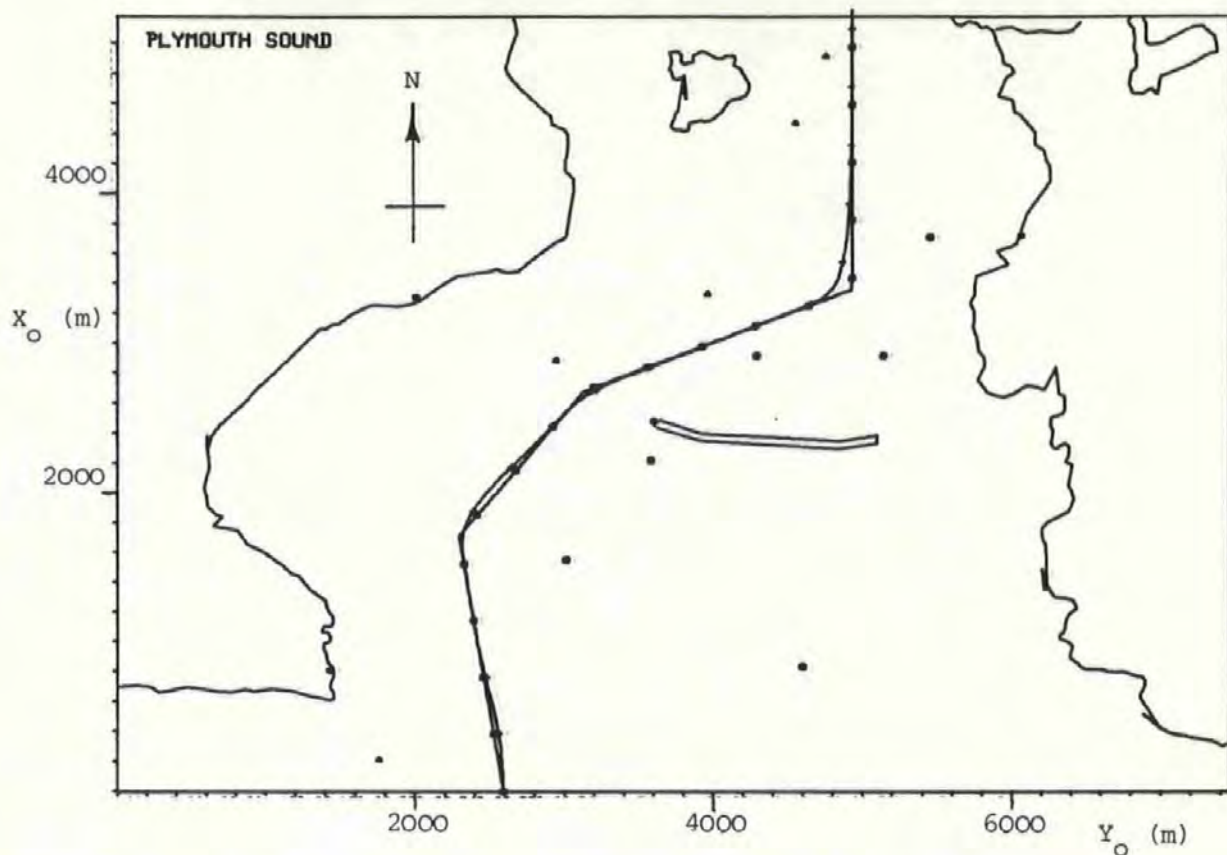


Figure 6.13(b)

Simulation 16

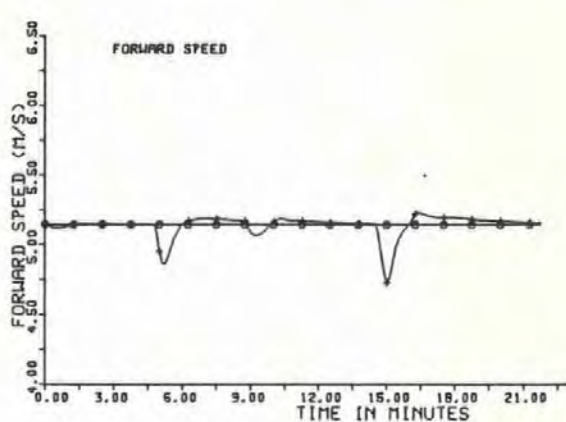
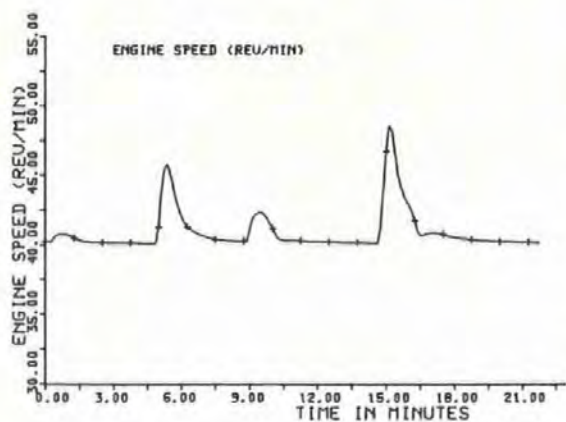
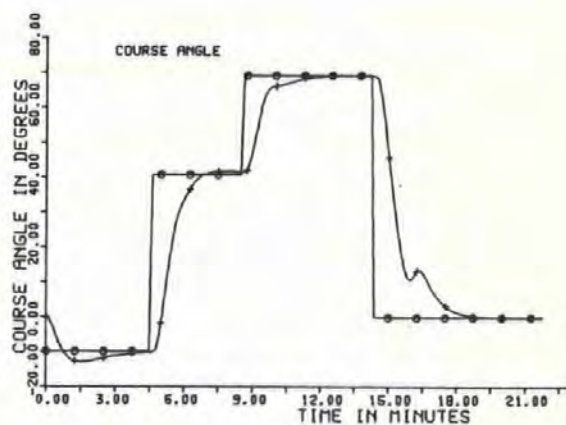
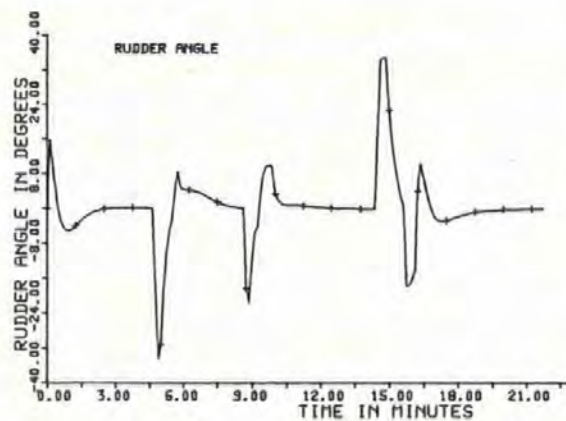
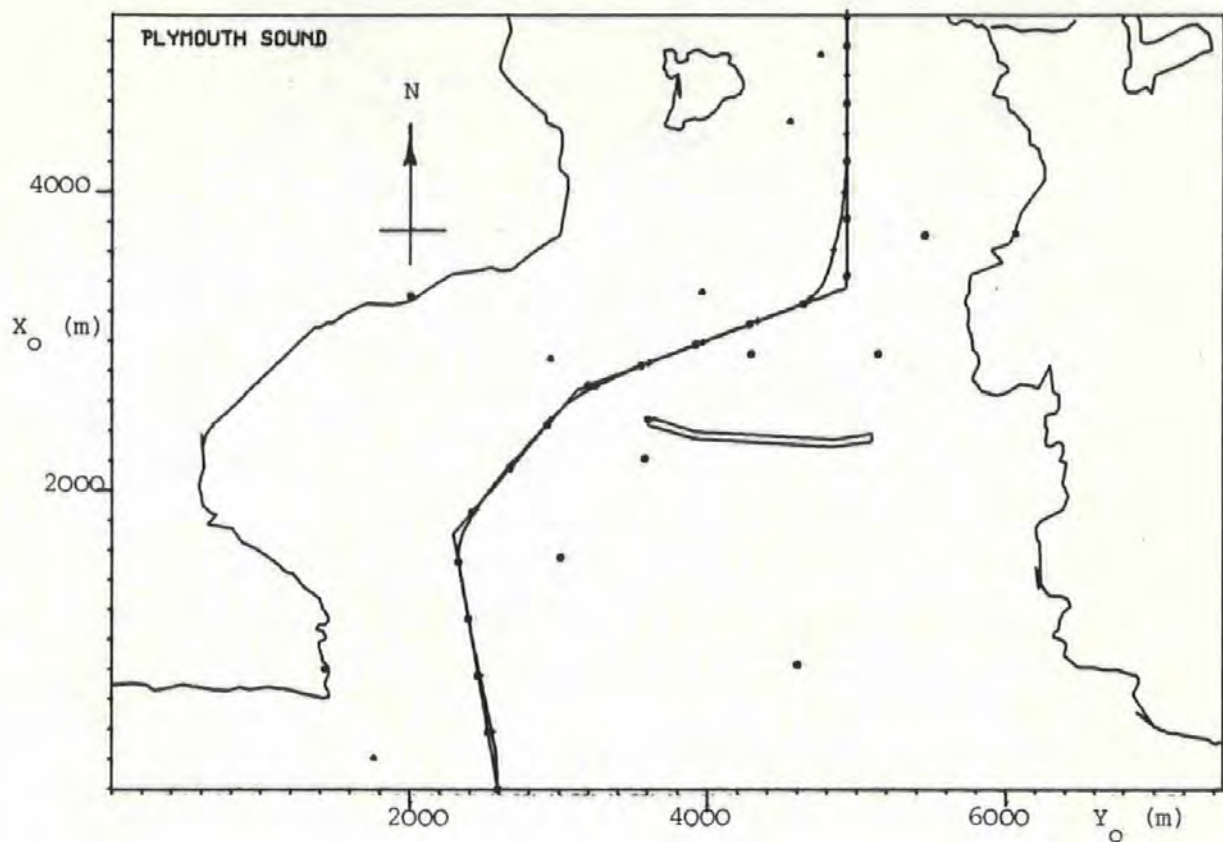


Figure 6.14(a)

Simulation 14

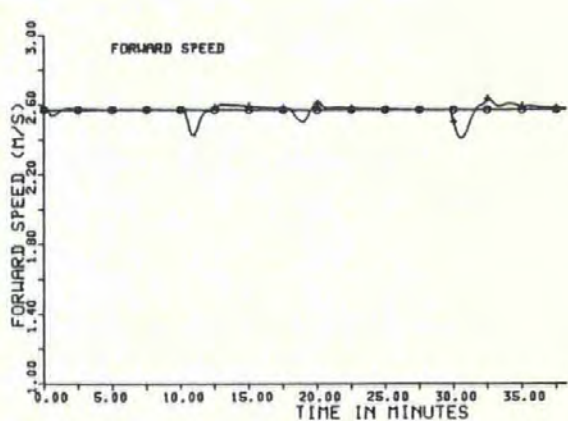
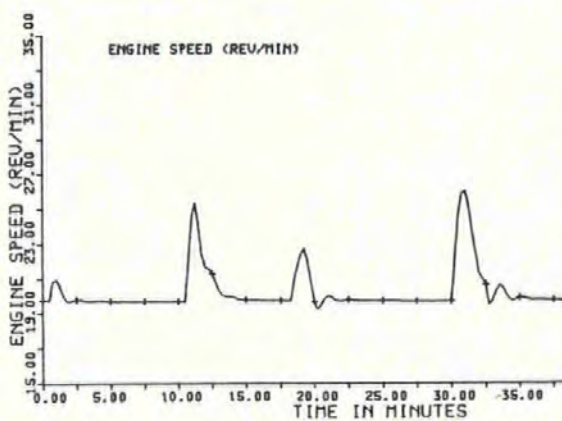
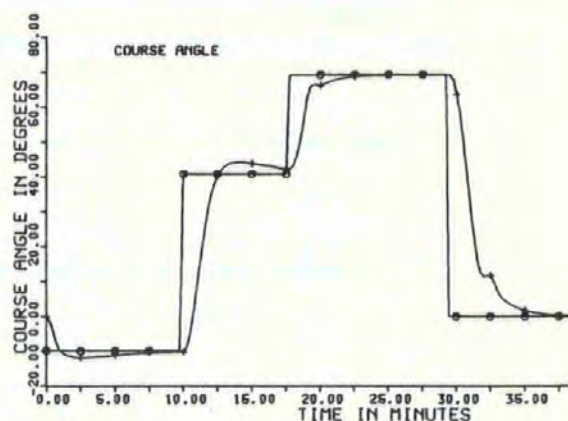
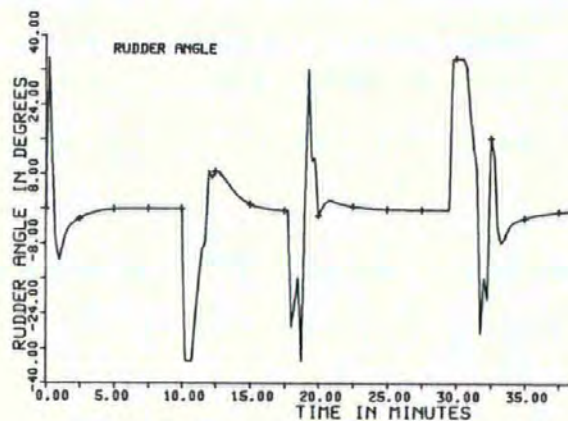
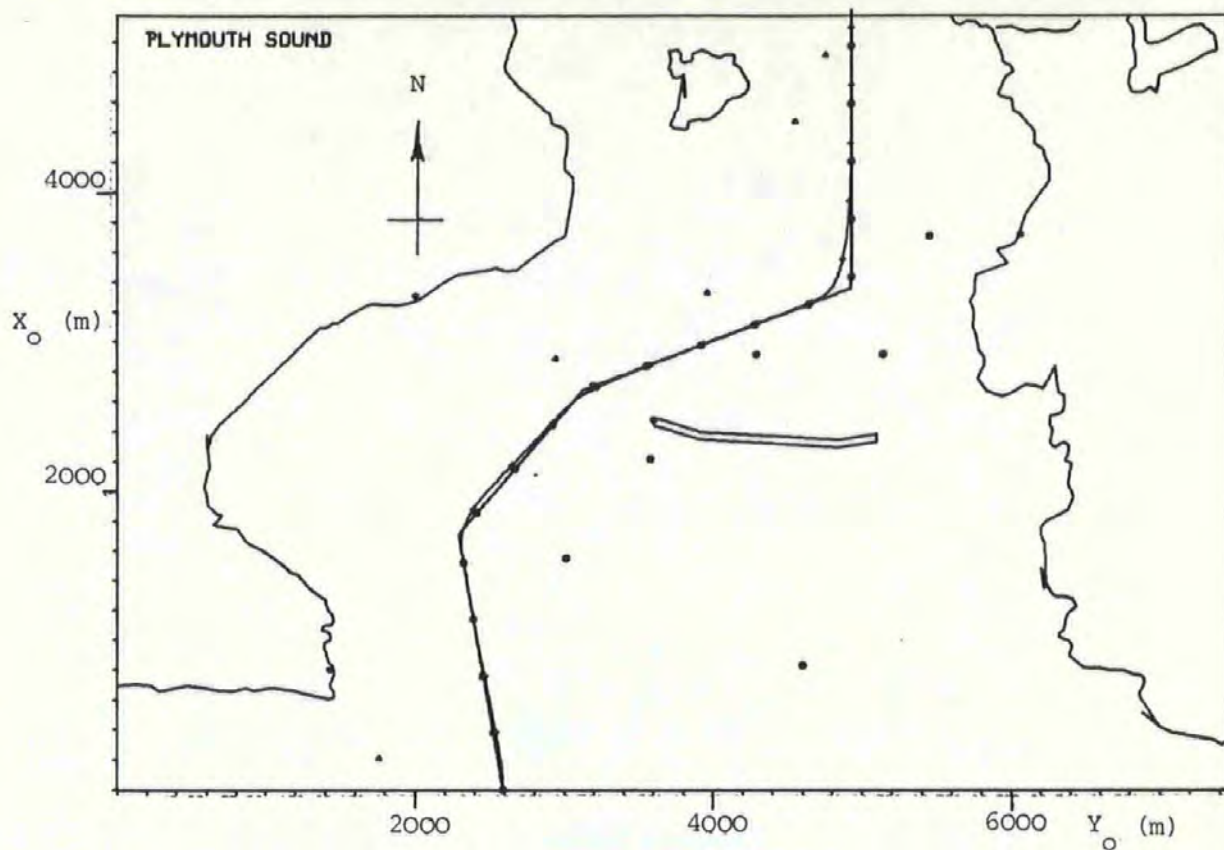


Figure 6.14(b)

Simulation 17

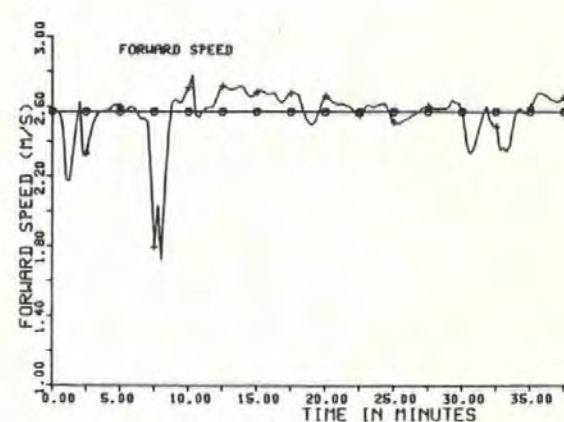
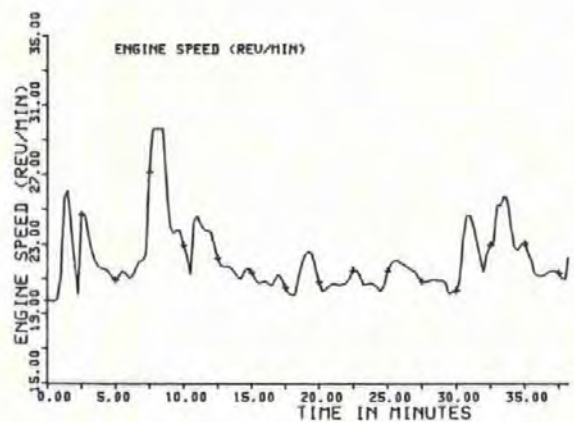
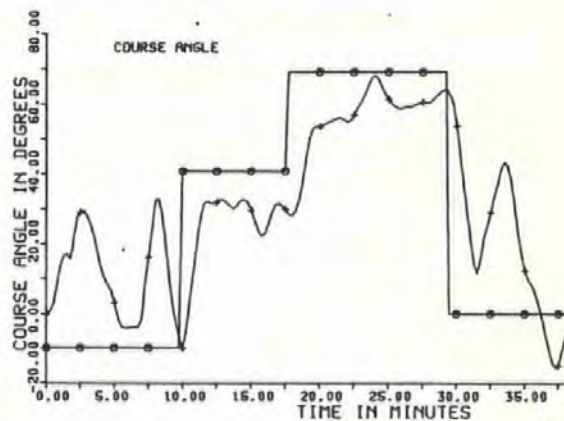
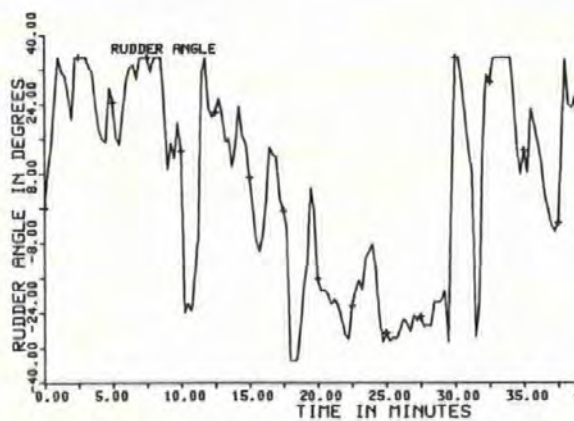
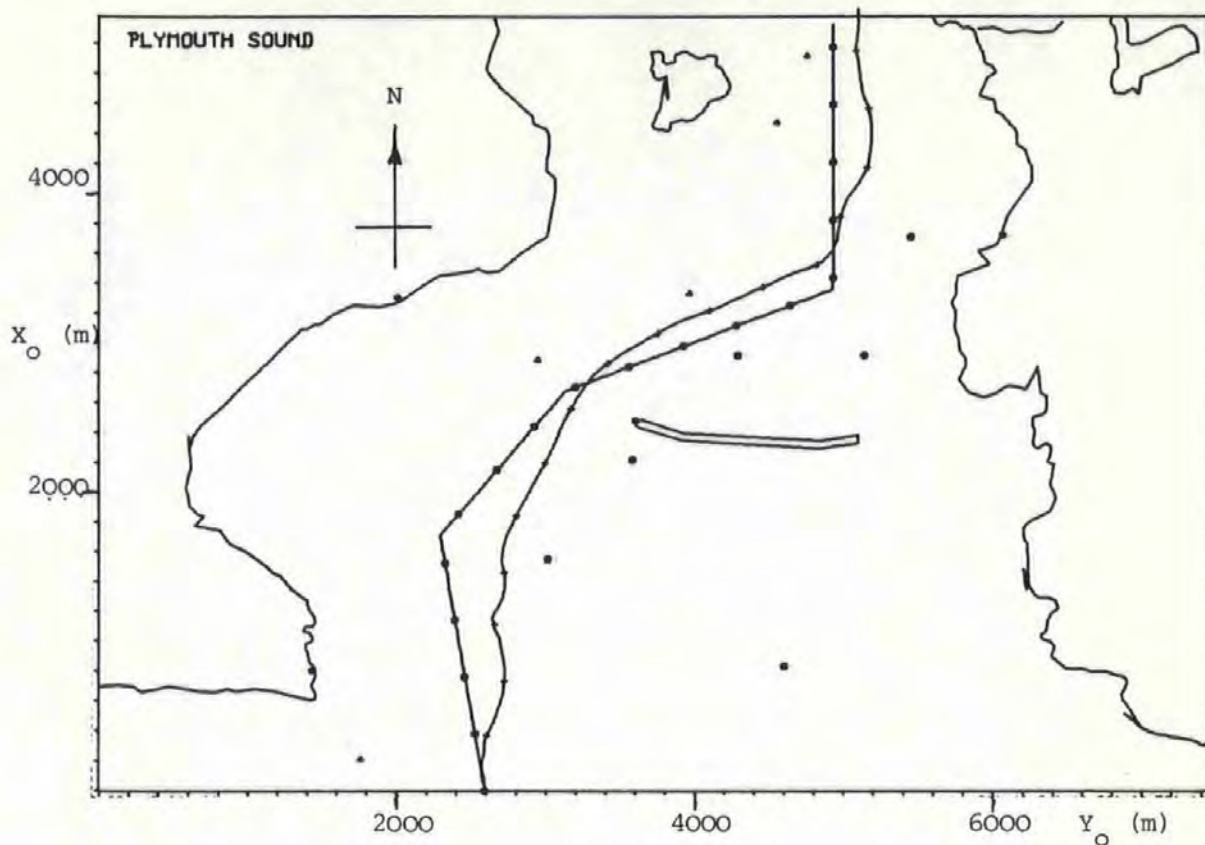


Figure 6.15(a)

Simulation 18

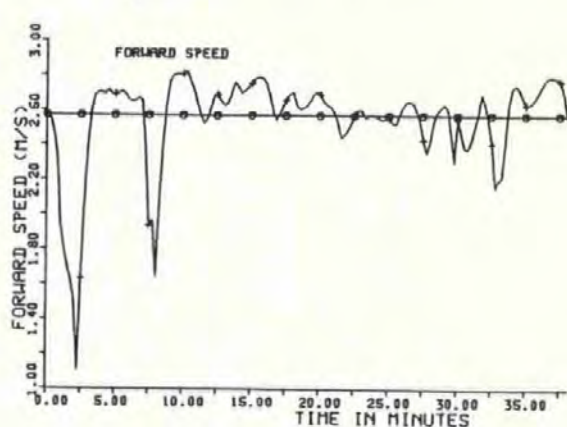
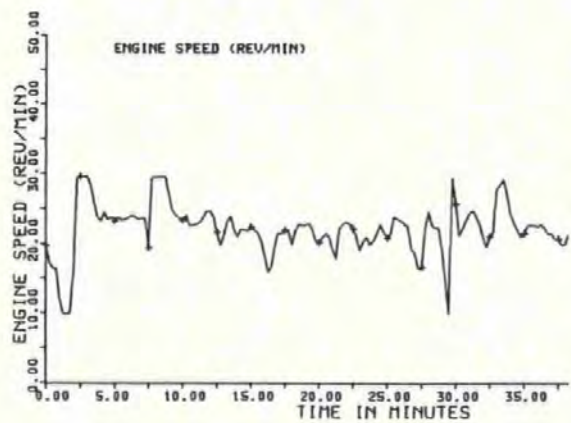
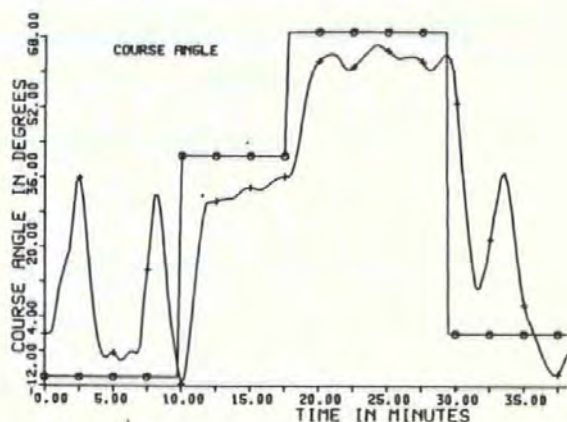
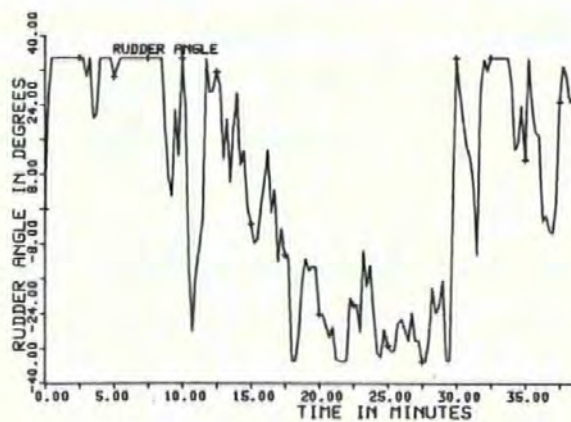
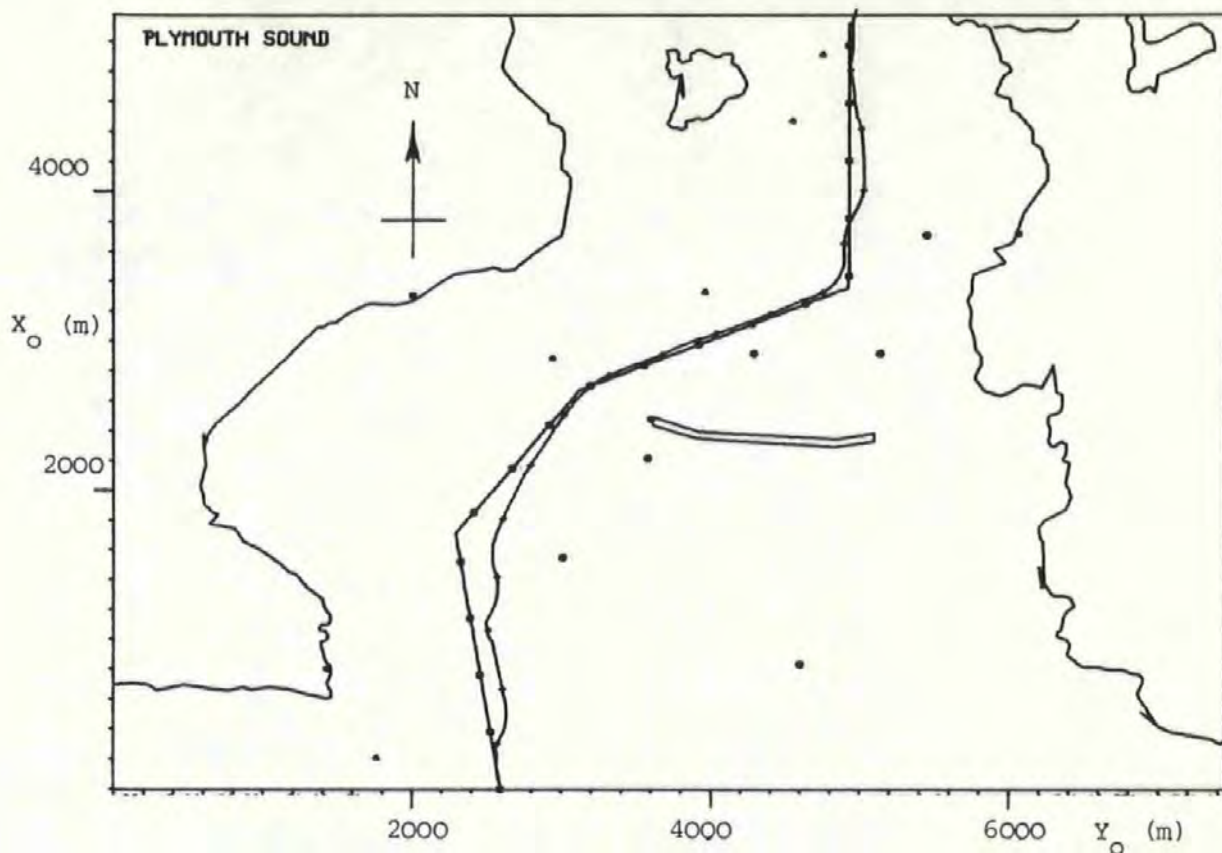


Figure 6.15(b)

Simulation 19

CHAPTER 7

SYSTEM IMPLEMENTATION

7.1 Introduction

The first step towards the physical realisation of a guidance system based on the controller design described in Chapter 5 together with the optimal filter of Dove was achieved by implementing the control and filter algorithms on a microprocessor situated on-board the model car ferry hull 5502. The complete system is shown schematically in Figure 7.1.

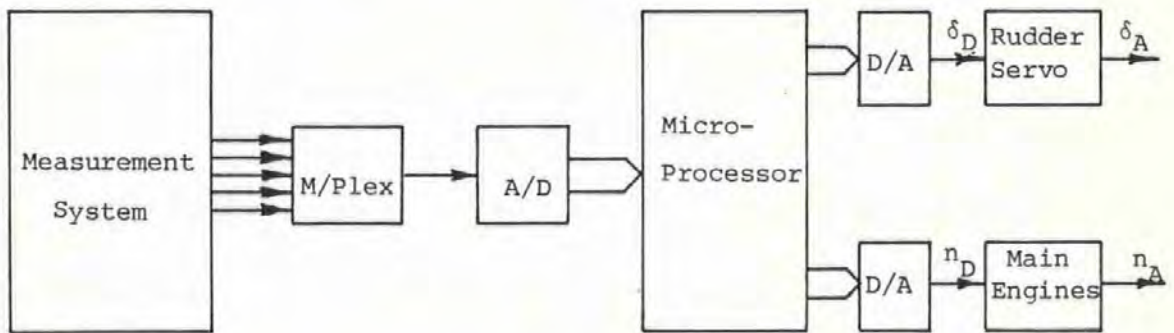


Figure 7.1

Schematic Representation of Guidance System

7.2 Measurement System

7.2.1 Review of Measurement Techniques

The selection of the state variables given in equations (2.4) and (2.5) were based upon quantities that not only describe the system

behaviour, but are also measureable by navigational aids on-board a full-size ship. When attempting to measure the same quantities within the constraints of a model vessel, problems of space restriction and cost dictate the need for a different approach.

Position Fixing

Since radio location is impractical, an underwater acoustic transponder system that uses localised grid co-ordinates was considered. A similar system, designed by Wood (81) is currently being used in the manoeuvring tank at the National Maritime Institute. The system employs a transmitter transducer mounted under the hull that transmits a 200 kHz signal in bursts of 100 μ s, once every second. The radial wave travels through the water and is received by four, equi-spaced transducers. The position of the vessel is a function of the transmission time to each receiver, and an accuracy of better than ± 7.5 cm over a distance of 40 m is claimed.

For control of a free-sailing vessel the system has the disadvantage that the positional information is shore-based and must be relayed back to the model via a telemetry link. The main problem however, was the high cost of the transmit and receive transducers and receive amplifiers. The fundamental idea is still attractive, and ways of 'in-house' transducer manufacture are being considered for future projects.

Linear Velocity Measurement

Measurement of the surge and sway velocity of the model hull pose a problem because of the small magnitude involved, particularly in the latter case, where even in a tight turn, values will not rise much above 0.1 m/s.

Conventional turbine and electro-magnetic logs lack in sensitivity, as do their doppler-sonar counterparts. A further

disadvantage is that both systems produce increased drag on the hull. Also of concern with the former systems is that they measure velocity relative to the water. Further investigation into doppler-sonar measurement revealed that two-axis systems were outside the project budget.

An alternative employed in aero-space applications is to measure the total linear acceleration vector and hence compute the components in the surge and sway directions, the respective velocities being obtained by integration. This type of inertial navigation system works well in aircraft, where accelerations are high. In the model hull however, a tight turn produces a sway acceleration in the region of 0.01 m/s^2 , and with a 1 g accelerometer (the most sensitive that could be obtained) this represents a signal of 10 mV. Another problem with inertial systems is that successive integration produces a progressively increasing error.

Angular Position and Velocity Measurement

The measurement of angular position (heading) and angular velocity (yaw-rate) fortunately did not present a problem. The Department of Mechanical Engineering had in its possession an accurate heading gyroscope, supplied by University College, London. Also it owned three servoed rate gyroscopes, mounted on orthogonal axes in order to measure pitch, roll and yaw-rates. The sensitivities of both heading and rate gyroscopes were sufficiently high to cope with the range of measurements expected.

7.2.2. Prototype Measurement System

Of the options available, a measurement system based on inertial principles (acceleration measurement) was the most viable in terms of performance and cost. Three servoed linear accelerometers were

purchased, and together with the existing gyroscopes formed the basis of an inertial sensing system.

Traditionally, inertial systems are mounted on a stabilised platform so that measurements of surge and sway accelerations are independent of pitch and roll. Also, if the platform is aligned to True North, accelerations relative to the earth's co-ordinate system are available.

Strap-down systems, of the type shown in Figure 7.2 are currently used in missiles and other aero-space applications.

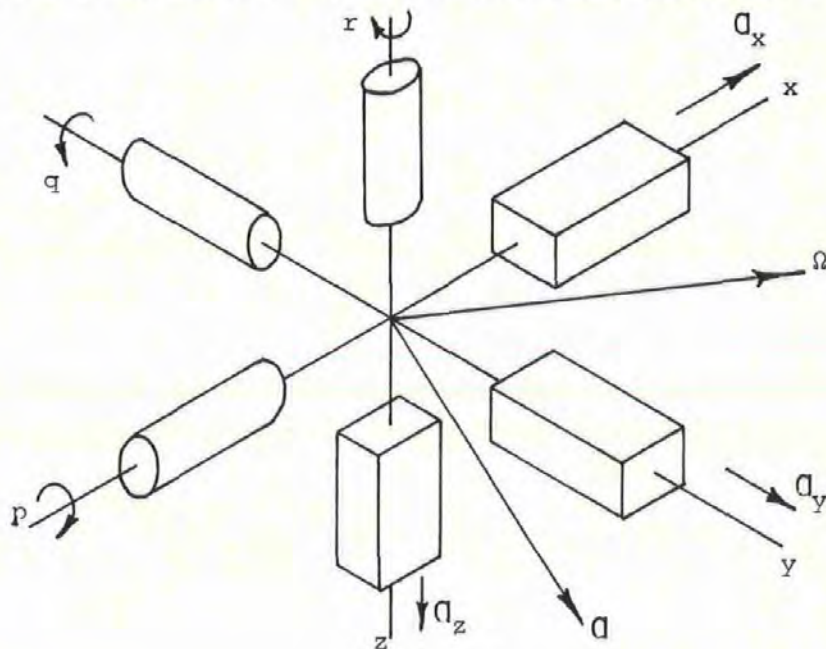


Figure 7.2

Strap-Down Inertial Navigation System

The instruments are mounted with respect to a local co-ordinate system and the total acceleration vector \mathbf{a} and angular rate vector $\mathbf{\Omega}$ computed according to the relationships:

$$\mathbf{a} = \mathbf{a}_x + \mathbf{a}_y + \mathbf{a}_z$$

$$\mathbf{\Omega} = \mathbf{p} + \mathbf{q} + \mathbf{r} \quad (7.1)$$

This allows accelerations and angular velocities to be calculated with respect to any other set of orthogonal axes. From a given set of initial conditions, other kinematic quantities may be obtained through successive integration.

A prototype measurement system consisting of 3 accelerometers and 3 rate gyroscopes conforming to the configuration in Figure 7.2 was constructed. In addition, heading was to be measured directly by the University College gyrocompass. The degree of redundancy of pitch, roll and heave transducers, at this stage, was unknown.

7.2.3. Initial Tests

To check how the accelerometers and rate gyroscopes would perform in a real manoeuvring situation, permission was obtained from Brittany Ferries to place the prototype system (excluding heading gyro) on the bridge of the 5000 tonne ferry Amorique. Recordings from the instruments were made on a Racal 4-channel tape-recorder whilst the Amorique manoeuvred in and out of Plymouth (and also Roscoff). In addition, use was made of the bridge radar, ship's log and rudder indicator to chart the actual track of the vessel and to collect information on forward velocity and rudder activity during the manoeuvres.

In this early stage, analysis of data was qualitative rather than quantitative. Play back of the tapes revealed that the ship's motions in yaw, roll and pitch were adequately measured by the rate gyros. Signals from surge and sway accelerometers (heave acceleration was not measured) were detectable during periods of high acceleration, but deeply buried in measurement noise (main engine vibration). Bearing in mind that all measurements in the final configuration would be passing through a Kalman filter, the decision was taken on the basis of these results to implement the inertial measurement system on

-board the model car ferry hull.

The positional and velocity data collected from the Amorique proved to be valuable when setting up the simulation programs described in Chapter 6. Also, what is difficult to quantify perhaps, is the insight given into the real problem of manoeuvring a large vessel in confined waters, as viewed from the bridge.

7.2.4 Measurement System Component Characteristics

800 ADA Servoed Linear Accelerometer

Manufactured by Smiths Industries, these accelerometers are of high sensitivity and operate as torque balance, closed-loop systems. As shown in Figure 7.3, accelerations along the input axis produce a force on the mass. Resultant movement of this mass is detected by an optical pick-off and fed back to the coil of a torque motor, which returns the mass to its null position. The magnitude of the torque motor current is a measure of the acceleration.

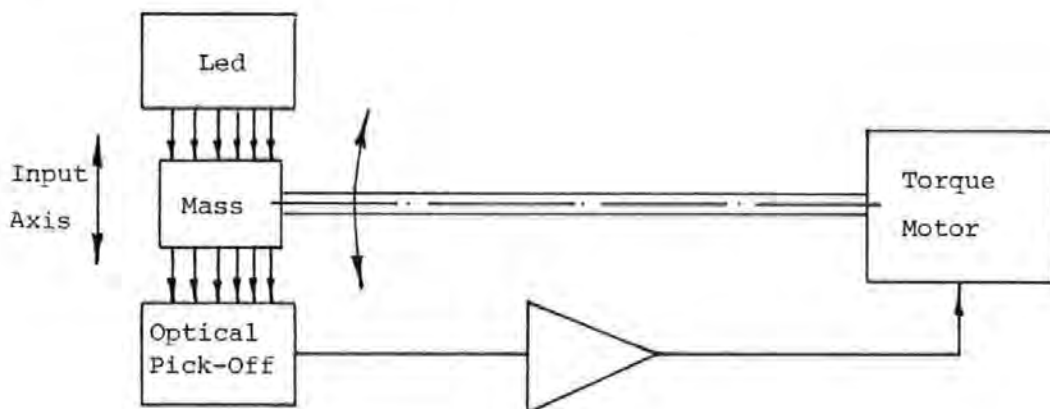


Figure 7.3

800 ADA Servoed Linear Accelerometer

Specification

Input Range: ± 1 g surge and sway directions
 ± 2 g heave direction.
Electrical Supply: ± 12 V d.c.

Output Range: ± 10 V d.c.

Sensitivity (As supplied by manufacturer and confirmed by calibration tests).

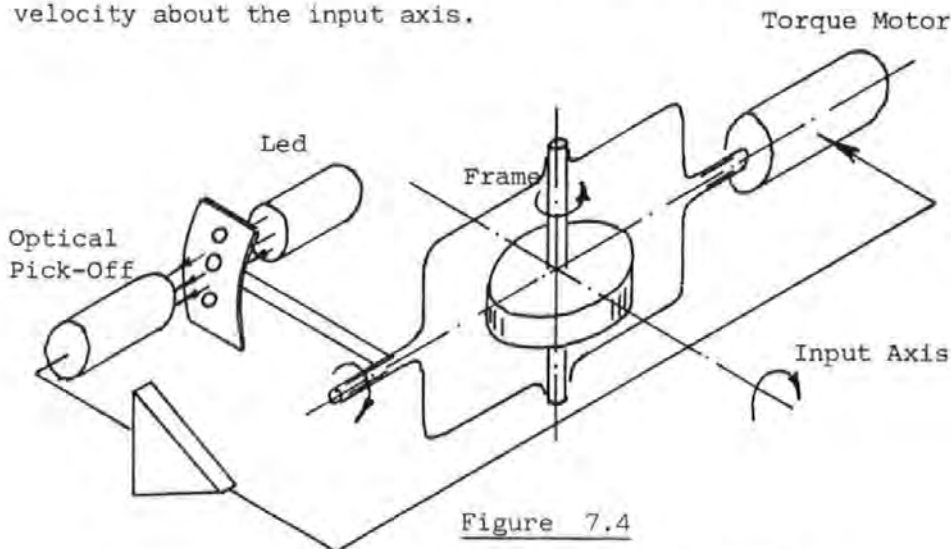
Surge Accelerometer: $1.018135 \text{ V s}^2/\text{m}$

Sway Accelerometer: $1.020191 \text{ V s}^2/\text{m}$

Heave Accelerometer: $0.509642 \text{ V s}^2/\text{m}$

900 Series Servoed Rate Gyroscope

Again a product of Smiths Industries, the rate gyroscopes employ a d.c. motor to drive a brass rotor at high speeds to obtain the necessary angular momentum. The deflection of the frame in Figure 7.4 due to the gyroscopic couple is detected by an optical pick-off and fed back to a torque motor, which returns the frame to its null position. The torque motor current is a measure of the angular velocity about the input axis.



900 Series Servoed Rate Gyroscope

Specification

Input Range: ± 50 degrees/s full scale.

Electrical Supply: ± 6 V d.c.

Output Range: ± 3 V d.c.

Sensitivity (As supplied by manufacturer and confirmed by calibration tests)

Yaw-Rate Gyroscope: -3.28549 V s/rad .

Pitch-Rate Gyroscope: -3.27138 V s/rad .

Roll-Rate Gyroscope: -3.17419 V s/rad .

ADC Heading Gyroscope

Supplied by University College, London, the heading gyroscope, seen in Figure 7.11, was manufactured by American Design Components (ADC) of New York. To operate the gyro, the inner frame is caged and the spin rotor run up to speed. When steady conditions exist the position motor is used to drive the inner frame to the null position on the measurement bridge shown in Figure 7.5.

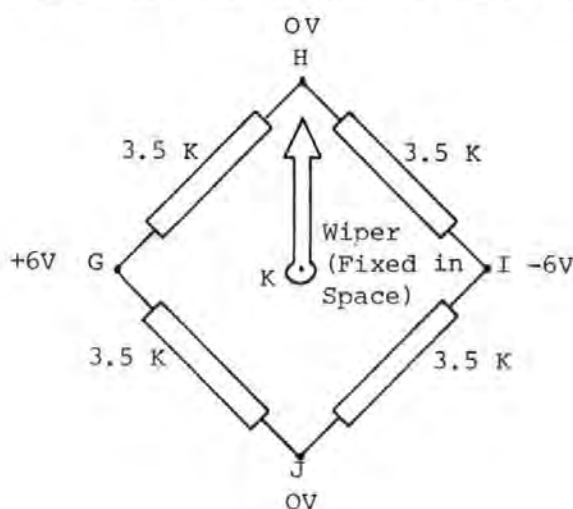


Figure 7.5

Heading Gyroscope Measurement Bridge

With the vessel pointing due North, the gyro is uncaged. If it is now set to point due East, the gyro outer frame and hence the bridge windings turn starboard through 90 degrees. Position G is now aligned with the wiper and the output signal is + 6 V d.c. Similarly, if the vessel points South, the output is 0 V d.c. and if it points West, - 6 V d.c.

The problem with this arrangement is that for each signal output, there exists two possible headings. For example:

0 V d.c. = 0 or 180 degrees
+3 V d.c. = 45 or 135 degrees
-3 V d.c. = 225 or 315 degrees.

To avoid confusing the guidance system, this placed a restriction that all test manoeuvres should be confined to ± 90 degrees.

Specification

Input Range: ± 90 degrees full scale

Electrical Supplies:

Measurement Bridge: ± 6 V d.c.

Output Range: ± 6 V d.c.

Gyro Spin Motor: + 12 V d.c.

Sensitivity (By calibration): 3.8993 V/radian

7.3 The Measurement Package

The measurement package consisted of the accelerometers and rate gyros mounted in a waterproof box as shown in Figure 7.6. This package, as with all other high cost equipment, was attached to the hull with quick-release screws.

In order to avoid signal contamination, the instrumentation and servo-motor power supplies were separated. The general arrangement of the former are shown in Figure 7.7.

7.4 Rudder and Engine Servo-Systems

7.4.1 Rudder Servos

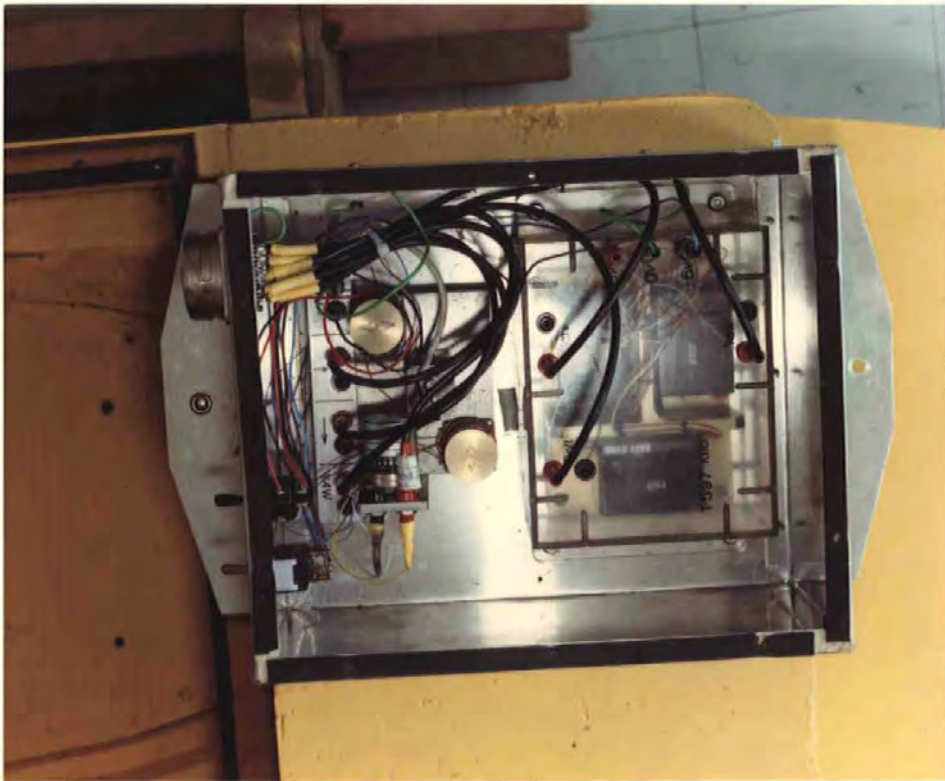
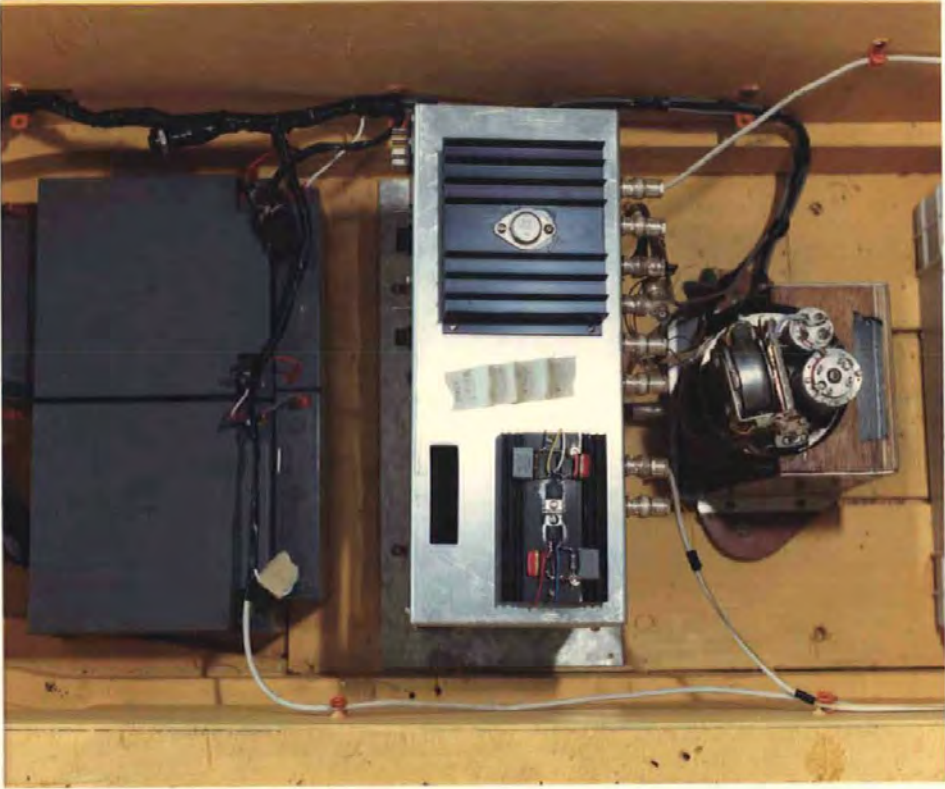
Each rudder had its own servo-drive (although eventually both were linked to a single unit) which consisted of a conventional feedback positional control system driven by a d.c. servo-motor. Conductive plastic potentiometers were employed to reduce signal noise and a 1.0 Amp power operational amplifier (National Semiconductor

Figure 7.6

Measurement Package

Figure 7.11

Top View of TMS 9900 Computer, Power
Supplies and Heading Gyroscope.



LH0021) was used to drive the servo-motor. The schematic diagram is given in Figure 7.8(a) and a photograph of the rudder servo-system is shown in Figure 7.8(b).

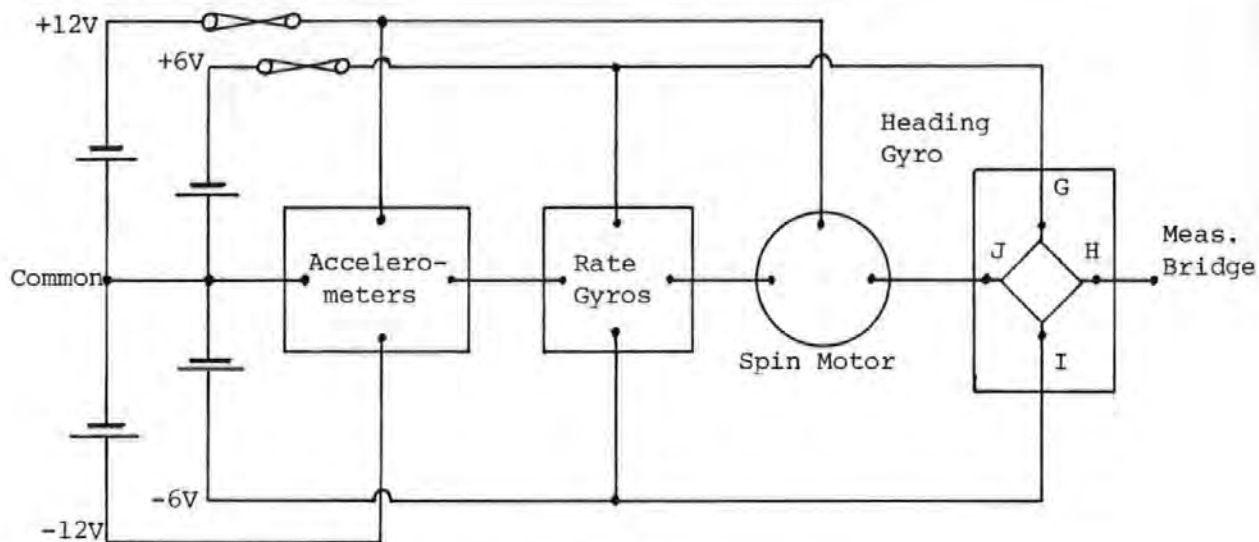


Figure 7.7

Instrumentation Power Supplies

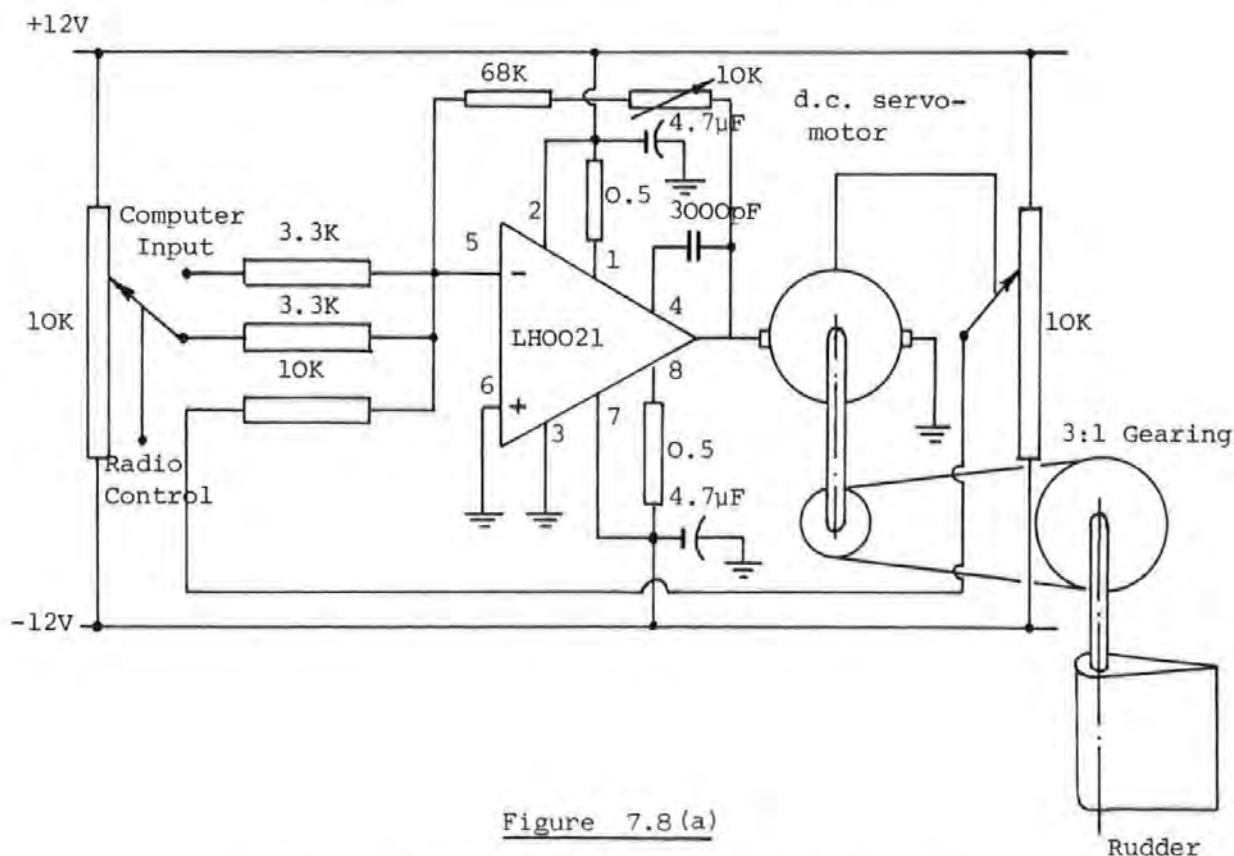
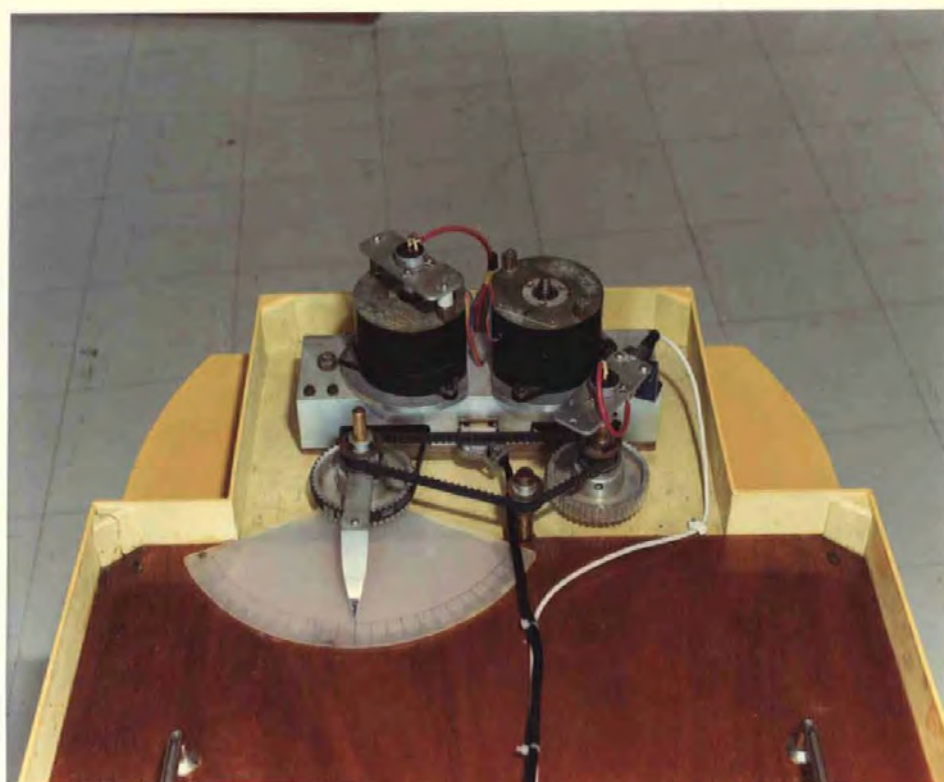


Figure 7.8 (a)

Schematic Diagram of Rudder Servo-System

Figure 7.8(b)
Rudder Servo-System

Figure 8.12
Model in a Tight Turn
on the Reservoir



The operational requirements of the system were:

- (i) To produce sufficient torque at the rudder to overcome friction and hydrodynamic moments.
- (ii) To achieve a rapid response with no more than 10% overshoot with rudder immersed in water.
- (iii) To provide ± 40 degrees rudder deflection from either radio control or computer input.

Although a fairly large d.c. motor was employed, there was insufficient torque at the motor shaft to meet requirement (i). The torque was increased by a factor of three to a suitable value by the use of a timing belt and pulleys.

The dynamic characteristics were tuned by varying the feedback resistance of the operational amplifier and the correct rudder deflection obtained by careful selection of input resistance values. The radio-control rudder deflection was finally increased to ± 50 degrees to allow for steerage under a computer malfunction "hard-over" command.

Rudder Servo Characteristics

Static

Sensitivity (computer input) : 0.4385 rad./V.

Dynamic

Rise Time: 0.2 seconds

Damping Ratio: 0.7

7.4.2 Engine Speed Control

As with the rudders each engine was equipped with its own speed control system. Since, at any given speed, the hydrodynamic moments on the propeller remain approximately constant, it was decided that open-loop speed control would give sufficient accuracy.

The d.c. motor power requirements, measured during towing-tank tests were known to be 2 A at 24 V to rotate the propeller at 712 rev./min. in water. This performance was obtained from a NPN/PNP darlington pair of power transistors (TIP 141 and TIP 146) which were used to supply the armature current to the d.c. motor, the base current to each transistor being provided by a 300 mA 759 operational amplifier as shown in Figure 7.9.

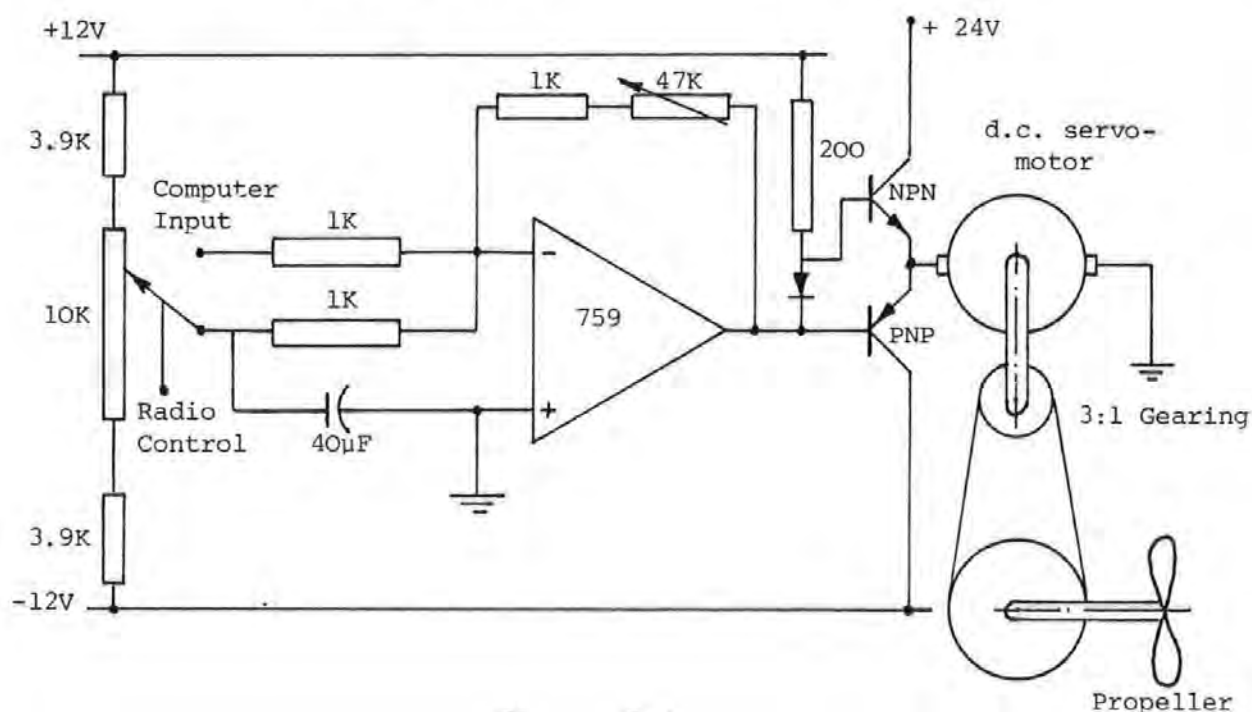


Figure 7.9

Schematic Diagram of Engine Speed Control

Initial tests on the system indicated that a maximum unloaded speed of 250 rev./min. was available at the motor. This was increased to 750 rev./min. at the propeller shaft by gearing, but fell to 500 rev./min. under normal operating load. Finally, an asymmetric power supply (+24 V, -12 V) was employed on the power transistors to provide the following performance characteristics:

Static

Maximum forward speed: 1,000 rev./min. unloaded
750 rev./min. loaded.

Maximum reverse speed: 750 rev./min. unloaded
500 rev./min. loaded

Sensitivity (computer input); 105.263 rad/sV

Dynamic

Time Constant: 0.15 seconds.

As with the rudder servo, sufficient control was available from the radio link to override any computer malfunction command.

When the rudder and engine servos were connected to the same power supplies, a certain amount of interaction took place during motor transients. This was overcome by inserting a 40 μ F capacitor between one of the engine inputs and ground.

7.5 Microcomputer Hardware

A Texas TMS 9900 microprocessor was used for the on-board computer facility. The machine was chosen because:

- (i) It has 16-bit capacity.
- (ii) Several TMS 9900 processors were already in use within the Department. With the given expertise of Academic and Technical Staff, a rapid implementation could be achieved.

7.5.1 General Features of the TMS 9900

The TMS 9900 is a 16-bit machine with bit, byte and word processing capability. It operates with 16-bit instructions which may be one, two or three words long. The instruction set comprises of 69 operations which employ a total of 5 addressing modes.

The Workspace Concept

The TMS 9900 chip contains the following registers:

- (1) Program Counter (PC)
- (2) Workspace Pointer (WP)
- (3) Program Status Register (ST)

Instead of hardware working registers, the processor has the ability to create a file of 16 general purpose registers in RAM. In principle, each of these registers can be used for any purpose the programmer chooses, though in practice some of the registers are usually reserved for particular functions in connection with software instructions and addressing modes. To create a workspace area, the workspace pointer register is loaded with the starting address.

Input/Output Capability

The TMS 9900 chip has separate 16-bit data and address busses, the latter giving the capability of accessing 64 k bytes of memory. Input/Output operations are performed by a Communication Register (CRU). This is a system whereby the information bits enter/leave the CPU in serial fashion and parallel series or series parallel conversion takes place under software control in synchronism with the CPU.

7.5.2 System Configuration

The TMS 9900 may be configured in various arrangements, depending upon the requirements of the programmer. When operating as an on-board controller/estimator/logger, the system must contain the following functions:

- (i) High-level language facility (BASIC)
- (ii) Program storage on EPROM
- (iii) A/D and D/A conversion
- (iv) Data logging capability

This was achieved by a four, printed circuit board system, the

memory-map details of which are given in Figure 7.10.

7.5.3 A/D and D/A Conversion

Analogue to digital and digital to analogue conversion is performed on the TMS 9900 by reading and writing, by means of a move-word instruction, to a small memory area hard-wired to a user-defined base address, in this case $9FF0_{16}$. Both A/D and D/A units are bipolar and contain 12-bit accuracy, so that ± 2047 separate increments are available. When set to unity gain, this provides an A/D resolution of 4.885 mV per bit. A summary of the functions are given below.

D/A Conversion (2 Channels)

Channel 1. Write to (Base Address + 2) i.e. MWD(09FF2H) = D1

Channel 2. Write to (Base Address + 0) i.e. MWD(09FF0H) = D2

A/D Conversion (16 Channels)

Select Channel. Write to (Base Address + 8) 0, 1, 2 etc.

Select Channel 1. MWD(09FF8H) = 0001H

Set Gain Write to (Base Address + 6)

00 Gain = 1

01 Gain = 2

10 Gain = 4

11 Gain = 8

For Gain = 2 MWD(09FF6H) = 0001H

Start Conversion. Initiated by Write to (Base Address + A)

End Conversion. Conversion complete if contents of (Base Address + C) are positive.

Conversion time = 25 μ s.

Read Data. Data contained in bytes (Base Address + E)
and (Base Address + F).

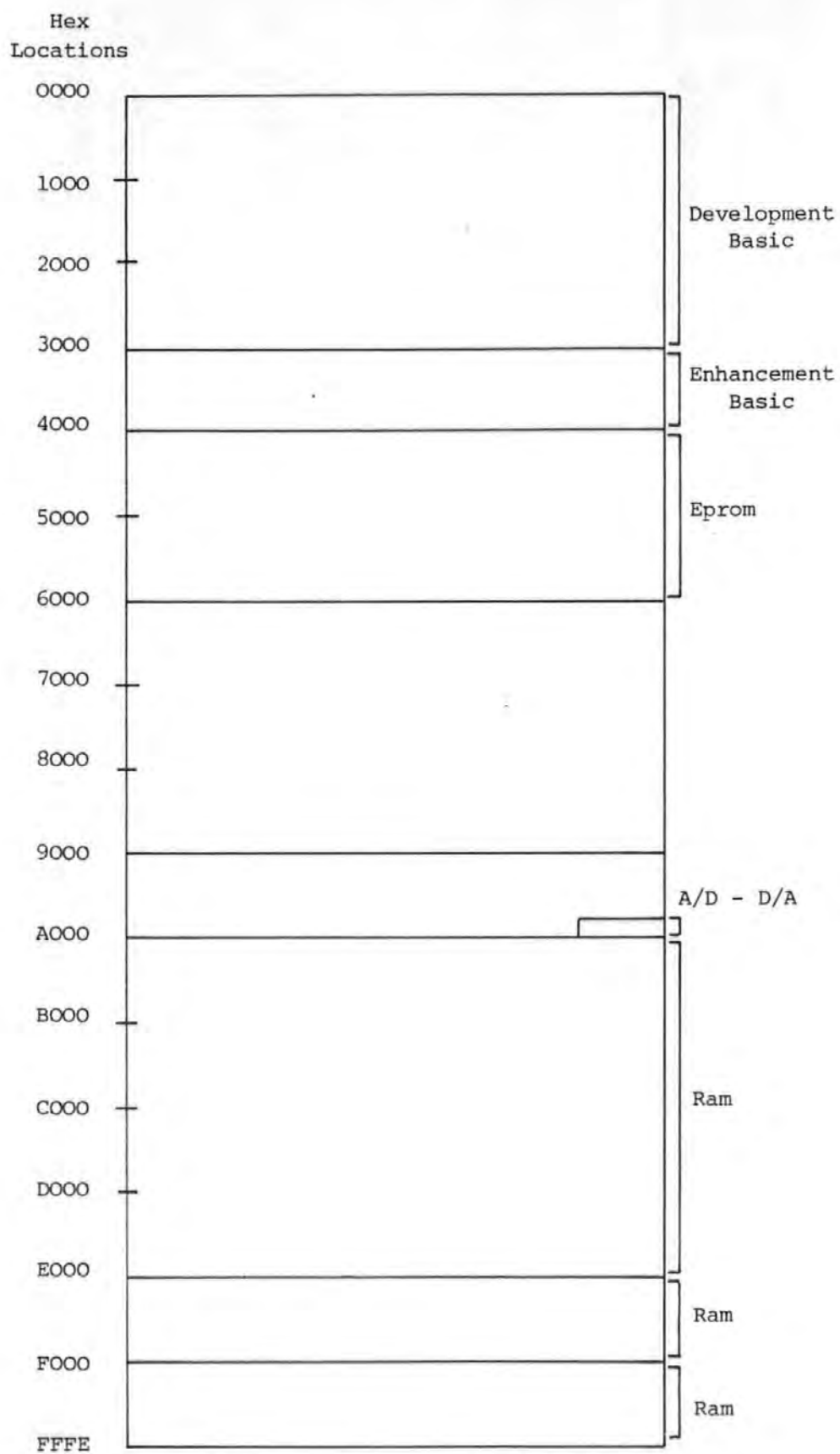


Figure 7.10

TMS 9900 Memory-Map.

An A/D subroutine would then be:

```
00  REM  ADC  SUBROUTINE
10  MWD(09FFAH) = OFFFH
20  CHK = MWD(09FFCH)
30  IF CHK<0 THEN GOTO 20
40  AC = MWD(09FFEh)
50  RETURN
```

Computer Power Supplies

The tolerances on the computer power supplies ($\pm 3\%$) were tighter than could be obtained directly from a battery. Three regulators (+5V, +12V and -12V) were mounted on heat sinks and attached to the top of the computer casing to obtain maximum heat transfer, as can be seen in Figure 7.11.

7.6 Commissioning Trials

7.6.1 Commissioning Test 1. 19.7.83

This first test was performed on the Rowing Club side of the River Plym under wind conditions of force 2/3 and a slightly choppy water surface. Signals from three accelerometers and 3 rate-gyros were relayed by cable to a shore-based 8-channel Racal tape-recorder. The heading gyro was inoperative due to transportation damage.

The objectives of the test were:

- (i) To commission the measurement package and servo-drives to rudders and main engines.
- (ii) To determine the degree of transducer redundancy.
- (iii) To qualify signal magnitudes.

The test consisted of driving the vessel, under radio control, 20 m in a straight line followed by a 180 degree turn to port. The vessel returned along a reciprocal course arriving at the start point

again by a further 180 degree turn to port.

Problems were experienced with:

- (a) Sea-weed fouling the propellers.
- (b) Cable drag in the water.
- (c) Main engines running at only 60% of design speed.

A reasonable set of results however, were recorded on the fourth run, and are shown in Figure 7.12. The points to be noted are:

- (i) Surge acceleration is small, a slight deceleration being evident during the turn.
- (ii) Sway acceleration very noisy, due to rolling (up to 20 degrees) of vessel.
- (iii) Heave acceleration negligible.
- (iv) Pitch-rate small.
- (v) Good yaw-rate signal, particularly in turn.
- (vi) Large roll rates (note correlation with sway accelerometer).

It is evident from the above that heave and pitch measurements are small enough to be neglected, thus simplifying vector equation 7.1. Under calmer conditions, this statement could equally apply to roll measurements.

The sensitivity of the sway accelerometer to roll gave cause for concern, since integration would give unreal harmonic variation in sway velocity.

7.6.2 Commissioning Test 2.3.8.83.

In order to avoid sea-weed complications, the site location was changed to the National Trust side of the River Plym, launching from Point Beach. To overcome cable drag problems, the test consisted of a turning circle around a moored sailing boat, on-board which sat the 8-

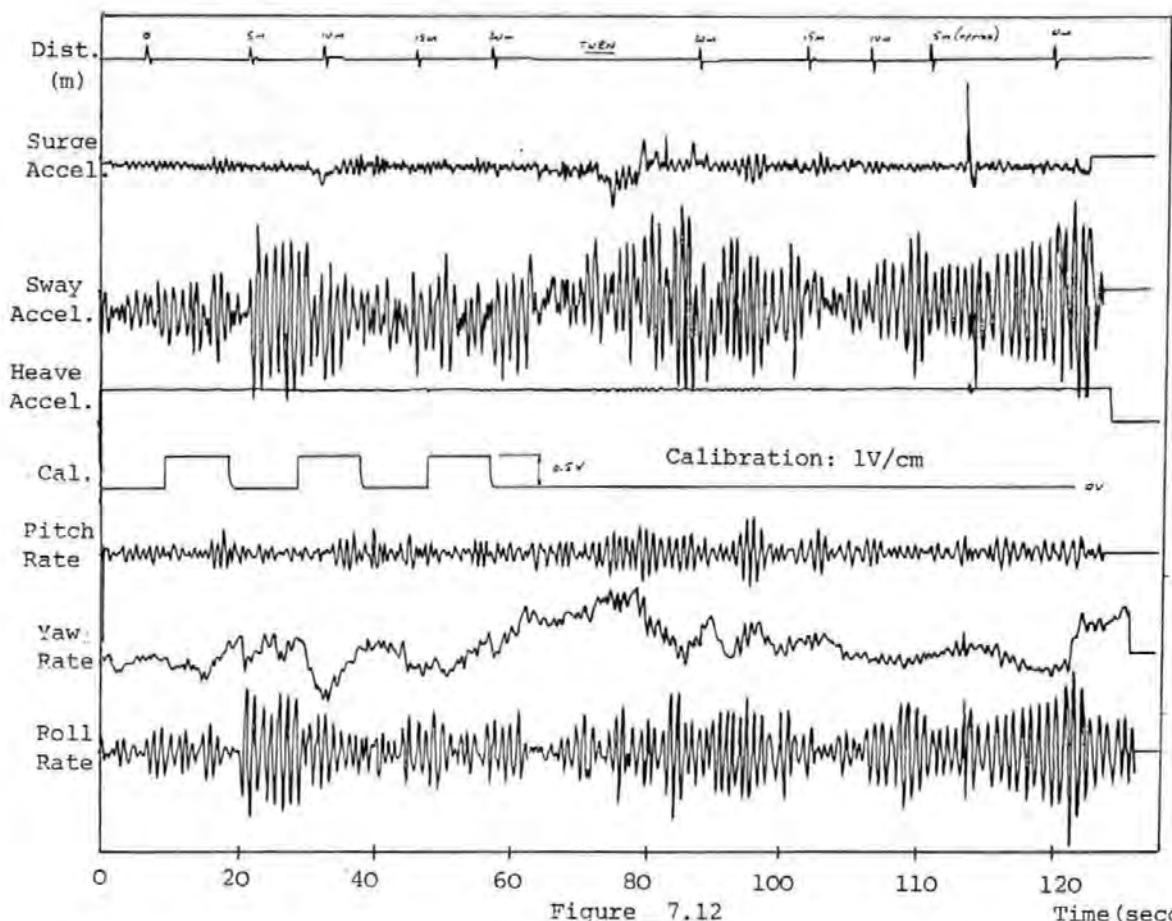


Figure 7.12

Time (seconds)

Commissioning Test 1

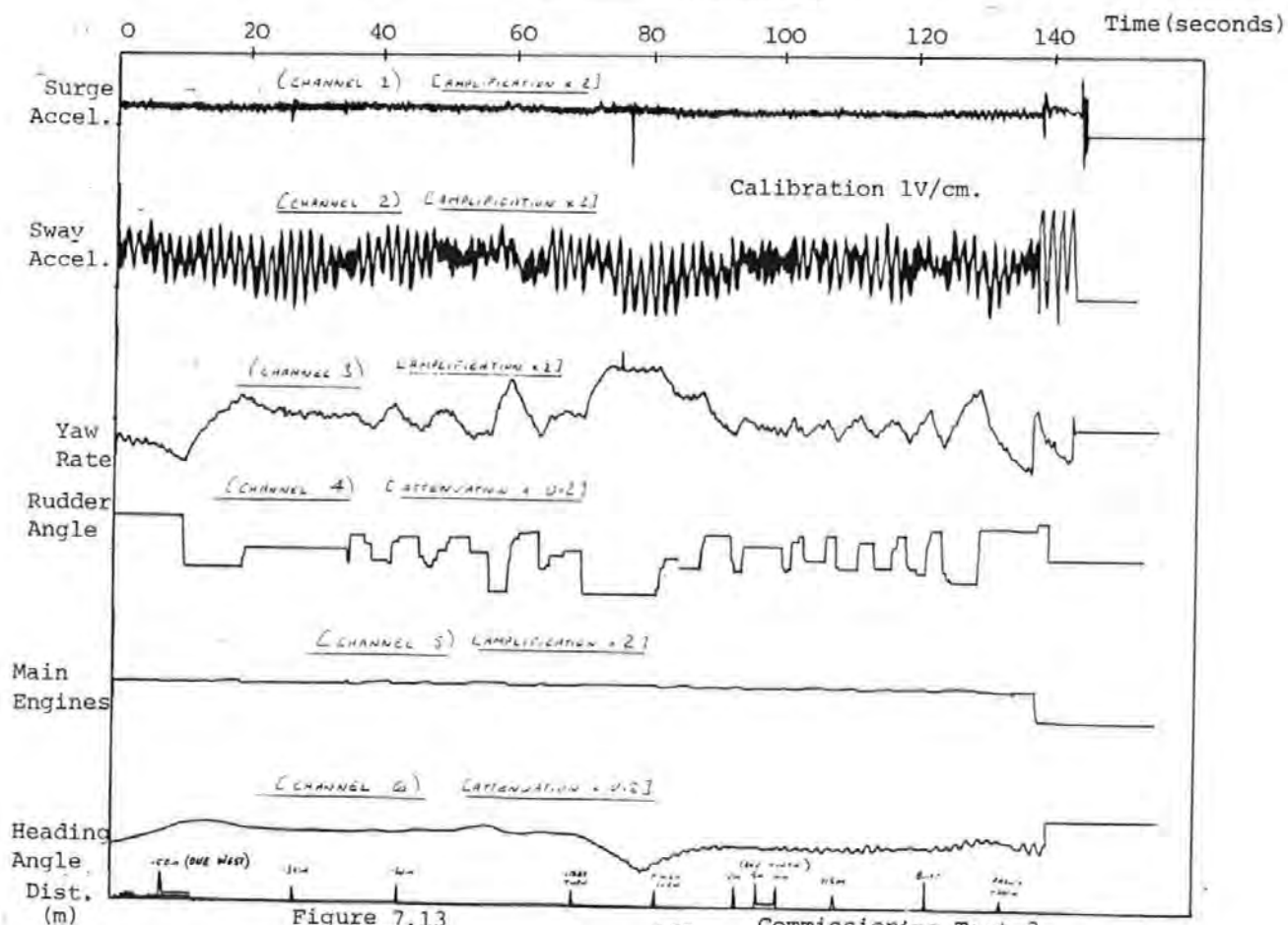


Figure 7.13

160

Commissioning Test 3

channel tape-recorder. The speed of the main engines had now been increased to their design value by the addition of a + 24V rail, as described in section 7.4.2.

The test was unsuccessful due to wind rising in the setting-up period from force 1 to force 3/4. When attempting to perform a turning circle around the moored vessel, the model hull became uncontrollable when it was beam-on to the wind.

Other problems encountered were again cable drag and also main engine malfunction which was diagnosed to be a faulty wiper contact on the 47k preset shown in Figure 7.9. The cure was to replace it with a standard potentiometer.

7.6.3. Commissioning Test 3. 12-20.9.83.

The frustrations of attempting to co-ordinate tide, weather and wind on the River Plym made the search for a more desirable site a high priority. Also, since much time was wasted in setting up, a site where the model could be left would be advantageous.

Such a site was eventually found at the South West Water Authority's water treatment works, Crownhill. Here, the reservoir measured 110 m x 110 m and, depending upon wind direction, usually contained at least one stretch of sheltered water. Further, the reservoir was used by Plymouth Model Boat Club and possessed an excellent winched launching platform facility. In addition, mains power was available for test instruments and battery charging.

The tests were performed around one of the four corners of the reservoir, depending upon wind direction. The vessel was driven towards the corner, parallel to, and about 3 m from the side for a distance of 50 m. It was then turned under radio control through 90 degrees and piloted away from the corner, again parallel to the side. The 8-channel tape-recorder was wheeled on a trolley along

the side of the reservoir, the connecting cable being held vertically above the model at all times by means of a boom.

Several runs were undertaken and Figure 7.13 shows a typical set of results. It can be seen that surge acceleration is fairly constant, but has a d.c. bias due to uneven balast. Sway acceleration still contains a large component of roll which will be considered as measurement noise by the optimal filter. Good correlation is obtained between rudder angle, heading and yaw-rate, all of which are reasonably noise-free signals.

Engine and rudder servos performed satisfactorily, although in the latter case, if too much trim was applied, the rudder angle could exceed 50 degrees. This allowed the feedback potentiometer to pass the $\pm 12V$ discontinuity point and the rudder would attempt to rotate through 360 degrees and end up jammed hard over. The problem was overcome by the use of mechanical stops at ± 40 degrees.

CHAPTER 8

FREE - SAILING TRIALS

8.1 Introduction

The aims that were set when planning the execution of the free-sailing trials on the model hull are listed below:

(i) Track-Keeping

To demonstrate the ability of the control system to lock onto a pre-defined track from any given combination of initial conditions.

(ii) Track-Changing

To show the system is able to change from one track to another when initially under: (a) steady-state conditions, (b) transient conditions (as may be experienced when way-points are close together).

(iii) Speed Control

To observe the characteristics of the forward velocity control of the vessel.

(iv) Comparison With Theoretical Predictions

To compare the trial results with those predicted by computer simulation.

(v) Measurement Accuracy

To determine the accuracy of the measurement system and the effectiveness of the filter/estimation algorithm. This analysis has been undertaken by Dove (78) and is not included here.

Limitations

The trials were conducted at constant forward speed under calm water conditions with the absence of tide, wind and waves. These limitations were imposed because:

- (a) Restrictions in speed and size of the on-board computing facility to fully implement the control and filter algorithms.
- (b) The problems of obtaining scaled disturbance effects on open water with known mean and statistical properties.

8.2 Selection of State Variables for Model

When a comparison between the model and a full-size vessel is made, two main differences exist:

- (a) No positional measurement takes place on the model.
- (b) The dynamics of the rudder and engines are rapid and may be neglected.

Under these conditions, the state vector as defined by equation (2.4) reduces to:

$$\begin{matrix} & T \\ X & = (u \ v \ \psi \ r) \\ & A \end{matrix} \quad (8.1)$$

It will be noted that all of these variables are measurable from the on-board instrumentation pack.

8.2.1 Reduced State Equations

The reduced state equations for the model, with no disturbance terms, become:

$$\begin{pmatrix} \dot{u} \\ \dot{v} \\ \dot{\psi}_A \\ \dot{r} \end{pmatrix} = \begin{pmatrix} f_{11} & f_{12} & 0 & f_{14} \\ f_{21} & f_{22} & 0 & f_{24} \\ 0 & 0 & 1 & 0 \\ f_{41} & f_{42} & 0 & f_{44} \end{pmatrix} \begin{pmatrix} u \\ v \\ \psi_A \\ r \end{pmatrix} + \begin{pmatrix} g_{11} & g_{12} \\ g_{21} & g_{22} \\ 0 & 0 \\ g_{41} & g_{42} \end{pmatrix} \begin{pmatrix} \delta_D \\ n_D \end{pmatrix} \quad (8.2)$$

The elements of the reduced F and G matrices all exist in the original non-linear state equations and are defined in Appendix A1.3.

F Matrix

Reduced Element Designation: $f_{11} f_{12} f_{14} f_{21} f_{22} f_{24} f_{41} f_{42} f_{44}$

Original Element Designation: $f_{44} f_{46} f_{48} f_{64} f_{66} f_{68} f_{84} f_{86} f_{88}$

G Matrix

Reduced Element Designation: $g_{11} g_{12} g_{21} g_{22} g_{41} g_{44}$

Original Element Designation: $f_{41} f_{42} f_{61} f_{62} f_{81} f_{82}$

8.3 Controller Parameters

The design and simulation package used to determine controller parameters for the full-size vessel was now used to compute the parameters for the model hull. It was anticipated that the weightings of the Q and R matrices given in equation (6.11) would remain unchanged for two dimensionally similar hulls. This, however, was not the case and the feedback matrix computed for the model heavily emphasised course-keeping, rather than track-keeping performance.

The implication from this result suggests that for both hulls the course-keeping control parameters are approximately the same, but the track-keeping parameters for the model hull need to be increased. This, with hindsight, is explained by the fact that for both hulls the expected course error is of a similar magnitude whereas track errors might be of an order of ten times smaller for the model hull, requiring larger feedback gains to produce similar rudder deflections.

The optimal root locus diagram technique outlined in Chapter 5

was again employed and the selected weightings, together with the corresponding feedback matrix for a forward speed of 0.75 m/s are given in equations (8.3) and (8.4)

$$\begin{aligned} Q &= \text{diag. } \{0 \ 0 \ 0.0005 \ 0.5 \ 0.1 \ 0 \ 1 \ 0\} \\ R &= \text{diag. } \{1 \ 1\} \end{aligned} \quad (8.3)$$

$$S = \begin{bmatrix} 0.026 & 0 & 0 & 0 & -0.06795 & 2.765 & -0.9329 & -3.1029 \\ 0 & 0.19\text{E-}5 & 0.00107 & 0.0479 & 0 & 0 & 0 & 0 \end{bmatrix} \quad (8.4)$$

The reduced version of equation (8.4) is:

$$S = \begin{bmatrix} -0.06795 & 2.765 & -0.9329 & -3.1029 \\ 0.00107 & 0.0479 & 0 & 0 \end{bmatrix} \quad (8.5)$$

with track and forward position terms s_{11} and s_{21} retained.

Of interest is that the course-keeping terms s_{13} and s_{14} in equation (8.5) are almost identical to those calculated before the Q weightings were varied. This implies that dual-mode control switching from track to course-keeping may be implemented by simply setting s_{11} to zero without fear of instability.

The optimal closed-loop eigenvalues for the 8-state system with feedback matrix (8.4) are:

$$\begin{aligned} s &= -4.8235 ; \ -0.3998 ; \ -0.1427 ; \ -0.2521 ; \\ &0.0 ; \ -0.0317 ; \ -0.105\text{E-}4 ; \ -4.9999. \end{aligned} \quad (8.6)$$

Figure 8.1 shows a simulation of a 90 degree track-changing situation using the reduced state equations (8.2) together with the feedback matrix (8.5) when the forward speed is 0.75 m/s. Here the dual-mode controller switches from track to course-keeping when the course error exceeds 30 degrees. The way-point advance is 15.75 m and

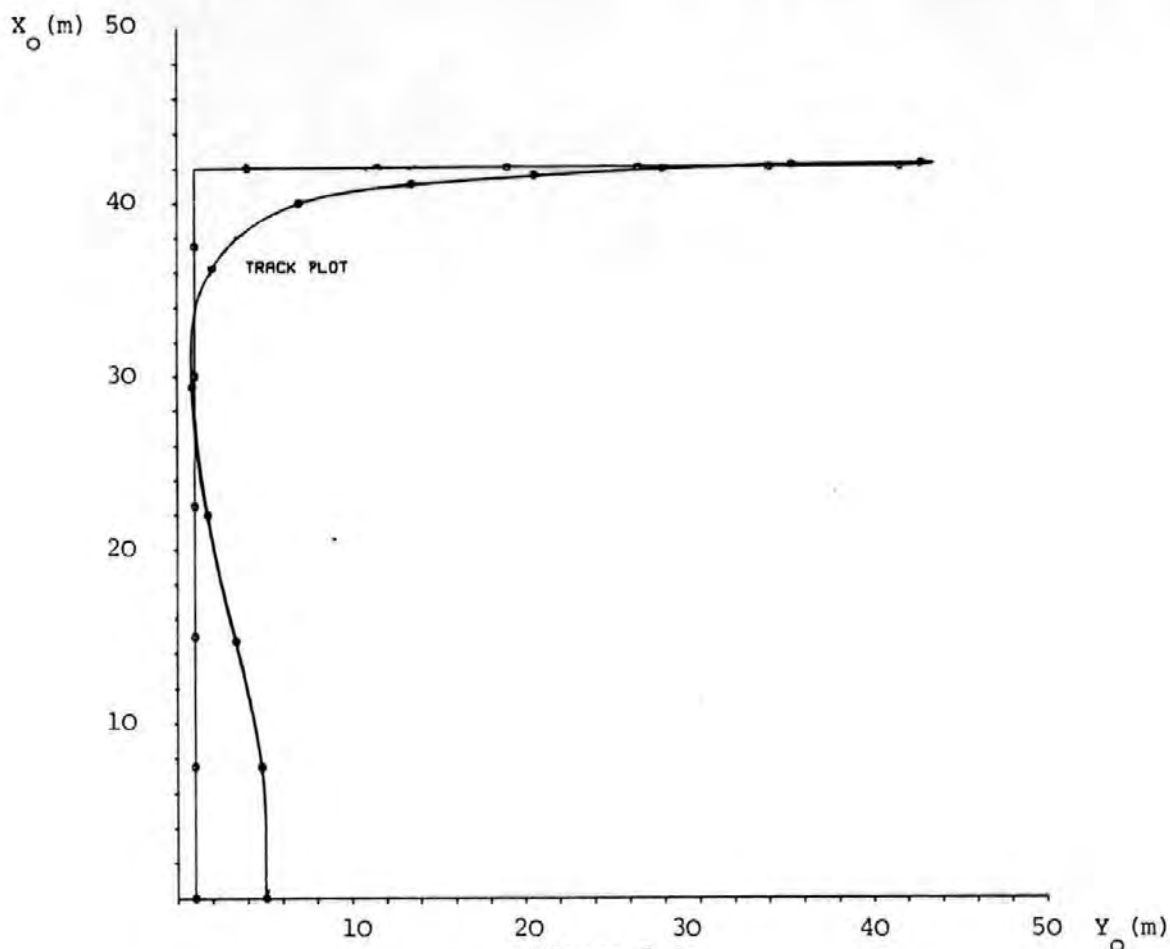


Figure 8.1

90 Degree Track-Changing Simulation (Model), Dual-Mode Control.

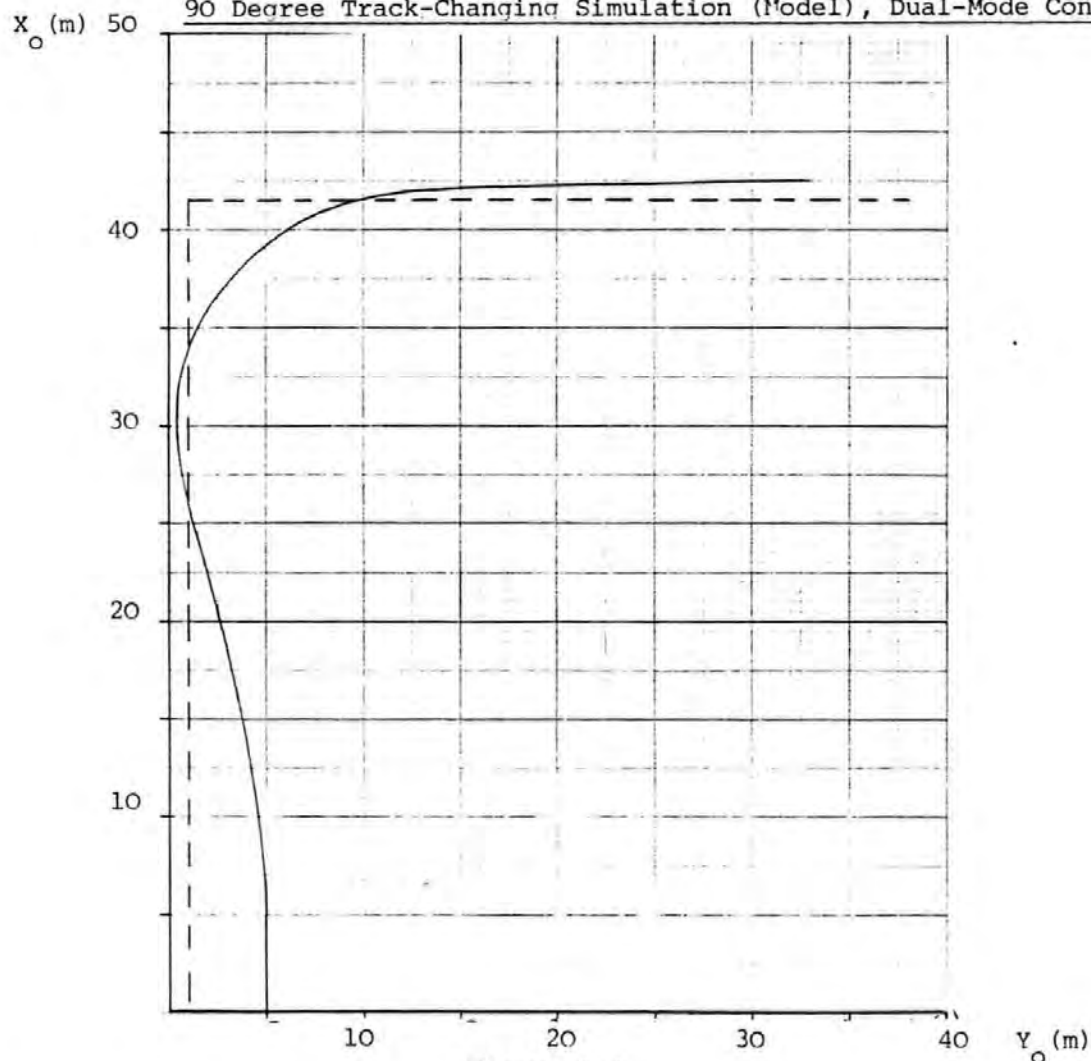


Figure 8.3

Bench-Test: TMS 9900 Microcomputer Interfaced to Instrumentation Package

the sampling time is one second.

8.4 Real-Time Software Development

Mainframe simulations of the type shown in Figure 8.1 reveal that system performance deteriorates rapidly when the sampling time is much above one second. This imposes the restriction that all real-time computation has to be carried out within this time interval. A problem to be faced at the development stage was that the TMS 9900, in common with many other microprocessors, used an interpretive, rather than a compiled version of BASIC. The former, although easy to use is slow in operation because of its line-by-line interpretation from source to object code.

Figure 8.2 shows the order of operations, together with their estimated time values, to be performed within one sampling interval.

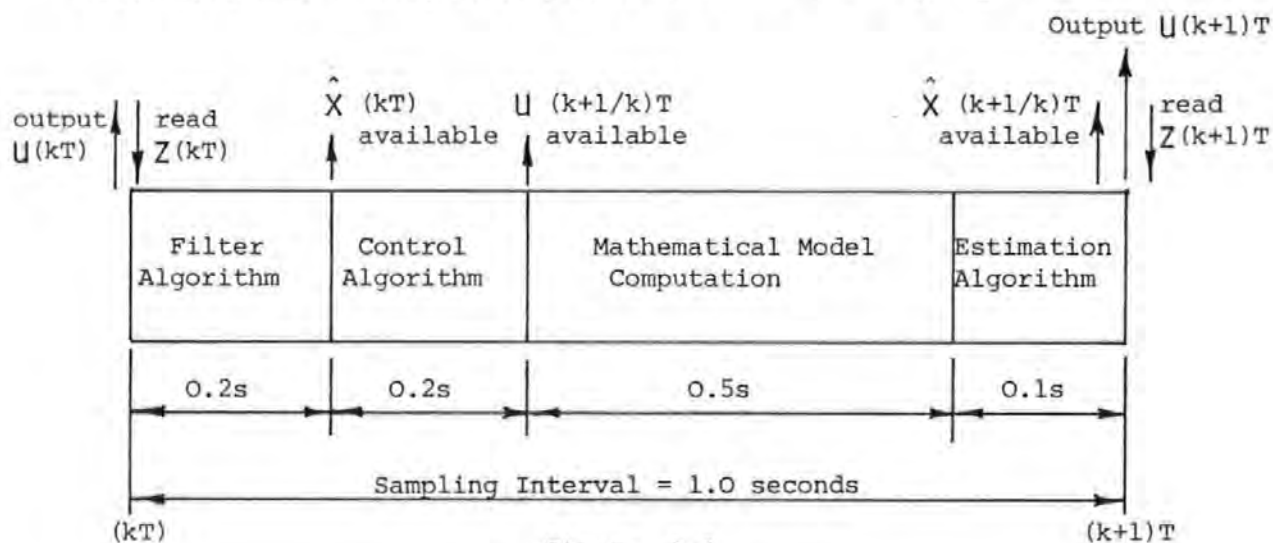


Figure 8.2

Order of Operations in Real-Time Program

It will be noted that 0.4 seconds has elapsed before the control vector U , based upon the best estimate of the state variables at time kT , becomes available. Since this information can only be output at the end of the sampling interval, it means that the control variables are computed from the immediate previous, and not the current state

estimates, the latter being unavailable. This dilemma is unavoidable in a real-time situation.

8.4.1 Program Structure

Apart from the obvious functions of estimation, filtering and control, an important programming feature is that of logging measured and computed data. The following parameters are stored at each sampling instant:

- (a) Raw measurements of state variables: forward and lateral velocity, heading and yaw-rate (4 x 112).
- (b) Best estimates of state variables (4 x 112).
- (c) Demanded and actual rudder angle and engine speed (4 x 112).
- (d) Computed track co-ordinates (2 x 112).

The final sizing of the DIMENSION statements were left until the end to use up all available memory space.

Subroutines

The program employs the following main subroutines (BASIC) and utility subroutines (Assembly Language)

Main Subroutines

<u>Statement Number</u>	<u>Subroutine Function</u>
3000	Estimation Algorithm
3100	Filter Algorithm
10000	Measurement Subroutine
12000	Control Algorithm
13000	Mean and Standard Deviation
15000	Mathematical Model

Utility Subroutines

10400	Analogue/Digital Conversion
10500	Digital/Analogue Conversion

8.4.2 Computation of Mathematical Model

The discrete mathematical model of the vessel is recalculated for the estimation algorithm during each sampling interval. Initially, this was performed in a similar manner to the mainframe program, i.e. by determining the elements of the F and G matrices and then calculating the discrete state and control transition matrices A and B using the power series expansion technique outlined in Appendix A1.5.

The mainframe subroutine TRNMAC takes into account the first 50 terms in the expansion and when the routine was performed in BASIC on the TMS 9900 the following run times were observed:

<u>Number of Terms</u> <u>in Expansion</u>	<u>Run Time</u> <u>(seconds)</u>
50	30
20	12
5	3

In order to maintain an accuracy up to 3 decimal places in both A and B matrices, the absolute minimum number of terms in the expansion was 5. Unfortunately, a total program run time of 3.4 seconds was still too high to be considered.

An alternative approach based on perturbation theory was finally employed to calculate A and B directly.

If it is assumed that:

$$A = F(u, v, r, t)$$

$$B = (u, v, r, \delta_D, n_D, t) \quad (8.7)$$

then, for small perturbations in u, v, r, δ_D and n_D ,

$$\begin{aligned}
 a_{11} &= \frac{\partial A_{11}}{\partial u} \bigg|_a u + \frac{\partial A_{11}}{\partial v} \bigg|_b v + \frac{\partial A_{11}}{\partial r} \bigg|_c r \\
 &\vdots \\
 b_{42} &= \frac{\partial B_{42}}{\partial u} \bigg|_a u + \frac{\partial B_{42}}{\partial v} \bigg|_b v + \dots + \frac{\partial B_{42}}{\partial n_D} \bigg|_e n_D
 \end{aligned} \tag{8.8}$$

The TRNMAC routine was run varying u, v, r, δ_D and n_D in turn over their expected ranges and the partial derivatives for each element calculated. A summary is given in Appendix 5.

When tested on the TMS 9900 the perturbation technique gave an accuracy equal to ten terms in the power series expansion and took 0.58 seconds to run. Dove undertook further mainframe simulation tests using both methods in order to validate the precision of state variable computation (78).

A complete listing of the real-time program, including the control, modelling and estimation routines, is given in Appendix A6.4.

8.4.3 Bench Testing

So that the final version of the program could be tested, the instrument pack, together with the heading gyroscope were mounted on a trolley and interfaced with the TMS 9900. Since, in reality, the vessel would be moving with very small accelerations, signals from the instruments were obtained by rotating the trolley, at a suitable rate, through some prescribed angle. The x_o, y_o filtered track parameters were fed to D/A converters and output to an analogue X-Y plotter. Figure 8.3 shows the trace from a typical run.

The instruments, computer and servo-systems were now mounted in the 5502 hull (re-named St. Nicholas, after Sealink's flag-ship, a car-ferry of similar size and displacement) and the hull re-painted prior to the final tests.

8.5 Test Procedure

The reservoir is shown in Figure 8.4.

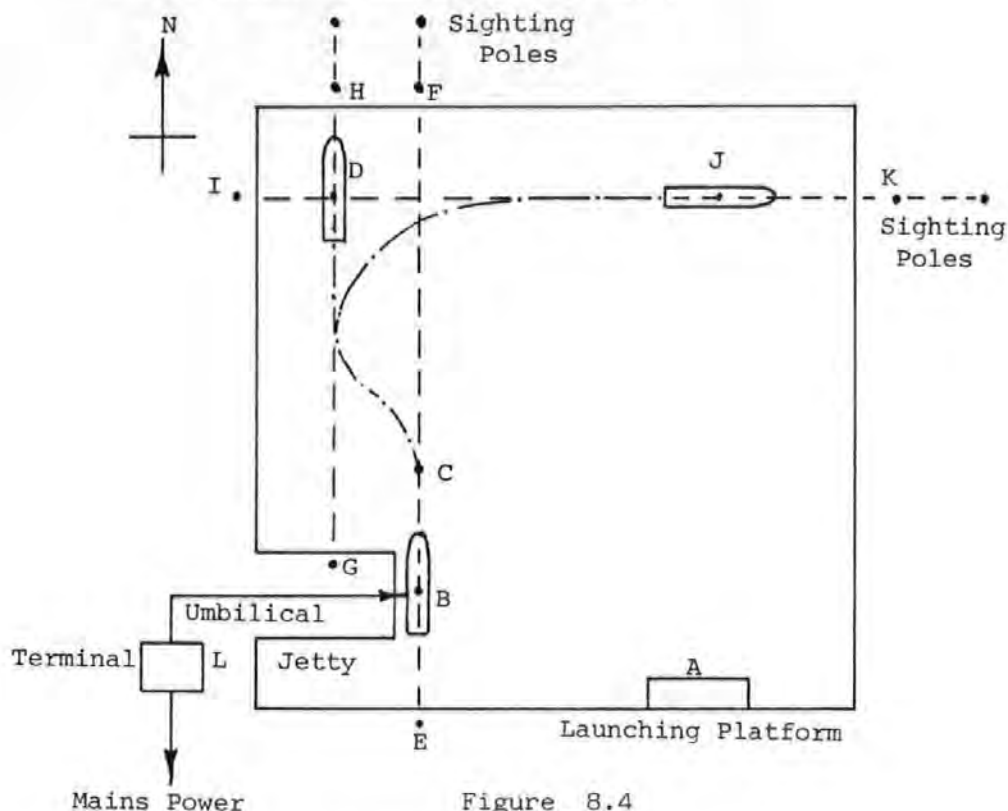


Figure 8.4

Plan of Crownhill Reservoir

Calm water conditions usually exist on the southern or western sides of the reservoir making either A or B suitable test starting positions. Assuming the latter, the model is positioned at the end of the jetty and connected to the keyboard/printer terminal by a communications umbilical chord. All systems are now switched on and the following test procedure initiated:

1. Load program from EPROM and run.
2. Input time delay necessary to manoeuvre vessel under radio-control from B to C, the latter being the start position for the run.
3. Input details regarding desired track and way-point advance.

4. Specify which measurements are to be filtered and adjust Kalman gain matrix.
5. Allow vessel to float freely for 1 minute to enable 60 measurements from each instrument to be made. Calculate and print mean and standard deviation, the former being subtracted from any future measurements, the latter being used in the filter measurement noise covariance matrix.
6. Un-plug the umbilical and pilot vessel to position C. This is performed by the radio-control operator standing at E and lining model up with sighting poles F.
7. During the test, still and video cameras monitor the vessel's progress, either from G for track-keeping, or from I for a track-changing.
8. Upon completion, manoeuvre model under radio-control back to B, plug in umbilical and dump data to terminal.

A similar procedure may be employed when operating from position A.

Typically, a test would require 5 minutes to align the heading gyroscope, input the track and filter data and measure the mean and standard deviation of the instrument signals. The run itself would take 2 minutes and a further period of about 25 minutes would be required to print the data to the terminal. During this 32 minute time interval the computer 5V power supply regulator became extremely hot and a 10 minute cooling down period was allowed, prior to the execution of the next test. At every opportunity (i.e. during data print-out) batteries were placed on charge. In this manner, 3 successive runs could be undertaken before a complete re-charge of all

batteries became necessary. This enabled, weather permitting, up to 9 runs to be performed in a single day.

8.6 Test Results

A total of 19 runs were conducted during the period 30th May - 8th June 1984, the details of which are given in Table 8.1. It must be remembered that the effectiveness of the filter as well as the controller was being studied, and not all tests have significance in context with the latter. Runs 1, 4, 6, 7 and 8 are particularly concerned with filter tuning and detailed discussion is presented by Dove (78). In Runs 3 and 5, the filter closely resembled its final form, and the test results may be considered to be valid.

With Run 2, the heading gyroscope was inadvertently left caged, and as the measurement was unfiltered, this led to the condition of no heading feedback. This set of circumstances was considered in 5.5 where it appeared that no stable solution existed. This was indeed the case and the system became dynamically unstable, highlighting the fact that if system integrity is to be maintained, a filtered estimate must always be available under conditions of gyro malfunction. No data was printed from this run.

The following runs were selected for detailed analysis:

<u>Run No.</u>	<u>Objective</u>	<u>Reason for Choice</u>
3 and 5	Track-Keeping	Positive initial track error
9	Track-Keeping	Negative initial track error
10	Track-Changing	Steady-state conditions at change, no disturbances.
12	Track-Changing	Steady-state conditions at change with wind gusting force 3/4.
19	Track-Changing	Initial track error, producing transient conditions at change.

Run No.	Date and Time	Test Type	Initial Track Offset. (m)	Number of Samples (T _{SAMP} = 1 s)	Filtered Measurements	Recorded Video/ Still	Start Position	Comments
1	30.5.84 11.00	Track-keeping	4.11	80	All filtered	-	B	Light Westerly Wind.
2	12.00	Track-keeping	4.11	80	u & v filtered	-	B	Gyro Caged.
3	12.30	Track-keeping	4.11	80	u & v filtered	-	B	Light Westerly Wind.
4	14.15	Track-keeping	0.0	80	All unfiltered	V & S	A	Light Southerly Wind.
5	15.00	Track-keeping	5.0	80	u & v filtered	V & S	A	Light Southerly Wind.
6	16.00	Track-keeping	5.0	80	All filtered	V & S	A	Light Southerly Wind.
7	17.00	Track-keeping	5.0	80	All filtered	S	A	Light Southerly Wind.
8	18.00	Track-keeping	-5.0	110	u & v filtered	S	A	Diagonal Run.
9	31.5.84 9.15	Track-keeping	-5.0	80	All filtered	V & S	A	Calm Conditions.
10	13.00	Track-Changing	0.0	110	All filtered		A	Light Southerly Wind.
11	14.30	Track-Changing	0.0	110	All filtered		A	Wind Increasing. 14 rows of data missing.
12	15.00	Track-Changing	0.0	110	All filtered		A	Wind Gusting 3/4.
13	1.6.84 9.15	Track Changing	-1.0	110	u & v filtered		A	Reduced Way-Point Advance. Calm Conditions.
14	11.00	Track Changing	-2.4	110	All filtered		A	Increased Way-Point Advance.
15	12.00	Track Changing	-2.4	110	All filtered		A	Track Change During Transient.
16	14.30	Track Changing	-2.4	110	All filtered		A	Wind Gusting 3/4.
17	5.6.84 11.00	Track Changing	0.0	110	u & v filtered	-	B	Wind Gusting 3/4.
18	8.6.84 11.00	Track Changing	0.0	110	All filtered	-	B B	Slight Wind, South-West.
19	15.00	Track-Changing	4.0	110	All filtered	S	A	Calm Conditions.

Table 8.1
Details of Test Runs.

8.7 Analysis of Results

In assessment of system performance it must be clearly understood that:

- (i) Any difference between the filtered measurements and the actual states of the vessel is a measure of the performance of the optimal filter.
- (ii) Any difference between the filtered measurements and the desired states is a measure of the performance of the optimal controller.

It must be with respect to (ii) above that the analysis of the controller is conducted. However, for the purpose of comparison, the final position of the vessel relative to the sighting poles is shown on track plots.

Figures 8.11(a) and (b) are repeated exposure photographs for runs 5 (track-keeping) and 10 (track-changing). In the former, the sighting poles at H and F (as defined in Figure 8.4) can be seen on the far bank, and in the latter the sighting pole at position K.

Figure 8.12, mounted beneath Figure 7.8(b) in Chapter 7, shows the model in a tight turn during a track-changing manoeuvre.

The measured data for all runs was input from keyboard into the mainframe PRIME 9950 and a common database established. Computer simulations were then conducted for each run, matching in every case simulated and measured initial conditions. Raw and filtered measurements (again the former for comparison only) were superimposed upon simulation data. Figures 8.5 through to 8.10 are the graphics output for Runs 3, 5, 9, 10, 12 and 19 respectively.

When attempting to quantify the "goodness" of a control system, one is really asking the question: what error exists between the

Figure 8.11(a)

Run 5: Track-Keeping

Figure 8.11(b)

Run 10: Track-Changing



desired value and the measurement of the actual value over the control interval? The answer must lie in the form of a performance index, and the quadratic form of those given in equations (6.3) relate best to the optimal control law employed here.

Where mathematical modelling techniques are used in the design of dynamic systems and some optimal solution is sought, the ultimate response of the simulation model must be considered as an ideal that the real system will approach. The measure of the degree of closeness of the two systems will be reflected in their respective performance indices.

The generalised performance indices (with the exception of J_x which has no relevance to the present set of state variables) for both the mathematical model and the physical model are given in Table 8.2.

Apart from control quality analysis, it is also necessary to validate the accuracy of the mathematical model. Since both physical and mathematical models are responding to almost identical inputs, the integral of the square of the residuals over the control period may be used to define the following mathematical model validity indices:

$$\begin{aligned}
 J_{uu} &= \int_{t_0}^{t_1} (u - \hat{u})^2 dt \\
 J_{yy} &= \int_{t_0}^{t_1} (y - \hat{y})^2 dt \\
 J_{\psi\psi} &= \int_{t_0}^{t_1} (\psi_A - \hat{\psi}_A)^2 dt \\
 J_{\delta\delta} &= \int_{t_0}^{t_1} (\delta_A - \hat{\delta}_A)^2 dt \\
 J_{nn} &= \int_{t_0}^{t_1} (n_A - \hat{n}_A)^2 dt
 \end{aligned} \tag{8.9}$$

A list of mathematical model validity indices for the trials on the reservoir are given in Table 8.3.

Run	Performance Indices				
No.	J_u	J_y	J_ψ	J_δ	J_n
	Mathematical Model				
3	0.0216	920.00	3.545	0.8472	0.00183
5	0.1038	1868.09	6.972	1.1769	0.00392
9	0.0024	311.82	1.309	0.2706	0.00062
10	0.3212	306.49	22.781	3.2329	0.00042
12	0.3279	314.79	23.169	3.2758	0.00045
19	0.3614	611.29	24.913	3.5469	0.00104
	Physical Model				
3	0.0668	1057.86	3.437	2.2287	0.00469
5	0.1491	2516.01	5.674	2.6414	0.00080
9	0.5316	402.28	3.346	4.9479	0.00056
10	0.9215	564.24	19.605	10.9555	0.00763
12	1.2365	1834.19	32.361	8.7313	0.01053
19	1.0063	824.81	22.084	9.9549	0.00847

Table 8.2

Generalised Performance Indices for Mathematical
and Physical Models

Run	Mathematical Model Validity Indices.				
No.	J_{uu}	J_{yy}	$J_{\psi\psi}$	$J_{\delta\delta}$	J_{nn}
3	0.049	22.010	1.209	1.612	9.050
5	0.157	146.173	2.044	2.035	0.495E-2
9	0.509	17.477	0.406	3.629	0.111E-2
10	0.271	86.009	1.730	9.244	0.762E-2
12	0.454	1311.126	9.108	7.818	0.105E-1
19	0.261	67.758	0.346	8.354	0.932E-2

Table 8.3

Mathematical Model Validity Indices

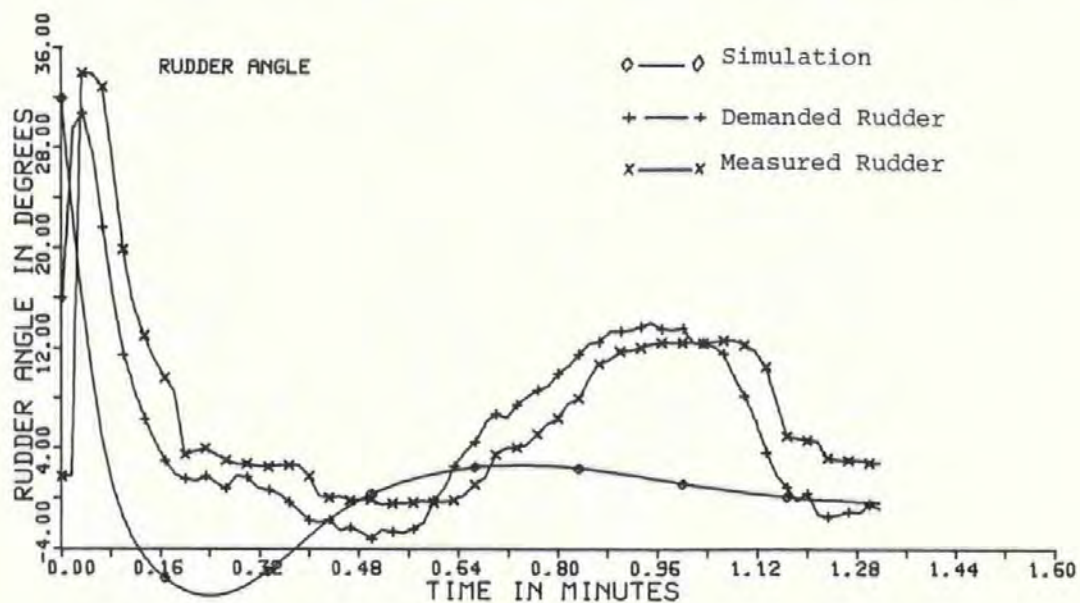
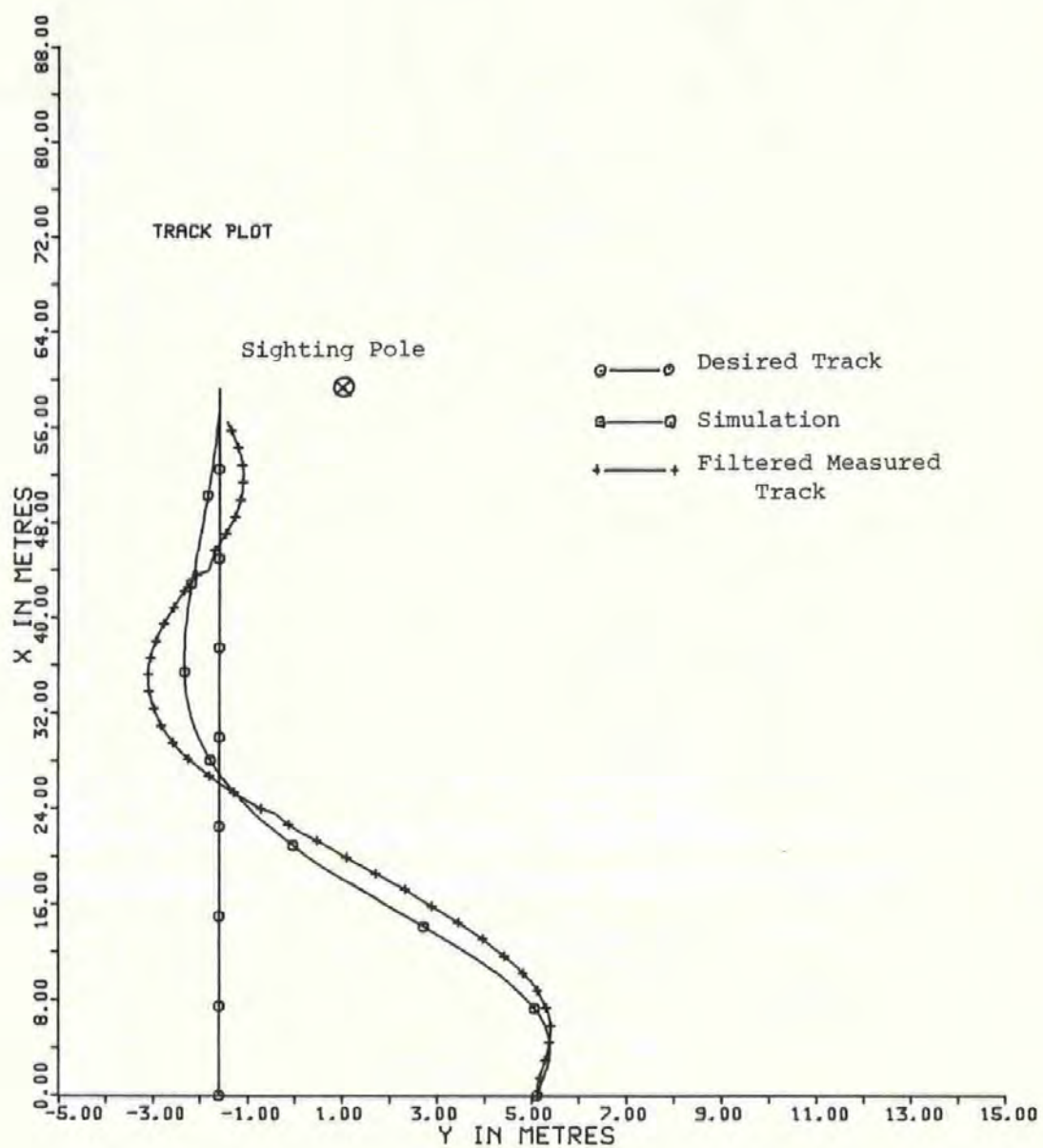


Figure 8.5(a)

Run 3

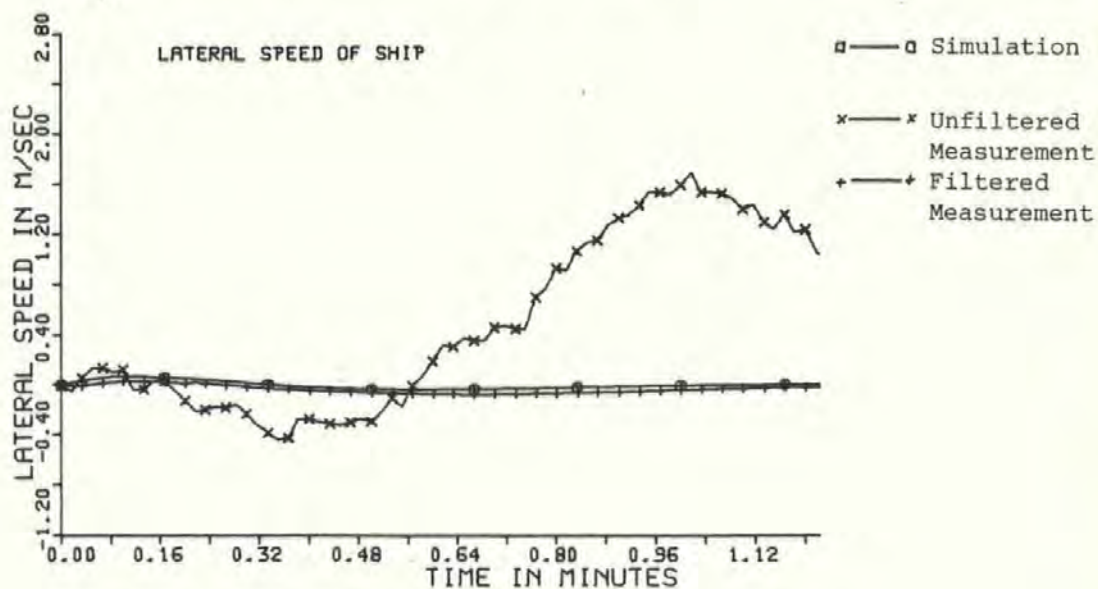
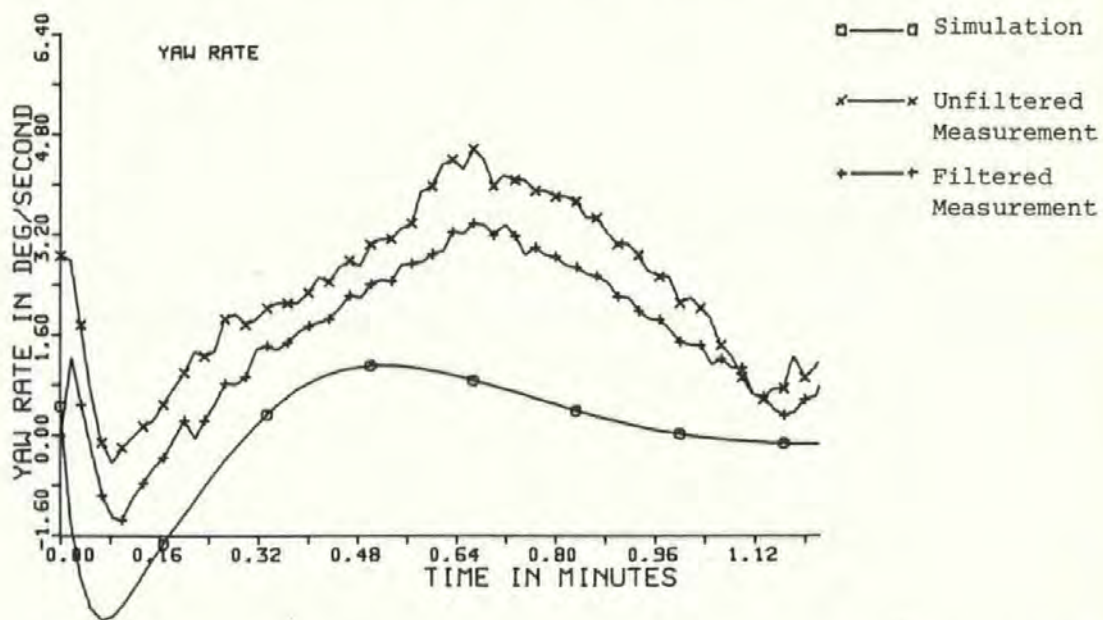
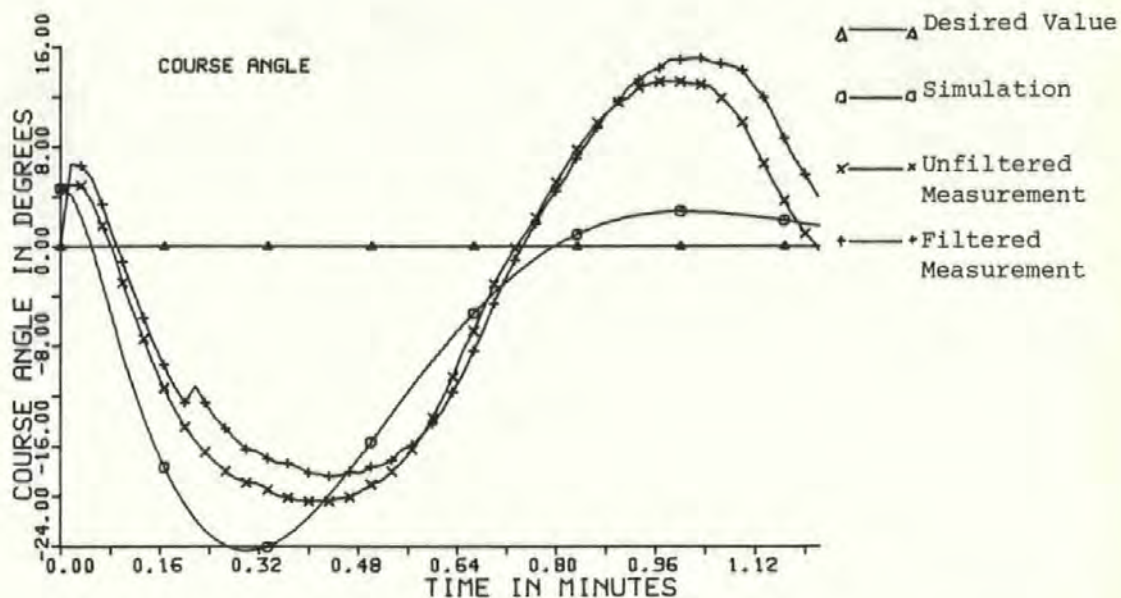


Figure 8.5(b)

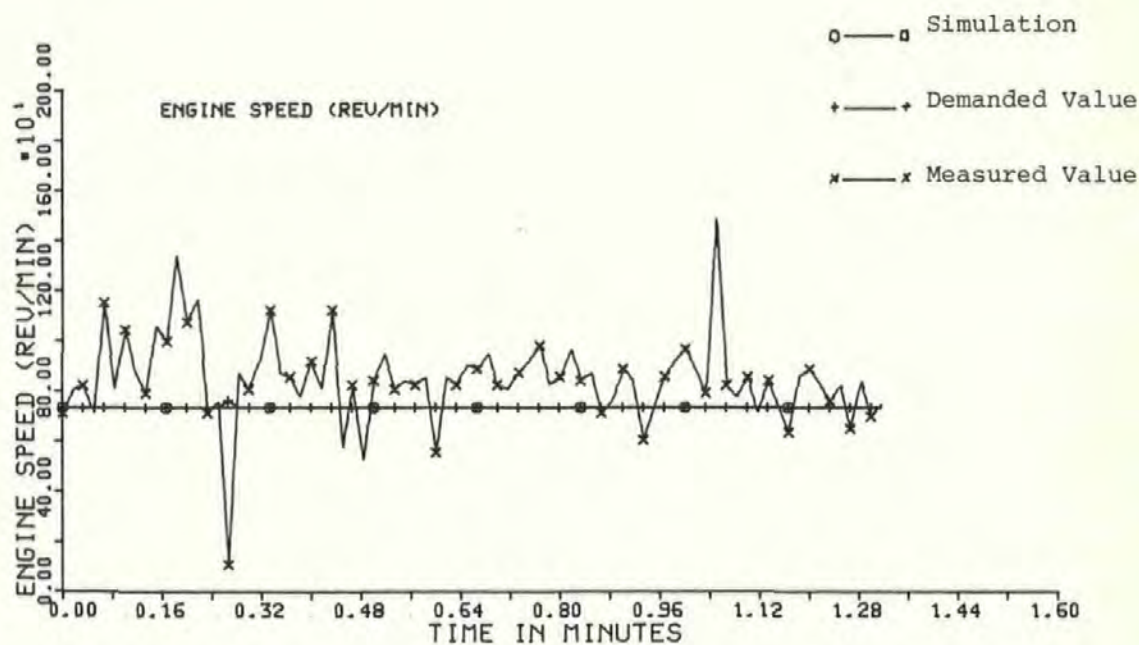
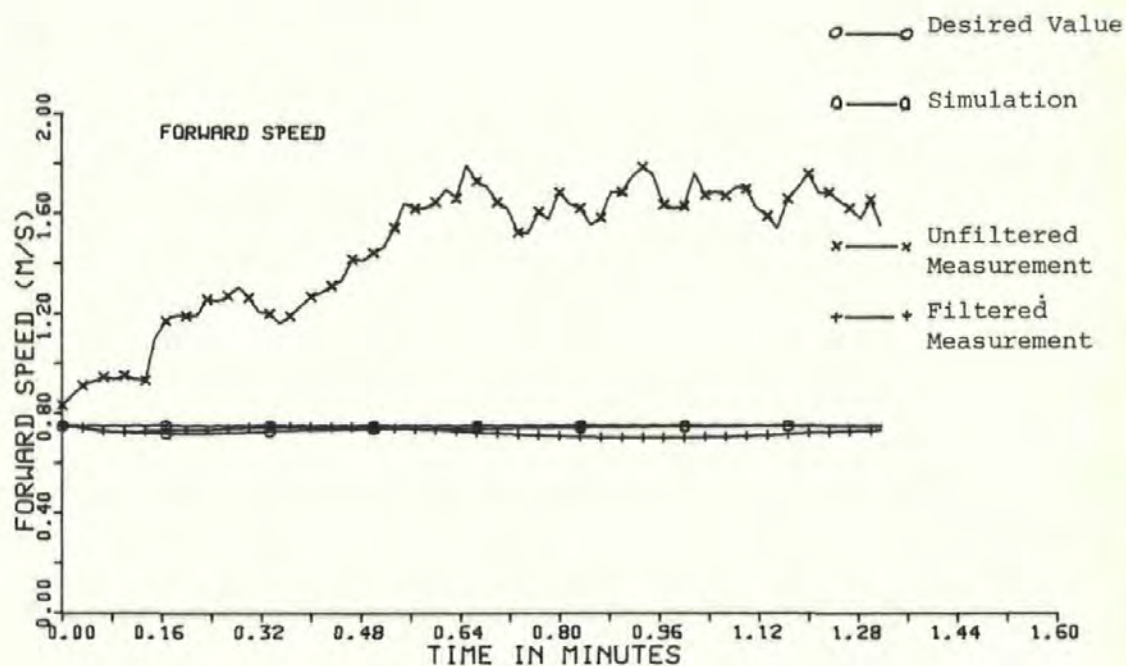


Figure 8.5(c)

Run 3

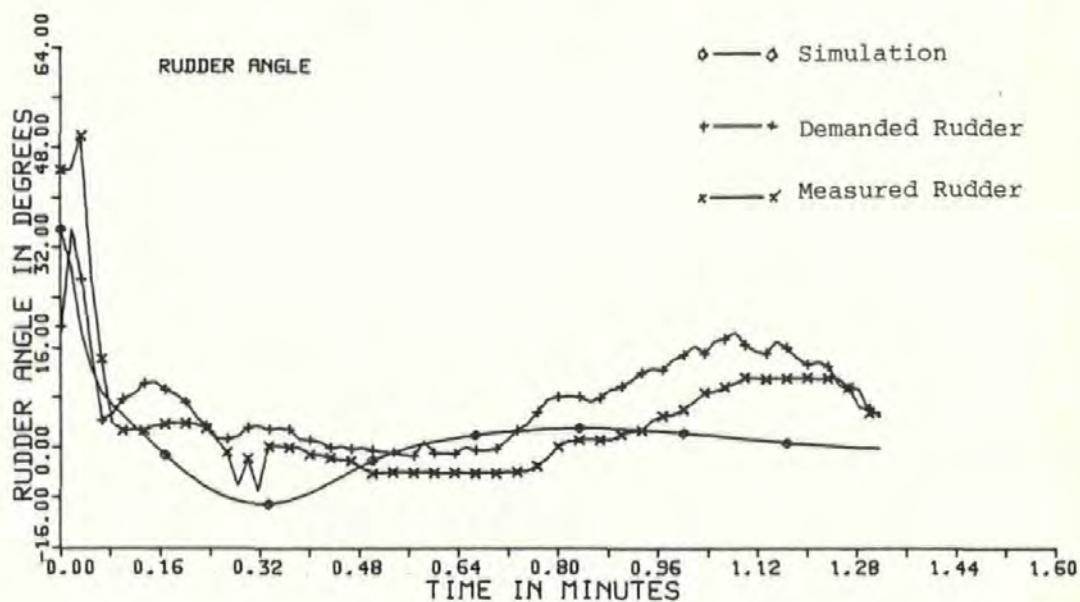
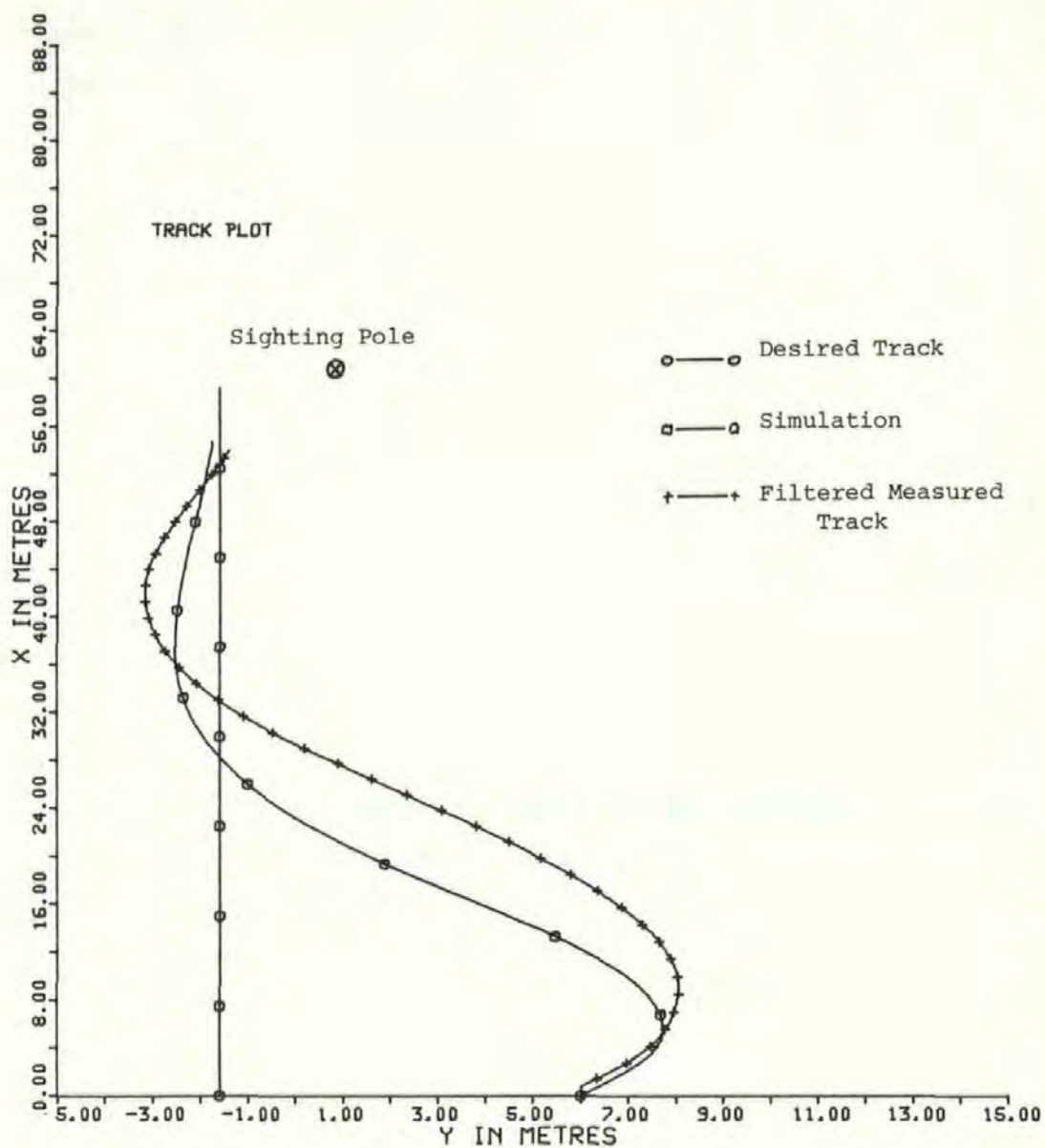


Figure 8.6(a)

Run 5

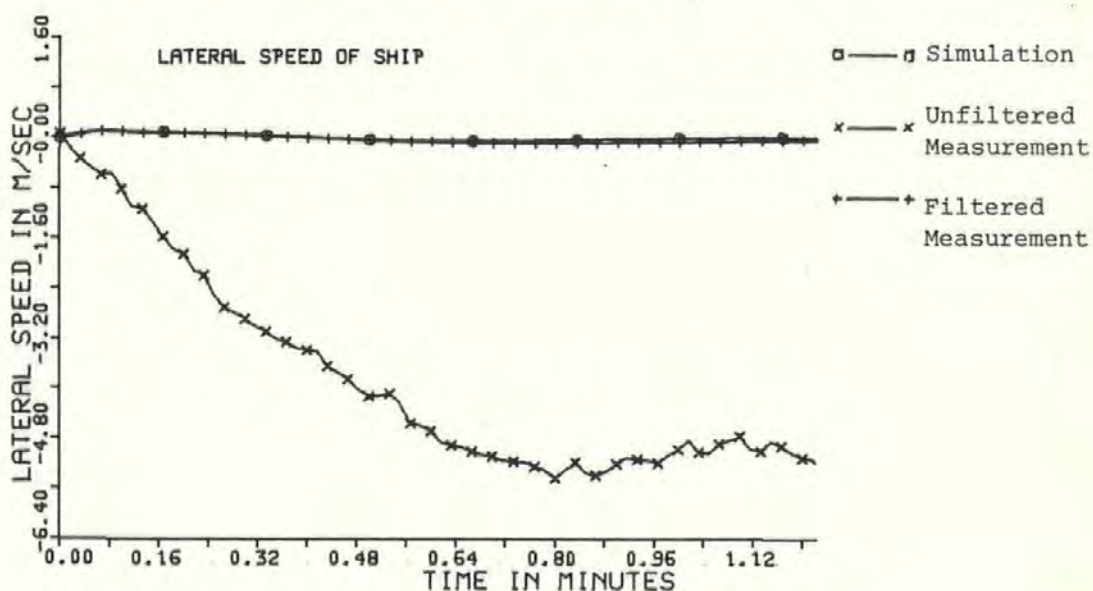
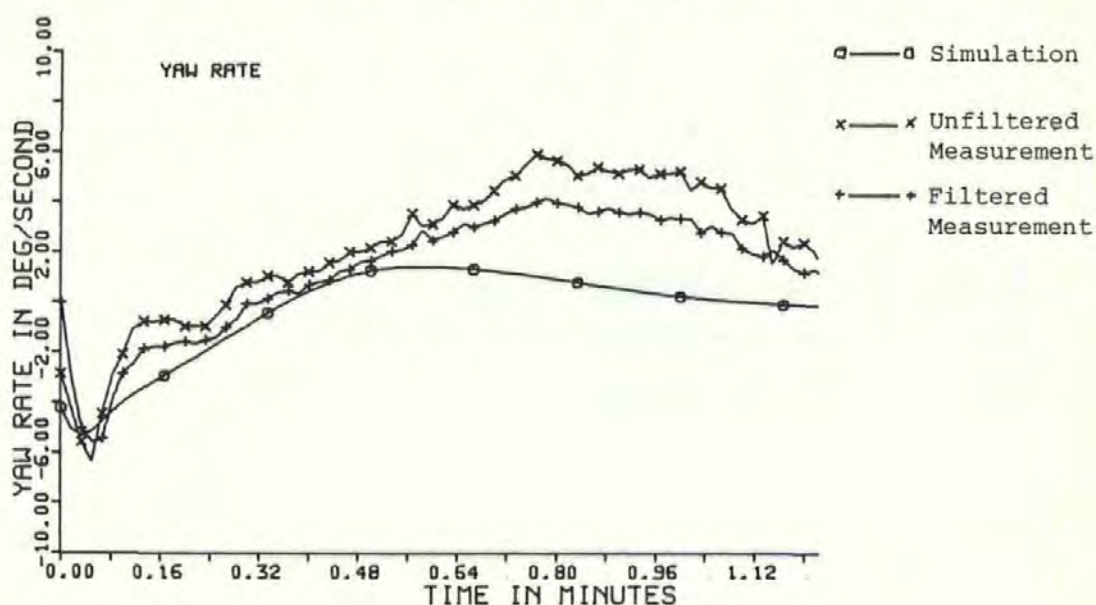
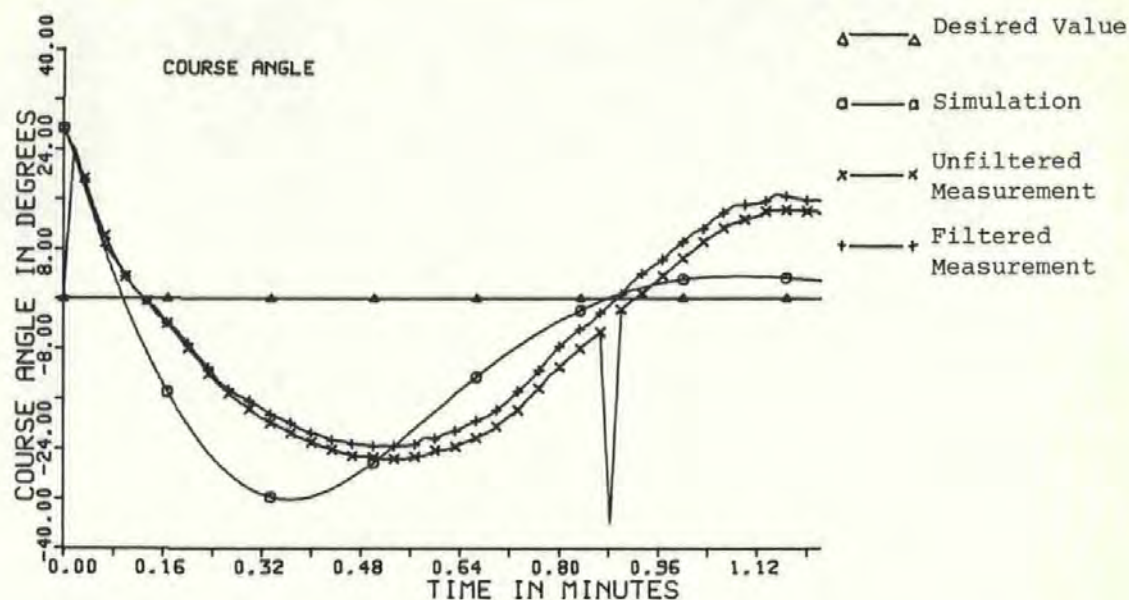


Figure 8.6(b)

Run 5

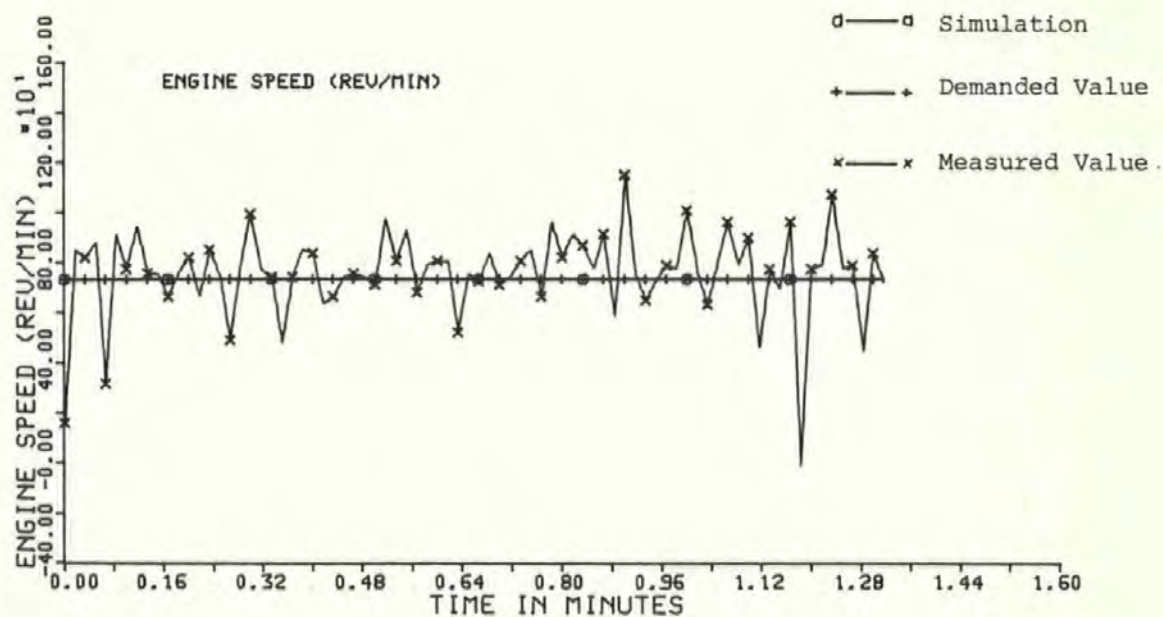
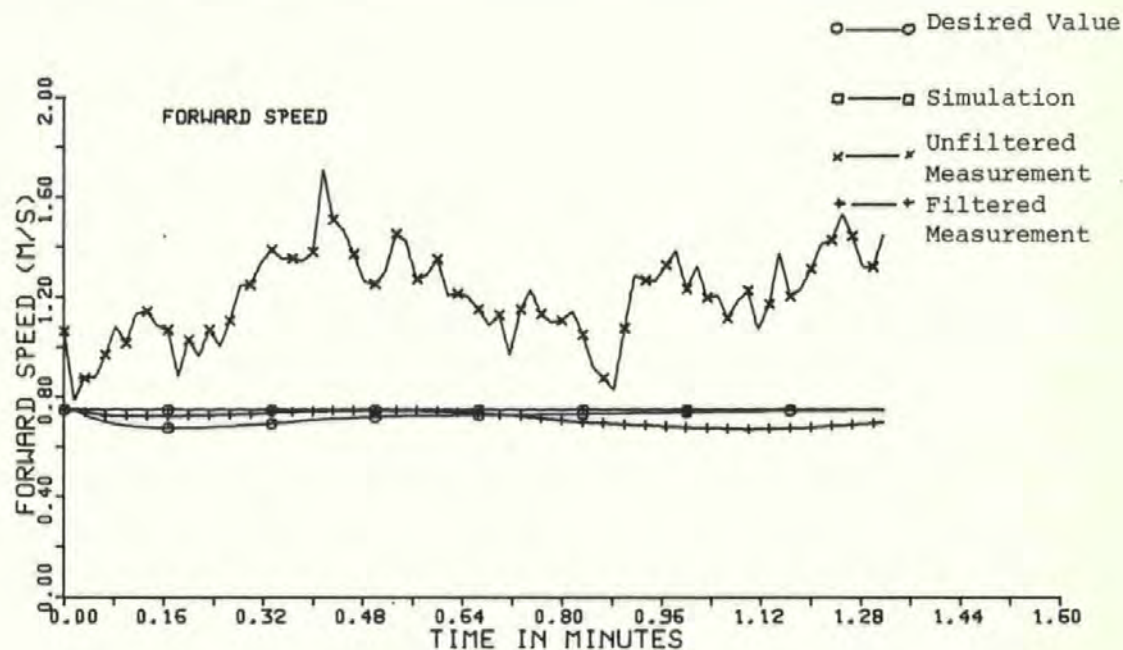


Figure 8,6(c)

Run 5

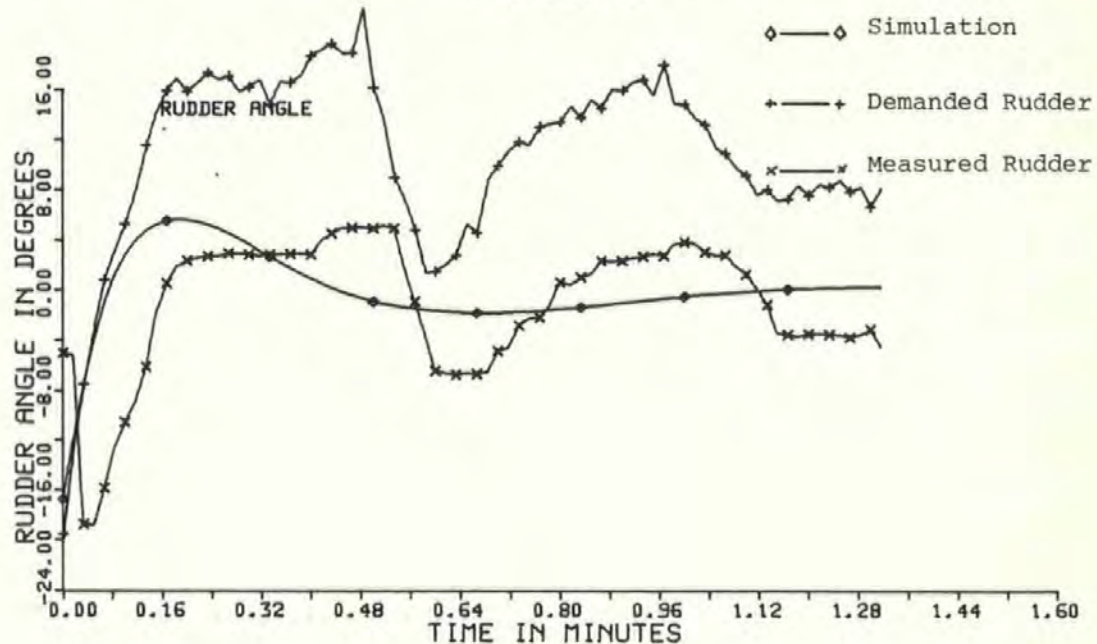
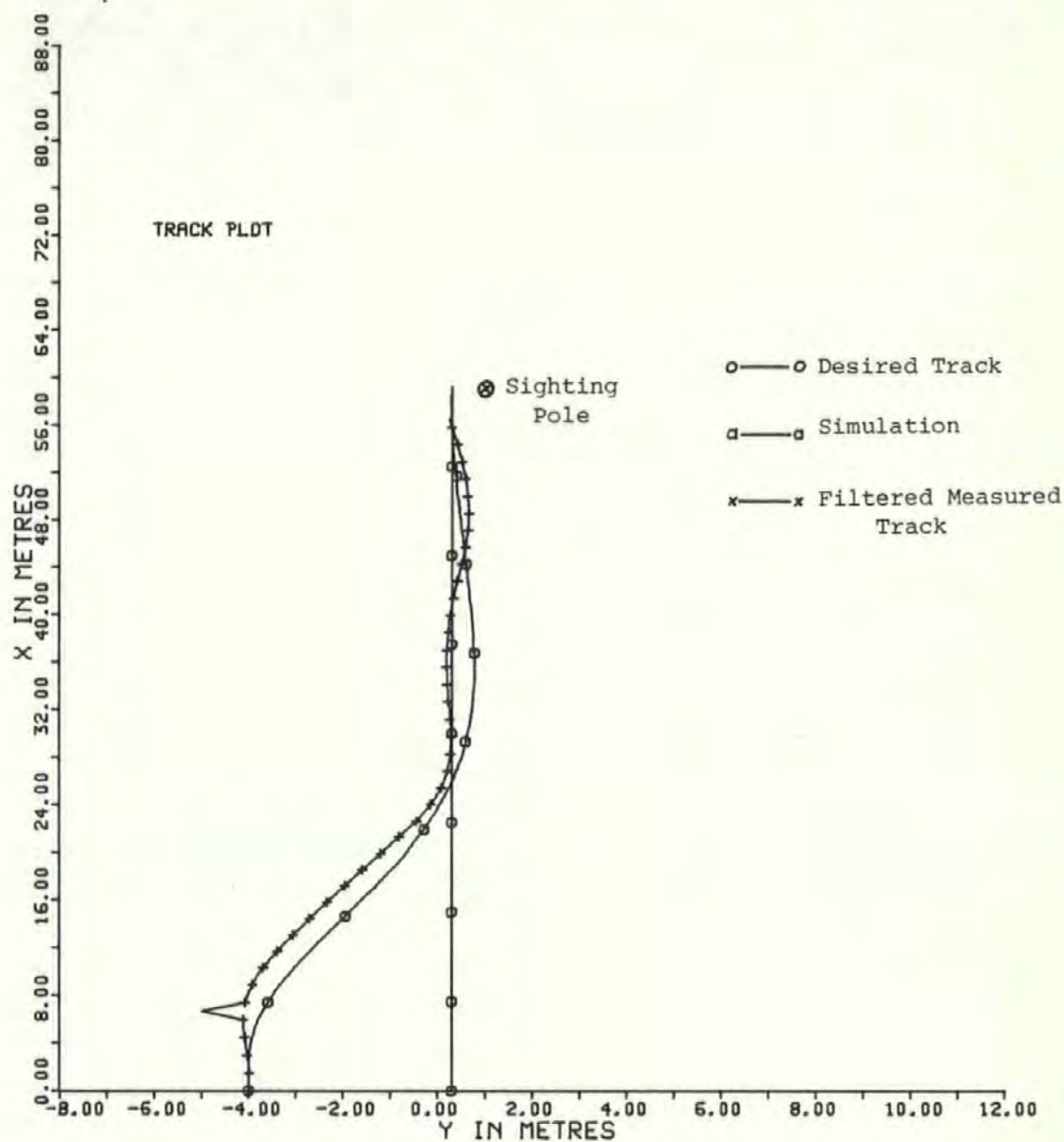


Figure 8.7(a)

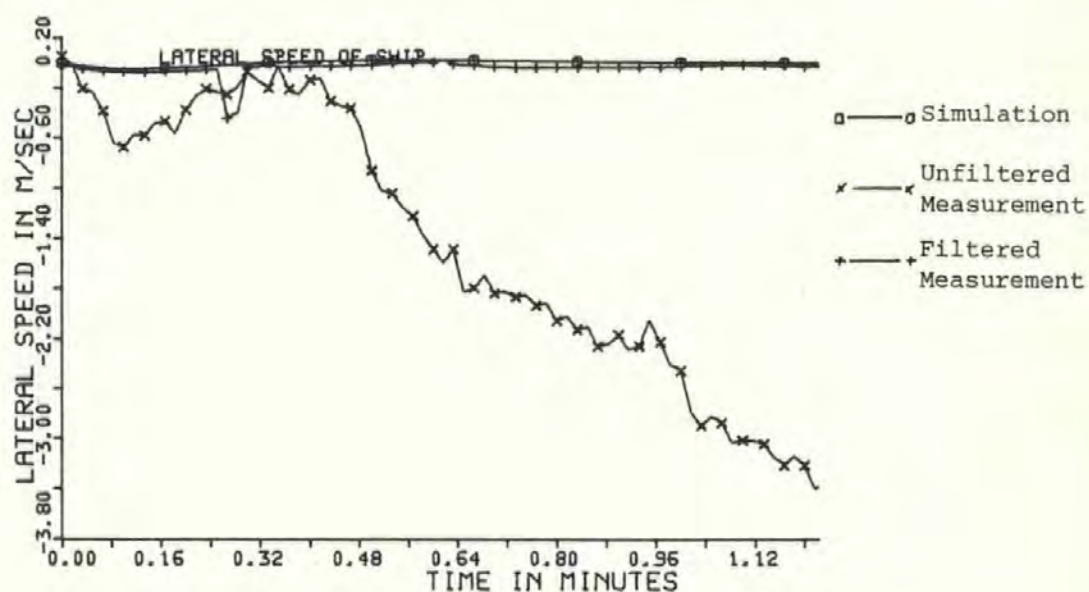
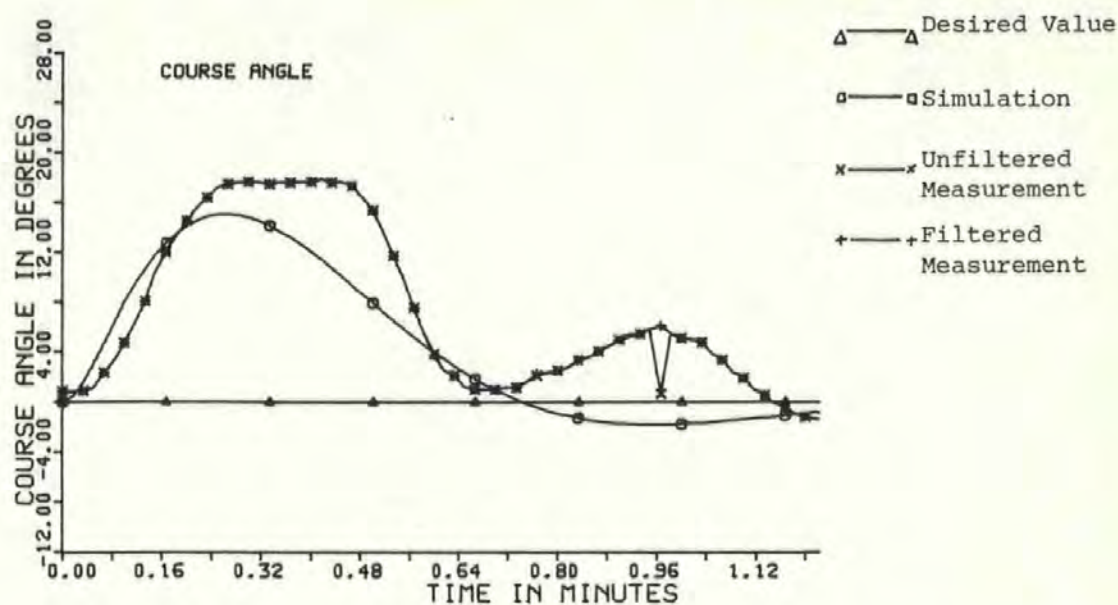


Figure 8.7(b)

Run 9

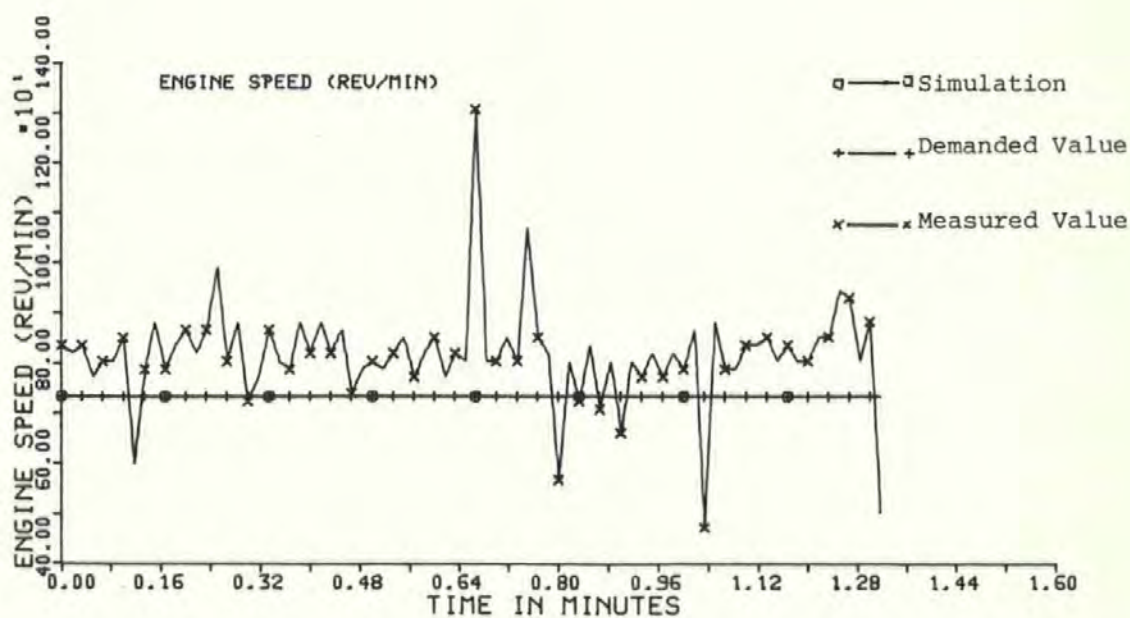
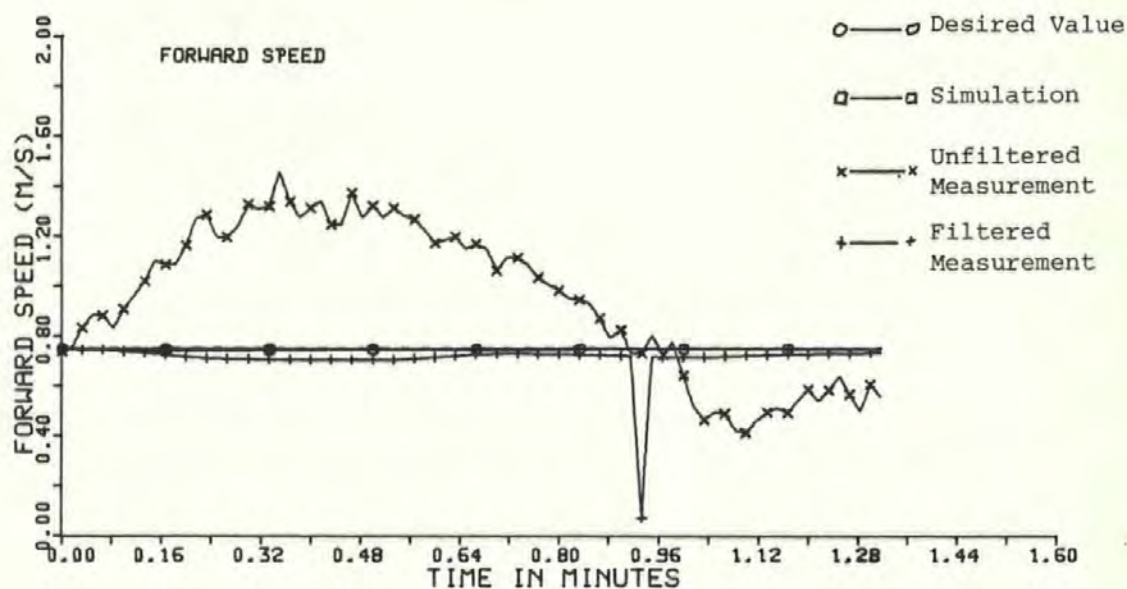


Figure 8.7(c)

Run 9

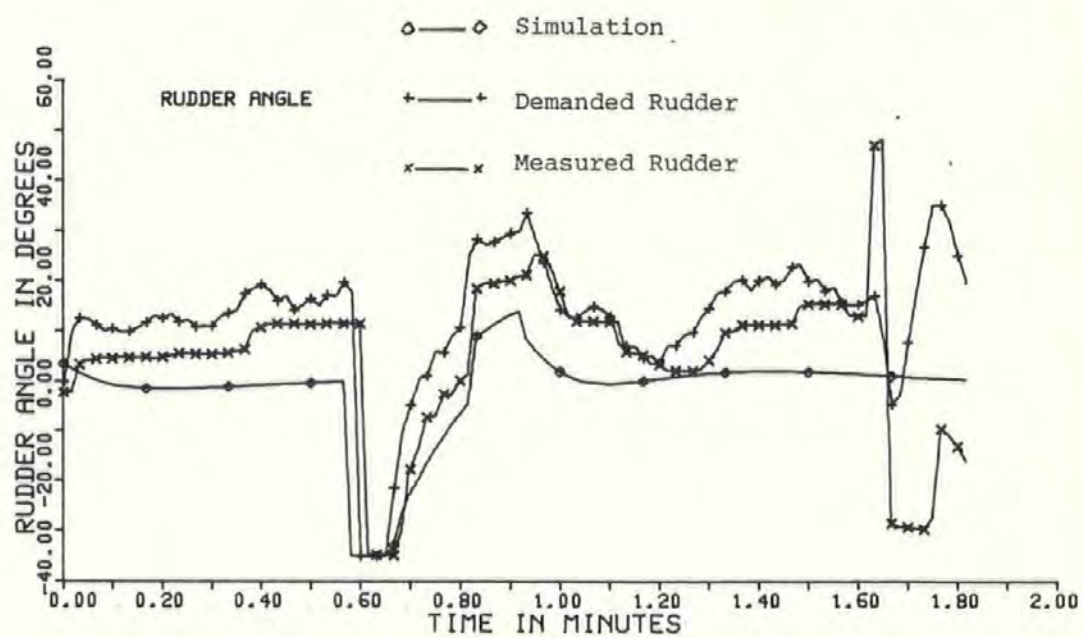
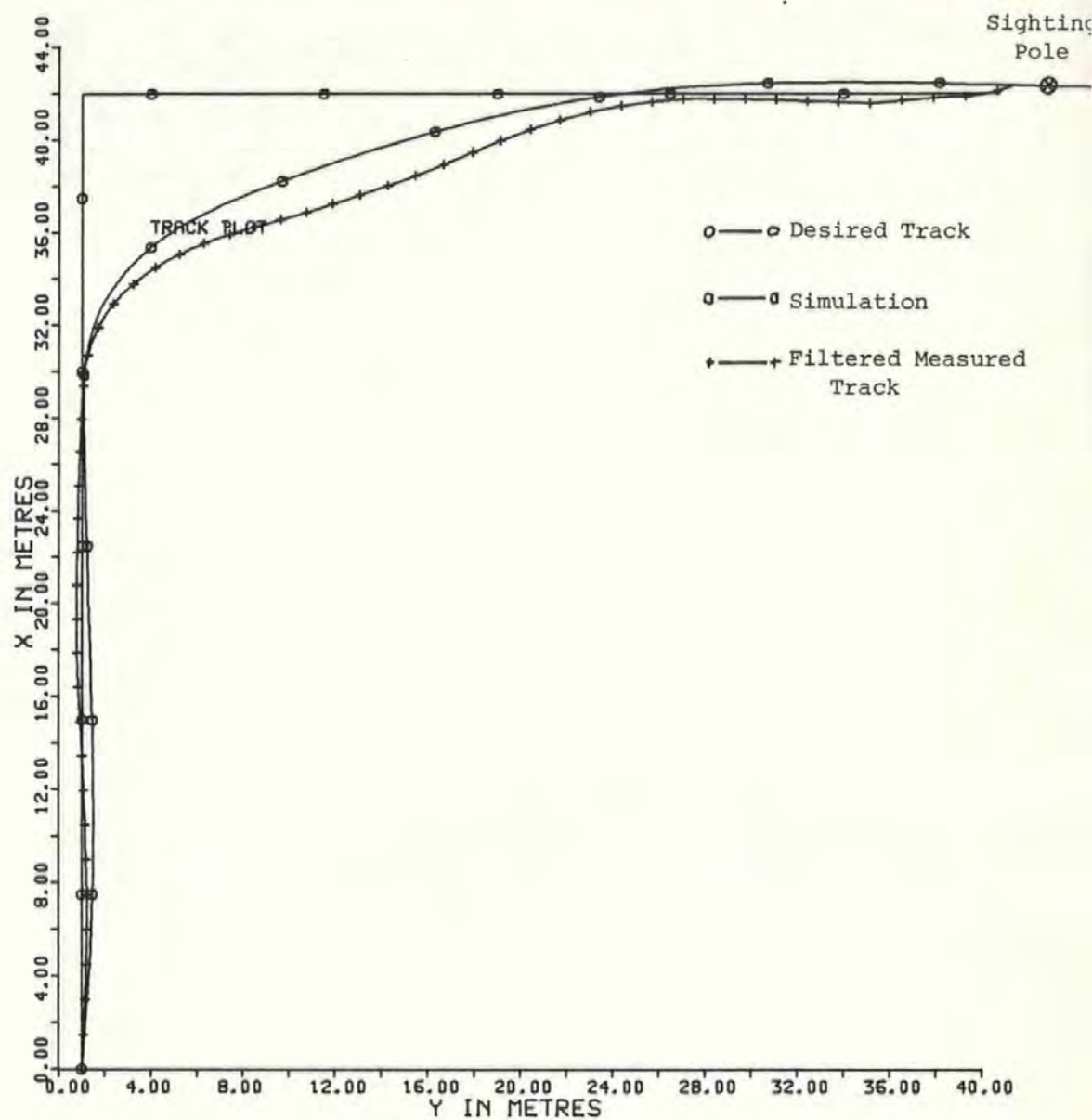


Figure 8.8(a)

Run 10

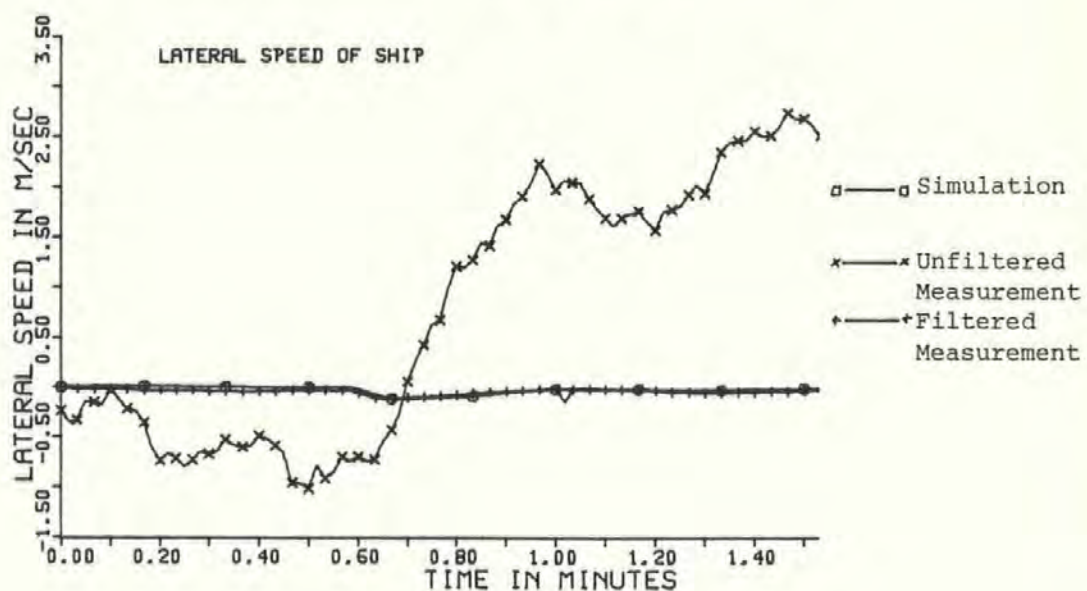
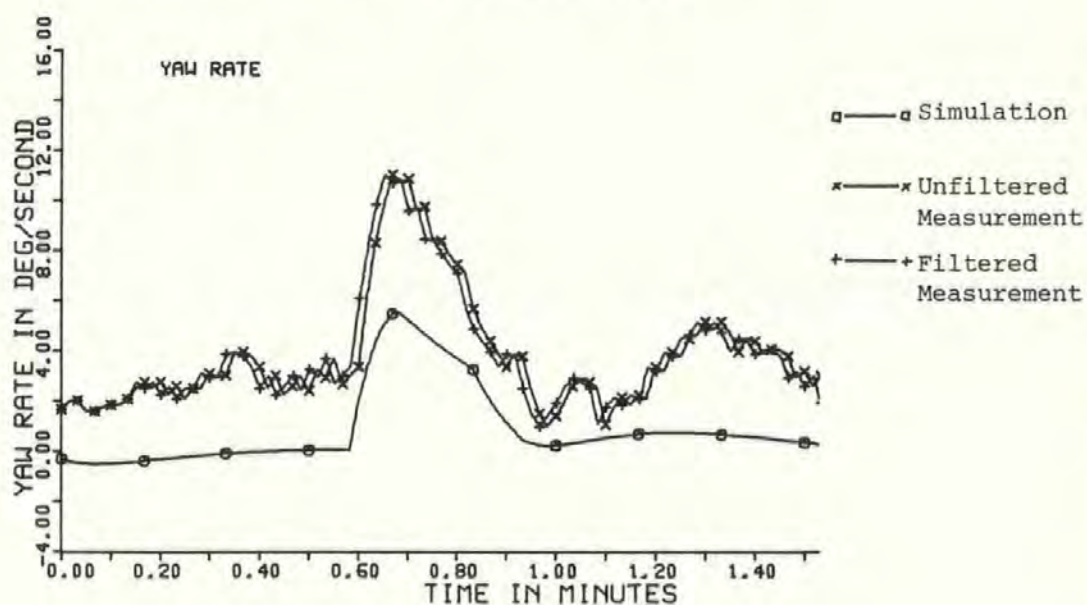
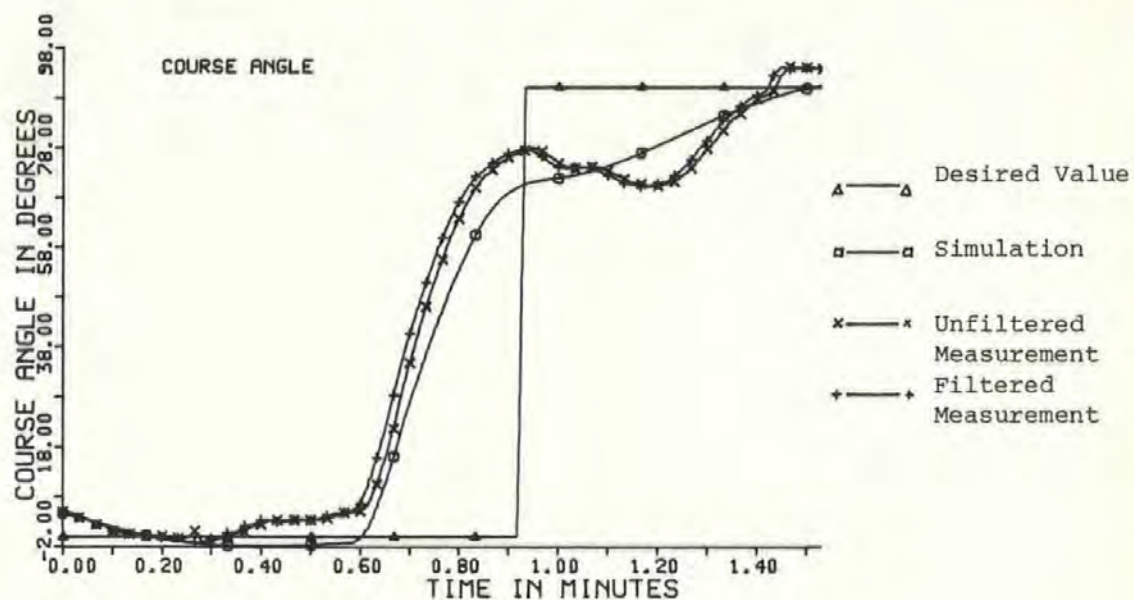


Figure 8.8(b)

Run 10

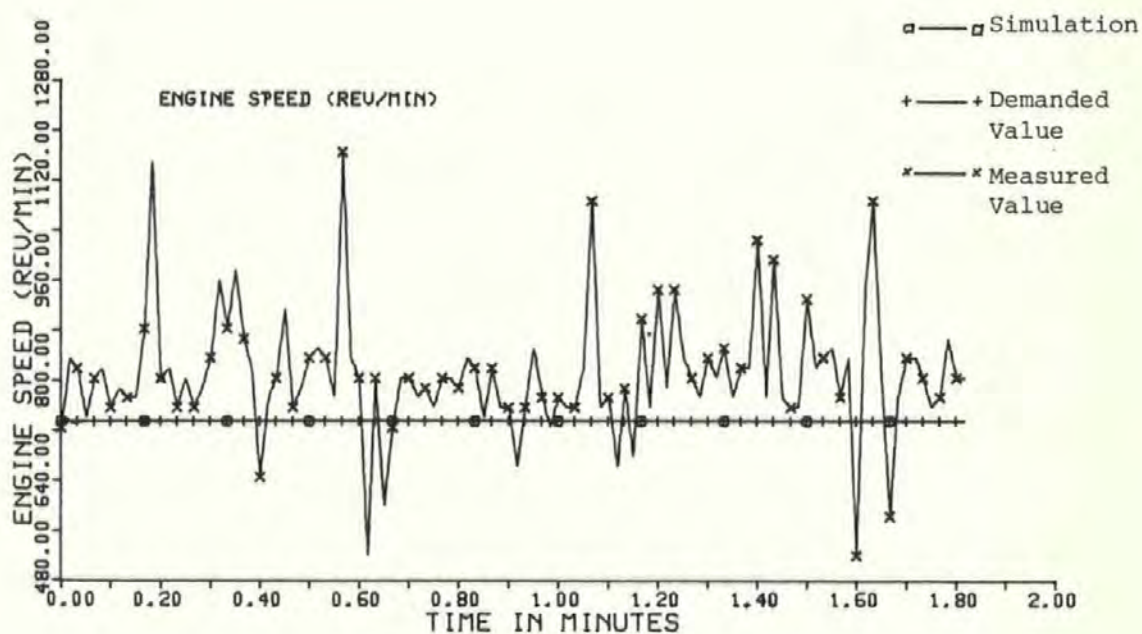
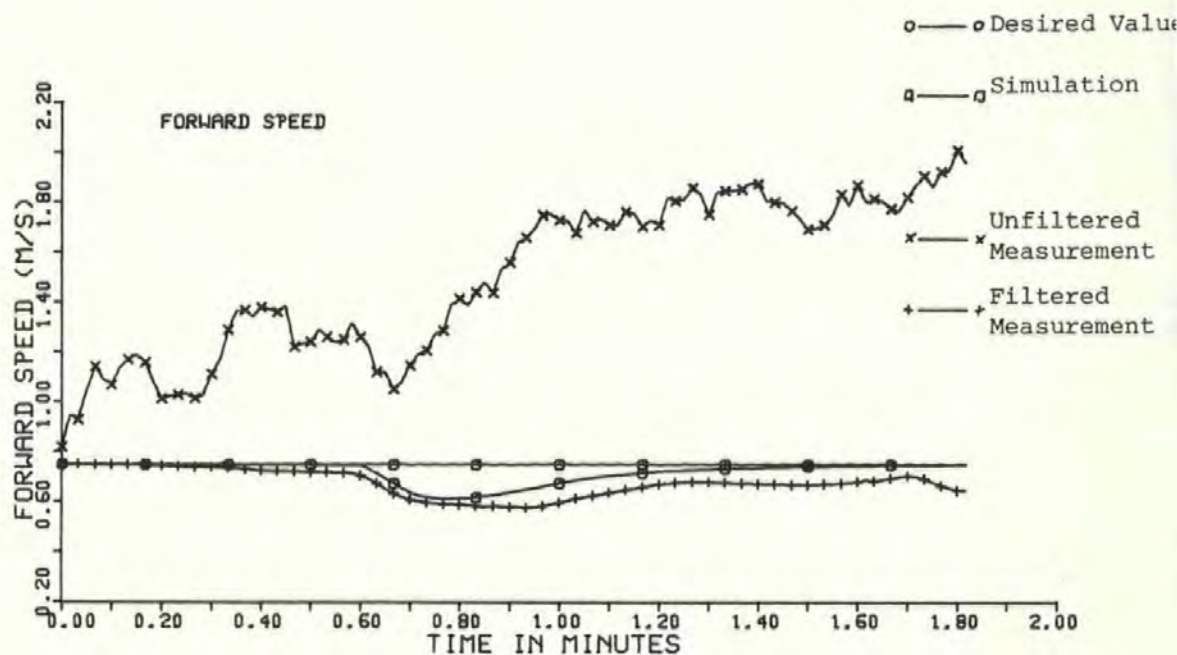


Figure 8.8(c)

Run 10

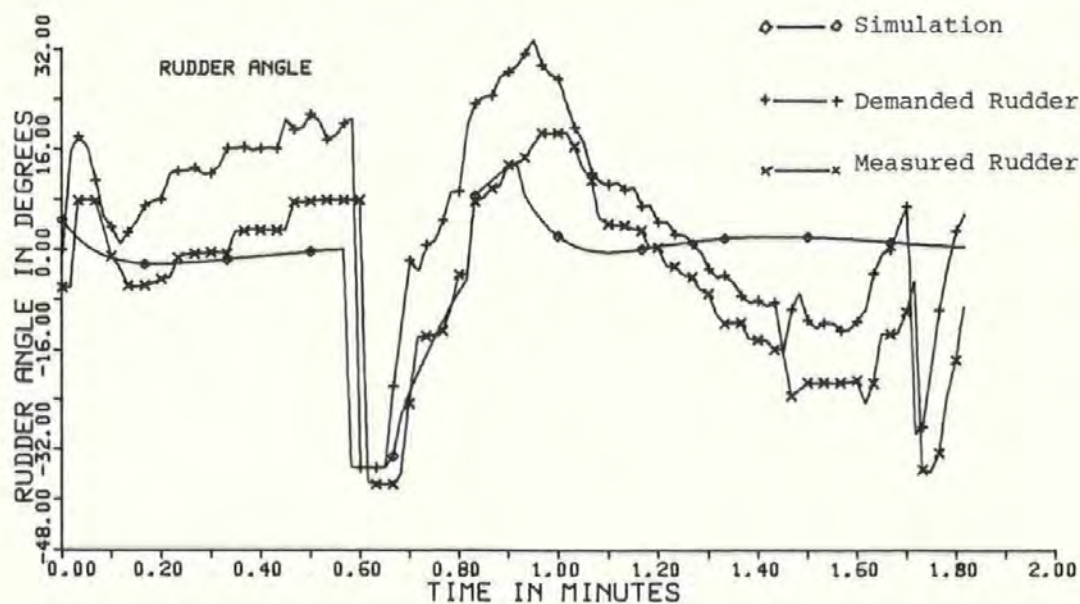
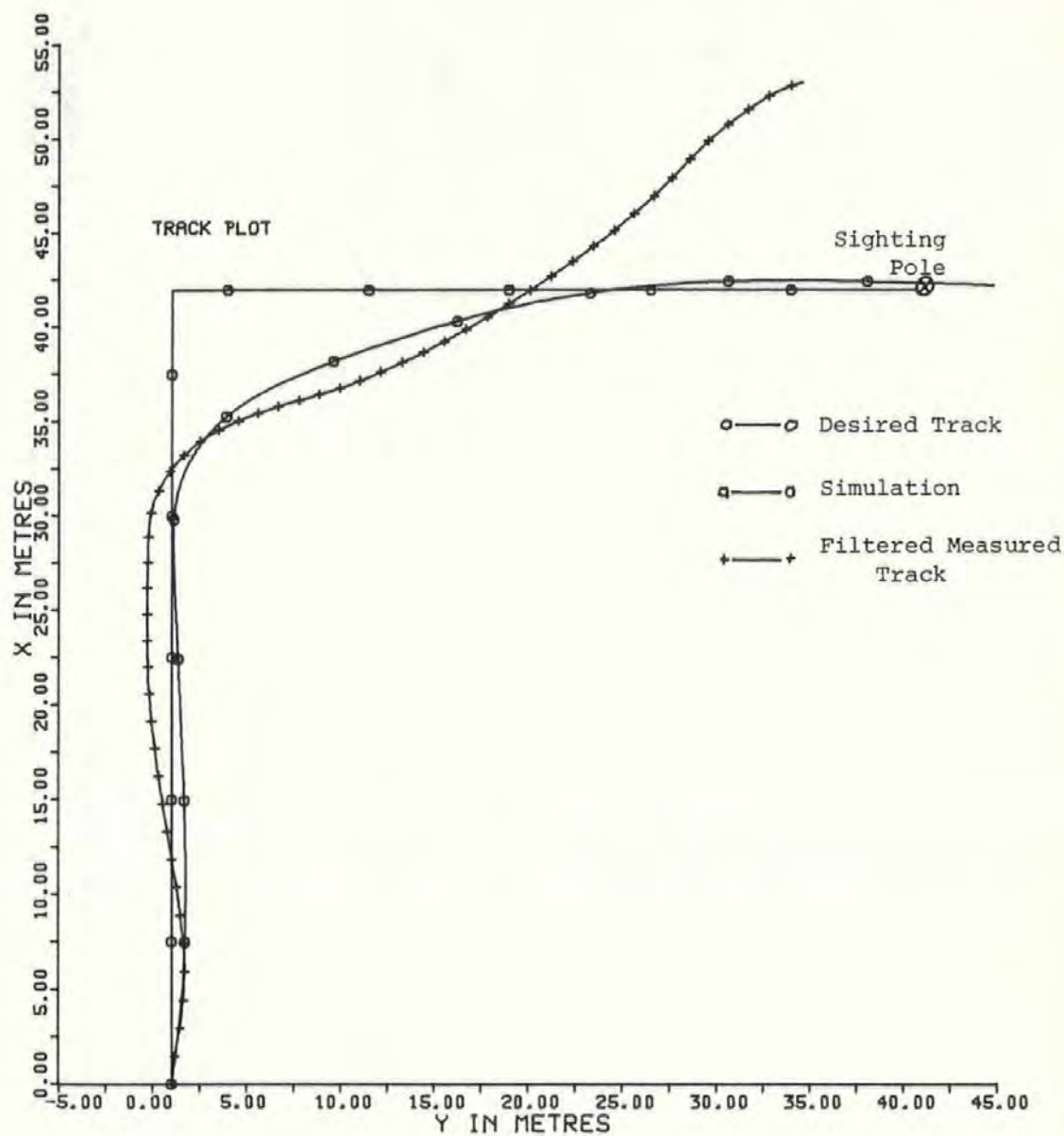


Figure 8.9(a)

Run 12

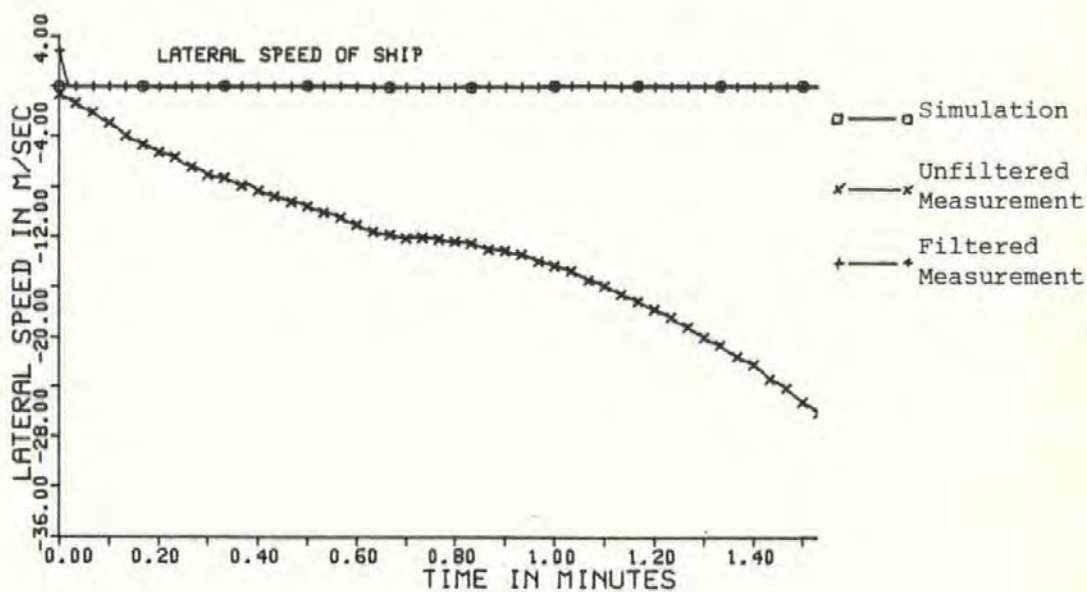
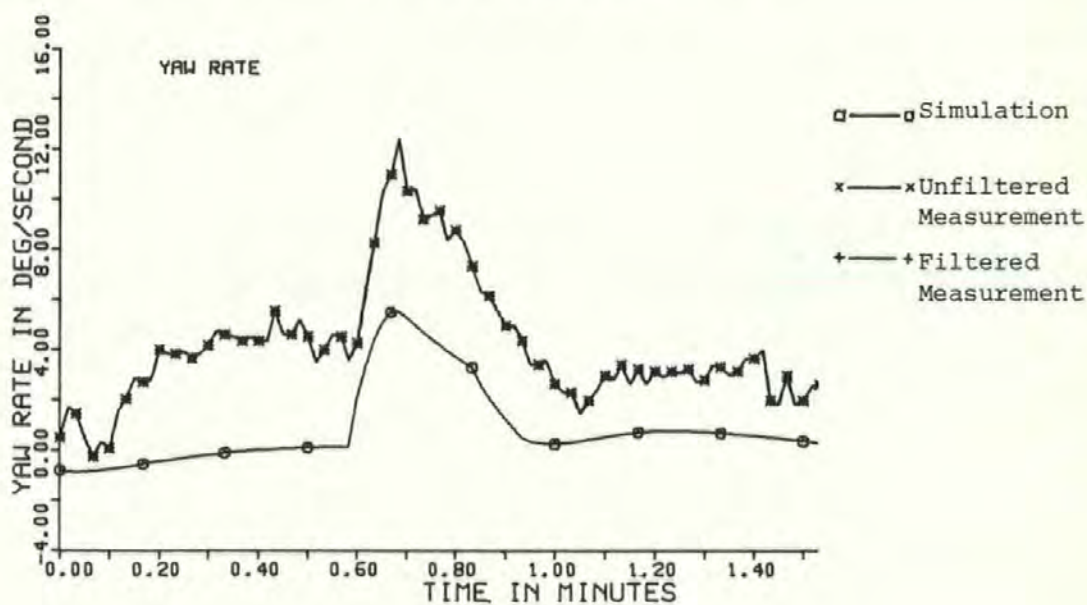
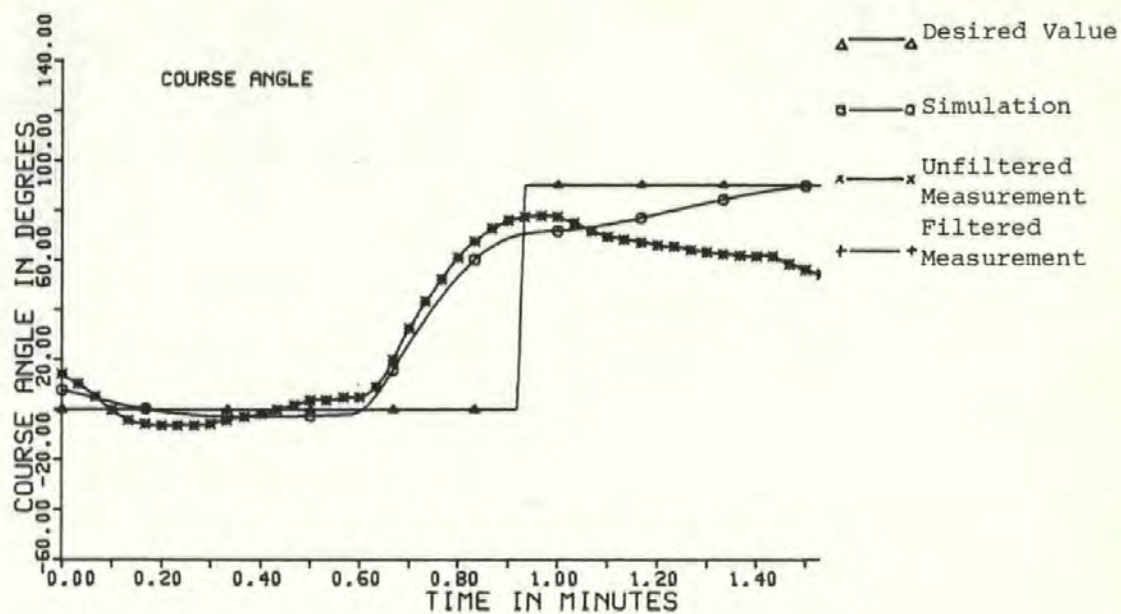


Figure 8.9(b)

Run 12

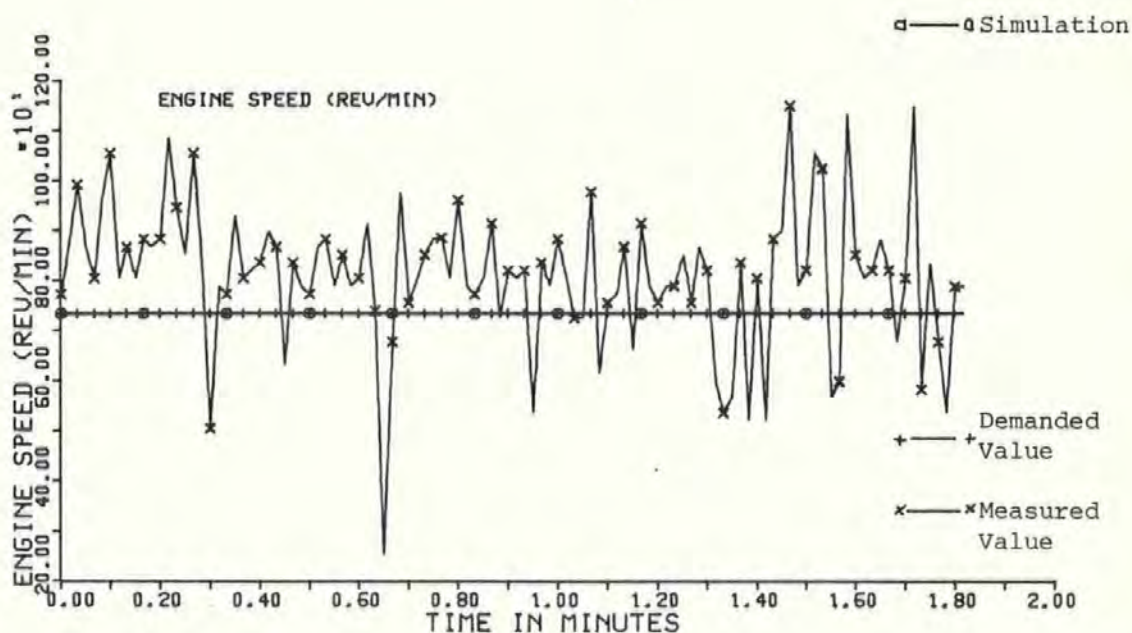
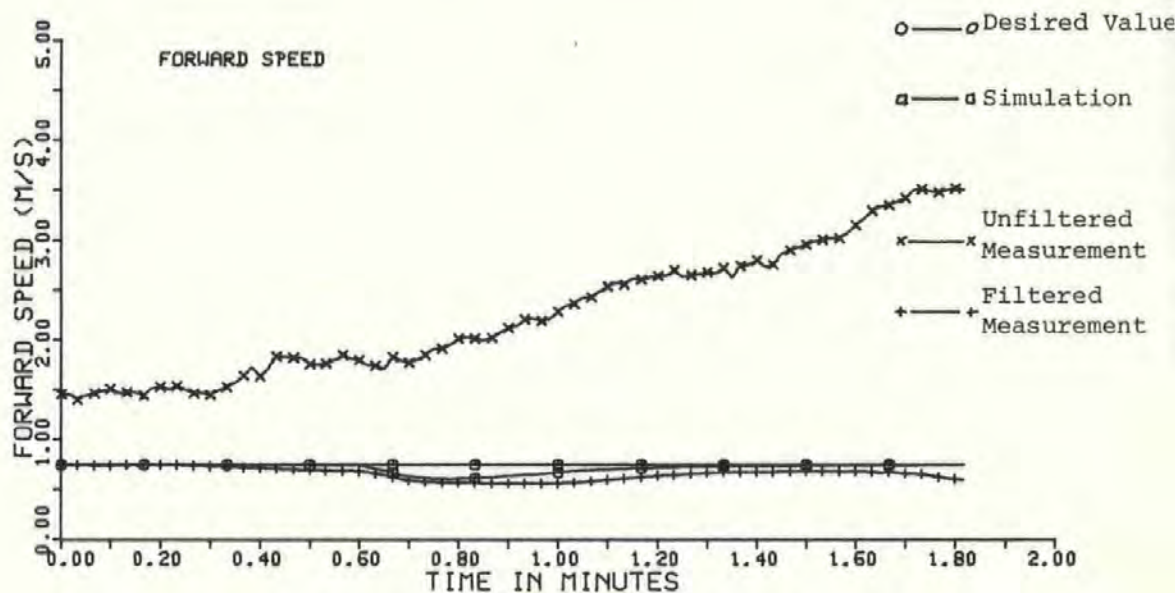


Figure 8.9(c)

Run 12

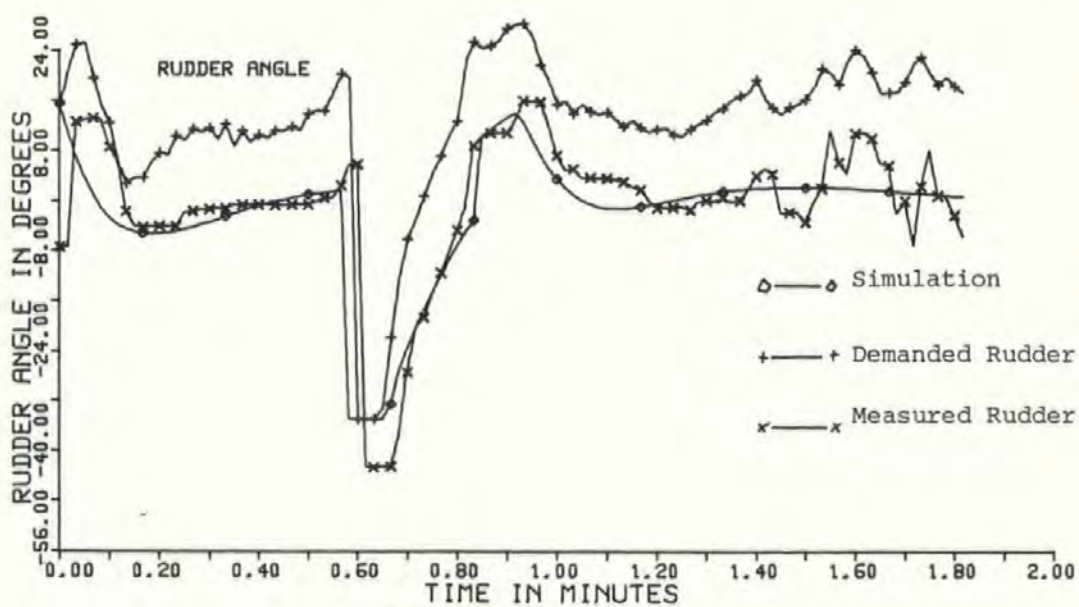
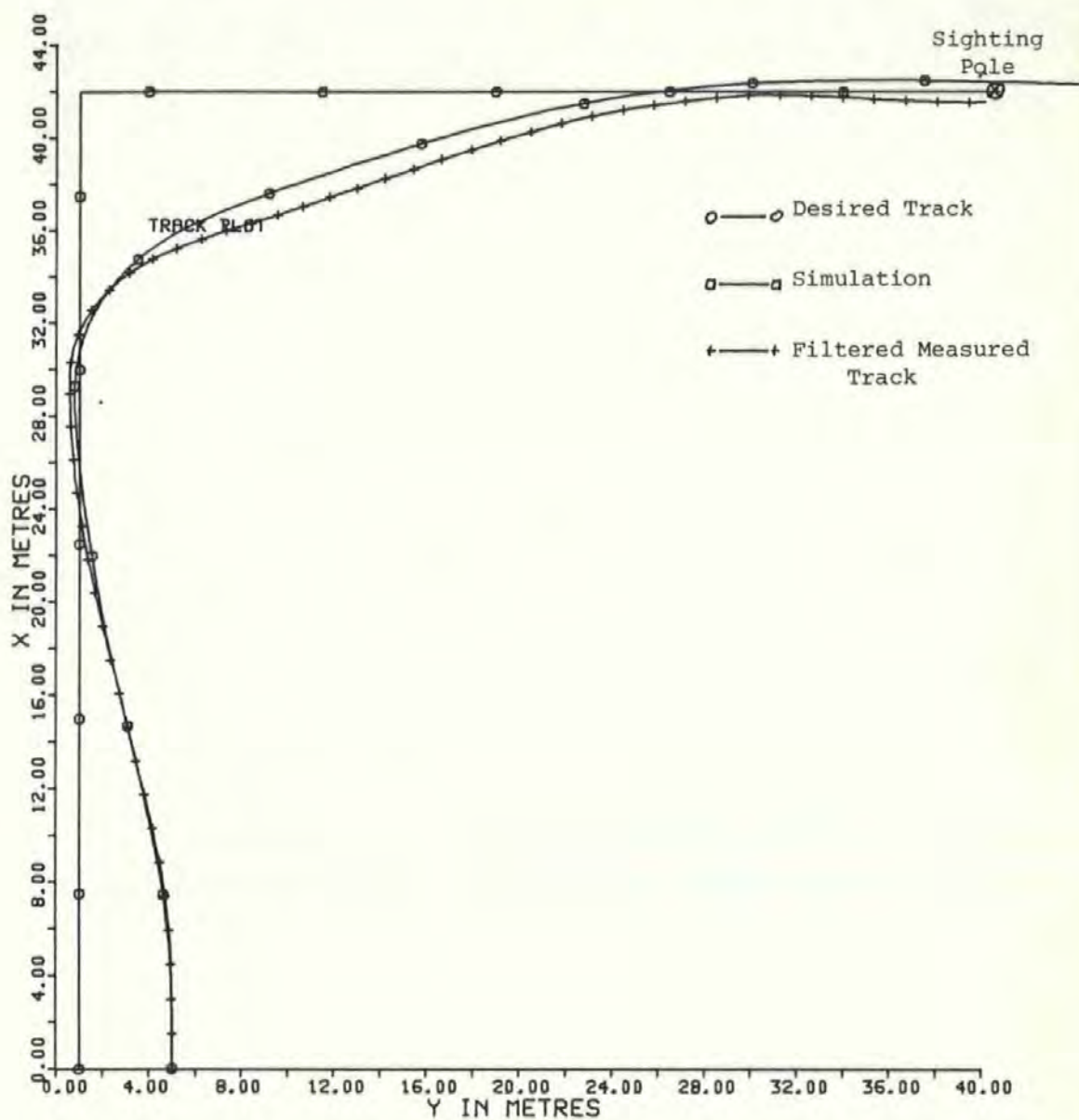


Figure 8.10(a)

Run 19

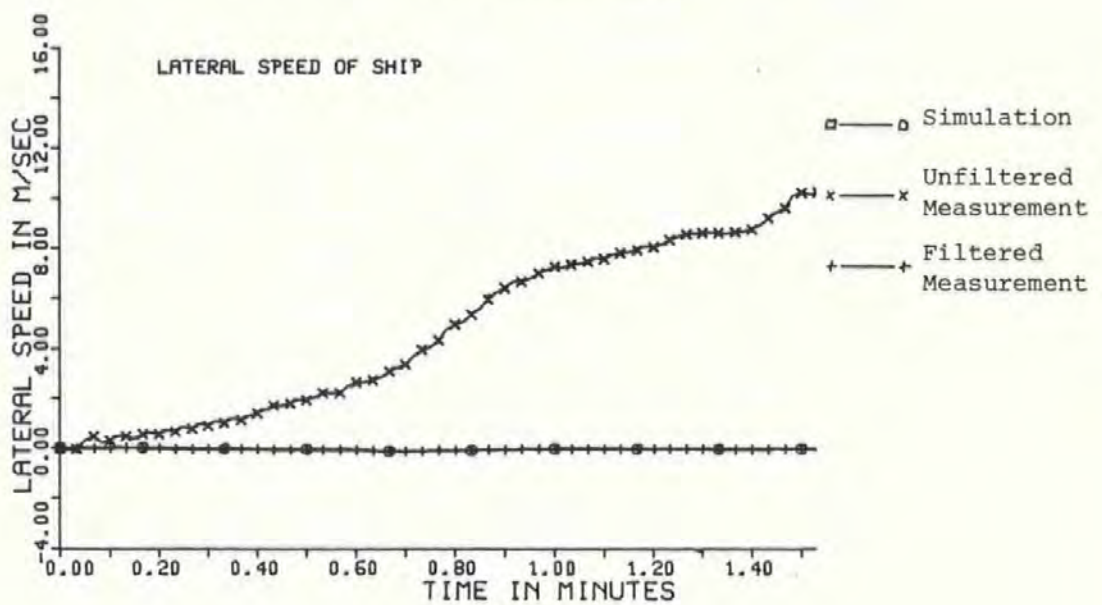
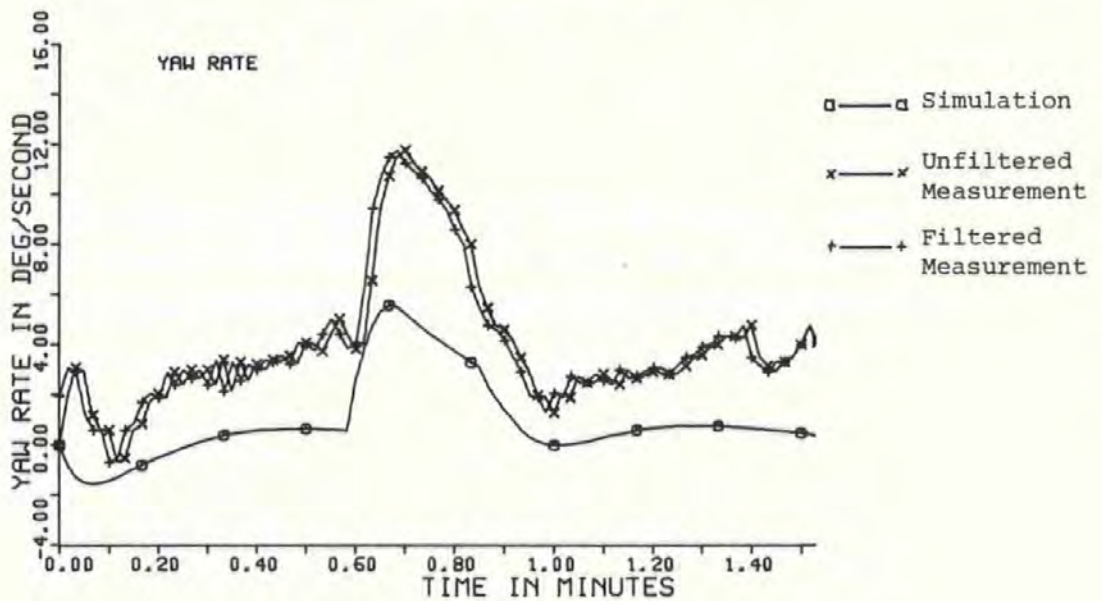
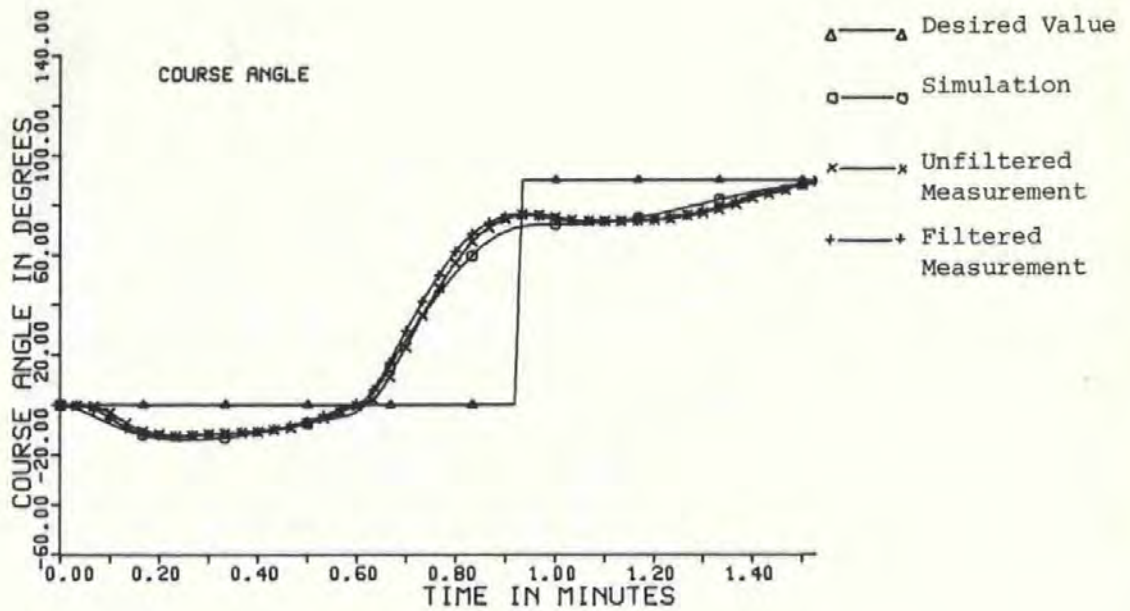


Figure 8.10(b)

Run 19

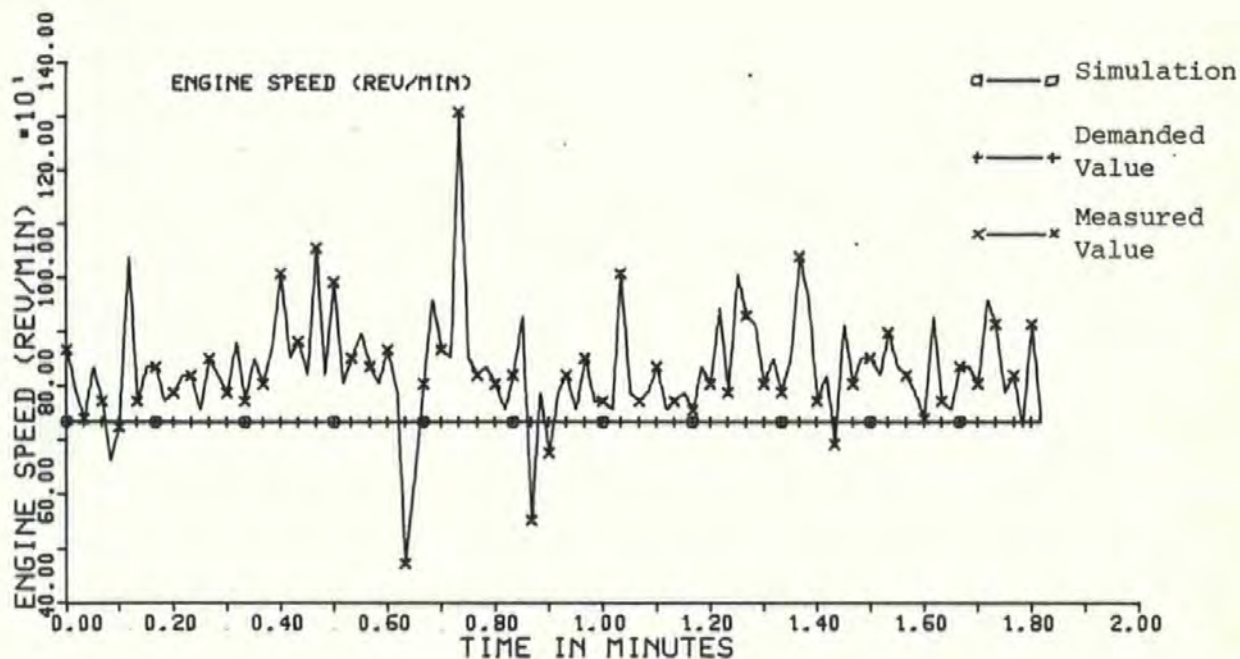
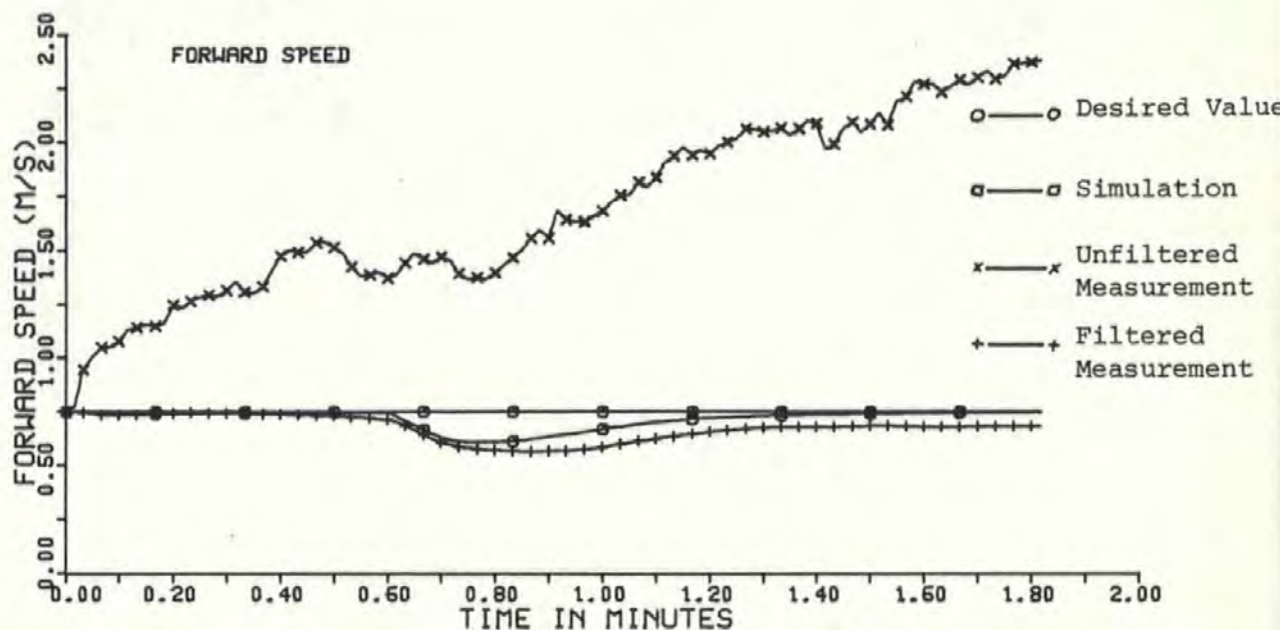


Figure 8.10(c)

Run 19

CHAPTER 9

CONCLUSIONS

9.1 Introduction

The research summarised in this thesis has been concerned with the design and evaluation of a control system which could be utilised for automatic pilotage of surface ships in confined or restricted waters. This final chapter reviews some of the principal conclusions and observations based on the work and considers the possibility of future developments.

9.2 Modelling Techniques

Mariner Hull

The first section of work was devoted to the development of a mathematical model that adequately describes the motion of a vessel in a manoeuvring situation. A comprehensive computer simulation study was conducted on the Mariner hull form using hydrodynamic data from the work of Chislett and Strom-Tejsen (67). A comparative evaluation with full-scale measurements taken by Morse and Price for the USS Compass Island (66) showed that a non-linear, time-varying model most accurately represented the motion of the hull in surge, sway and yaw, particularly with tight manoeuvres.

The model gives good correlation with the full-size ship in terms of both transient and steady-state behaviour over a range of forward velocities from 2.572 to 7.717 m/s and yaw-rates up to ± 1.0 degrees/second, which corresponds to 25 degrees of rudder. It does not however cater for:

- (i) Changes in handling qualities due to operational loading or trim.
- (ii) Shallow water and bank effects.
- (iii) The action of passing ships.

Disturbances were modelled in terms of hydrodynamic effects of current and aerodynamic effect of wind. The aerodynamic data for the Mariner hull was taken from wind-tunnel tests performed by Eda (62). The disturbances were considered to contain both mean and stochastic components which could be scaled to simulate a range of weather conditions that might occur in Plymouth Sound. The stochastic nature of the disturbances were correlated in terms of magnitude and direction.

Use was made of the disturbances to deflect the vessel from some desired track and, in the absence of measured data, no attempt was made to quantify the resulting motion. The effect of waves on the hull was not considered.

Car-Ferry Hull

As a consequence of the Mariner modelling exercise, there existed a simulation package that had been extensively tested on a single vessel but was as yet untried on other ship types. Due to time limitation and lack of availability of the large number of hydrodynamic coefficients required, it was decided that future validation of the simulation package could be made using experimental data derived from tests on the model car-ferry hull.

The towing-tank tests at the National Maritime Institute resulted in a set of accurately measured steady-state hydrodynamic coefficients for the model car-ferry, the yaw-rate dependent coefficients being obtained later from free-sailing tests. No measurements were taken, however, of the added mass coefficients which

affect the transient behaviour of the vessel. The assumption that the ratio of non-dimensional added mass to non-dimensional ship mass was the same for both Mariner and car-ferry, due to their similar block coefficients, was shown to be true from the magnitude of the validity indices obtained by comparison of real and simulated data.

The aerodynamic coefficients for the car-ferry hull are based on equations (3.18) and must be assumed to be approximate in the absence of measured data.

9.3 Controller Design and Evaluation

The design of a multivariable system to control simultaneously track, heading and velocity of a ship modelled by a set of non-linear, time-varying differential equations is a challenging requirement.

Linear Analysis

The task is simplified when the time-varying and non-linear effects are removed, and it was for these conditions that the system was demonstrated to be fully state controllable. What effect variations in forward velocity, yaw-rate and other parameters have on controllability still as yet remain unanswered.

Optimal control of systems with linear dynamics using quadratic performance criteria (LQP control) has an explicit solution giving directly the optimal control law. The matrix recursive equations (5.19) and (5.20) integrate in reverse time to give the solution of the steady-state matrix Riccati equation together with the parameters of the feedback matrix. The time interval required for steady-state convergence is equal to the settling time of the dominant closed-loop eigenvalues, needing many recursions when the sampling time is small. This means that the algorithm is demanding in terms of processor utilisation and a more efficient technique might be to use the Potter

algorithm(82). This requires that a $2n \times 2n$ matrix is formed, the eigenvalues of which correspond to those of the optimal system.

The use of optimal root loci is a very visual approach and gives great insight into the effect of changing parameter weightings in the Q and R matrices. An important outcome of linear design analysis is the dependence of dynamic stability upon heading feedback.

Non-Linear Analysis

When the effects of system non-linearities were considered, it was discovered that the optimal closed-loop poles had very little departure from their assigned positions, even in very tight turns. From this it was concluded that controller adaption was unnecessary for turning manoeuvres.

Adaptive Optimal Control

Variations in forward velocity has the effect of radically changing system open and closed-loop poles and a system tuned to provide satisfactory response at 7.717 m/s will be highly oscillatory at 2.572 m/s.

A method of adaption was proposed whereby the complex closed-loop poles maintain their original optimally assigned positions. The controller synthesised from the variations of required feedback matrix elements takes the form of a "gain scheduling controller" where, in general, the gain of the time-varying elements is inversely proportional to the square of the forward velocity.

Disturbance Control

It is not possible under an optimal policy to employ integral control action without affecting the closed-loop poles. An alternative method, referred to as active disturbance control, was investigated. The technique relies upon knowledge of the disturbance model of the vessel, together with the nature of the disturbances. It

was found that complete instantaneous force and moment cancellation was not possible due to the dynamics of the controls themselves, together with their force/moment characteristics. A compromise solution was proposed whereby emphasis was placed upon the balancing of disturbance and control moments.

9.4 Performance Characteristics

The performance evaluation of three different types of control strategy was undertaken. The first of these, Reverse-Time Integration provides the only true means of anticipating desired state trajectories. A reverse-time command vector is generated from knowledge of the ship's closed-loop dynamics together with the desired state vector. Inbuilt into the command vector, which must be available prior to the vessel entering port, is the inverse of all transient and steady-state errors.

The technique was found to possess good transient anticipation but suffered from a lack of steady-state accuracy, the latter being sensitive to controller setting.

The second control strategy incorporates dual-mode control with way-point anticipation. This is a simple concept that allows the command vector to be replaced by a method of advancing way-points so that track-changing occurs without overshoot. At the advanced way-point position, a switch is made from track to course-keeping. This initiates a turning manoeuvre and when the course error is less than a prescribed amount (thirty degrees was found to be suitable) the track-keeping mode is re-established.

Dual-mode control was found to possess excellent track-keeping capability as can be seen in Figure 6.7. The generalised performance indices given in Table 6.4 show that for this run, J_y and J_u , which

relate to track-keeping ability and forward velocity control, both have a global minimum. It will be observed by comparing J_y with J_ψ that good track-keeping performance is achieved at the expense of good course-keeping, for when a vessel pulls onto track it must always incur a course penalty.

The third policy uses a combination of ship and earth related state variables to allow a multivariable control strategy, referred to as dynamic position-keeping, to be used to control the vessel's heading and forward speed, together with its position on the earth's surface. The method has the advantage that filtered positional information taken from navigational equipment may be used directly in the feedback loop, but suffers from the problem that the feedback matrix becomes a function of the desired heading.

It will be observed that the performance indices in Table 6.4 for position-keeping runs 7 and 8 correspond to those for the dual-mode simulations 5 and 6, i.e. the net outcome of both strategies is the same, the difference lying in the manner in which the problem has been tackled.

It was concluded that reverse-time integration is a sophisticated solution but with practical difficulties, whilst dual-mode control and dynamic position-keeping ultimately perform the same function, the former being more straight-forward to use. Hence a dual-mode policy with way-point anticipation was selected as the best control strategy to implement in the physical model.

Adaptive Control Performance

As predicted at the design stage, oscillatory track-keeping performance occurs when a vessel travels at low forward speed with a fixed gain feedback matrix as shown in Figure 6.12(b). The gain scheduling controller proposed in Chapter 5 provided the vessel with

unchanging yaw dynamics as its forward speed varied. This had the effect of reducing track transient errors but with the penalty of significant increase in rudder activity.

It was observed, however, that when adaption takes place with constant Q and R matrices at each forward speed, the ship always moves along an identical track. This form of adaption was considered more desirable than the fixed eigenvalue policy and the parameters for a gain scheduling controller were again computed. These were found, in general, to be proportional to the inverse of the forward speed.

Disturbance Control Performance

Comparison of Figures 6.10 and 6.11(a) show quite clearly the benefits that can be obtained by the use of disturbance control. In the latter, however, it is assumed that the nature of the disturbances are known, i.e. that they can be measured. The use of anemometers to measure wind strength and direction presents no problem but difficulties arise in the measurement of current. One possibility is to place current-meters at strategic points in port approaches and radio information to passing vessels. Alternatively, dopplar sonar may be used to monitor surge and sway velocity relative to (a) seabed, (b) water, the difference being the velocity of the current.

If, however, no measurements exist, but an approximate mean estimate for both wind and current is available as input to the controller, some improvement will result as seen in Figure 6.11(b).

At reduced forward speeds disturbance control is less effective because of the corresponding reduction in rudder control moments and forces. Eventually, a saturation point occurs when the maximum control effort available is insufficient to counteract the disturbance effects.

9.5 Implementation and Testing

The factors that governed the selection of measurement and control system hardware for the physical model were:

- (a) cost
- (b) size
- (c) accuracy
- (d) "in house" availability
- (e) "in house" expertise.

This resulted in a system that was not ideal, but had the potential to work. Initial tests on the bridge of the Amorique demonstrated that the prototype measurement system had sufficient sensitivity to detect motions of a full-size vessel.

Apart from tuning feedback loops, the rudder servos on the model gave little trouble. There was a problem, however, with the main engine drive amplifiers, which were always working close to their upper saturation level in order that the propellers could operate at the mean design speed. As a result, when testing on the reservoir, the speed control system was unable to cope with a wide range of demanded engine speeds about the mean value. To avoid the possibility of amplifier malfunction due to frequent overload, the optimal controller weightings were adjusted to provide a constant demanded speed with only small perturbations, with the incurred penalty of largely ineffective forward velocity control.

Although the sides of the reservoir were sheltered, the central area always remained exposed. Track-keeping runs therefore, could be performed in conditions of moderate wind, but track-changing runs required calm weather, usually found early in the morning or late evening. Run 12 in Figure 8.9 is a good example of where the model is

deflected off-track by a force 3/4 wind experienced in the middle of the reservoir.

However, in calm water, the model responded well and the dominant closed-loop dynamic characteristics for both simulated and measured systems can be extracted from runs 3 and 5 and are listed in Table 9.1.

Run No.	Simulation or Measured	ω_D (rad/s)	ζ	ω_n (rad/s)	Closed-Loop Eigenvalues
3	Simulation	0.0668	0.581	0.0821	$-0.0477 \pm j0.0668$
3	Measured	0.073	0.437	0.0812	$-0.0355 \pm j0.073$
5	Simulation	0.0654	0.590	0.0810	$-0.0478 \pm j0.0654$
5	Measured	0.0654	0.500	0.0755	$-0.0378 \pm j0.0654$

Table 9.1

Closed-Loop Characteristics of Model

Table 9.1 reinforces the data presented in the form of validity indices that in general the closed-loop dynamics of both physical and mathematical models are very close. The damping in the physical system is slightly less than that in the mathematical one and is thought to be due to small inaccuracies in the yaw-rate coefficients measured from free-sailing tests on the River Plym.

9.6 Future Developments

Within the given limitations of the reservoir trials, the performance of the physical model closely corresponded to theoretical predictions, and demonstrates the effectiveness and accuracy of the synthesis and analysis techniques employed. Although these trials

conclude the present programme of work, they are also the starting point for the next phase of research.

It has been appreciated throughout, that the detailed information obtained for the ship mathematical model was for one carefully defined set of conditions only. Further, data regarding dynamic characteristics (added mass) was missing and had to be approximated.

The handling characteristics of surface ships undergo significant changes depending upon operational and environmental conditions. It is important therefore to have within the system a parameter estimation algorithm that provides the controller and filter with frequent updates of the mathematical model. Parsons and Cuong (37) in 1980 studied the effectiveness of a two-loop system, an inner control loop and an outer gain update loop, the latter taking the form of either a weighted least-squares, or a minimum variance parameter estimator. Bouncer (83) has used on-line methods of identification and parameter estimation for a noisy electrohydraulic system and Kallstrom (84) has employed similar techniques to investigate ship steering properties. Abkowitz (85) employs an extended Kalman filter technique to identify hydrodynamic characteristics from ship manoeuvring trials. Slender body theory has been applied by Hwang (86) in the identification of non-linear hydrodynamic coefficients and to show the cancellation effect.

The integrated use of identification, estimation and control algorithms to form optimal self-tuning systems has been explored by Grumble et. al. (87), (88) with particular reference to the dynamic positioning problem. This is an area where there has been much activity and optimal self-tuning systems for dynamic positioning now exist. Saelid et. al. (89) discusses an instability problem on the ALBATROSS system and points out that the real life situation often

results in a sub-optimal solution due to compromise in terms of performance, physical costs and the technical costs of modelling and tuning.

The track-keeping performance of a vessel is very dependent upon accurate positional measurement. Apart from the development of satellite navigational systems such as GPS, there is a growing interest in localised position-fixing systems. A state-space controller has been designed by Gilles et. al. (90) that locks a ship onto an underwater pilot or leader cable and the system was successfully tested over a distance of 4 km.

An offshoot from dynamic positioning technology is the use of acoustic transponders that lie on the sea-bed in port approaches to provide positional information to ships in close proximity. Smith (91) reports that Krupp Atlas-Elektronik have developed an automatic position fixing system that uses a laser beam to measure dynamically both range and bearing from shore to ship. The system is claimed to have decimeter accuracy.

The danger with automatic track-keeping is always the risk of collision. The potential integration of automatic track-keeping with collision avoidance systems very much depends upon how reliable and accurate the measurement of relative position and velocity of nearby ships can be made.

The main problems are noise on radar data coupled with small perturbation of ship motion. Merz (92) is investigating the use of an optimal filtering algorithm to obtain best estimates. Lanka (93) has developed a continuously adaptive Kalman filter for tracking manoeuvring radar targets. Stockel and Colley (94) have been working on collision avoidance algorithms that enable a vessel to follow the

"rules of the road" in a potential collision situation.

It is envisaged that in the immediate future, developments in the continuing ship dynamics and control research programme at Plymouth Polytechnic will take place in the following areas:

(a) Identification and Parameter Estimation

Carrying on the work of Bouncer, the free-sailing car-ferry model will be used as a vehicle to investigate on-line identification techniques such as Linear Least Squares and Maximum Likelihood for comparative evaluation with existing towing-tank data.

(b) Integrated Track-Keeping and Collision Avoidance

The guidance system devised by Burns and Dove will be implemented on the Polytechnic survey vessel for further testing and evaluation. The system will then be expanded to encompass the collision avoidance algorithms of Stockel and Colley and the feasibility of a fully integrated track-keeping and collision avoidance system investigated.

REFERENCES

1. E. SPERRY
"Automatic Steering".
Trans. SNAME, 1922.
2. N. MINORSKY
"Directional Stability of Automatically Steered Bodies."
Journal of American Society of Naval Engineers, 1922.
3. K. NOMOTO
"Directional Stability of Automatically Steered Ships with
Particular Reference to Their Bad Performance in Rough
Seas."
Proc. of First Symposium on Ship Manoeuvrability, DTMB,
May, 1960, DTMB Report No. 1461, Oct. 1960.
4. R.M. LUKE and F. WEST
"An Integrated Steering System."
New England Section, SNAME, June, 1960.
5. S. MOTORA
"On the Automatic Steering and Yawing of Ships in Rough
Seas."
Journal of S.N.A. of Japan, 1953.
6. L.J. RYDILL
"A Linear Theory for the Steered Motion of Ships in Waves."
Trans. RINA, 1958.

7. M.I. BECH
"Some Aspects of the Stability of Automatic Course Control of Ships."
Journal Mech. Eng. Science, Vol. 14, No. 7, 1972, p 123-131
8. C.R. WESNER
"An Advanced Autopilot for Ships."
Third Ship Control Symposium, Bath, Sept. 1972, Paper 111B-2.
9. D.L. BROOK
"The Design of a New Autopilot for the Commercial Ship."
Ship Operation Automation IFAC/IFIP Symposium, Oslo, July, 1973, Paper 9.4.
- 10 G. HONDERD and J.E.W. WINKELMAN
"An Adaptive Autopilot for Ships."
Third Ship Control Symposium, Bath, Sept 1971, Paper 111B-1
- 11 J. VAN AMERONGEN and A.J. UDINK TEN CATE
"Adaptive Autopilots for Ships".
Ship Operation Automation IFAC/IFIP Symposium, Oslo, July 1973, Paper 9.3.
12. D.R. INGWERSON
"A Modified Liapunov Method for Non-Linear Stability Analysis."
IRE Trans. on Auto. Control. Vol. AC-6, 1961.
13. C.A. WINSOR and R.J. ROY
"Design of Model Reference Adaptive Control Systems by Liapunov's Second Method."

14. A.J. UDINK TEN CATE and N.D.L. VERSTOEP
"Improvement of Liapunov Model Reference Adaptive Control Systems in a Noisy Environment."
Int. J. Control, 1974, Vol. 20, No. 6, p 977-996.
15. K.J. ASTROM and P. EYKHOFF
"System Identification - A Survey."
Automatica, Vol. 7, 1971, p 123-162.
16. K.J. ASTROM and B. WITTENMARK
"On Self Tuning Regulators."
Automatica, Vol. 9, 1973, p 185-199.
17. D.W. CLARKE and P.J. GAWTHROP
"Self-Tuning Controller.'
Proc. IEE 122, No. 9, Sept. 1975, p 929-934.
18. N. MORT and D.A. LINKENS
"Self-Tuning Controllers for Surface Ship Course and Track-Keeping."
Symposium on Ship Steering Automatic Control, Genova, June 1980, p 175-188.
19. S.M. HODDER and D.N. SHIELDS
"Application of Self-Tuning Control to Ships' Autopilots."
Second International Conference on Systems Engineering.
Coventry Lanchester Polytechnic, Sept. 1982, p 187-198.
20. K.J. ASTROM and C.G. KALLSTROM
"Identification of Ship Steering Dynamics."
Automatica, Vol. 12, 1976, p 9-22.

21. K.J. ASTROM and C.G. KALLSTROM et. al.
"The Identification of Linear Ship Steering Dynamics Using
Maximum Likelihood Parameter Estimation."
Swedish State Shipbuilding Experimental Tank, 1975, Nr. 75.
22. C.G. KALLSTROM and K.J. ASTROM et. al.
"Adaptive Autopilots for Tankers."
Automatica, Vol. 15, 1979, p 241-254.
23. K. NOMOTO and T. MOTOYAMA
"Loss of Propulsive Power Caused by Yawing with Particular
Reference to Automatic Steering."
Japan Shipbuilding and Marine Eng., 120, 1960, p 71-80.
24. T. KOYAMA
"On the Optimum Automatic Steering System of Ships at Sea."
Journal of Soc. Nav. Arch., Japan, Vol. 4, 1970.
25. N.H. NORRBIN
"On the Added Resistance due to Steering a Straight Course."
Thirteenth ITTC Berlin/ Hamburg, 1972.
26. D.R. BROOME and T.H. LAMBERT
"An Optimising Function for Adaptive Ships' Autopilots."
Fifth Ship Control Systems Symposium, Vol. 3, Paper J2 1-1,
1978, Maryland, U.S.A.
27. L. MARSHALL and D.R. BROOME
"A Cost Function Indicator for Optimal Ship Course Keeping."
Automation for Safety in Shipping and Offshore Petroleum
Operations. IFIP, 1980, p 103-108.

28. D. CLARKE
"Development of a Cost Function for Auto-pilot Optimisation.
Symposium on Ship Steering Automatic Control, Genova, June
1980, p 59-77.
29. J. GOCLOWSKI and A. GELB
"Dynamics of an Automatic Ship Steering System."
Automatic Control, Vol. AC-11, No. 3, July 1966, p 513-524.
30. IR J.A.M. TER HORST
"Automatic Track Guidance of a Minesweeper."
Third Ship Control Systems Symposium, Bath, Sept. 1972,
Paper 11B-2.
31. J.K. ZUIDWEG
"Automatic Guidance of Ships as a Control Problem."
Thesis, Technische Hogeschool, Delft, 1970.
32. J.K. ZUIDWEG
"Automatic Track-Keeping as a Control Problem."
Third Ship Control Systems Symposium, Bath, Sept. 1972,
Paper 11B-1.
33. H.F. MILLERS
"Modern Control Theory Applied to Ship Steering."
Ship Operation Automation - IFAC/IFIP Symposium, Oslo, July
1973, Paper 9.2.
34. W.H.P. CANNER
"Automatic Path Guidance."
Ship Operation Automation - IFAC/IFIP Symposium, Oslo, July
1973 p 115-129.

35. W.H.P. CANNER

"The Accuracy Requirements of Automatic Path Guidance."

Proc. Fourth Ship Control Systems Symposium, Royal

Netherlands Naval College, Oct. 1975, p 1.141-1.169.

36. A.A. YAKUSHENKOV

"Automation of Ship Steering Control on a Desired Track."

Ship Operation Automation IFAC/IFIP Symposium, Oslo, July

1973, p 138-144.

37. M.G. PARSONS and H.T. CUONG

"Adaptive Path Control of Surface Ships in Restricted

Waters."

Dept. of Nav. Arch. and Marine Eng. University of Michigan,

Report No. 211, March 1980.

38. J. VAN AMERONGEN and E.F.A. LAND

"An adaptive Autopilot for Trackkeeping."

Ship Operation Automation 111 IFPA, 1980, p 105-114.

39. A. SARGENT and G. COWGILL

"Design Considerations for Dynamically Positioned Utility

Vessels."

Offshore Tech. Conf. 1976, Dallas, U.S.A.

40. N.A. JENSSEN et. al.

"Dynamic Positioning System Using Kalman Filtering Technique

From Theory to Practice."

Automation for Safety in Shipping and Offshore Petroleum

Operations, IFIP, 1980, p 211-219.

41. A.L. COLEMAN and B.P. WANG
"Developments in Automatic Control of Ship Steering."
Symposium on Ship Steering Automatic Control, Genova, June
1980, p 361-375.
42. R.E. KALMAN and R.S. BUCY
"New Results in Linear Filtering and Prediction Theory."
J. of Basic Eng., Trans. of the Am. Soc. of Mech. Eng.,
March 1961, p 95-108.
43. M.J. DOVE
"Kalman Filter Techniques in Marine Integrated
Navigational Systems."
J. Inst. Nav. (U.K.), Vol. 30, No. 1, Jan. 1977, p 135-145.
44. M.J. GRIMBLE
"Adaptive Kalman Filter for Control of Systems with Unknown
Disturbances."
Research Report EEE/56/1980. Dept. of Elect. and
Electronic Eng., Sheffield City Polytechnic, July, 1980.
45. A.J. ROBINS
"The Extended Kalman Filter and its Use in Estimating
Aerodynamic Derivatives."
Aerospace Dynamics, Issue 9, Sept. 1982, p 16-24.
46. S. HASHIGUCHI
"Integrated Automatic Navigational System."
Ship Operation Automation 1111, IFIP, 1980, p 173-181.
47. R.S. BURNS, T.H. BOUNCER and M.J. DOVE
"Automatic Pilotage of Large Ships in Confined Waters - A
Multivariable Approach."

Symposium on Application of Multivariable Systems Theory,
Plymouth, Oct. 1982, p 71-80.

48. M.A. ABKOWITZ

"Lectures on Ship Hydrodynamics - Steering and
Manoeuvrability."

Hydro-Og Aerodynamisk Laboratorium, Lyngby, Denmark, Report
No. Hy-5, May 1964.

49. P. MANDEL

"Ship Maneuvering and Control."

Principles of Naval Architecture (revised), SNAME, New York
1967.

50. J.A. CADZOW and H.R. MARTENS

"Discrete-Time and Computer Control Systems."

Prentice Hall Inc., New Jersey, 1970.

51. T.H. BOUNCER

"Discrete-Time Solution of the State Equations."

Internal Technical Note, Dept. of Mech. Eng., Plymouth
Polytechnic, 1980.

52. K. NOMOTO

"Response Analysis of Manoeuvrability and its Application
to Ship Design.

60th Anniversary Series, Vol. 11, Soc. of Naval Arch. of
Japan, Tokyo, 1966.

53. J. DZIEDZIC and L. MORAWSKI

"Algorithm of Control of Ship's Motion According to Desired
Trajectory."

Symposium on Ship Steering Automatic Control,
Genova, June 1980, p 141-151.

54. M. BECH and L. WAGNER SMITT

"Analogue Simulation of Ship Manoeuvres."

Hydro-Og Aerodynamisk Laboratorium, Lyngby, Denmark, Report
No. Hy-14, Sept. 1969.

55. J. STROM-TEJSEN

"A Digital Computer Technique for Prediction of Standard
Maneuvers of Surface Ships."

Dept. of Navy Research and Development Report No. 2130,
David Taylor Model Basin, Washington D.C., Dec. 1965.

56. G.R.G. LEWISON

"The Development of Ship Manoeuvring Equations."

National Physical Laboratory, Report Ship 176, Dec. 1973.

57. A.D. GILL

"The Identification of Manoeuvring Equation from Ship
Trials Results."

R.I.N.A., 1975.

58. H. EDA and C.L. CRANE

"Steering Characteristics of Ships in Calm Water and Waves.

Presented at the Annual SNAME Meeting, New York, Nov. 1965.

59. T.P. O'BRIEN

"The Design of Marine Screw Propellers."

Hutchingson, London, 1968.

60. D. CLARKE

"A New Nonlinear Equation for Ship Manoeuvring."

61. K.F. BOWDEN and J. PROUDMAN

"Observations on the Turbulent Fluctuations of a Tidal Current."

Proc. Roy. Soc., A199, 1949, p 311-327.

62. H. EDA.

"Low Speed Controllability of Ships in Wind."

Journal of Ship Research, Sept. 1968, p 181-200.

63. I. VAN DER HOVEN

"Power Spectrum of Horizontal Wind in the Frequency Range from 0.0007 to 900 Cycles/Hour."

J. Met. 14, 160, 1957.

64. A. WATTS

"Wind and Sailing Boats."

Adlard Coles Ltd., London, 1965.

65. B.S.R.A.

"Code of Procedure for Steering and Manoeuvring Trials."

B.S.R.A. Report NS. 353, 1972.

66. R.V. MORSE and D. PRICE

"Manoeuvring Characteristics of the MARINER Type Ship (USS Compass Island) in Calm Seas."

Sperry Polaris Management, Sperry Gyroscope Company, New York, Dec. 1961.

67. M.S. CHISLETT and J. STROM-TEJSEN

"Planar Motion Mechanism Tests and Full-Scale Steering and

Manoeuvring Predictions for a MARINER Class Vessel."

International Shipbuilding Progress, May 1965, Vol. 12,
p 201-224.

68. H.NYQUIST

"Regeneration Theory".

Bell Syst. Tech. J., 1932, Vol. 11, p 126-147.

69. H.W. BODE

"Relations Between Attenuation and Phase in Feedback
Amplifier Design."

Bell Syst. Tech. J., 1940, Vol. 19, p 421-454.

70. W.R. EVANS

"Graphical Analysis of Control Systems."

Trans. Am. Inst. Elect. Engrs., 1948, Vol. 67, p 547-551.

71. R.E. KALMAN

"On the General Theory of Control Systems."

Proc. First International Congress of Automatic Control,
Moscow, 1960.

72. L.J. PONTYAGIN

"Optimal Control Processes."

U.S.P. Mat. Nank 14, 3, 1959.

73. R.E. BELLMAN

"Dynamic Programming."

Princeton University Press,
Princeton, N.J., 1959.

74. K.J. ASTROM

"Introduction to Stochastic Control Theory."

Academic Press, N.J., 1970.

75. H.H. ROSENBROCK

"Design of Multivariable Control Systems using the Inverse Nyquist Array."

Proc. Instn. Elect. Engrs., 1969, Vol. 116, p 1929-1936

76. D.Q. MAYNE

"The Design of Linear Multivariable Systems."

Automatica, 1973, Vol. 9, p 201-207.

77. A.G.J. MACFARLANE and I. POSTLETHWAITE

"The Generalised Nyquist Stability Criterion and Multivariable Root Loci."

Int. J. Control, 1977, Vol. 25, p 81-127.

78. M.J. DOVE

"A Digital Filter/Estimator for the Control of Large Ships in Confined Waters."

Ph.D. Thesis, Plymouth Polytechnic, Oct. 1984.

79. R.S. BURNS

"Application of Minicomputers to Numerical Control of Electrohydraulic Machine Tool Profiling Systems."

M.Phil. Thesis, Plymouth Polytechnic, April 1978.

80. B. KOUVARITAKIS

"The Optimal Root Loci of Linear Multivariable Systems."

Int. J. Control, 1978, Vol. 28, p 33-62.

81. R.J. WOOD

"An Ultrasonic Position Plotting System for Free Mode

Manoeuvring and Seakeeping Experiments."

National Maritime Institute Report NMI TM 58, June 1981.

82. J.E. POTTER

"Matrix Quadratic Solutions."

Siam J. Appl. Math. 1966, Vol. 14, p 495-501.

83. T.H. BOUNCER

"On-Line Methods of Identification and Parameter Estimation
for a Noisy Electrohydraulic System."

M.Sc. Thesis, Dept. of Eng. Science,

University of Exeter, April 1978.

84. C.G. KALLSTROM and K.J. ASTROM

"Experiences of System Identification Applied to Ship
Steering."

Automation, Jan. 1981, Vol. 17, No. 1, p 187-198.

85. M.A. ABKOWITZ

"Measurement of Hydrodynamic Characteristics from Ship
Maneuvering Trials by System Identification."

Soc. of Nav Archit and Mar Eng., New York., 1981, p 283-318

86. W.Y. HWANG

"Cancellation Effect and Parameter Identifiability of Ship
Steering Dynamics."

Int. Shipbuild Prog v 29, n 332, Apr 1982, p 90-102.

87. M.J. GRIMBLE, M.A. JOHNSON and P.T.K. FUNG

"Optimal Self-Tuning Control Systems: Theory and
Application - 1. Introduction and Controller Design."

Trans Inst Meas Control v 2, n 3, Jul-Sept 1980, p 115-120.

88. M.J. GRIMBLE, P.T.K. FUNG and M.A. JOHNSON
"Optimal Self-Tuning Control Systems: Theory and
Application - 2. Identification and Self-Tuning."
Trans. Inst Meas Control V 4, n 1 Jan-Mar 1982 p 25-36.
89. S. SAELID, N.A. JENSSEN and J.G. BALCHEN
"Design and Analysis of a Dynamic Positioning System Based
on the Kalman Filtering and Optimal Control."
IEEE Trans Autom Control v AC-28, n 3, Mar 1983, p 331-339.
90. E.D. GILLES and K. STARK
"Automatical Navigation of Ships Along a Pilot Cable."
Regelungstechnik v 24, n 11, Nov 1976, p 371-376.
91. J.G. SMITH
"New High Precision Range/Azimuth Position Fixing System."
Sea Technol V 24, n 3, Mar 1983, p 33, 35-36.
92. A.W. MERZ and C.R. TRIMBLE
"Data Processing in Ship Relative Position Estimation."
J. Navigation v 29, n 3, 1982 p 199-203.
93. O. LANKA
"Adaptive Kalman Tracking Filter for Manoeuvring Radar
Targets."
Tesla Electron V 15, n 2, Jun 1982 p 35-41.
94. B.A. COLLEY, R.G. CURTIS and C.T. STOCKEL
"On Marine Traffic Flow and Collision Avoidance Computer
Simulation by the RDRR Method."
J. Navigation V 37, n 2, 1984

NOMENCLATURE

a_0, a_1, a_2, a_3	Constants in control equation.
a_a, a_{ad}	Constants in Gauss-Markov functions for wind.
a_c, a_{cd}	Constants in Gauss-Markov functions for current.
A	Cost function coefficient.
A/D	Analogue to digital converter.
A_p	Projected propeller blade area.
A_v	Radius of track-changing arc.
A_{wp}	Way-point advance.
A_x, A_y	Projected area in x and y directions.
\vec{Q}	Total acceleration vector.
Q_x, Q_y, Q_z	Components of \vec{Q} in x, y and z directions.
A	State transition matrix.
b_a, b_{ad}	Constants in Gauss-Markov functions for wind.
b_c, b_{cd}	Constants in Gauss-Markov functions for current.
B	Cost function coefficient.
B	Control transition matrix.
c_0, c_1, c_2, c_3	Coefficients in cubic polynomial expression.
cov{ }	Covariance.
C	Cost function coefficient.
CPU	Central processing unit.
CRU	Communications register.
$c_{d1}, c_{d2}, c_{d3}, c_{d4}$	Scaling factors in disturbance equations.
C_x, C_y	Drag and lift coefficients.
C	Disturbance transition matrix.
d	Propeller diameter.

D	Height of vessel above waterline.
D/A	Digital to analogue converter.
D	Reverse-time command transition matrix.
$E\{\cdot\}$	Expected value.
E	Reverse-time control transition matrix.
$f(\cdot)$	Function of.
$f_{11}, f_{12}, \dots, f_{87}, f_{88}$	Elements of system matrix.
F_x, F_y	Aerodynamic drag and lift forces.
F	System matrix.
F_c	Closed-loop system matrix.
$g(\cdot)$	Function of.
$g_{11}, g_{12}, \dots, g_{85}, g_{86}$	Elements of forcing matrix.
G	Forcing matrix.
G_c	Disturbance control matrix.
G_d	Disturbance forcing matrix.
$h(\cdot)$	Function of.
$H(\cdot)$	Non-linear function of.
I_x, I_y, I_z	Moments of inertia about mass centre.
I	Identity matrix.
J	Cost function/performance criterion.
J_a	Screw advance coefficient.
$J_x, J_u, J_y, J_\psi, J_\delta, J_n$	Generalised performance indices.
$J_{uu}, J_{yy}, J_{\psi\psi}, J_{\delta\delta}, J_{nn}$	Mathematical model validity indices.
k, k_1, k_2	Increment counters.
K	Sum of all external moments about roll axis.
K_1, K_2, K_3, K_4	Constants in control equation.
K_n	Constant in Nomoto equation.
K_R, K_{CR}	Rudder and counter rudder gain.
K_t	Propeller thrust coefficient.

L, L_{pp}	Ship length between perpendiculars.
L_b	Beam..
m	Total mass of ship.
m'	Non-dimensional mass of ship.
M	Sum of all external moments about pitch axis.
M_p	Axial momentum across propeller.
\mathbf{m}	Command vector.
n_A, n_D	Actual and demanded engine speed.
N	Sum of all external moments about yaw axis.
N_c	Sum of moments due to current about yaw axis.
N_{rd}	Rudder moment to counteract disturbances.
N_{rudd}	Rudder disturbance coefficient.
$N_v, N_v', N_r, N_r', N_\delta$	
N_n, N_a	Linear yaw hydrodynamic coefficients.
$\bar{N}_{nn}, \bar{N}_{vvv}, \bar{N}_{rvv}$	
$\bar{N}_{\delta\delta\delta}, \bar{N}_{\delta vv}, N_{uva}$	Non-Linear yaw hydrodynamic coefficients.
N_w	Sum of moments due to wind about yaw axis.
p	Roll-rate.
p_1, p_2	Coefficients in propeller equation.
PC	Program counter.
q	Pitch-rate
q_1	Weighting matrix scalar.
$q_{11}, q_{22} \dots q_{77}$	
q_{88}	Elements of state error weighting matrix.
q_a, q_{ad}, q_c, q_{cd}	Variance of wind and current.
Q	State error weighting matrix.
Q_c	Controllability matrix.
r	Yaw-rate.

r_1	Weighting matrix scalar.
r_{11}, r_{22}	Elements of control weighting matrix.
r_D	Desired value of r .
RAM	Random access memory.
r	Desired state vector.
r_o	Desired earth-related state vector.
R	Control weighting matrix.
s	Laplace operator.
$s_{11}, s_{12} \dots s_{27}$	
s_{28}	Elements of feedback gain matrix.
ST	Program status register.
S	Feedback gain matrix.
t	Continuous time.
t'	Non-dimensional time.
t_p	Thrust deduction fraction.
T	Sampling time interval.
T_1, T_2, T_3	Time constants in Nomoto equation.
T_c	Current time constant.
T_D	Damping time constant.
T_N	Engine time constant.
T_p	Propeller thrust.
T_{PH}	Automatic permanent helm.
T_R, T_{CR}	Rudder and counter rudder time constant.
T	Transformation matrix.
u	Surge velocity.
u_a	Wind velocity in surge direction.
u_{am}, u_{cm}	Mean velocities of wind and current.
u_{av}	Speed of advance of propeller.
u_c	Velocity of current in surge direction.

u_D	Desired value of surge velocity.
u_O	Earth-related velocity (due North).
u_{OD}	Desired value of u_O .
u_r	Velocity of propeller race.
U	Vector sum of surge and sway velocities.
U_a	Total wind velocity.
U_c	Total velocity of current.
U	Vector of inputs to system.
U_a'	Horizontal gust magnitude, parallel to wind direction.
U_c	Vector of control inputs to system.
U_{dc}	Vector of disturbance control inputs to system.
U_g'	Total horizontal gust magnitude.
U_{opt}	Optimal control.
v	Sway velocity.
v_a	Wind velocity in sway direction.
v_c	Velocity of current in sway direction.
v_D	Desired value of sway velocity.
v_O	Earth-related velocity (due East).
v_{OD}	Desired value of v_O .
V_a'	Horizontal gust magnitude, perpendicular to wind.
V	Liapunov function.
w	Heave velocity.
w_a, w_{ad}, w_c, w_{cd}	Gaussian random processes for wind and current.
w_T	Wake fraction.
WP	Workspace pointer.
W	Vector of disturbances.
W_a'	Vertical gust magnitude perpendicular to wind

	direction..
W	Riccati matrix.
x	Distance travelled in surge direction ($\int u dt$).
x'	Non-dimensional length.
$x(i)$	Earth-related co-ordinate of i th way-point.
x_D	Desired value of x .
x_o	Earth-related distance co-ordinate (Northing).
x_{oD}	Desired value of x_o .
x_t	Parallel distance travelled from way-point.
X	Sum of all external forces in surge direction.
X_c	Sum of forces due to current in surge direction.
X_G	Distance to mass centre in surge direction.
X_p	Propeller thrust to counteract disturbances.
X_{pr}	Propeller disturbance coefficient.
X_u, X_u^*, X_n, X_a	Linear surge hydrodynamic coefficients.
X_{un}, \bar{X}_{nn}	Non-linear propeller hydrodynamic coefficients.
$\bar{X}_{uu}, \bar{X}_{uuu}, \bar{X}_{vv},$	
$\bar{X}_{rr}, \bar{X}_{\delta\delta}$	Non-linear surge hydrodynamic coefficients.
X_w	Sum of forces due to wind in surge direction.
X	Ship-related state vector.
\hat{X}	Best estimate of state vector.
y	Distance travelled in sway direction ($\int v dt$)
$y(i)$	Earth related co-ordinate of i th way-point.
y_D	Desired value of y .
y_o	Earth related distance co-ordinate (Easting).
y_{oD}	Desired value of y_o .
y_t	Perpendicular distance off track.
Y	Sum of all external forces in sway direction.
Y_c	Sum of forces due to current in sway direction.

Y_G	Distance to mass centre in sway direction.
Y_r	Lateral force on hull due to rudder.
$Y_v, Y_v', Y_r, Y_r', Y_\delta,$	
Y_n, Y_a	Linear sway hydrodynamic coefficients.
$Y_{nn}, Y_{vvv}, Y_{rvv},$	
$Y_{\delta\delta\delta}, Y_{\delta vv}$	Non-linear sway hydrodynamic coefficients.
Y	Earth related state vector.
z	Distance travelled in heave direction ($\int w dt$)
z	Earth related height co-ordinate.
z_o	
Z	Sum of all external forces in heave direction.
Z_G	Distance to mass centre in heave direction.
Z	Vector of measured values.

Greek Symbols

α_a	Earth related wind angle.
α_{am}, α_{cm}	Mean angle of wind and current.
α_c	Earth related current angle.
β	Drift angle.
δ_A, δ_D	Actual and demanded rudder angles.
ζ	Damping ratio.
λ	Weighting factor.
λ_a, λ_{ay}	Aspect ratio - x and y directions.
Λ	Aspect ratio correction factor.
ρ, ρ_a	Density of water and air.
σ_a, σ_c	Standard deviations of wind and current.
ψ_A, ψ_D	Actual and desired course angle.
ψ_e	Course error.
ψ_{DA}, ψ_{DB}	Track angles.
ψ_m	Course angle of mathematical model.

ω_D, ω_n

Damped and undamped natural frequency.

 Ω

Angular rate vector.

Special Notations

Dot notation is used for time derivatives.

$$\text{i.e. } \dot{\psi}_A = \frac{d\psi_A}{dt} ; \quad \ddot{y}_t = \frac{d^2 y_t}{dt^2}$$

Clarke's bar notation is used for non-linear hydrodynamic coefficients.

$$\bar{x}_{uu} = \frac{1}{2} \frac{\partial^2 x}{\partial u^2} ; \quad \bar{x}_{uuu} = \frac{1}{6} \frac{\partial^3 x}{\partial u^3}$$

Hat notation is used when referring to best estimates.

i.e. \hat{x} is the best estimate of x

APPENDIX 1

MATHEMATICAL MODEL PARAMETERS

A1.1. Linear Time-Invariant Model

$$f_{11} = -\frac{1}{T_R}$$

$$f_{22} = -\frac{1}{T_N}$$

$$f_{61} = \frac{Y_\delta (I_z - N_r) + Y_r N_\delta}{(m - Y_v) (I_z - N_r) - Y_r N_v}$$

$$f_{62} = \frac{Y_n (I_z - N_r) + Y_r N_n}{(m - Y_v) (I_z - N_r) - Y_r N_v}$$

$$f_{66} = \frac{Y_v (I_z - N_r) + Y_r N_v}{(m - Y_v) (I_z - N_r) - Y_r N_v}$$

$$f_{68} = \frac{(Y_r - \mu u) (I_z - N_r) + Y_r N_r}{(m - Y_v) (I_z - N_r) - Y_r N_v}$$

$$f_{81} = \frac{N_\delta (m - Y_v) + N_v Y_\delta}{(m - Y_v) (I_z - N_r) - Y_r N_v}$$

$$f_{82} = \frac{N_n (m - Y_v) + N_v Y_n}{(m - Y_v) (I_z - N_r) - Y_r N_v}$$

$$f_{86} = \frac{N_v (m - Y_v) + N_v Y_v}{(m - Y_v) (I_z - N_r) - Y_r N_v}$$

$$f_{88} = \frac{N_r (m - Y_v) + N_v (Y_r - \mu u)}{(m - Y_v) (I_z - N_r) - Y_r N_v}$$

$$g_{11} = \frac{1}{T_R}$$

$$g_{22} = \frac{1}{T_N}$$

$$g_{64} = \frac{Y_v (I_z - N_r) + Y_r N_v}{(m - Y_v) (I_z - N_r) - Y_r N_v}$$

$$g_{66} = \frac{Y_a (I_z - N_r) + Y_r N_a}{(m - Y_v) (I_z - N_r) - Y_r N_v}$$

$$g_{84} = \frac{N_v (m - Y_v) + N_v Y_v}{(m - Y_v) (I_z - N_r) - Y_r N_v}$$

$$g_{86} = \frac{N_a (m - Y_v) + N_v Y_a}{(m - Y_v) (I_z - N_r) - Y_r N_v}$$

A1.2 Quasi-Linear Time-Variant Model

Parameters required in addition to, or instead of, those listed in A1.1.

$$f_{42} = \frac{X_n}{m - X_u}$$

$$f_{44} = \frac{X_u}{m - X_u}$$

$$f_{46} = \frac{mr}{m - X_u}$$

$$f_{64} = \frac{-mr(I_z - N_r)}{(m - Y_v) (I_z - N_r) - Y_r N_v}$$

$$f_{68} = \frac{Y_r (I_z - N_r) + Y_r N_r}{(m - Y_v) (I_z - N_r) - Y_r N_v}$$

$$f_{84} = \frac{-N_v mr}{(m - Y_v) (I_z - N_r) - Y_r N_v}$$

$$f_{88} = \frac{N_r(m-Y_v) + N_v Y_r}{(m-Y_v)(I_z-N_r) - Y_r N_v}$$

$$g_{43} = \frac{x_u}{m-x_u}$$

$$g_{45} = \frac{x_a}{m-x_u}$$

A1.3 Non-Linear Time-Variant Model

$$f_{11} = -\frac{1}{T_R}$$

$$f_{22} = -\frac{1}{T_N}$$

$$f_{41} = \frac{\bar{X}_{\delta\delta} \delta_A}{m - X_u}$$

$$f_{42} = \frac{X_{un} u + \bar{X}_{nn} n_A}{m - X_u}$$

$$f_{44} = \frac{X_u + \bar{X}_{uu} u + \bar{X}_{uuu} u^2}{m - X_u}$$

$$f_{46} = \frac{\bar{X}_{vv} v + mr}{m - X_u}$$

$$f_{48} = \frac{\bar{X}_{rr} r}{m - X_u}$$

$$f_{61} = \frac{(Y_\delta + \bar{Y}_{\delta\delta\delta} \delta_A^2)(I_z - N_r) + Y_r(N_\delta + \bar{N}_{\delta\delta\delta} \delta_A^2)}{(m-Y_v)(I_z-N_r) - Y_r N_v}$$

$$f_{62} = \frac{Y_{nn} n_A (I_z - N_r) + Y_r N_{nn} n_A}{(m-Y_v)(I_z-N_r) - Y_r N_v}$$

$$f_{64} = \frac{-mr(I_z - N_r)}{(m-Y_v)(I_z-N_r) - Y_r N_v}$$

$$f_{66} = \frac{(Y_v + \bar{Y}_{rvv} rv + \bar{Y}_{vvv} v^2 + \bar{Y}_{\delta vv} \delta_A v)(I_z - N_r)}{(m-Y_v)(I_z-N_r) - Y_r N_v} +$$

$$\frac{Y_r(N_\delta + \bar{N}_{rvv} rv + \bar{N}_{vvv} v^2 + \bar{N}_{\delta vv} \delta_A v)}{(m-Y_v)(I_z-N_r) - Y_r N_v}$$

$$f_{68} = \frac{Y_r(I_z - N_r) + Y_r N_r}{(m-Y_v)(I_z-N_r) - Y_r N_v}$$

$$f_{81} = \frac{(N_\delta + \bar{N}_{\delta\delta\delta} \delta_A^2)(m-Y_v) + N_v(Y_\delta + \bar{Y}_{\delta\delta\delta} \delta_A^2)}{(m-Y_v)(I_z-N_r) - Y_r N_v}$$

$$f_{82} = \frac{N_{nn} n_A (m-Y_v) + N_v Y_{nn} n_A}{(m-Y_v)(I_z-N_r) - Y_r N_v}$$

$$f_{84} = \frac{-N_v mr}{(m-Y_v)(I_z-N_r) - Y_r N_v}$$

$$f_{86} = \frac{(N_v + \bar{N}_{rvv} rv + N_{vvv} v^2 + \bar{N}_{\delta vv} \delta A v) (m - Y_v)}{(m - Y_v) (I_z - N_r) - Y_r N_v} +$$

$$\frac{N_v (Y_v + \bar{Y}_{rvv} rv + \bar{Y}_{vvv} v^2 + \bar{Y}_{\delta vv} \delta A v)}{(m - Y_v) (I_z - N_r) - Y_r N_v}$$

$$g_{11} = \frac{1}{T_R} \quad g_{22} = \frac{1}{T_N}$$

$$g_{43} = \frac{X_u + \bar{X}_{uu} u_c + \bar{X}_{uuu} u_c^2}{m - X_u} \quad g_{45} = \frac{X_a}{m - X_u}$$

$$g_{64} = \frac{(Y_v + \bar{Y}_{rvv} rv + \bar{Y}_{vvv} v^2 + \bar{Y}_{\delta vv} \delta A v) (I_z - N_r)}{(m - Y_v) (I_z - N_r) - Y_r N_v} +$$

$$\frac{Y_r (N_v + \bar{N}_{rvv} rv + \bar{N}_{vvv} v^2 + \bar{N}_{\delta vv} \delta A v)}{(m - Y_v) (I_z - N_r) - Y_r N_v}$$

$$g_{66} = \frac{Y_a (I_z - N_r) + Y_r (N_a + N_{uva} u_a)}{(m - Y_v) (I_z - N_r) - Y_r N_v}$$

$$g_{84} = \frac{(N_v + \bar{N}_{rvv} rv + \bar{N}_{vvv} v^2 + \bar{N}_{\delta vv} \delta A v) (m - Y_v)}{(m - Y_v) (I_z - N_r) - Y_r N_v} +$$

$$\frac{N_v (Y_v + \bar{Y}_{rvv} rv + \bar{Y}_{vvv} v^2 + \bar{Y}_{\delta vv} \delta A v)}{(m - Y_v) (I_z - N_r) - Y_r N_v}$$

$$g_{86} = \frac{(N_a + N_{uva} u_a) (m - Y_v) + N_v Y_a}{(m - Y_v) (I_z - N_r) - Y_r N_v}$$

A1.4. Nomoto Model

$$\frac{1}{T_1 T_2} = \frac{Y_v N_r - N_v (Y_r - \mu u)}{(m - Y_v) (I_z - N_r) - Y_r N_v}$$

$$\frac{1}{T_1} + \frac{1}{T_2} = \frac{T_1 + T_2}{T_1 T_2} = \frac{-N_r (m - Y_v) - Y_v (I_z - N_r) - Y_r N_v - N_v (Y_r - \mu u)}{(m - Y_v) (I_z - N_r) - Y_r N_v}$$

$$T_3 = \frac{N_v Y_\delta + (m - Y_v) N_\delta}{N_v Y_\delta - Y_v N_\delta}$$

$$K_n = \frac{N_v Y_\delta - Y_v N_\delta}{Y_v N_r - N_v (Y_r - \mu u)}$$

$$\frac{K_n T_3}{T_1 T_2} = \frac{N_\delta (m - Y_v) + N_v Y_\delta}{(m - Y_v) (I_z - N_r) - Y_r N_v} = f_{81} \quad (\text{linear model})$$

A1.5. Computation of the Discrete State and Control Matrices

For the linear constant coefficient system:

$$\dot{X}(t) = FX(t) + GU(t)$$

the discrete solution is:

$$X((k+1)T) = e^{FT} X(kT) + \int_0^T e^{F(T-\tau)} G U(\tau) d\tau$$

If $U(\tau)$ is piecewise constant over the interval T , then

$$X((k+1)T) = A(T) X(kT) + B(T) U(T)$$

where, $A(T) = e^{FT}$

and, $B(T) = (e^{FT} - I) F^{-1} G$

For general applications the exponential matrix may be evaluated by a digital computer program based on the following arrangement of the equation

$$A(T) = I + FT + F^2 \frac{T^2}{2!} + \dots + F^{L-1} \frac{T^{L-1}}{(L-1)!} + F^L \frac{T^L}{L!}$$

$$= (I + FT) \left(I + F \frac{T}{2} \left(I + F \frac{T}{3} \left(I + \dots \dots \dots \right. \right. \right. \\ \left. \left. \left. \dots + F \frac{T}{(L-2)} \left(I + F \frac{T}{(L-1)} \left(I + F \frac{T}{L} \right) \right) \right) \right) \right)$$

Similarly,

$$B(T) = T \left(I + F \frac{T}{2} \left(I + F \frac{T}{3} \left(I + \dots \dots \dots \right. \right. \right. \\ \left. \left. \left. \dots + F \frac{T}{(L-2)} \left(I + F \frac{T}{(L-1)} \left(I + F \frac{T}{L} \right) \right) \right) \right) \right) G$$

Starting with the innermost factor, the number of terms L in the series approximation must be decided beforehand. When implemented in subroutine TRNMAC, a value of $L = 50$ was found to be sufficiently accurate.

APPENDIX 2

MARINER HULL HYDRODYNAMIC COEFFICIENTS

Particulars of Full-Size Vessel

Hull

Length between perpendiculars $L_{pp} = 160.9 \text{ m}$

Draught = 9.07 m Displacement = 17.1024×10^6 kg

Beam = 23.17 m Block Coefficient = 0.6
9 2

I_z about mass centre = $21.74962 \times 10^{-6} \text{ kg m}^2$

Rudder

Maximum Design Angle = 37-40 degrees

Maximum Rudder Rate = 2.5 - 3.7 degrees/second

Closed-Loop Time Constant $T_R = 2$ seconds

Propeller

Number of Propellers = 1

Number of Blades = 4

Propeller Diameter = 6.706 m

Direction of Rotation = right-handed

Closed-Loop Engine Time Constant $T_N = 2$ seconds

Surge Hydrodynamic Coefficients				Sway Hydrodynamic Coefficients			
Coefficient	Non-Dimensional Value		Dimensionalising Factor	Coefficient	Non-Dimensional Value		Dimensionalising Factor
	Quasi-Linear	Non-Linear			Linear and Quasi-Linear	Non-Linear	
X_n'	0.0000462		$4\rho L^3$	Y_δ'	0.0027	0.00255	$4\rho L^2 u_r$
X_u', X_u	-0.0012	-6000*	$4\rho L^2 U$	Y_n'	0.52	-	$4\rho L^3$
X_u'	-0.0005384	-0.00042	$4\rho L^3$	Y_{nn}	-	2104.307*	-
\bar{X}_{uu}	-	-1860.436*	-	Y_v'	-0.01243	-0.0116	$4\rho L^2 U$
\bar{X}_{uuu}	-	-272.047*	-	Y_v'	-0.0070384	-0.00748	$4\rho L^3$
X_{un}	-	-15155.8*	-	Y_r'	0.0028616	0.0022	$4\rho L^3 U$
X_a'	-0.015	-0.015	$4\rho L^2 U_A$	Y_r'	-0.00027	-0.000086	$4\rho L^4$
\bar{X}_{vv}'	-	-0.008988	$4\rho L^2$	Y_a'	-0.056	-0.056	$4\rho L^2 U_A$
\bar{X}_{rr}'	-	0.00018	$4\rho L^4$	\bar{Y}_{vvv}'	-	-0.080782	$(4\rho L^3)/U$
$\bar{X}_{\delta\delta}'$	-	-0.000948	$4\rho L^2 U^2$	\bar{Y}_{rvv}'	-	0.15356	$(4\rho L^3)/U$
\bar{X}_{nn}	-	21855.5*		$\bar{Y}_{\delta\delta\delta}'$	-	-0.00082	$4\rho L^2 u_r$
				$\bar{Y}_{\delta vv}'$	-	0.011896	$4\rho L^2$

* dimensionalised form

Table A2.1

Mariner Hull Hydrodynamic Coefficients

Yaw Hydrodynamic Coefficients			
Coefficient	Non-Dimensional Value		Dimensionalising Factor
	Linear and Quasi-Linear	Non-Linear	
N_δ'	-0.00126	-0.001274	$4\rho L^3 u_r$
N_n'	-0.26	-	$4\rho L^4$
N_{nn}	-	-169291.5*	-
N_v'	-0.00351	-0.002635	$4\rho L^4 U$
N_v'	0.00005	-0.000227	$4\rho L^4$
N_r'	-0.00227	-0.00166	$4\rho L^4 U$
N_r'	-0.0000165	-0.000437	$4\rho L^5$
N_a'	-0.0017	-0.0017	$4\rho L^3 U_A$
N_{uva}'	-0.0046	-0.0046	$4\rho L^3$
\bar{N}_{vvv}'	-	0.016361	$(4\rho L^3)/U$
\bar{N}_{rvv}'	-	-0.05483	$(4\rho L^4)/U$
$\bar{N}_{\delta\delta\delta}'$	-	0.00041	$4\rho L^3 u_r$
$\bar{N}_{\delta vv}'$	-	-0.00489	$4\rho L^3$

* dimensionalised form

APPENDIX 3

TOWING TANK RESULTS CAR FERRY HULL 5502

A3.1. Hull Resistance

Forward Velocity u. (m/s)	Force in x-Direction (N)
0.255	-0.428
0.505	-1.833
0.750	-4.213
1.003	-7.518
1.250	-11.731
1.500	-17.126

Table A3.1

Hull Resistance

Figure A3.1 shows a least-squares fit of the following cubic polynomial to the data in Table A3.1:

$$X = 0.038462u - 7.293782u^2 - 0.227298u^3 \quad (A3.1)$$

so that,

$$\begin{aligned} X_u &= 0.038462 \\ \bar{X}_{uu} &= -7.293782 \\ \bar{X}_{uuu} &= -0.227298 \end{aligned} \quad (A3.2)$$

A3.2 Bollard Pulls

A least-squares straight line fit of thrust against n_A^2 as shown in Figure A3.2(a) gives:

$$X = -0.0482 + 1.1563 \times 10^{-3} n_A^2 \quad (A3.3)$$

or,

$$\bar{X}_{nn} = 1.1563 \times 10^{-3} \quad (A3.4)$$

Propeller Speed n_A (rad/s)	n_A^2 (rad/s) ²	Thrust (N)
10.47	109.66	0.120
20.94	438.65	0.480
31.42	986.96	1.079
41.89	1754.60	1.918
52.36	2741.56	3.117
62.83	3947.84	4.367
73.30	5373.45	6.148
83.78	7018.39	8.135

Table A3.2 (a)

Bollard Pulls - Both Propellers Ahead

It will be observed that the relationship Thrust = $\bar{X}_{nn} n_A^2$ suffers from the disadvantage that a positive thrust results, whether or not the screws are ahead or astern.

Propeller Speed n_A (rad/s)	Thrust (N)
83.78	3.853
73.30	2.877
62.83	2.124
52.36	1.387
41.89	0.891
31.42	0.462
20.94	0.154
10.47	0.069
0.0	0.0
-10.47	-0.103
-20.94	-0.154
-31.42	-0.393
cont..	cont..

Propeller Speed n_A (rad/s)	Thrust (N)
cont..	
-41.89	-0.617
-52.36	-0.976
-62.83	-1.559
-73.30	-2.021
-83.78	-2.791

Table A3.2(b)

Port Screw Ahead and Astern

A least-squares cubic polynomial fit to the data in Table A3.2(b) is shown in Figure A3.2(b). The cubic thrust-speed law is:

$$X = 0.0107875n_A + 0.8073 \times 10^{-4} n_A^2 + 0.4201 \times 10^{-5} n_A^3 \quad (A3.5)$$

A3.3 Self Propulsion Points.

Propeller Speed n_A (rad/s)	u (m/s)	R (N)	$T = \bar{X}_{nn} n_A^2$ (N)	$T + R =$ $\bar{X}_{un} u n_A$	$u \cdot n_A$	$\bar{X}_{un} =$ $\frac{T + R}{u \cdot n_A}$
25.13	0.25	-0.449	0.718	0.268	6.283	-0.04267
50.27	0.50	-1.823	2.872	1.048	25.133	-0.04170
74.61	0.754	-4.215	6.327	2.112	56.258	-0.03754

Mean Value. $\bar{X}_{un} = -0.040637$

Table A3.3

Self Propulsion Points - Both Screws Ahead

A3.4 Rudder Experiments

Rudder Angle δ_A		X'	Y'	N'
Degrees	Radians	$\times 10^{-3}$	$\times 10^{-3}$	$\times 10^{-3}$
5	0.087	0.005	0.268	0.126
10	0.175	-0.052	0.537	-0.264
15	0.262	-0.172	0.784	-0.406
20	0.349	-0.303	1.218	-0.550
25	0.436	-0.449	1.528	-0.687
30	0.524	-0.699	1.693	-0.772
35	0.611	-0.882	1.899	-0.833
-10	-0.175	-0.083	-0.619	0.273
-20	-0.349	-0.271	-1.218	0.579
-30	-0.524	-0.744	1.757	0.786

Table A3.4

Non-Dimensional Rudder Forces and Moments on Hull

From Figure A3.3(b),

$$X' = -0.00221\delta_A^2 \quad (A3.6)$$

hence, $\bar{X}_{\delta\delta} = -0.00221 \quad (A3.7)$

The non-dimensional sway-force/rudder relationship is shown in Figure A3.4(a) and is expressed by:

$$Y' = 0.0034178\delta_A - 0.0009569\delta_A^3 \quad (A3.8)$$

so that,

$$\begin{aligned} Y_{\delta}' &= 0.0034178 \\ \bar{Y}_{\delta\delta\delta}' &= -0.0009569 \end{aligned} \quad (A3.9)$$

Figure A3.4(b) gives the non-dimensional yaw-moment/rudder relationship and the polynomial fit is:

$$N' = -0.0016011\delta_A + 0.0007421\delta_A^3 \quad (A3.10)$$

or

$$\begin{aligned} N_{\delta}' &= -0.0016011 \\ \bar{N}_{\delta\delta\delta}' &= 0.0007421 \end{aligned} \quad (A3.11)$$

The linear coefficients Y_{δ}' and N_{δ}' in equations A3.9 and A3.11 were checked by fitting a straight line through the points over the range ± 20 degrees.

A3.5 Drift Angle Experiments

The straight-line fit of non-dimensional X-force against v^2 as shown in Figure A3.5 is:

$$X' = -0.00617v^2 \quad (A3.12)$$

i.e. $\bar{X}_{vv}' = -0.00617 \quad (A3.13)$

Figure A3.6(a) shows non-dimensional sway force against lateral velocity. The least-squares fit is:

$$Y' = -0.0098675v - 0.441178v^3 \quad (A3.14)$$

hence,

$$\begin{aligned} Y_v' &= -0.0098675 \\ \bar{Y}_{vvv}' &= -0.441178 \end{aligned} \quad (A3.15)$$

Figure A3.6(b) gives the non-dimensional yaw-moment/sway velocity relationship. The polynomial fit is:

$$N' = -0.0043535v - 0.0326335 \quad (A3.16)$$

where,

$$\begin{aligned} N_v' &= -0.0043535 \\ \bar{N}_{vvv}' &= -0.0326335 \end{aligned} \quad (A3.17)$$

As with the rudder coefficients, the linear terms Y_v' and N_v' were checked by a straight line fit over the sway velocity range ± 0.08 m/s.

A3.6 Added Mass Coefficients

From equations (4.1)

$$X_u' = -0.05263 \text{ m'}$$

$$Y_v' = -0.93734 \text{ m'}$$

$$Y_r' = -0.21939 \text{ I}_z'$$

$$N_v' = -0.028446 \text{ m'}$$

$$N_r' = -1.1148 \text{ I}_z'$$

For hull 5502,

$$m' = 0.00809$$

$$I_z' = 0.0006236 \quad (A3.18)$$

$$U = 0.754 \text{ m/s}$$

$$v = U \sin \beta$$

Rudder Angle δ_A Degrees	Drift Angle β Degrees	X' $\times 10^{-3}$	Y' $\times 10^{-3}$	N' $\times 10^{-3}$	Drift Angle β Degrees	X' $\times 10^{-3}$	Y' $\times 10^{-3}$	N' $\times 10^{-3}$
0	10	-0.083	2.186	0.633	-10	-0.139	-2.288	-0.618
10	10	-0.217	2.839	0.881	-10	-0.150	-1.675	-0.887
20	10	-0.470	3.554	0	-10	-0.191	-1.226	-1.066
30	10	-0.955	4.208	-0.220	-10	-0.594	-1.389	-0.974
-20	10	-0.315	1.062	1.182	-10	-0.516	-3.656	-0.008
-30	10	-0.676	0.613	1.389	-10	-0.976	-4.085	0.248
0	8	-0.067	1.593	0.470	-8	-0.072	-1.655	-0.436
10	8	-0.191	2.308	0.158	-8	-0.119	-1.001	-0.724
20	8	-0.403	2.900	-0.140	-8	-0.253	-0.429	-0.991
30	8	-0.914	3.513	-0.383	-8	-0.589	-0.020	-1.220
-20	8	-0.289	0.286	0.984	-8	-0.460	-3.023	0.127
-30	8	-0.687	-0.020	1.205	-8	-0.935	-3.452	0.373
0	6	-0.021	1.021	0.338	-6	-0.052	-1.103	-0.328
10	6	-0.145	1.695	0.025	-6	-0.103	-0.388	-0.594
20	6	-0.382	2.369	-0.228	-6	-0.268	0.184	-0.886
30	6	-0.852	2.839	-0.491	-6	-0.620	0.654	-1.077
-20	6	-0.320	-0.184	0.869	-6	-0.392	-2.226	0.236
-30	6	-0.697	-0.633	1.079	-6	-0.909	2.778	0.494
0	4	-0.041	0.470	0.256	-4	-0.119	-0.531	-0.225
10	4	-0.139	1.185	-0.038	-4	-0.191	-0.041	-0.503
20	4	-0.392	1.838	-0.325	-4	-0.356	0.613	-0.789
30	4	-0.826	2.431	-0.563	-4	-0.723	1.164	-0.981
-20	4	-0.310	-1.675	0.796	-4	-0.475	-1.736	0.313
-30	4	-0.687	-1.920	0.984	-4	-0.924	-2.186	0.554
0	2	-0.057	0.123	0.143	-2	-0.098	-0.082	-0.107
10	2	-0.124	0.756	-0.154	-2	-0.166	0.368	-0.388
20	2	-0.315	1.389	-0.435	-2	-0.387	1.001	-0.686
30	2	-0.754	1.940	-0.649	-2	-0.749	1.491	-0.907
-20	2	-0.299	-0.919	0.691	-2	-0.439	-1.409	0.410
-30	2	-0.692	-1.348	0.869	-2	-0.847	-1.797	0.639

Table A3.5 Drift Angle Experiments

this gives,

$$X_u' = -0.000426$$

$$Y_v' = -0.007583$$

$$Y_r' = -0.0001368$$

$$N_v' = -0.00023$$

$$N_r' = -0.0006952 \quad (A3.19)$$

A3.7 Free-Sailing Tests

The steady-state forces and moments acting on the hull during a turning circle are obtained by substitution of the data in 4.7.7 into equations (4.2)

Steady-State Sway Equation

$$\begin{aligned} -2.11485 &= -1.05959 - 0.04189Y_r + 1.02698 - 1.65868 \\ &\quad - 0.13995 \times 10^{-3} Y_{rvv} - 0.07883 \end{aligned} \quad (A3.20)$$

From equation (4.3),

$$\bar{Y}_{rvv}rv^2 = 1.630 Y_r \quad (A3.21)$$

Substitution of equation (A3.21) into (A3.20) gives:

$$\begin{aligned} Y_r &= 3.129053 \\ \bar{Y}_{rvv} &= 1526.64 \end{aligned} \quad (A3.22)$$

hence,

$$\begin{aligned} Y_r' &= 0.0004926 \\ \text{and, } \bar{Y}_{rvv}' &= 0.022934 \end{aligned} \quad (A3.23)$$

Steady-State Yaw Equation

Substitution into equation (4.2) gives,

$$\begin{aligned} 0 &= -1.59833 - 0.04189N_r - 1.64488 - 0.41948 - 0.0001399\bar{N}_{rvv} \\ &\quad + 0.2090156 \end{aligned} \quad (A3.24)$$

From equation (4.3),

$$\bar{N}_{rvv}rv^2 = 0.771 N_r \quad (A3.25)$$

Combine equations (A3.24) and (A3.25),

$$\begin{aligned} N_r &= -46.54237 \\ \bar{N}_{rvv} &= -10750.586 \end{aligned} \quad (A3.26)$$

giving,

$$\begin{aligned} N_r' &= -0.002143 \\ \text{and, } \bar{N}_{rvv}' &= -0.047235 \end{aligned} \quad (A3.27)$$

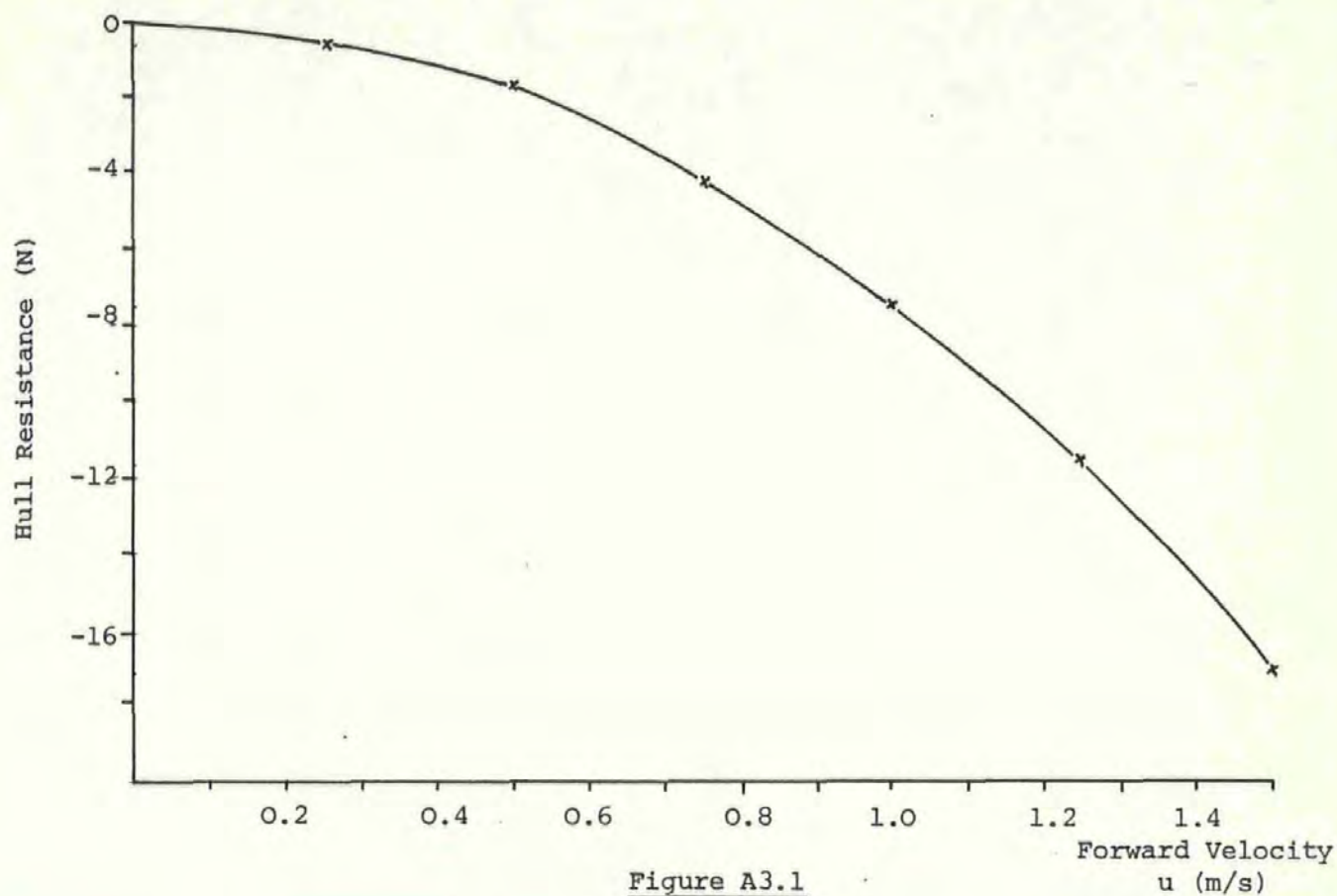


Figure A3.1
Hull Resistance

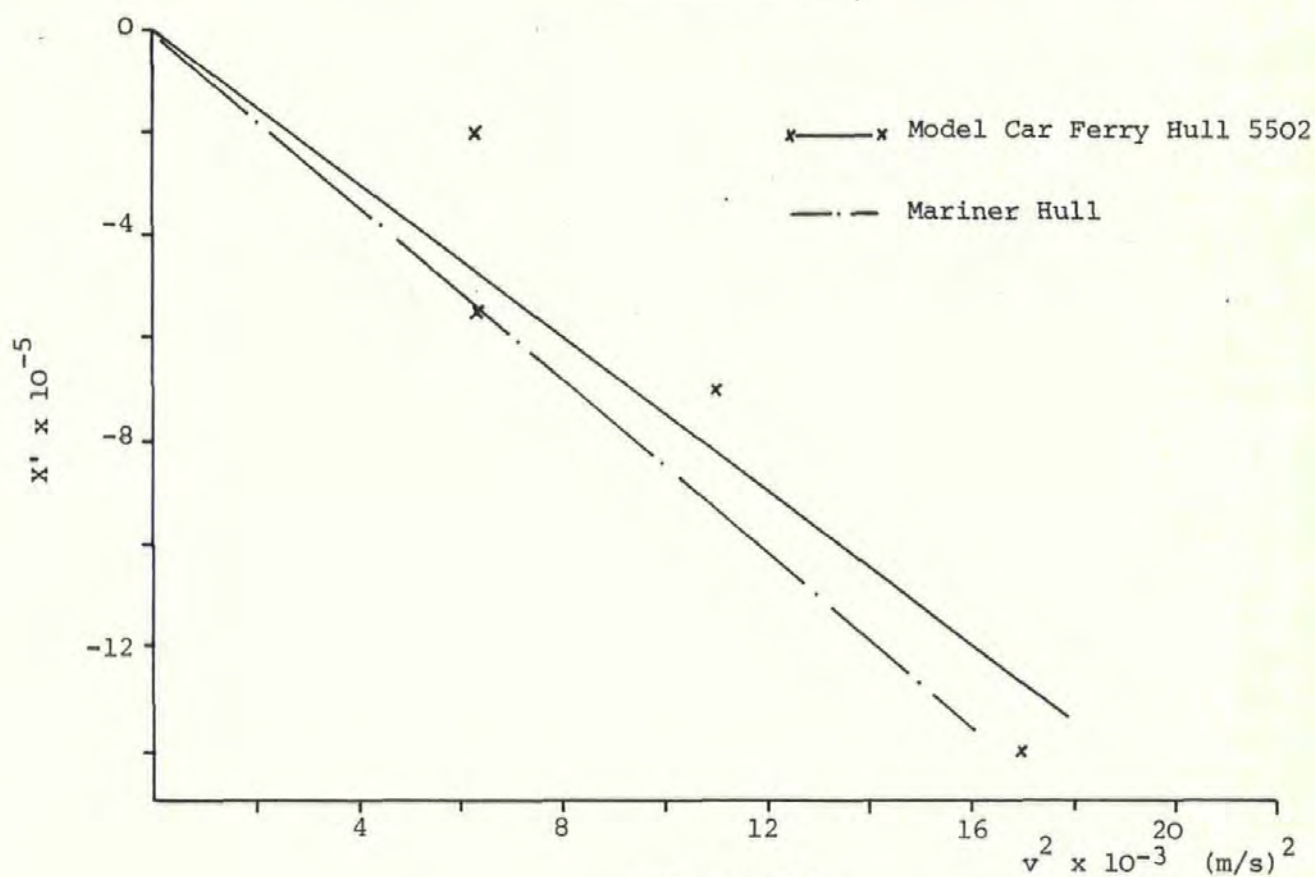
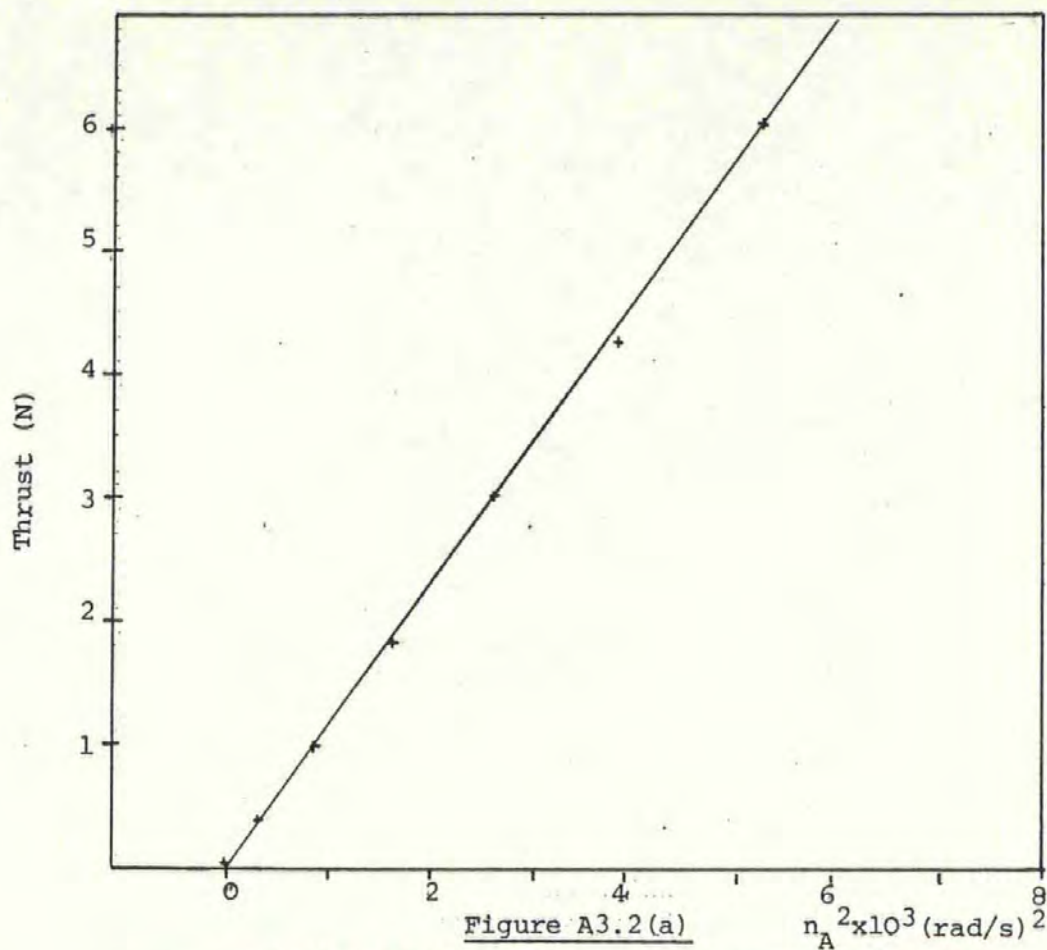


Figure A3.5
Determination of \bar{X}_{vv}'



Bollard Pulls; Both Propellers Ahead

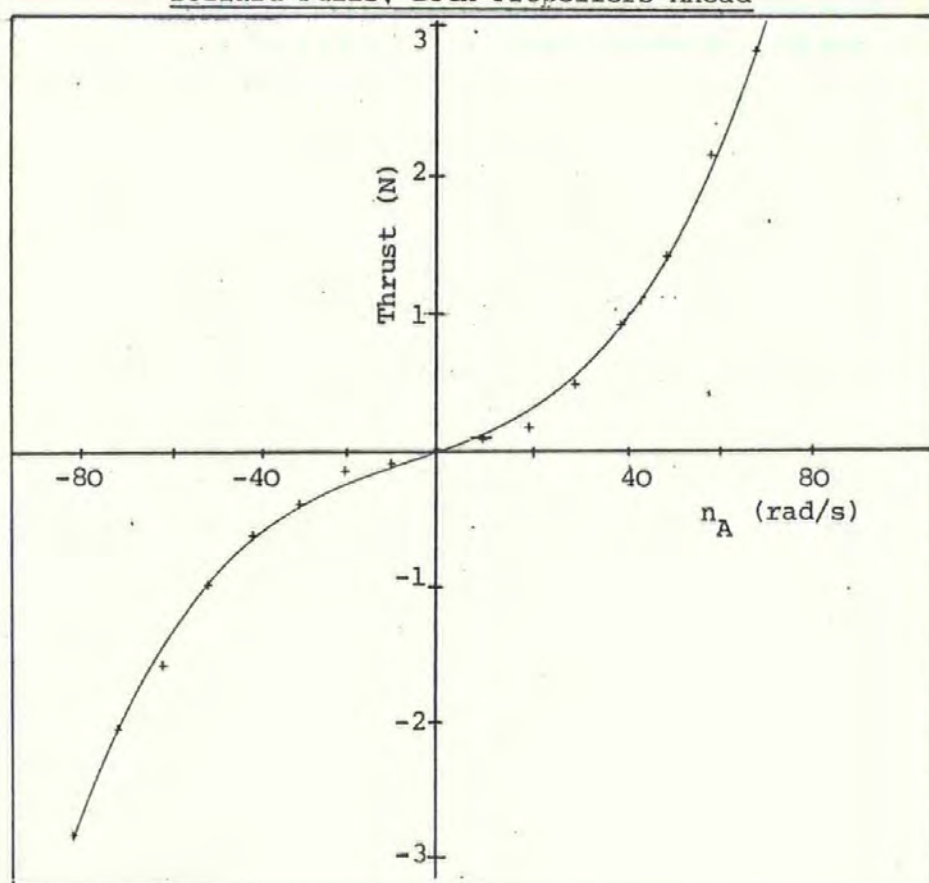


Figure A3.2(b)

Bollard Pulls: Port Screw Ahead and Astern

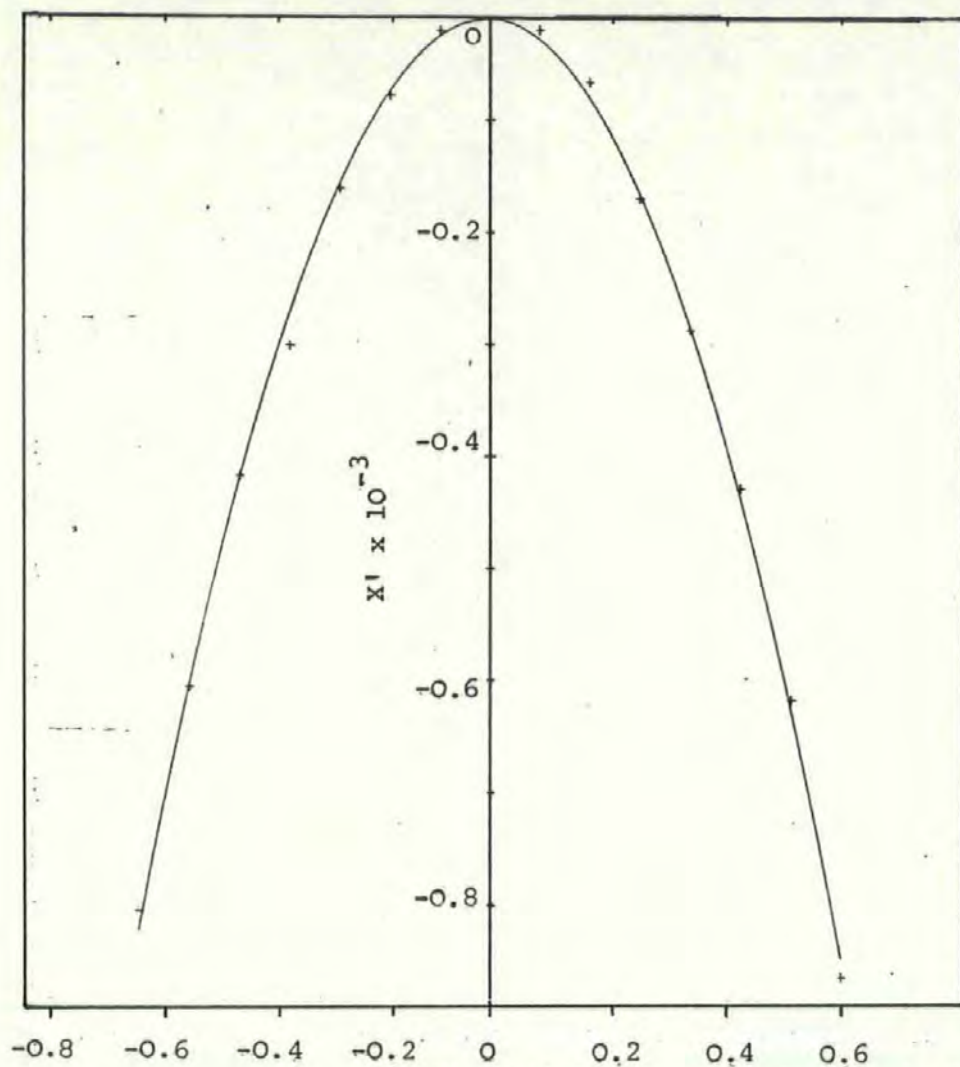


Figure A3.3(a)

Rudder Angle δ_A (rad)

Non-Dimensional X-Direction Rudder Force: Both Rudders

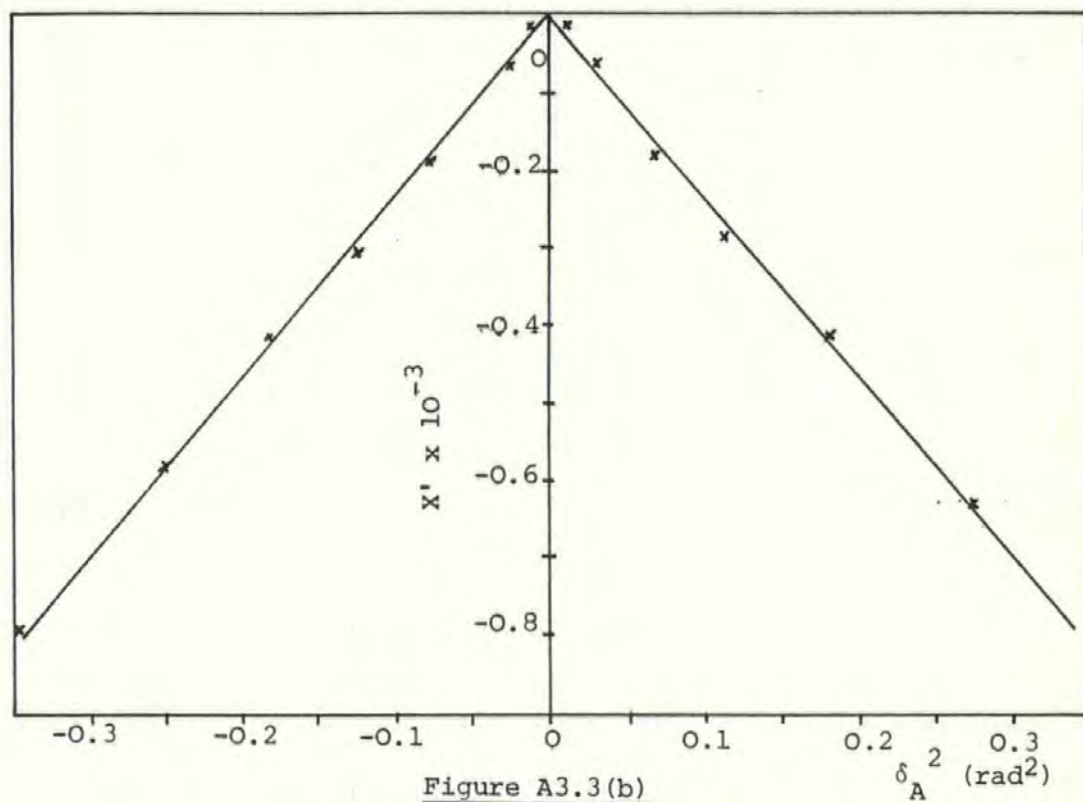


Figure A3.3(b)

δ_A^2 (rad^2)

Determination of $\bar{X}_{\delta\delta}'$

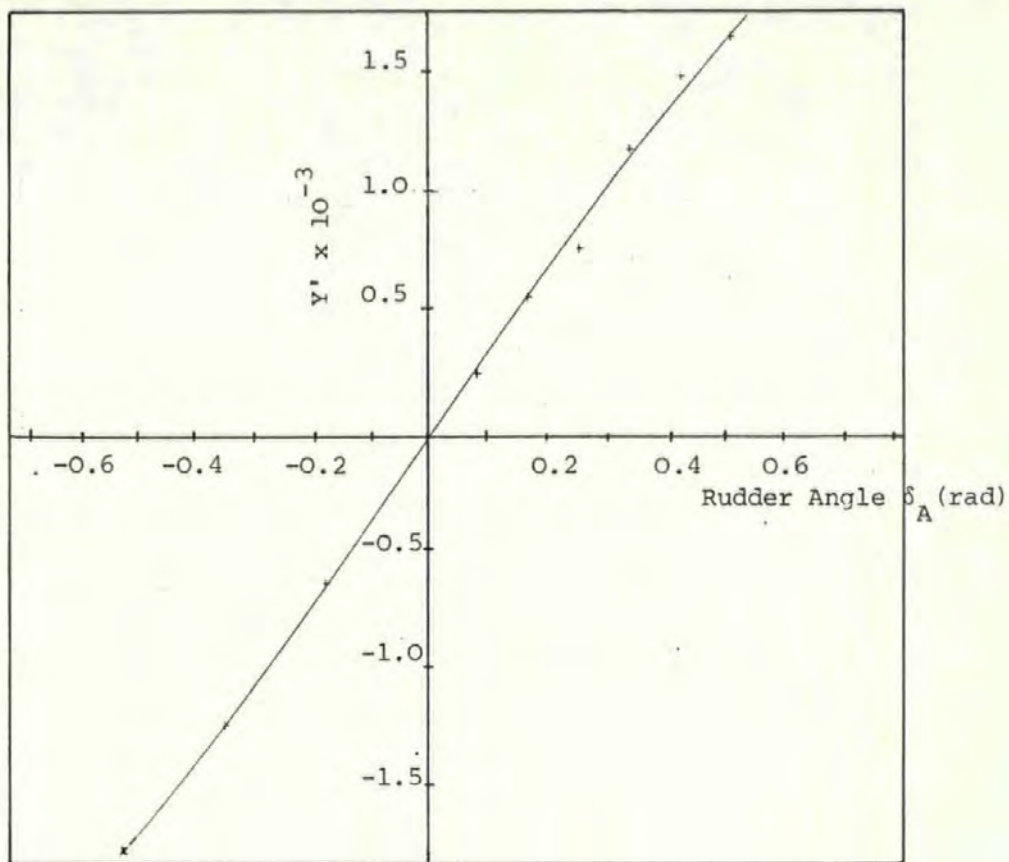


Figure A3.4(a)

Non-Dimensional Y-Force Against Rudder Angle

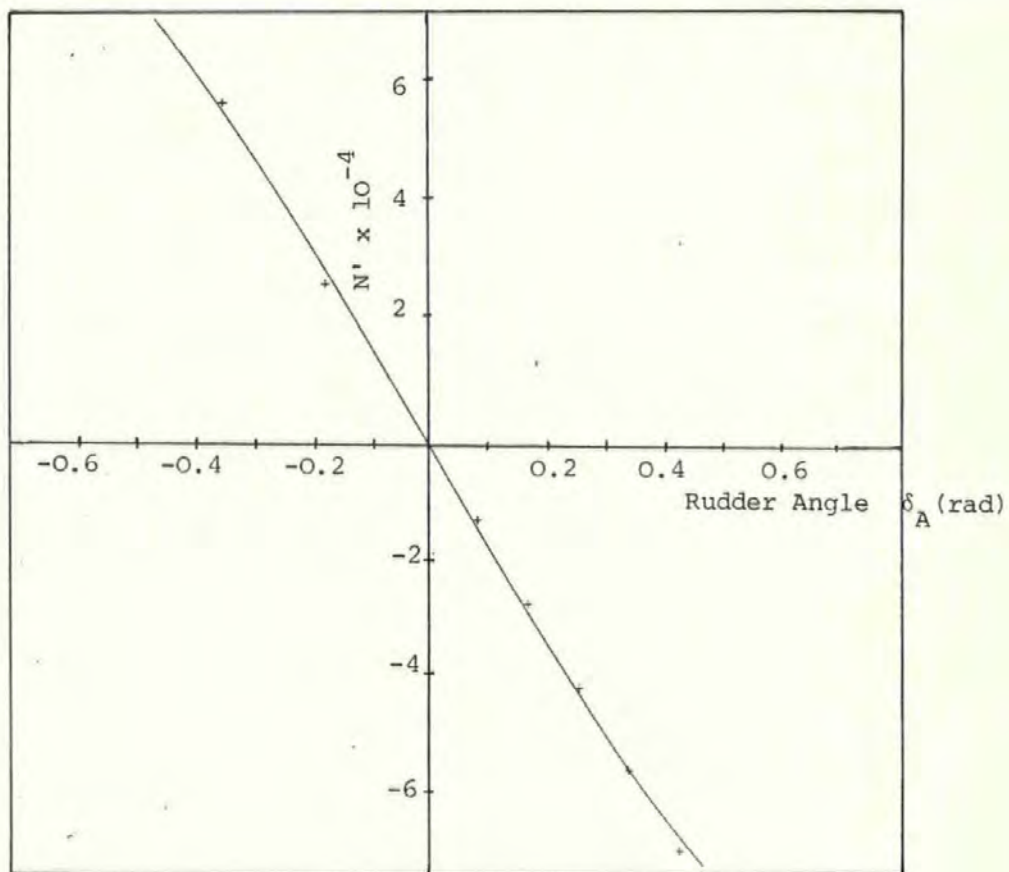


Figure A3.4(b)

Non-Dimensional N-Moment Against Rudder Angle

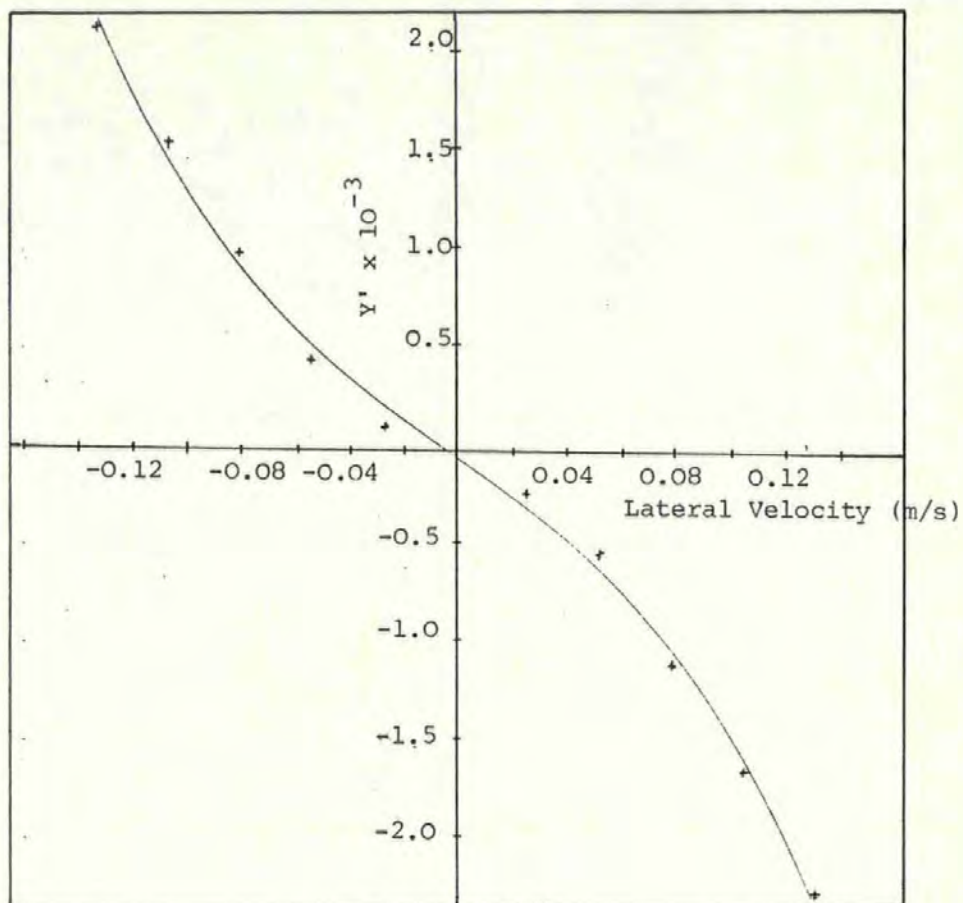


Figure A3.6(a)

Non-Dimensional Y-Force Against Lateral Velocity

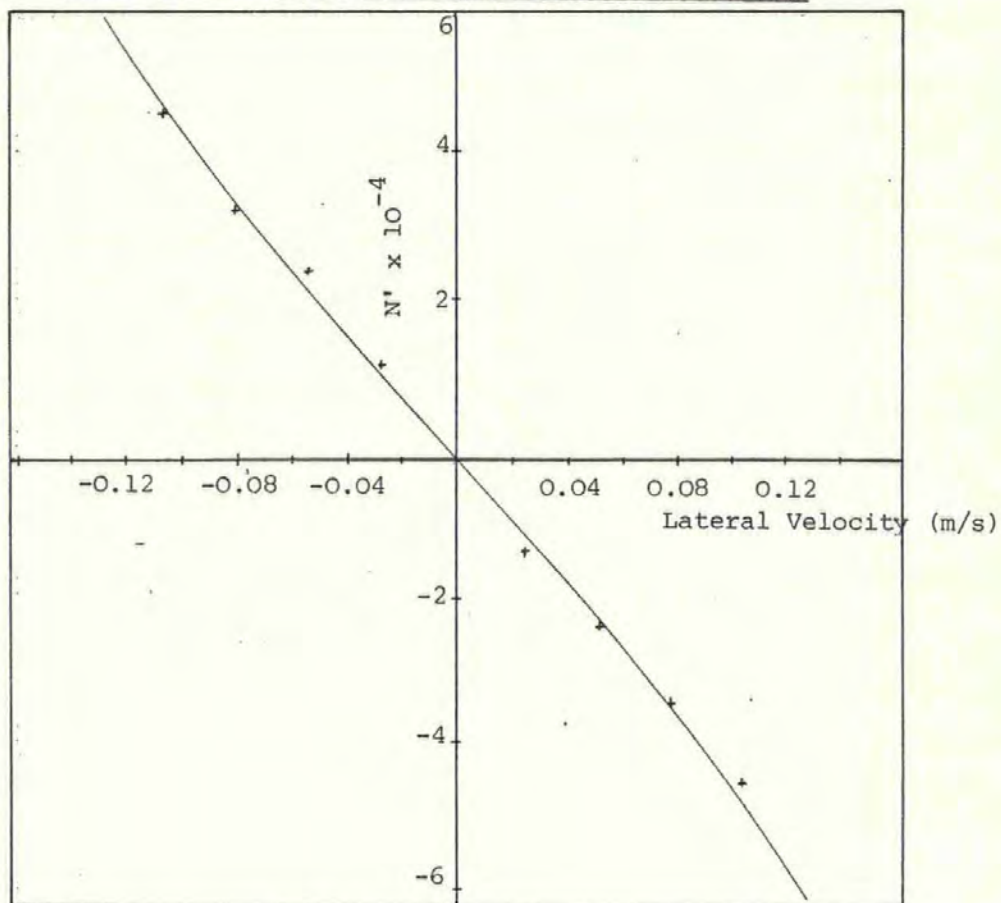


Figure A3.6(b)

Non-Dimensional N-Moment Against Lateral Velocity

APPENDIX 4

OPTIMAL FILTER

The optimal filter has been designed by Dove and was used in conjunction with the optimal controller during computer simulation and free-sailing model tests. It comprises of a recursive algorithm which remembers past data, receives future measurements, and bases the estimate of the state vector upon a combination of past and present information.

The block diagram of the filter model is shown in Figure A4.1.

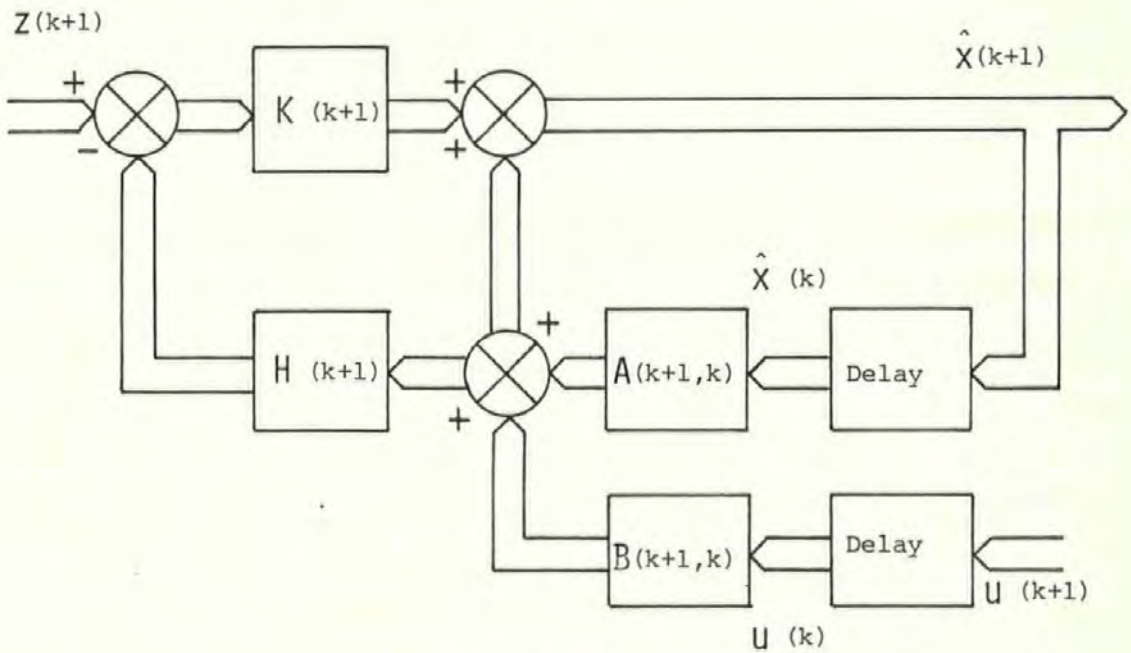


Figure A4.1

Optimal Filter

The filter equations are summarised in the paper presented in Appendix 7, and are numbered (14) to (16) consecutively.

APPENDIX 5

ELEMENTS OF A AND B MATRICES

Using small perturbation analysis, the elements of the 4 x 4 discrete state transition matrix A and 4 x 2 control transitionmatrix B have been computed in real-time using the following relationships:

$$\begin{aligned}
 a_{11} &= 1 - 0.0410116u - 0.02119 r \\
 a_{12} &= 1.06725 r \\
 a_{13} &= 0 \\
 a_{14} &= 0.0140048 r \\
 a_{21} &= 0.446096 r \\
 a_{22} &= 0.995 - 0.1593785u - 2.05168 \text{ ABS}(r) \\
 a_{23} &= 0 \\
 a_{24} &= 0.005 + 0.028376u - 0.02429 \text{ ABS}(r) \\
 a_{31} &= 0.015758 r \\
 a_{32} &= 0.01 - 0.101248u + 0.6868 \text{ ABS}(r) \\
 a_{33} &= 1 \\
 a_{34} &= 0.989 - 0.195818u \\
 a_{41} &= 0.03377 r \\
 a_{42} &= -0.0295 - 0.17164u + 1.29186 \text{ ABS}(r) \\
 a_{43} &= 0 \\
 a_{44} &= 0.967 - 0.35436u \\
 b_{11} &= -0.0316267\delta_D \\
 b_{12} &= -0.000195 + 0.0000065n_D + 0.000478 \text{ ABS}(r) \\
 b_{21} &= 0.0195 + 0.071189u - 0.0045258 \text{ ABS}(\delta_D) \\
 b_{22} &= 0 \\
 b_{31} &= 0.017 - 0.059506u - 0.00146 \text{ ABS}(\delta_D) \\
 b_{32} &= 0 \\
 b_{41} &= 0.0315 - 0.1130267u \\
 b_{42} &= 0
 \end{aligned}$$

APPENDIX 6

COMPUTER PROGRAMS

All mainframe simulation programs have been run on a PRIME 9950 CPU with 10 MB memory and 1 x 600, 3 x 300 MB disc file storage. The subroutines listed in A6.1, 2 and 3 are written in FORTRAN and form the essential core of the simulation package.

The real-time ship control program, implemented on the TMS 9900 microprocessor, is listed in A6.4.

A6.1 Main Subroutines

- Subroutine NAB : Computes the non-linear system matrices F and G and discrete transition matrices A , B and C .
- Subroutine RICAL : Determines the Riccati matrix W , feedback matrix S , command vector M and reverse-time tracking matrices D and E .
- Subroutine RICATI : Is called by RICAL to obtain the discrete solution of the matrix Riccati equation.
- Subroutine OPTCON : Calculates the optimal control law and confines the maximum and minimum control values to remain within specified limits.

```

SUBROUTINE HAB(A,B,C,N,NX,NG,NB,NC,NN,IPIN,K,LOOP,T,
&WUM,TSAMP,XOLD,UVEL,UA,WU,UD1,UD2,U)

C THIS SUBROUTINE COMMENCES WITH THE NON-DIMENSIONALISED
C HYDRODYNAMIC COEFFICIENTS AND CALCULATES THE CONTINUOUS
C TIME STATE AND FORCING MATRICES. IT THEN CALLS TRNMAC TO
C CONVERT THESE TO THE DISCRETE TIME MATRICES A,B & C.
C
C
C   DIMENSION F(8,8),G(8,6),XP(14),YP(14),ANP(14)
C   DIMENSION A(8,8),B(8,2),C(8,4),WU(4),WUM(4)
C   DIMENSION R(500),XOLD(8),T(500)
C   DIMENSION U(2)
C
C   IF(K-1)6,6,7
C 6 READ(5,101)RO,AL,AM,TAUR,TAUN,ZI
C   IFIM=IPIN+1
C   NX=1
C   WRITE(6,103)RO,AL,AM,TSAMP,TAUR,TAUN,ZI
C   WRITE(6,104)N,NG,NN,IPIN
C
C READ IN NON-DIMENSIONALISED HYDRODYNAMIC DERIVATIVES
C USING MATRED AND PRINT VALUES USING MATPRN
C CONVENTION:
C   XP(1)=XDELT'   YP(1)=YDELT'   ANP(1)=NDELT'
C   XP(2)=XN'      YP(2)=YNN'     ANP(2)=NNN'
C   XP(3)=XU'      YP(3)=YU'      ANP(3)=NU'
C   XP(4)=XUDOT'   YP(4)=YUDOT'   ANP(4)=NUDOT'
C   XP(5)=XUU'     YP(5)=YV'      ANP(5)=NV'
C   XP(6)=XUUU'    YP(6)=YVDOT'   ANP(6)=NVDOT'
C   XP(7)=XUN'     YP(7)=YR'      ANP(7)=NR'
C   XP(8)=XRODOT'  YP(8)=YRDOT'   ANP(8)=NRDOT'
C   XP(9)=XUA'     YP(9)=YUA'     ANP(9)=NUVA'
C   XP(10)=XVA'    YP(10)=YVA'    ANP(10)=NVA'
C   XP(11)=XVV'    YP(11)=YVVV'   ANP(11)=NVVV'
C   XP(12)=XRR'    YP(12)=YRVV'   ANP(12)=NRVV'
C   XP(13)=XDD'    YP(13)=YDDD'   ANP(13)=NDDD'
C   XP(14)=XNN'    YP(14)=YDVV'   ANP(14)=NDVV'
C
C   CALL MATRED(XP,14,1,28)
C   CALL MATPRN(XP,14,1,28,12HNDX)
C
C   CALL MATRED(YP,14,1,28)
C   CALL MATPRN(YP,14,1,28,12HNDY)
C
C
C   CALL MATRED(ANP,14,1,28)
C   CALL MATPRN(ANP,14,1,28,12HNDN)
C
C COMPUTE DIMENSIONALISED HYDRODYNAMIC DERIVATIVES
C THAT CORRESPOND TO SHIP FORWARD VELOCITY. (UVEL)
C
C 7 CALL DIMEN(RO,AL,XP,YP,ANP,UVEL,XOLD,UA,U,
C 1XDELT,XN,XU,XUDOT,XUU,XUUU,XUN,XRODOT,XUA,XVA,XVV,XRR,
C 2XDD,XNN,YDELT,YN,YU,YUDOT,YV,YVDOT,YR,YRDOT,YUA,YVA,
C 3YVV,YRVV,YDDD,YDVV,ANDELT,ANNN,ANU,ANUDOT,ANV,ANVDOT,
C 4ANR,ANRDOT,ANUA,ANVA,ANVVV,ANRVV,ANDDD,ANDVV)
C
C COMPUTE X,B AND C COEFFICIENTS
C
C   CALL CALXBC(AM,ZI,XOLD,UVEL,WU,UD1,UD2,K,WUM,
C 1XN,XU,XUDOT,XUU,XUUU,XUN,XUA,XVA,XVV,XRR,XDD,XNN,
C 2YDELT,YN,YV,YVDOT,YR,YRDOT,YUA,YVA,YVVV,YRVV,YDDD,YDVV,
C 3ANDELT,ANNN,ANV,ANVDOT,ANR,ANRDOT,ANUA,ANVA,ANVVV,ANRVV,
C 4ANDDD,ANDVV,X1,X2,X4,X6,X8,XU3,XU5,
C 5B1,B2,B4,B6,B8,BU4,BU6,
C 6C1,C2,C4,C6,C8,CU4,CU6,U)
C
C COMPUTE F MATRIX
C
C   CALL FMAT(X4,X6,X8,XOLD,B4,B6,B8,C4,C6,C8,F,N,NN)
C
C COMPUTE G MATRIX
C
C   CALL GMAT(X1,X2,XU3,XU5,B1,B2,C1,C2,
C 1BU4,BU6,CU4,CU6,G,N,NG,NN)
C
C COMPUTE DISCRETE TIME STATE TRANSITION MATRIX A(T),
C CONTROL TRANSITION MATRIX B(T) & DISTURBANCE TRANSITION
C MATRIX C(T).
C
C   CALL TRNMAC(F,G,A,B,C,N,NG,NB,TSAMP,NN)
C
C   WRITE WHEN K=1,LOOP,2LOOP,3LOOP ETC.
C   IF (K-1)2,2,3
C 3 IF (K-LOOP)4,5,5
C 5 LOOP=LOOP+20
C 2 CONTINUE
C   WRITE(6,102)T(K)
C   CALL MATPRN(F,N,NN,12HF MATRIX)

```

```

CALL MATPRN(G,N,NG,NN,12HG MATRIX)
CALL MATPRN(A,N,N,NN,12HA MATRIX)
CALL MATPRN(B,N,NB,NN,12HB MATRIX)
CALL MATPRN(C,N,NC,NN,6H C)
C
101 FORMAT(6F12,4)
102 FORMAT(1H,'TIME=',F10,5,'SECONDS')
103 FORMAT(1H,'LOX,RO=',E14.7,'KG/M**3/LOX,LENGTH=',E14.7,
1'M'/LOX,MASS=',E14.7,'KG/LOX,TSAMP=',E14.7,'SEC'/LOX,
2'TAUR=',E14.7,'SEC'/LOX,TAUN=',E14.7,'SEC'/LOX,IZ=',
3 E14.7,'KG M**2')
104 FORMAT(1H,'LOX,N=',I5/LOX,NG=',I5/LOX,NN=',I5/LOX,
1'IPIN=',I5)
C
4 RETURN
END
C
SUBROUTINE RICAT(F,G,GU,AA,BB,Q,R,S,W,
&XD,YD,VFOR,TSAMP,N,NB,NN,IPIN)
C
C * SUBROUTINE CALCULATES THE RICCATI FEEDBACK MATRIX
C * AND COMMAND MATRIX
C
C   DIMENSION AA(8,8),BB(8,2),Q(8,8),R(2,2),W(8,8),WPI(8,8)
C   DIMENSION S(2,8),F(8,8),G(8,6),GU(8,2),D(8,8),E(8,8)
C   DIMENSION REVIN(8,500),GT(2,8),RGT(2,8)
C   DIMENSION RGTM(2,8),UREV(8),DM(8,1),EU(8,1)
C   DIMENSION OLDM(8),VREV(2),VFOR(2,500),C(8,4)
C   DIMENSION XD(500),YD(500)
C   COMMON RIN(8,500),YOUT(8,250)
C
C * PUT W MATRIX TO TERMINAL(NULL)VALUE
C   DO 15 J=1,N
C   DO 15 I=1,N
C 15 W(I,J)=0.0
C
C   DO 10 M=1,IPIN
C   CALL RICATI(AA,BB,Q,R,S,W,WPI,TSAMP,N,NB,NN)
C
C * UPDATE W MATRIX
C
C   DO 20 J=1,N
C   DO 20 I=1,N
C 20 W(I,J)=WPI(I,J)
C 10 CONTINUE
C   S(1,3)=-S(1,3)
C   S(1,5)=-S(1,5)
C   CALL MATPRN(S,NB,N,NN,6HS)
C   CALL MATPRN(W,N,N,NN,6HW)
C   WRITE(1,114)
C 114 FORMAT(1H,'OK')
C
C * DETERMINE GU(8X2) MATRIX FROM G(8X6)
C
C   DO 45 I=1,N
C   DO 45 J=1,NB
C 45 GU(I,J)=G(I,J)
C
C * CALCULATE REVERSE TIME TRACKING MATRICES D AND E
C   CALL TRACK(F,GU,R,Q,W,S,D,E,TSAMP,N,NB,NN)
C   CALL MATPRN(D,N,N,NN,6HD)
C   CALL MATPRN(E,N,N,NN,6HE)

```



```

C   WHERE Q IS A 8X8 DIAGONAL MATRIX
Q   W,S,T,R,A AND B DEFINED EARLIER
C
C * TRANSPOSE OF S MATRIX
CALL MATRNS(ST,S,NB,N,N)
C
C * PRODUCT OF S' AND SCALAR TSAMP
CALL MATSCL(STT,TSAMP,ST,N,NB,N,N)
C
C * PRODUCT OF STT AND R
CALL MATMUL(STTR,STT,R,N,NB,NB,N,N)
C
C * PRODUCT OF STTR AND S
CALL MATMUL(STTRS,STTR,S,N,NB,N,N,N,N)
C
C * PRODUCT OF Q AND SCALAR TSAMP
CALL MATSCL(QT,TSAMP,Q,N,N,N,N)
C
C * ADD QT AND STTRS
CALL MATADD(PA,QT,STTRS,N,N,N,N)
C
C   ONEM=-1.0
C
C * PRODUCT OF B AND S
CALL MATMUL(BS,B,S,N,NB,N,N,N)
CALL MATSCL(BSM,ONEM,BS,N,N,N,N)
CALL MATADD(V,A,BSM,N,N,N,N)
C
C * TRANSPOSE OF V
CALL MATRNS(VT,V,N,N,N,N)
C
C * PRODUCT OF VT AND W AND V
CALL MATMUL(VTW,VT,W,N,N,N,N,N)
CALL MATMUL(VTWV,VTW,V,N,N,N,N,N)
C
C * NEW VALUE FOR W MATRIX=WP1
CALL MATADD(WP1,PA,VTWV,N,N,N,N)
C
C   RETURN
C   END

SUBROUTINE OPTOON(XOLD,K,S,VFOR,UD1,UD2,U,N,NB,NX,N,N,
  *TSAMP,DRUDD,MODE,ABCE,CERROR,XO,YO,PTRACK)
C
C * SUBROUTINE TO COMPUTE OPTIMAL CONTROL LAW
C
C   DIMENSION XOLD(8),VFOR(2,500),S(2,8),SX(2),U(2),DRUDD
C   1(500)
C   DIMENSION XO(250),YO(250)
C   COMMON RIN(8,500),YOUT(8,250)
C
C * RECALCULATE XOLD(5) USING CO-ORDINATE TRANSFORMATION
C
C   IF(K.GT.1) TO TO 20
C   PTRACK=0.0
C 20 IF(K.GT.46) GO TO 21
C   YI=2590.0
C   XI=0.0
C   RIN7=-0.173076
C   GO TO 22
C 21 IF(K.GT.79) GO TO 23
C   YI=2290.974
C   XI=1710.378
C   RIN7=0.7135
C   GO TO 22
C 23 IF(K.GT.129) GO TO 24
C   YI=3124.321
C   XI=2673.084
C   RIN7=1.209397
C   GO TO 22
C 24 YI=4928.924
C   XI=3355.213
C   RIN7=0.0
C
C 22 TEMP=XOLD(5)
C   XOLD(5)=(YO(K)-YI)*COS(RIN7)-(XO(K)-XI)*SIN(RIN7)
C   PTRACK=PTRACK+(XOLD(5)**2)*TSAMP
C
C * UOPT=VFOR-S*X
C
C * CHANGE TO COURSE-KEEPING
C * IF COURSE ERROR EXCEEDS 20 DEGREES.
C
C   UD1=0.0

```

```

UD2=0.0
CERROR=RIN(7)*XOLD(7)
ABCE=ABS(CERROR)
CALL MATMUL(SX,S,XOLD,NB,N,NX,N,N)
IF(ABCE.GT.0.349) GOTO 18
U(1)=VFOR(1,K)-SX(1)+UD1
GO TO 19
18 U(1)=-(CERROR-30.0*XOLD(8))+UD1
19 U(2)=VFOR(2,K)-SX(2)+UD2
C
C * LIMIT ENGINE SPEED
C
C   U2LIM1=1.5*RIN(2,K)
C   U2LIM2=0.5*RIN(2,K)
C   IF(U(2).GT.U2LIM1) U(2)=U2LIM1
C   IF(U(2).LT.U2LIM2) U(2)=U2LIM2
C
C   XOLD(5)=TEMP
C   IF(MODE)1,1,2
C
C MAXIMUM RUDDER ANGLE = +OR- 35 DEGREES.
C
C   1 IF(U(1).LT.0.610865) GOTO 3
C   U(1)=0.610865
C   3 CONTINUE
C   IF(U(1).GT.-0.610865) GOTO 5
C   U(1)=-0.610865
C   5 CONTINUE
C
C MAXIMUM RATE OF CHANGE OF RUDDER IS 2.5DEG/SEC.
C
C
C MAXRTE IS MAXIMUM RATE OF CHANGE OF RUDDER ANGLE
C CURRTE IS CURRENT RATE OF CHANGE OF RUDDER ANGLE
C
C   MAXRTE=0.0436332313
C   IF(K-1)12,12,13
C 12 CURRTE=U(1)/TSAMP
C   IF(CURRTE.LT.0.0436) GOTO 14
C   U(1)=0.0436*TSAMP
C 14 CONTINUE
C   IF(CURRTE.GT.-0.0436) GOTO 66
C   U(1)=-0.0436*TSAMP
C   GO TO 66

```

```

13 CURRTE=(U(1)-DRUDD(K-1))/TSAMP
IF(CURRTE.LT.0.0436) GOTO 44
U(1)=DRUDD(K-1)+(0.0436*TSAMP)
44 CONTINUE
IF(CURRTE.GT.-0.0436) GOTO 66
U(1)=DRUDD(K-1)-(0.0436*TSAMP)
66 CONTINUE
C
2 RETURN
END

```

A6.2 Utility Subroutines

```

Subroutine DIMEN :      Dimensionalises the hydrodynamic coefficients.
                        Called by NAB.

Subroutine CALXBC :      Computes the elements of the F and G
                        matrices. Called by NAB.

Subroutine FMAT :      Sets up the F matrix. Called by NAB.

Subroutine GMAT :      Sets up the G matrix. Called by NAB.

Subroutine TRNMAC :      Evaluates discrete transition matrices A, B
                        and C. Called by NAB.

Subroutine TRACK :      Generates the reverse-time discrete transition
                        matrices D and E. Called by RICAL.

Subroutine REVMAT :      Evaluates reverse-time discrete transition
                        matrices D and E. Called by TRACK.

```

A6.3 Matrix Operations

Subroutine MATINV :	Performs matrix inversion.
Subroutine MATADD :	Performs matrix addition.
Subroutine MATMUL :	Performs matrix multiplication.
Subroutine MATONE :	Produces a One's matrix.
Subroutine MATRED :	Reads in a matrix.
Subroutine MATEQL :	Makes matrix A equal to matrix B.
Subroutine MATIDN :	Produces an Identity matrix.
Subroutine MATSCL :	Multiplies a matrix by a scalar.
Subroutine MATZER :	Produces a null matrix.
Subroutine MATPRN :	Prints out a matrix.
Subroutine MATRNS :	Provides the transpose of a matrix.


```

SUBROUTINE DIMEN(RO,AL,XP,YP,ANP,UVEL,XOLD,UA,U,
1XDELTA,XN,XU,XUDOT,XUU,XUUU,XUN,XRDOT,XUA,XVA,XVV,XRR,
2XDD,XNN,YDELTA,YNN,YU,YUDOT,YV,YVDOT,YR,YRDOT,YUA,YVA,
3YVV,YRUV,YDDD,YDVV,ANDELTA,ANN,ANU,ANUDOT,ANV,ANVDOT,
4ANR,ANRDOT,ANUA,ANVA,ANVV,ANRUV,ANDDD,ANDVV)
DIMENSION XP(14),YP(14),ANP(14),XOLD(8),U(2)
C
C X DIMENSIONALISED HYDRODYNAMIC DERIVATIVES
C FOR NON-LINEAR MODEL
C
RO2=0.5*RO
RA2=0.5*1.28
C
XDELTA=XP(1)*RO2*AL**2*UVEL**2
XN=(XP(2)*RO2*AL**3*7.752)/(2.*3.14159)
XU=XP(3)
XUDOT=XP(4)*RO2*AL**3
XUU=XP(5)
XUUU=XP(6)
XUN=XP(7)
XRDOT=0.0
XUA=XP(9)*RA2*AL**2*UA
XVA=0.0
XVV=XP(11)*RO2*AL**2
XRR=XP(12)*RO2*AL**4
XDD=XP(13)*RO2*AL**2*UVEL**2
XNN=XP(14)
C
C Y DIMENSIONALISED HYDRODYNAMIC DERIVATIVES
C FOR NON-LINEAR MODEL
C
UCOR2=(0.84*UVEL**2+0.000015331*U(2)**2)
YDELTA=YP(1)*RO2*AL**2*UCOR2
YNN=YP(2)
YU=0.0
YUDOT=0.0
YV=YP(5)*RO2*AL**2*UVEL
YVDOT=YP(6)*RO2*AL**3
YR=YP(7)*RO2*AL**3*UVEL
YRDOT=YP(8)*RO2*AL**4
YUA=0.0
YVA=YP(10)*RA2*AL**2*UA
YVV=YP(11)*RO2*AL**2*UVEL
YRVV=YP(12)*RO2*AL**3*UVEL
YDDD=YP(13)*RO2*AL**2*UCOR2
YDVV=YP(14)*RO2*AL**2
C
C M DIMENSIONALISED HYDRODYNAMIC DERIVATIVES
C FOR NON-LINEAR MODEL
C
ANDELTA=ANP(1)*RO2*AL**3*UCOR2
ANN=ANP(2)
ANU=0.0
ANUDOT=0.0
ANV=ANP(5)*RO2*AL**3*UVEL
ANVDOT=ANP(6)*RO2*AL**4
ANR=ANP(7)*RO2*AL**4*UVEL
ANRDOT=ANP(8)*RO2*AL**5
ANUA=ANP(9)*RA2*AL**3
ANVA=ANP(10)*RA2*AL**3*UA
ANVV=ANP(11)*RO2*AL**3*UVEL
ANRVV=ANP(12)*RO2*AL**4*UVEL
ANDDD=ANP(13)*RO2*AL**3*UCOR2
ANDVV=ANP(14)*RO2*AL**3
C
RETURN
END

```

```

SUBROUTINE CALXBC(AM,ZI,XOLD,UVEL,WU,UD1,UD2,K,WUM
1XN,XU,XUDOT,XUU,XUUU,XUN,XUA,XVA,XVV,XRR,XDD,XNN,
2YDELTA,YNN,YV,YVDOT,YR,YRDOT,YUA,YVA,YVVV,YRVV,YDDD,YDVV
3ANDELTA,ANN,ANV,ANVDOT,ANR,ANRDOT,ANUA,ANVA,ANVV,ANRUV
4ANDDD,ANDVV,X1,X2,X4,X6,X8,XU3,XU5,
5B1,B2,B4,B6,B8,BU4,BU6,
6C1,C2,C4,C6,C8,CU4,CU6,U)
C
DIMENSION XOLD(8),WU(4),WUM(4),U(2)
C
C X COEFFICIENTS
C
XUDOTM=AM-XUDOT
C
X1=(XDD*U(1))/XUDOTM
X2=((XUN*UVEL)+(XNN*U(2)))/XUDOTM
X4=(XU+XUU*XOLD(1)+XUUU*XOLD(1)**2)/XUDOTM
X6=(XVV*XOLD(2)+AM*XOLD(4))/XUDOTM
X8=(XRR*XOLD(4))/XUDOTM
XU3=(XU+XUU*WU(1)+XUUU*WU(1)**2)/XUDOTM
XU5=XUA/XUDOTM
C
C Y COEFFICIENTS
C
YVDOTM=AM-YVDOT
C
Y1=(YDELTA+YDDD*U(1)**2)/YVDOTM
Y2=(YNN*U(2))/YVDOTM
Y4=(-AM*XOLD(4))/YVDOTM
Y6=(YV+YRVV*XOLD(4)*XOLD(2)+YVVV*XOLD(2)**2+YDVV*U(1)
1*XOLD(2))/YVDOTM
Y8=YR/YVDOTM
Y88=YRDOT/YVDOTM
YU4=(YV+YRVV*XOLD(4)*WU(2)+YVVV*WU(2)**2+YDVV*U(1)
1*WU(2))/YVDOTM
YU6=YVA/YVDOTM
C
C N COEFFICIENTS
C
ANRDOI=ZI-ANRDOT
C
AN1=(ANDELTA+ANDDD*U(1)**2)/ANRDOI
AN2=(ANN*U(2))/ANRDOI
AN4=0.0
C
AN6=(ANV+ANRVV*XOLD(4)*XOLD(2)+ANVVV*XOLD(2)**2+ANDVV
1*U(1)*XOLD(2))/ANRDOI
AN66=ANVDOT/ANRDOI
AN8=ANR/ANRDOI
AN4=(ANV+ANRVV*XOLD(4)*WU(2)+ANVVV*WU(2)**2+ANDVV*U(1)
&*WU(2))/ANRDOI
C
C * EDA'S TERM
C
ANU6=(ANVA+ANUA*WU(3))/ANRDOI
C
C * DISTURBANCE CONTROL TERMS
C
TC=(XU3*XUDOTM)*WU(1)
TA=(XUA*WU(3))
TP=(XUN*UVEL)+(XNN*U(2))
UD2=(TC+TA)/TP
C
ANC=(ANU4*ANRDOI)*WU(2)
ANA=(ANVA+ANUA*WU(3))*WU(4)
ANR=(ANDELTA+ANDDD*U(1)**2)
UD1=(ANC+ANA)/ANR
C
C B COEFFICIENTS
C
BDEN=1.0-Y88*AN66
C
B1=(Y1+Y88*AN1)/BDEN
B2=(Y2+Y88*AN2)/BDEN
B4=(Y4)/BDEN
B6=(Y6+Y88*AN6)/BDEN
B8=(Y8+Y88*AN8)/BDEN
BU4=(YU4+Y88*ANU4)/BDEN
BU6=(YU6+Y88*ANU6)/BDEN
C
C C COEFFICIENTS
C
CDEN=1.0-AN66*Y88
C
C1=(AN1+AN66*Y1)/CDEN
C2=(AN2+AN66*Y2)/CDEN
C4=(AN66*Y4)/CDEN
C6=(AN6+AN66*Y6)/CDEN
C8=(AN8+AN66*Y8)/CDEN

```

```

CU4=(ANU4+AN66*YU4)/CDEN
CU6=(ANU6+AN66*YU6)/CDEN

```

```

RETURN
END

```

```

SUBROUTINE FMAT(TAUR,TAUN,X1,X2,X4,X6,X8,XOLD,
1B1,B2,B4,B6,B8,C1,C2,C4,C6,C8,F,N,NN)

```

```

DIMENSION F(N,N),XOLD(8)
CALL MATZER(F,N,N,NN)
F(1,1)=(-1.0)/TAUR
F(2,2)=(-1.0)/TAUN
F(3,4)=1.0
F(4,1)=X1
F(4,2)=X2
F(4,4)=X4
F(4,6)=X6
F(4,8)=X8
F(5,6)=1.0
F(6,1)=B1
F(6,2)=B2
F(6,4)=B4
F(6,6)=B6
F(6,8)=B8
F(7,8)=1.0
F(8,1)=C1
F(8,2)=C2
F(8,4)=C4
F(8,6)=C6
F(8,8)=C8

```

```

RETURN
END

```

```

SUBROUTINE GMAT(TAUR,TAUN,XU3,XU5,
1BU4,BU6,CU4,CU6,G,N,NG,NN)

```

```

DIMENSION G(N,NG)
CALL MATZER(G,N,NG,NN)
G(1,1)=1.0/TAUR
G(2,2)=1.0/TAUN
G(4,3)=XU3
G(4,5)=XU5
G(6,4)=BU4
G(6,6)=BU6
G(8,4)=CU4
G(8,6)=CU6

```

```

RETURN
END

```

```

SUBROUTINE TRNMAC(F,G,A,B,C,N,NG,NB,TSAMP,NN)

```

```

C
C EVALUATES DISCRETE STATE TRANSITION MATRIX A(T)
C CONTROL TRANSITION MATRIX B(T) AND DISTURBANCE
C TRANSITION MATRIX C(T).
C

```

```

DIMENSION ST(8,8),F(8,8),A(8,8),INTEGA(8,8)
DIMENSION BUD(8,6),G(8,6),B(8,2),C(8,4)
REAL INTEGA
INTEGER POWER
NORMFT=0.0
DO 1 I=1,N
DO 1 J=1,N
ST(I,J)=F(I,J)*TSAMP
1 A(I,J)=ST(I,J)
POWER=50
DO 7 I=2,POWER
FPOWER=POWER-I+2
DO 5 J=1,N
DO 3 K=1,N
3 INTEGA(J,K)=A(J,K)/FPOWER
5 INTEGA(J,J)=INTEGA(J,J)+1.0
CALL MATMUL(A,ST,INTEGA,N,N,N,NN)
7 CONTINUE
DO 9 J=1,N
A(J,J)=A(J,J)+1.0
DO 9 K=1,N
9 INTEGA(J,K)=TSAMP*INTEGA(J,K)
CALL MATMUL(BUD,INTEGA,G,N,N,NG,NN)

```

```

C
C * SPLIT BUD(8,6) INTO B(8,2) AND C(8,4)
C

```

```

DO 10 I=1,N
DO 10 J=1,NB
10 B(I,J)=BUD(I,J)
DO 20 I=1,N
DO 20 J=3,NG
K=J-2
20 C(I,K)=BUD(I,J)

```

```

RETURN
END

```

```

SUBROUTINE TRACK(F,GU,R,Q,W,S,D,E,TSAMP,N,NB,NN)
C
C * THE SUBROUTINE GENERATES THE REVERSE TIME DISCRETE
C * TRACKING MATRICES D AND E BY SOLVING THE EQUATION:
C MDOT=FF*M+GG*RI
C WHERE, FF=(F-G*R**(-1)*G'*W)'
C GG=-Q
C R**(-1)*G'*W=S
C
C DIMENSION F(8,8),GU(8,2),R(2,2),Q(8,8),W(8,8),S(2,8)
C DIMENSION D(8,8),E(8,8),GM(8,2),GMS(8,8),FGMS(8,8)
C DIMENSION FF(8,8),GG(8,8)
C
C ONEM=-1.0
C CALL MATSCL(GM,ONEM,GU,N,NB,NN)
C
C * PRODUCT OF -G AND S
C CALL MATMUL(GMS,GM,S,N,NB,N,NN)
C
C * ADD F AND GMS
C CALL MATADD(FGMS,F,GMS,N,N,NN)
C
C * FF IS TRANSPOSE OF FGMS
C CALL MATRNS(FF,FGMS,N,N,NN)
C
C * GG IS -Q
C CALL MATSCL(GG,ONEM,Q,N,N,NN)
C
C * USE REVMAT(REVERSE TRMAT) TO FIND DISCRETE MATRICES D
C AND E
C CALL REVMAT(FF,GG,D,E,N,N,TSAMP,NN)
C
C RETURN
C END

```

```

SUBROUTINE REVMAT(F,G,A,B,N,NG,TSAMP,NN)
C
C EVALUATES DISCRETE STATE TRANSITION MATRIX A(T)
C AND DISCRETE FORCING MATRIX B(T)
C
C DIMENSION ST(8,8),F(8,8),A(8,8),INTEGA(8,8),B(8,8),G(8,8)
C REAL INTEGA
C INTEGER POWER
C NORMFT=0.0
C DO 1 I=1,N
C DO 1 J=1,N
C ST(I,J)=F(I,J)*TSAMP
1 A(I,J)=ST(I,J)
C POWER=50
C DO 7 I=2,POWER
C FPOWER=POWER-I+2
C DO 5 J=1,N
C DO 3 K=1,N
3 INTEGA(J,K)=A(J,K)/FPOWER
5 INTEGA(J,J)=INTEGA(J,J)+1.0
C CALL MATMUL(A,ST,INTEGA,N,N,N,NN)
7 CONTINUE
C DO 9 J=1,N
C A(J,J)=A(J,J)+1.0
C DO 9 K=1,N
9 INTEGA(J,K)=TSAMP*INTEGA(J,K)
C CALL MATMUL(B,INTEGA,G,N,N,NG,NN)
C
C RETURN
C END

```

```

SUBROUTINE MATINV(A,N,NA)
C DIMENSION A(NA,N),PIVOT(20),INDEX(20,2)
C EQUIVALENCE (IROW,JROW),(ICOL,JCOL),(AMAX,T,SWA)
C IF(N=1)10,5,10
5 AT=A(1,1)
C A(1,1)=1./AT
C RETURN
10 DETERM=1.0
15 DO 20 J=1,N
20 IPIVOT(J)=0
30 DO 550 I=1,N
40 AMAX=0.0
45 DO 105 J=1,N
50 IF(IPIVOT(J)-1)60,105,60
60 DO 100 K=1,N
70 IF (IPIVOT(K)-1)80,100,740
80 IF (ABS(AMAX)-ABS(A(J,K)))85,100,100
85 IROW=J
90 ICOL=K
95 AMAX=A(J,K)
100 CONTINUE
105 CONTINUE
110 IPIVOT(ICOL)=IPIVOT(ICOL)+1
130 IF(IROW=ICOL)140,260,140
140 DETERM=-DETERM
150 DO 200 L=1,N
160 SWAP=A(IROW,L)
170 A(IROW,L)=A(ICOL,L)
200 A(ICOL,L)=SWAP
260 INDEX(I,1)=IROW
270 INDX(I,2)=ICOL
310 PIVOT(I)=A(ICOL,ICOL)
320 DETERM=-DETERM*PIVOT(I)
330 A(ICOL,ICOL)=1.0
340 DO 350 L=1,N
350 A(ICOL,L)=A(ICOL,L)/PIVOT(I)
380 DO 550 LI=1,N
390 IF(LI=ICOL)400,550,400
400 T=A(LI,ICOL)
420 A(LI,ICOL)=0.0
430 DO 450 L=1,N
450 A(LI,L)=A(LI,L)-A(ICOL,L)*T
550 CONTINUE

```

```

600 DO 710 I=1,N
610 L=N+1-I
620 IF(INDEX(L,1)-INDEX(L,2))630,710,630
630 JROW=INDEX(L,1)
640 JCOLUMN=INDEX(L,2)
650 DO 700 K=1,N
660 SWAP=A(K,JROW)
670 A(K,JROW)=A(K,JCOLUMN)
700 A(K,JCOLUMN)=SWAP
710 CONTINUE
740 RETURN
C END

```

```

SUBROUTINE MATADD(A,B,C,N,M,NN)
C
C MATADD A=B+C
C
C N IS THE NUMBER OF ROWS IN B AND C
C M IS THE NUMBER OF COLUMNS IN B AND C
C
C DIMENSION A(N,M),B(N,M),C(N,M)
C DO 10 I=1,N
C DO 10 J=1,M
C A(I,J)=B(I,J)+C(I,J)
10 CONTINUE
C RETURN
C END

```

```

SUBROUTINE MATMUL(A,B,C,N,M,L,NN)
C
C MATMUL A=B*C
C
C N IS NUMBER OF ROWS IN B
C M IS NUMBER OF COLUMNS IN B AND ROWS IN C
C L IS NUMBER OF COLUMNS IN C
C
  DIMENSION A(N,L),B(N,M),C(M,L)
  DO 10 I=1,N
    DO 10 K=1,L
      A(I,K)=0.0
      DO 10 J=1,M
10    A(I,K)=A(I,K)+B(I,J)*C(J,K)
      RETURN
    END
  END

```

```

SUBROUTINE MATONE(A,N,M,NN)
C
C PRODUCES A ONE'S MATRIX
C
  DIMENSION A(N,M)
  DO 10 I=1,N
    DO 10 J=1,M
10    A(I,J)=1.0
  RETURN
  END

```

```

SUBROUTINE MATRED(A,N,M,NN)
C
  DIMENSION A(N,M)
  DO 10 I=1,N
10    READ(5,20) (A(I,J),J=1,M)
20    FORMAT(8F10.0)
  RETURN
  END

```

```

SUBROUTINE MATEQL(A,B,N,M,NN)
C
C MATEQL A=B
C
C N IS THE NUMBER OF ROWS
C M IS THE NUMBER OF COLUMNS
C
  DIMENSION A(N,M),B(N,M)
  DO 10 I=1,N
    DO 10 J=1,M
10    A(I,J)=B(I,J)
  RETURN
  END

```

```

SUBROUTINE MATIDN(A,N,NN)
C
C MATIDN PRODUCES A UNITY MATRIX A
C
C N IS THE NUMBER OF ROWS AND COLUMNS
C
  DIMENSION A(N,N)
  DO 10 I=1,N
    DO 10 J=1,N
      A(I,J)=0.0
10    CONTINUE
    DO 20 I=1,N
      A(I,I)=1.0
20    CONTINUE
  RETURN
  END

```

```

SUBROUTINE MATSCL(A,S,B,N,M,NN)
C
C N IS NUMBER OF ROWS,M NUMBER OF COLUMNS
C
  DIMENSION A(N,M),B(N,M)
  DO 10 I=1,N
    DO 10 J=1,M
      A(I,J)=S*B(I,J)
10    CONTINUE
  RETURN
  END

```

```

SUBROUTINE MATZER(A,N,M,NN)
C
  DIMENSION A(N,M)
  DO 10 I=1,N
    DO 10 J=1,M
      A(I,J)=0.0
10    CONTINUE
  RETURN
  END

```

```

SUBROUTINE MATPRN(A,N,M,NN,NAME)
C
C PRINTS OUT MATRIX A
C
C N IS NUMBER OF ROWS
C M IS NUMBER OF COLUMNS
C
  DIMENSION A(N,M),NAME(2)
  WRITE(6,30)
  WRITE(6,40) NAME(1),NAME(2),N,M
  DO 10 I=1,N
    WRITE(6,20) (A(I,J),J=1,M)
10    CONTINUE
20    FORMAT(1X,SE14.7)
30    FORMAT(//)
40    FORMAT(12H REAL MATRIX,3X,2A4,10X,I3,3H X ,I3//)
  RETURN
  END

```

```

SUBROUTINE MATRNS(A,B,N,M,NN)
C
C A=TRANPOSE OF B
C
  DIMENSION A(M,N),B(N,M)
  DO 10 I=1,M
    DO 10 J=1,N
      A(I,J)=B(J,I)
10    CONTINUE
  RETURN
  END

```

A6.4 Real-Time Ship Control Program

```

100 DIM AK(4,4), A(4,4), AXT(4)
110 DIM B(4,2), BU(4)
120 DIM CR(4,4)
130 DIM ER(4,2), F(4,4), G(4,2)
150 DIM KZ(4)
180 DIM S(2,4), ST(4,4)
190 DIM TR(112), TT(4,4)
200 DIM U(2,112), UZ(2,112)
210 DIM XT(4), XTA(4), XTB(4,112), XO(112)
220 DIM YO(112)
230 DIM Z(4,112), ZD(4)
232 N=4: NB=2
235 XT(1)=0.75: XT(2)=0: XT(3)=0: XT(4)=0
240 INPUT "TIME DELAY(SECS)=";TD
245 INPUT "YO(M)=";YO(0)
250 INPUT "RUDDER CHANGE=";RC;"TRACK CHANGE=";TC
255 INPUT "NEW HEADING(RAD)=";HC
260 INPUT "FIN=";FIN
262 INPUT "FILTERED FORWARD VELOCITY?(Y/N)";$FU
264 INPUT "FILTERED LATERAL VELOCITY?(Y/N)";$FV
266 INPUT "FILTERED HEADING?(Y/N)";$FH
268 INPUT "FILTERED YAW RATE?(Y/N)";$FY
269 UZ(1,0)=0: UZ(2,0)=76.9442
270 U(1,0)=0: U(2,0)=76.9442
280 XD=0: X=0: XO(0)=0
285 S1=0.982188: S2=0.980209: S3=0.256456: TP=1
290 S4=0.304369: S5=0.248: S6=337.8
292 DR=2.2805: DE=0.0095
295 M1=0: M2=0: M3=0
300 M4=0: M5=0: M6=0
310 GOSUB 13000
315 FOR I=1 TO N
320 Z(I,0)=XT(I)
325 NEXT I
340 DATA 0.00006816,4.478E-09,-0.0000912,-0.0000644
345 DATA 7.876E-08,5.174E-12,-1.058E-07,-7.442E-08
350 DATA -4.443E-09,-2.93E-13,0.01189,4.325E-09
355 DATA -1.099E-08,-7.226E-13,1.516E-08,1.039E-08
360 FOR I=1 TO N: FOR J=1 TO N
370 READ AK(I,J)
380 NEXT J: NEXT I
400 PRINT "AK MATRIX"
410 FOR I=1 TO N: FOR J=1 TO N
420 PRINT AK(I,J)

```

```

430 NEXT J: PRINT : NEXT I: PRINT
440 INPUT "CHANGE AK MATRIX ?(Y/N)";$CK
450 IF $CK="N" THEN GOTO 500
460 INPUT "I=";I;"J=";J
470 INPUT "AK(I,J)=";AK(I,J)
480 INPUT "MORE ?(Y/N)";$MK
490 IF $MK="Y" THEN GOTO 460
500 INPUT "ABORT ?(Y/N)";$AB
510 IF $AB="Y" THEN GOTO 1345
515 PRINT "START"
520 FOR K=1 TO TD
530 FOR JJ=1 TO 14: FOR KK=1 TO 95
540 NEXT KK: NEXT JJ: NEXT K
1000 FOR K=0 TO FIN
1006 IF K=0 THEN GOSUB 10500
1010 GOSUB 12000
1015 GOSUB 15000
1200 GOSUB 3010
1220 GOSUB 10500
1270 NEXT K
1271 MWD(09FF2H)=0
1272 MWD(09FF0H)=0
1273 INPUT $CO
1274 PRINT : PRINT
1275 PRINT "XHAT2"
1280 FOR K=0 TO FIN
1285 PRINT XTB(1,K),XTB(2,K),XTB(3,K),XTB(4,K)
1290 NEXT K
1294 PRINT : PRINT
1295 PRINT "Z"
1300 FOR K=0 TO FIN
1305 PRINT Z(1,K),Z(2,K),Z(3,K),Z(4,K)
1310 NEXT K
1314 PRINT : PRINT
1315 PRINT "U"
1320 FOR K=0 TO FIN
1322 PRINT U(1,K),U(2,K),UZ(1,K),UZ(2,K)
1324 NEXT K
1325 PRINT : PRINT : PRINT "K,XO,YO"
1330 FOR K=0 TO FIN
1335 PRINT K,XO(K),YO(K)
1340 NEXT K
1345 STOP
3010 FOR I=1 TO N

```

```

3015 AXT(I)=0: FOR J=1 TO N
3020 AXT(I)=AXT(I)+A(I,J)*XT(J)
3030 NEXT J: NEXT I
3040 FOR I=1 TO N
3045 BU(I)=0: FOR J=1 TO NB
3050 BU(I)=BU(I)+B(I,J)*U(J,K)
3060 NEXT J: NEXT I
3070 FOR I=1 TO N
3080 XTA(I)=AXT(I)+BU(I)
3090 NEXT I
3095 GOSUB 10000
3096 GOSUB 10500
3100 FOR I=1 TO N
3110 ZD(I)=Z(I,K+1)-XTA(I)
3120 NEXT I
6000 FOR I=1 TO N
6005 KZ(I)=0: FOR J=1 TO N
6010 KZ(I)=KZ(I)+AK(I,J)*ZD(J)
6020 NEXT J: NEXT I
6030 FOR I=1 TO N
6040 XTB(I,K+1)=XTA(I)+KZ(I)
6050 NEXT I
6060 FOR I=1 TO N
6070 XT(I)=XTB(I,K+1)
6080 NEXT I
6082 IF $FU="N" THEN XT(1)=Z(1,K+1)
6084 IF $FV="N" THEN XT(2)=Z(2,K+1)
6086 IF $FH="N" THEN XT(3)=Z(3,K+1)
6088 IF $FY="N" THEN XT(4)=Z(4,K+1)
6100 RETURN
10000 REM MEASUREMENT SUBROUTINE
10010 MWD(09FF8H)=OFF01H
10020 MWD(09FF6H)=OFF00H
10030 GOSUB 10400
10040 SA=(AC/204.7)-M1)*S1
10050 Z(1,K+1)=Z(1,K)+(SA*TP)
10055 IF $A="SD" THEN Z(1,K+1)=SA
10060 MWD(09FF8H)=OFF02H
10070 MWD(09FF6H)=OFF00H
10080 GOSUB 10400
10090 SW=(AC/204.7)-M2)*S2
10100 Z(2,K+1)=Z(2,K)+(SW*TP)
10105 IF $A="SD" THEN Z(2,K+1)=SW
10110 MWD(09FF8H)=OFF03H

```

```

10120 MWD(09FF6H)=OFF00H
10130 GOSUB 10400
10140 Z(3,K+1)=(AC/204.7)-M3)*S3
10150 MWD(09FF8H)=OFF04H
10160 MWD(09FF6H)=OFF00H
10170 GOSUB 10400
10180 Z(4,K+1)=(AC/204.7)-M4)*S4
10190 MWD(09FF8H)=OFF05H
10200 MWD(09FF6H)=OFF00H
10210 GOSUB 10400
10220 UZ(1,K+1)=(AC/204.7)*S5-M5
10230 MWD(09FF8H)=OFF06H
10240 MWD(09FF6H)=OFF00H
10250 GOSUB 10400
10260 UZ(2,K+1)=(AC/204.7)*S6-M6
10270 RETURN
10400 REM ADC SUBROUTINE
10410 MWD(09FFAH)=OFFFFH
10420 CHK=MWD(09FFCH)
10430 IF CHK<0 THEN GOTO 10420
10440 AC=MWD(09FFEH)
10450 RETURN
10500 REM DAC CONVERSION
10510 D1=(DR*204.7)*U(1,K)
10515 IF K>0 THEN D1=(DR*204.7)*U(1,K+1)
10520 D2=(DE*204.7)*U(2,K)
10525 IF K>0 THEN D2=(DE*204.7)*U(2,K+1)
10530 MWD(09FF2H)=D1
10540 MWD(09FF0H)=D2
10550 RETURN
12000 REM CONTROL SUBROUTINE
12010 GOSUB 12500
12020 R1=0.75: R2=0: R3=0: R4=0
12030 IF K>RC THEN R3=HC
12050 IF K>TC THEN GOTO 12080
12060 YI=1: XI=0: RA=0
12070 GOTO 12090
12080 YI=1: XI=42: RA=HC
12090 TR(K+1)=(YO(K+1)-YI)*COS(RA)-(XO(K+1)-XI)*SIN(RA)
12100 CR=R3-XT(3)
12110 ACR=ABS(CR)
12130 ER(1,1)=TR(K+1)
12140 ER(2,1)=R2-XT(2)
12150 ER(3,1)=R3-XT(3)

```

```

12160 ER(4,1)=R4-XT(4)
12170 XD=XD+R1*TP
12180 X=X+XT(1)*TP
12185 IF K=0 THEN XD=0: X=0
12190 ER(1,2)=XD-X: ER(3,2)=0
12200 ER(2,2)=R1-XT(1): ER(4,2)=0
12210 GOSUB 12600
12215 SP=S(1,1)
12220 IF ACR>0.524 THEN S(1,1)=0
12230 U(1,K+1)=0: U(2,K+1)=0
12240 FOR I=1 TO 2: FOR J=1 TO 4
12250 U(I,K+1)=U(I,K+1)+S(I,J)*ER(J,1)
12260 NEXT J: NEXT I
12270 S(1,1)=SP
12300 U(2,K+1)=U(2,K+1)+76.9442
12310 IF U(1,K+1)>0.6109 THEN U(1,K+1)=0.6109
12320 IF U(1,K+1)<-0.6109 THEN U(1,K+1)=-0.6109
12330 IF U(2,K+1)>100 THEN U(2,K+1)=100
12340 IF U(2,K+1)<50 THEN U(2,K+1)=50
12350 RETURN
12500 REM POSITIONAL CO-ORDINATES
12520 XO(K+1)=XO(K)+(XT(1)*COS(XT(3))-XT(2)*SIN(XT(3)))*TP
12530 YO(K+1)=YO(K)+(XT(2)*COS(XT(3))+XT(1)*SIN(XT(3)))*TP
12540 RETURN
12600 REM S MATRIX
12610 S(1,1)=-0.06795: S(1,2)=2.76508
12620 S(1,3)=-0.93291: S(1,4)=-3.10289
12630 S(2,1)=0.001067: S(2,2)=0.047929
12640 S(2,3)=0: S(2,4)=0
12650 RETURN
13000 REM MEAN AND STANDARD DEVIATION
13010 Z(1,0)=0: Z(2,0)=0: Z(3,0)=0: Z(4,0)=0
13020 $A="SD"
13030 FOR K=0 TO 59
13040 GOSUB 10000
13050 FOR JJ=1 TO 11: FOR KK=1 TO 95
13060 NEXT KK: NEXT JJ: NEXT K
13070 $A="RN"
13080 X1=0: X2=0: X3=0: X4=0: X5=0: X6=0
13090 FOR K=1 TO 60
13100 X1=X1+Z(1,K): X2=X2+Z(2,K)
13110 X3=X3+Z(3,K): X4=X4+Z(4,K)
13120 X5=X5+UZ(1,K): X6=X6+UZ(2,K)
13130 NEXT K

13140 M1=X1/60: M2=X2/60: M3=X3/60
13150 M4=X4/60: M5=X5/60: M6=X6/60
13160 X1=0: X2=0: X3=0: X4=0: X5=0: X6=0
13170 FOR K=1 TO 60
13180 X1=X1+(Z(1,K)-M1)*(Z(1,K)-M1)
13190 X2=X2+(Z(2,K)-M2)*(Z(2,K)-M2)
13200 X3=X3+(Z(3,K)-M3)*(Z(3,K)-M3)
13210 X4=X4+(Z(4,K)-M4)*(Z(4,K)-M4)
13240 NEXT K
13250 CR(1,1)=SQR(X1/59)
13260 CR(2,2)=SQR(X2/59)
13270 CR(3,3)=SQR(X3/59)
13280 CR(4,4)=SQR(X4/59)
13290 PRINT: PRINT "MEAN"
13300 PRINT M1,M2,M3
13310 PRINT M4,M5,M6
13320 PRINT: PRINT "STANDARD DEVIATION"
13330 PRINT CR(1,1),CR(2,2),CR(3,3),CR(4,4)
13340 RETURN
15000 A(1,1)=1-0.0410116*XT(1)-0.02119*XT(4)
15010 A(1,2)=1.06725*XT(4)
15020 A(1,3)=0
15030 A(1,4)=0.0140048*XT(4)
15040 A(2,1)=0.446096*XT(4)
15050 A(2,2)=0.995-0.1593785*XT(1)-2.05168*ABS(XT(4))
15060 A(2,3)=0
15070 A(2,4)=0.005+0.028376*XT(1)-0.02429*ABS(XT(4))
15080 A(3,1)=0.015758*XT(4)
15090 A(3,2)=-0.01-0.101248*XT(1)+0.6868*ABS(XT(4))
15100 A(3,3)=1
15110 A(3,4)=0.989-0.195818*XT(1)
15120 A(4,1)=0.03377*XT(4)
15130 A(4,2)=-0.0295-0.17164*XT(1)+1.29186*ABS(XT(4))
15140 A(4,3)=0
15150 A(4,4)=0.967-0.35436*XT(1)
15160 B(1,1)=-0.0316267*U(1,K)
15170 B(1,2)=-0.000195+0.0000065*U(2,K)+0.000478*ABS(XT(4))
15180 B(2,1)=0.0195+0.071189*XT(1)-0.0045258*ABS(U(1,K))
15190 B(2,2)=0
15200 B(3,1)=0.017-0.059506*XT(1)-0.00146*ABS(U(1,K))
15210 B(3,2)=0
15220 B(4,1)=0.0315-0.1130267*XT(1)
15225 B(4,2)=0
15226 GOTO 15300

15230 PRINT "AA MATRIX"
15240 FOR I=1 TO N: FOR J=1 TO N
15250 PRINT A(I,J),
15260 NEXT J: PRINT: NEXT I: PRINT
15270 PRINT "BB MATRIX"
15280 FOR I=1 TO N: FOR J=1 TO NB: PRINT B(I,J),
15290 NEXT J: PRINT: NEXT I: PRINT
15300 RETURN

```

APPENDIX 7

APPLICATION OF MULTIVARIABLE SYSTEMS THEORY, OCTOBER 1982

AUTOMATIC PILOTAGE OF LARGE SHIPS IN CONFINED WATERS - A MULTIVARIABLE APPROACH

R.S. Burns, M.J. Dove, T.H. Bouncer,

Plymouth Polytechnic.

The feasibility of a guidance system for automatically controlling a large ship in the pilotage phase of a voyage is investigated. Identification, Optimal Control and Estimation Techniques are applied to a mathematical model of a vessel in the approaches to Plymouth.

INTRODUCTION

It is beyond question that the overall standard of navigation at sea is very high indeed, and the probability of completing a voyage successfully must be very close to unity. However, (1), a brief summary of marine traffic accidents shows that the majority occur within congested waters, particularly within port limits. Congestion, coupled with the increased size and complexity of operation, has focussed attention on the control of pilotage and berthing, for, not only must the safety and cost factors be considered, but also the environmental aspects of, say, the spillage of large quantities of crude oil at, or near, the approaches to a port.

This paper investigates the possibilities of employing multivariable control theory to the problem of automatically piloting a large vessel in the approaches to a port.

A discrete, time-varying non-linear model has been developed based upon eight system states, namely forward and lateral position and velocity, heading, yaw-rate, rudder angle and engine speed. The model has two deterministic inputs - demanded rudder and engine speed plus four stochastic disturbance inputs in the form of wind and current vectors. The measurements of the state vector, contaminated with random noise, are passed through an optimal, time-varying filter.

The best estimate of the state variables are used by an adaptive optimal controller to compute those inputs (demanded rudder and engine speed) which minimise a given performance criterion. The dynamics of both the filter and controller are updated frequently by a system identification algorithm that can be either based upon apriori knowledge of the hydrodynamic coefficients of the vessel, or by on-line measurements of the state variables.

An outline of the proposed system is given in Figure 1.

MATHEMATICAL MODELEquations of Motion

The ship is considered to be a rigid body with three degrees of freedom, in surge, sway and yaw. Ship motions in the other three degrees of freedom, roll, pitch and heave are considered small enough to be neglected. It is convenient to describe the motion in terms of a moving system of axes coincident with the mass centre of the hull as illustrated in Figure 2. This gives rise to an Eulerian set of equations of motion which may be written in the form

$$\begin{aligned} m\dot{u} - mrv &= X \\ m\dot{v} + mur &= Y \\ I_z \dot{r} &= N \end{aligned} \quad (1)$$

Techniques employed in obtaining expressions for hydrodynamic forces and moments are well covered in the literature (2) and the usual method is to apply a Taylor series expansion. For applications such as course-keeping, where changes in rudder and heading angles do not usually exceed five degrees, a linear approximation, using only the first order terms in the expansion, is normally quite adequate. In a track-keeping situation where large changes in heading can be expected, it becomes necessary to include second and third order expansion terms.

Surge Equation. The complete surge equation in dimensionalised form is

$$\begin{aligned} m\dot{u} - mrv &= X_u \dot{u} + X_u(u + u_c) + \bar{X}_{uu} u^2 + \bar{X}_{uuu} u^3 + \bar{X}_{uv} v^2 + \bar{X}_{rr} r^2 + \bar{X}_{\delta\delta} \delta^2 + \bar{X}_{uu} u n_A + \bar{X}_{nn} n_A^2 \\ &+ \bar{X}_{u_a} u_a \end{aligned} \quad (2)$$

In the above equation a shorthand subscript and bar notation has been adopted, for instance

$$X_u = \frac{\partial X}{\partial u}, \quad \bar{X}_{uu} = \frac{1}{2} X_{uu} = \frac{1}{2} \left(\frac{\partial^2 X}{\partial u^2} \right)$$

The dimensionalised hydrodynamic coefficients are obtained from the non-dimensional values in the usual manner

$$X_u = \left(\frac{1}{2} \rho L^2 U \right) X_u'$$

Sway and Yaw Equations. The dimensionalised sway and yaw equations are

$$\begin{aligned} m\dot{v} + mur &= Y_v \dot{v} + Y_v(v + v_c) + Y_r \dot{r} + Y_r r + \bar{Y}_{nn} n_A^2 + \bar{Y}_{vvv} v^3 + \bar{Y}_{rvv} rv^2 + \bar{Y}_{nn\delta} n_A^2 \delta_A + \bar{Y}_{nn\delta\delta} n_A^2 \delta_A^2 \\ &+ \bar{Y}_{\delta vv} \delta_A v^2 + Y_{v_a} v_a \end{aligned} \quad (3)$$

$$\begin{aligned} I_z \dot{r} = & N_v \dot{v} + N_v (v + v_c) + N_r \dot{r} + N_r r + \bar{Y}_{nn} n_A^2 + \bar{N}_{vvv} v^3 + \bar{N}_{rvv} r v^2 + \bar{N}_{nn\delta} n_A^2 \delta_A + \bar{N}_{nn\delta\delta} n_A^2 \delta_A^2 \\ & + \bar{Y}_{\delta vv} \delta_A v^2 + Y_{v_a} v_a \dots \dots \dots (4) \end{aligned}$$

Steering Gear and Main Engine. These are both modelled by first order linear differential equations

$$\dot{\delta}_A = \frac{1}{T_R} \delta_D - \frac{1}{T_R} \delta_A \dots \dots \dots (5)$$

$$\dot{n}_A = \frac{1}{T_N} n_D - \frac{1}{T_N} n_A \dots \dots \dots (6)$$

Where δ_D and n_D are the demanded rudder angle and demanded engine speed respectively.

State Space Formulation

Much attention was devoted to the choice of state variables in relationship to the tracking problem and the state vector was finally based on the ship body axes

$$X^T = (\delta_A \ n_A \ x \ u \ y \ v \ \psi \ r) \dots \dots \dots (7)$$

This state is affected by the forcing vector

$$U^T = (\delta_D \ n_D \ u_c \ v_c \ u_a \ v_a) \dots \dots \dots (8)$$

Equations (5), (6), (2), (3) and (4) can be arranged in the following set

$$\begin{aligned} \dot{\delta}_A &= -\frac{1}{T_R} \delta_A + \frac{1}{T_R} \delta_D \\ \dot{n}_A &= -\frac{1}{T_N} n_A + \frac{1}{T_N} n_D \\ \dot{x} &= u \\ \dot{u} &= A_1 \delta_A + A_2 n_A + A_4 u + A_6 v + A_8 r + A_{u3} u_c + A_{u5} u_a \\ \dot{y} &= v \\ \dot{v} &= B_1 \delta_A + B_2 n_A + B_4 u + B_6 v + B_8 r + B_{u4} v_c + B_{u6} v_a \\ \dot{\psi} &= r \\ \dot{r} &= C_1 \delta_A + C_2 n_A + C_4 u + C_6 v + C_8 r + C_{u4} v_c + C_{u6} v_a \end{aligned} \dots \dots \dots (9)$$

The coefficients A, B, and C are all time-varying and so, for example

$$A_1 = \frac{\bar{X}_{\delta\delta} \cdot \delta_A}{m - X_{\dot{u}}} = \frac{(\frac{1}{2}\rho L^2 U) \cdot \bar{X}_{\delta\delta} \cdot \delta_A}{m - X_{\dot{u}}}$$

A_1 , therefore, is a function of the instantaneous total velocity U and rudder angle δ_A .

Equation set (9) represent the time-varying state equations for the ship and are expressed by the state matrix vector differential equation

$$\dot{X}(t) = F(t)X(t) + G(t)U(t) \quad \dots\dots\dots (10)$$

It is convenient to partition the G matrix in terms of the control forcing function δ_A and n_A and the disturbance forcing functions u_c , v_c , u_a and v_a so that

$$\dot{X}(t) = F(t)X(t) + G_c(t)U(t) + G_D(t)W(t) \quad \dots\dots\dots (11)$$

The corresponding discrete solution is

$$X((K+1)T) = A(T, KT)X(KT) + B(T, KT)U(KT) + C(T, KT)W(KT) \quad \dots\dots\dots (12)$$

MEASUREMENT AND FILTERING

Separation Principle

This is an important feature of stochastic optimal control theory that allows a given optimisation problem to be reduced into two problems whose solutions are known, namely an optimal filter in cascade with a deterministic optimal controller.

The Measurement Process. The measured state $Z(K+1)$ is considered to contain noise $V(K+1)$, where $V(K+1)$ is a stationary gaussian process with covariance M . The measurement process is then represented by

$$Z((K+1)T) = H((K+1)T)X((K+1)T) + V((K+1)T) \quad \dots\dots\dots (13)$$

Estimation of the State Vector

The Kalman filter used here is a recursive computational algorithm which remembers past data, receives future positions, and bases the estimate of the state upon a combination of past and present information. It should be noted however that this technique assumes the system is linear and the errors gaussian. As a ship constitutes a non-linear system, when parameters such as large alterations of course and speed, shallow water effects, and trim are considered there must be some limitations to the technique.

The filter is characterised by containing a model of the ship and the equations are

$$\hat{X}((K+1)T) = A(T,KT)\hat{X}(KT) + K((K+1)T) \left[Z((K+1)T) - H((K+1)T)A(T,KT)\hat{X}(KT) \right] \dots\dots\dots (14)$$

The filter gain matrix $K(K+1)$ and the two covariance matrices $P(K+1/K)$, $P(K+1/K+1)$ are governed by

$$\begin{aligned} P(K+1/K) &= A(T,KT)P(K/K)A^T(T,KT) + B(T,KT)N(K/K)B^T(T,KT) \\ K((K+1)T) &= P(K+1/K)H^T((K+1)T) \left[H((K+1)T)P(K+1/K)H^T((K+1)T) + M((K+1)T) \right]^{-1} \dots\dots (15) \\ P(K+1/K+1) &= \left[I - K((K+1)T)H((K+1)T) \right] P(K+1/K) \end{aligned}$$

In determining the value of the filter gain matrix consideration has to be given to the control vector $U(KT)$ and its associated control matrix $B(T,KT)$. A model of $B(T,KT)$ is required in the filter and the complete filter model is shown in Figure 3, leading to the overall filter equations as

$$\begin{aligned} \hat{X}((K+1)T) &= A(T,KT)\hat{X}(K/K) + B(T,KT)U(KT) + K((K+1)T) \left[Z((K+1)T) - H((K+1)T) \left\{ A(T,KT)\hat{X}(KT) \right. \right. \\ &\quad \left. \left. + B(T,KT)U(KT) \right\} \right] \dots\dots\dots (16) \end{aligned}$$

CONTROLLER DESIGN

Stochastic Optimal Control

The stochastic optimal control problem is to find a control U which causes the system

$$\dot{X} = g(X(t), U(t), W(t), t)$$

to follow an optimal trajectory $X(t)$ that minimises a performance criterion

$$J = \int_{t_0}^{t_1} h(X(t), U(t), t) dt$$

whilst being subjected to a measurement process

$$Z = f(X(t), V(t), t)$$

Deterministic Optimal Control

Tracking Problem with Quadratic Performance Criterion. The tracking or servomechanism problem is one of applying a control U to drive a ship so that its states follow a desired trajectory in some optimal sense. The regulator problem is a special case of the tracking problem, the desired trajectory being a zero state.

Continuous Form. The quadratic criterion to be minimised is

$$J = \int_{t_0}^{t_1} \left\{ (X - R)^T Q (X - R) + U^T R U \right\} dt \quad (17)$$

where R is the desired value of the state vector it can be shown (3) that constrained functional minimisation yields the matrix Riccati equations

$$\dot{W} = -WF - F^T W - Q + WGR^{-1}G^T W \quad (18)$$

together with the reverse-time differential equation set

$$\dot{M} = (F - GR^{-1}G^T W)^T M - Q_R \quad (19)$$

The boundary condition is

$$M(t_1) = 0$$

and the optimal control

$$U_{opt} = -R^{-1}G^T(WX + M) \quad (20)$$

Discrete Form. Discrete minimisation produces the recursive Riccati equations together with the difference equation

$$M_{((N-K)T)} = D(T,KT)M_{((N-(K+1))T)} + E(T,KT)R_{((N-(K+1))T)} \quad (21)$$

having the boundary condition

$$M_{(N-1)} = 0$$

and the optimal control at the K^{th} instant

$$U(KT)_{opt} = -S_{((N-(K+1))T)}X(KT) - R^{-1}G^T M_{((N-(K+1))T)} \quad (22)$$

The deterministic optimal controller for a ship tracking system is shown in Figure 4.

IDENTIFICATION

Method of Linear Least Squares

$$\text{Put } J = \sum (N_i^2), \quad i = 0, 1, 2, 3, \dots, K$$

$$= N_i^T N_i$$

$$= (Z_i - Y\beta)^T (Z_i - Y\beta)$$

If we differentiate with respect to $\hat{\beta}$ and set $\frac{\partial}{\partial \hat{\beta}}(J(\hat{\beta})) = 0$, we obtain the L.L.S. estimate given by

$$\hat{\beta} = P_K Y^T Z \quad \dots\dots\dots (23)$$

where

$$P_K^{-1} = Y^T Y$$

A recursive form of equation (23) is available, which has the form

$$P_{K+1} = P_K - P_K Y(1 + Y^T P_K Y)^{-1} Y^T P_K \quad \dots\dots\dots (24)$$

$$\hat{\beta}_{K+1} = \hat{\beta}_K + P_{K+1} Y(Z - Y^T \hat{\beta}_K) \quad \dots\dots\dots (25)$$

The pair of equations 24 and 25 enable revised estimates of the parameter matrix $\hat{\beta}_{K+1}$ to be calculated from the prior estimate $\hat{\beta}_K$, based on a knowledge of Y^T and Z obtained by measurements made at the $(K+1)$ th sampling instant.

COMPUTER SIMULATION

The vessel chosen for the simulation was of the Mariner Class. Good agreement between full-scale test results and data obtained from the mathematical model was found with all standard manoeuvres and Figure 5 shows a typical turning circle for 20 degree starboard rudder. The recommended track for deep draught vessels into Plymouth Sound was selected as a suitable design specification for the automatic guidance system. This requires simultaneous control of the ship's position, heading and forward velocity and implementation of the matrix control equation (22) produces the optimal trajectory illustrated in Figure 6 when the desired forward speed is 7.717 m/s (15 knots).

CONCLUSIONS

Much work is still to be done before automatic guidance systems of the type described here are actually fitted to surface ships. Manufacturers are, however, already moving towards the replacement of conventional analogue auto-pilots with adaptive microprocessor based minimum energy course-keeping systems and the possibility exists that in the none to distant future a new generation of auto-pilots with both course and track-keeping facilities will emerge.

REFERENCES

1. Dove, M.J., 1974, "Automatic Control of Large Ships in Pilotage and Berthing", J.Inst. Nav. (U.K.) 27, 4.
2. Abkowitz, M., 1964, "Lectures on Ship Hydrodynamics, Steering and manoeuvrability", Hy-A Report, Hy. 5., Denmark.
3. Kirk, D.E., 1970, "Optimal Control Theory - An Introduction", Prentice-Hall Inc., New Jersey.

APPLICATION OF MULTIVARIABLE SYSTEMS THEORY, OCTOBER 1982

NOTATION

Matrices and Vectors

A	Discrete State Transition Matrix.	P	Covariance of State Vector.
B	Discrete Control Matrix.	Q	State Error Weighting Matrix.
C	Discrete Disturbance Matrix.	R	Control Weighting Matrix.
D	Discrete Reverse Transition Matrix.	R	Desired State Vector.
E	Discrete Reverse Control Matrix.	S	Feedback Gain Matrix.
F	Continuous Time System Matrix.	U	Control Vector.
G	Continuous Time Forcing Matrix.	V	Command Matrix.
H	Measurement Matrix.	V	Noise Vector.
K	Kalman Gain Matrix.	W	Riccati Coefficient Matrix.
M	Covariance of Noise Vector.	W	Disturbance Vector.
M	Reverse Time State Vector.	X	State Vector.
N	Covariance of Control Vector.	\hat{X}	Best Estimate of State Vector.
N	Residual Vector.	Y	Combined State and Control Vector.
		Z	Measured State Vector.

Scalar Symbols

A,B,C	State Equation Coefficients.	U	Track velocity (m/s).
I_z	Moment of Inertia about z axis (kgm^2).	u	Forward velocity of ship (m/s).
L	Length of ship between perpendiculars (m).	u_a, u_c	Forward components of wind and current velocities (m/s).
m	Mass of ship (kg).	v	Lateral velocity of ship (m/s).
n_A, n_D	Actual and Demanded engine speeds (rad/s).	v_a, v_c	Lateral components of wind and current velocities (m/s).
N	Total moment applied to ship (Nm).	x,y,z	Ship related orthogonal co-ordinates (m).
N_u, N_δ	Yaw hydrodynamic coefficients.	X	Total force on ship in forward direction (N).
etc.		X_u, X_δ	Surge hydrodynamic coefficients.
r	Angular velocity of ship about z axis.	etc.	
T	Sampling time interval (s).	X_o, Y_o, Z_o	Earth related orthogonal co-ordinates.
t	Time (s).	Y	Total lateral force on ship (N).
T_N	Time constant of main engines (s).	Y_u, Y_δ	Sway hydrodynamic coefficients.
T_R	Time constant of rudder servo (s).	etc.	
K,i	Integer counters.		
J	Performance Index.		

GREEK SYMBOLS

$\beta, \hat{\beta}$	Transpose of Augmented State Transition Matrix and best estimate.	δ_A, δ_D	Actual and Demanded rudder angles (rad).
		ρ	Density of water (kg/m^3).
		ψ	Actual heading of ship (rad).

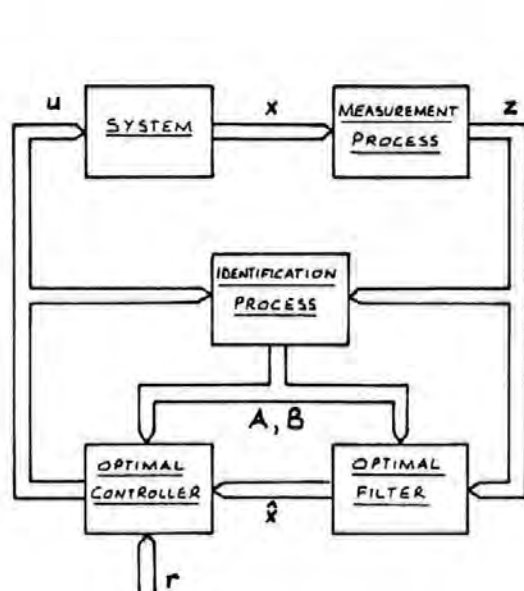


Figure 1 Proposed Automatic Guidance System

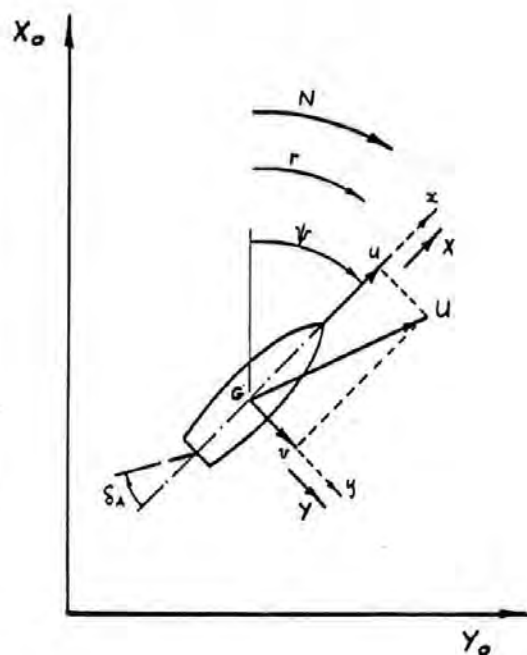


Figure 2 Co-ordinate Systems

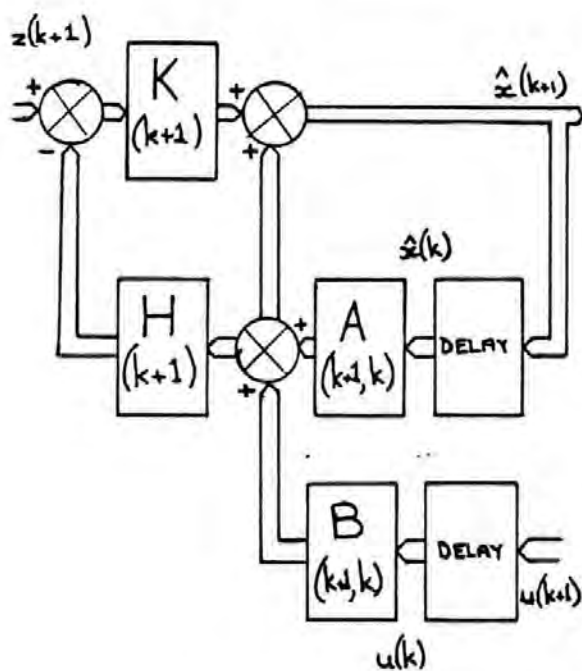


Figure 3 Optimal Filter

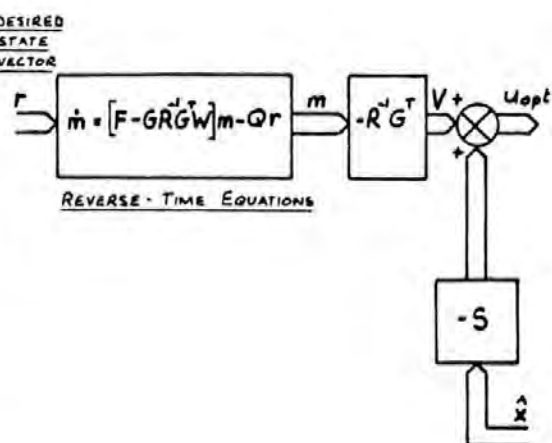


Figure 4 Optimal Controller

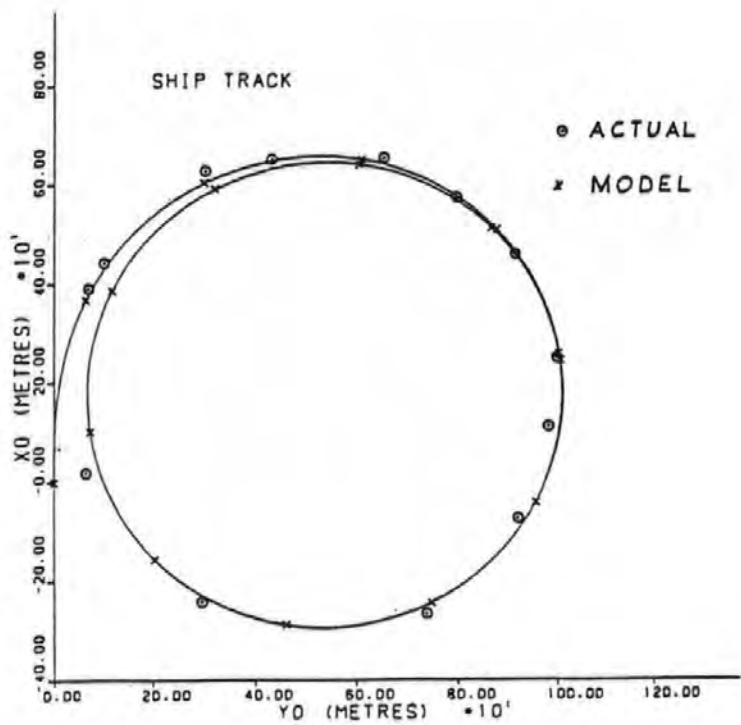


Figure 5 Turning Circle, 20° Starboard Rudder, 7.717 m/s.

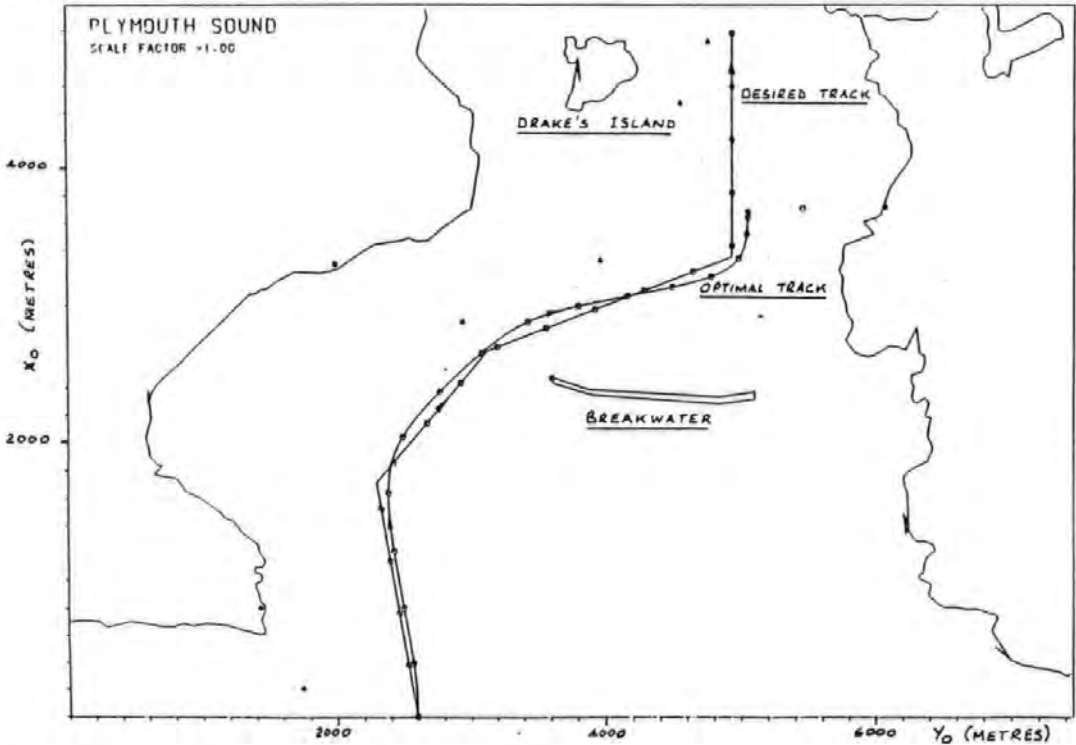


Figure 6 Optimal Trajectory into Plymouth Sound.